MATHEMATICAL METHODS AND SOLUTIONS IN BLACK HOLE ASTROPHYSICS

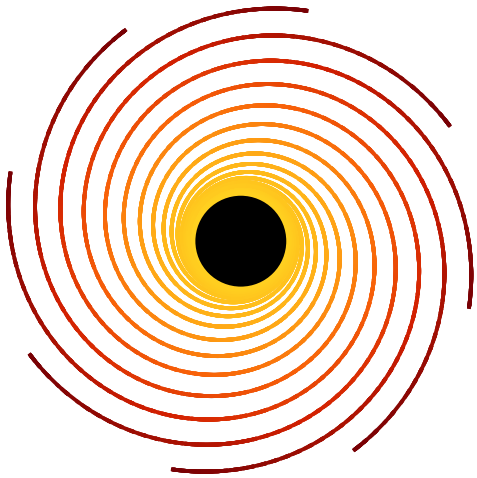

Dem Fachbereich Physik und Elektrotechnik der Universität Bremen
zur Erlangung des akademischen Grades eines

Doktor der Naturwissenschaften (Dr. rer. nat.)

vorgelegte Dissertation von

Mgr. Vojtěch Witzany

wohnhaft in Bremen

1. Gutachter: Prof., Dr. Claus Lämmerzahl
2. Gutachter: Prof., Dr. Jutta Kunz
Eingereicht am:
Datum des Promotionskolloquiums: 4. Oktober 2018

Bremen 2018

Acknowledgements

First of all, I would like to thank my loving parents and family for their unrelenting support throughout the years. It was this unconditional love and encouragement that ultimately made it possible for me to pursue a Ph.D.

Then, I would like to thank my supervisor Claus Lämmerzahl for his kind supervision during the time of the Ph.D., and all the work he invests into making ZARM and the Research Training Group *Models of Gravity* a fruitful scientific environment. At this point, I should mention that I have also greatly profited from numerous discussions about scientific topics with Volker Perlick, Eva Hackmann, Dirk Puetzfeld, Jan Steinhoff, Justin Vines, Charalampos Markakis, Domenico Giullini, Oldřich Semerák, and Georgios Lukes-Gerakopoulos, for which I express gratitude as well.

I should also mention the new friends I have made by coming to Bremen. Amongst the whole lively collective of people in the Research training group and at ZARM, I would like to specifically mention Pavel Jefremov, Efthimia Deligianni, Kris Schroven, and Dennis Philip as invaluable companions on the journey we have all embarked upon by taking on a Ph.D. Last but not least, I would like to thank for the partnership of my loving girlfriend.

This work would not have been possible without the support from a Ph.D. grant of the German Research Foundation (DFG) within the Research Training Group 1620 “Models of Gravity”, for which I am grateful. This thesis was typeset using the “PhD Thesis PSnPDF” template by Krishna Kumar.

Abstract

Black holes are nowadays widely accepted as the most likely explanation of a wide range of astrophysical phenomena from X-ray sources within our galaxy to powerfully radiating galactic cores billions of light-years away from us. The arguments that lead us to the conclusion that black holes of various masses indeed reside in such locations come from the observations in the electromagnetic spectrum and, since recently, also from gravitational-wave detections.

In this thesis, I first take the reader on a brief guided tour of the essential physics of black holes and the accretion of matter onto them that leads to the observed electromagnetic signal. Then, I explore the possibility of deepening the understanding of these topics with analytical methods in the appended papers.

The topics of the papers go as follows. In Witzany and Lämmerzahl [291], we have re-expressed exact relativistic equations of motion in general stationary space-times in a "pseudo-Newtonian" form, a form ready to be implemented in common Newtonian hydrodynamics codes while recovering all the essential properties of the evolution near a black hole. In Markakis et al. [163], we have explored various forms of equations of relativistic fluids and magnetized plasmas in curved space-time, deriving actions and Hamiltonians for fluid stream-lines, and corresponding conservation laws (such as the relativistic Kelvin theorem). In Witzany [288], I have investigated whether one can use deeper geometrical properties of spinning black-hole fields to derive new conservation laws that could be used to constrain numerical simulations. The conclusion is that only weak conservation laws of the character of a differential constraint can be found. In the fourth paper, Witzany and Jefremov [289], we have found new closed solutions for idealized equilibria of fluids near black holes. These represent a considerable expansion of the set of closed-form prescriptions with which numerical simulations of accretion disks can be initialized.

Last but not least, one of the chapters of the thesis is dedicated to my research on the so-called spin-curvature coupling, which is experienced by rapidly rotating astrophysical objects in curved space-time. My work on these topics greatly improves the understanding of the Hamiltonian formalism that captures this coupling, and the results are likely to become important for gravitational-wave modelling.

List of appended publications

Witzany, V., & Lämmerzahl, C. (2017). Pseudo-Newtonian Equations for Evolution of Particles and Fluids in Stationary Space-times. *The Astrophysical Journal*, 841(2), 105. Preprint at arXiv:1601.01034. (short ref.: [291])

Markakis, C., Uryū, K., Gourgoulhon, E., Nicolas, J. P., Andersson, N., Pouri, A., & Witzany, V. (2017). Conservation laws and evolution schemes in geodesic, hydrodynamic, and magneto-hydrodynamic flows. *Physical Review D*, 96(6), 064019. Preprint at arXiv:1612.09308. (short ref.: [163])

Witzany, V. (2017). Exploiting the hidden symmetry of spinning black holes: conservation laws and numerical tests. *Monthly Notices of the Royal Astronomical Society*, 473(2), 2434-2440. Preprint at arXiv:1709.03330. (short ref.: [288])

Witzany, V., & Jefremov, P. (2018). New closed analytical solutions for geometrically thick fluid tori around black holes – Numerical evolution and the onset of the magneto-rotational instability. *Astronomy & Astrophysics*, 614, A75. Preprint at arXiv:1711.09241. (short ref.: [289])

Preface

General theory of relativity, or Einstein gravity, published over a hundred years ago [82], is currently the leading theory of gravity. It is not that other theories fulfilling basic self-consistency conditions do not exist – a famous example of a self-consistent relativistic theory of gravity formulated even before Einstein was given by Nordström [197]. It is also not that Einstein gravity, or in more general the whole current "standard" set of laws, would not be under scrutiny due to observation and experiment – for example the problem of "missing mass" in the rotation curves of galaxies and the specific details of its phenomenology invite speculation as to whether a modified gravitational law is at play [177, 166].

What is it then that keeps General relativity (GR) reigning on the throne of gravity? The most convincing argument is that the paradigm of GR has an absolutely behemoth body of observational data behind it, obtained in a variety context and over many scales. Another argument is that Einstein gravity is in many senses of the word *robust*; it comes out *uniquely* from a set of theoretical requirements and heuristics. Consequently, if a theory attempts to add modified dynamics on top of GR, it might address a particular issue in a given context, but it will typically create an unwanted problem in a different one.

Consider the example of galactic rotation curves, that is, the average velocity of matter in the galaxy as a function of distance from the center as observed from its Doppler redshift. If we assume for a moment that the source of gravitation is a roughly spherical cloud of matter (as would be the case of e.g. bulge-dominated galaxies), then the rotational velocity v as a function of radius r should fulfill

$$v = \sqrt{\frac{GM(r)}{r}},$$

where $M(r)$ is the mass enclosed within a radius r, and G Newton's gravitational constant. However, it has long been observed that if we estimate $M(r)$ from the amount of glow coming from stars and hot gas visible in the galaxy, and use it to estimate the rotation velocity, we get a wildly inconsistent estimate for $v(r)$ in the galactic outskirts (see Fig. 1). This suggests that there is an additional, invisible component of $M(r)$ known as *dark matter* (see [30] for a historical review).

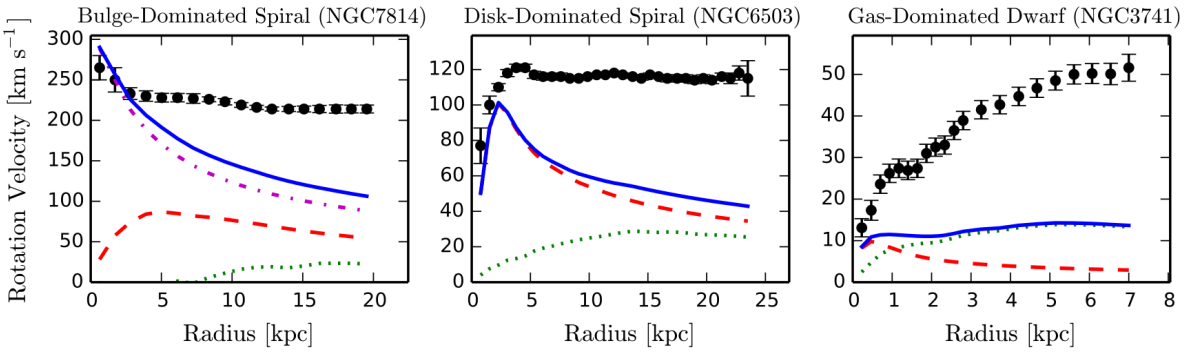

Fig. 1 Examples of mass models and rotation curves for individual galaxies taken from McGaugh et al. [166]. The black points with error bars are the observed rotation curves $v(r)$, and the solid blue line is the prediction based on the distribution of luminous matter.

However, a number of peculiar correlations can be observed between the observed rotation curve and the one predicted from luminous matter [84, 276, 174, 175, 166]. Let us formulate them in terms of an all-encompassing relation between the radial acceleration ($a = v^2/r$) predicted by the distribution of luminous mass $a_{\rm L}$ as compared to the observed one $a_{\rm obs}$

$$a_{\rm obs} = \frac{a_{\rm L}}{1-\exp(-\sqrt{a_{\rm L}/a_0})}\,, \tag{1}$$

where a_0 is a small acceleration constants. Relations like these have already been proposed for a long time [174–176] but they have recently been fit over 153 galaxies of various composition, mass, size, and morphology to yield $a_0 = 1.20 \pm 0.02(\text{intrinsic fit scatter}) \pm 0.24(\text{extrinsic modelling systematics}) \times 10^{-11}\,\text{m}\,\text{s}^{-2}$ [166]. From this, we can deduce that *independent of the size, composition, or shape of a galaxy*, at distances $r \gg \sqrt{GM_{\rm L}/a_0}$, where $M_{\rm L}$ is the luminous mass concentrated in the center of the galaxy, the dark matter halo density will behave as

$$\rho_{\rm DM} \approx \frac{\sqrt{GMa_0}}{r^2}\,. \tag{2}$$

However, the real density of dark matter (if dark matter is real) must have an eventual cut off, since this formula integrated to infinity corresponds to an infinitely heavy dark matter halo.

The remarkable scaling (1), of course, suggests the possibility that the phenomenon of dark matter is not linked to any invisible matter but rather a modified theory of gravitation that produces such dynamics sourced only by the luminous mass of the galaxies, as has been famously proposed in 1983 by Milgrom [174, 175, 176]. The basic idea is, quite naturally, that a new, somewhat arbitrary degree of freedom $\rho_{\rm DM}(r)$ chosen to fit the data is just a redundant

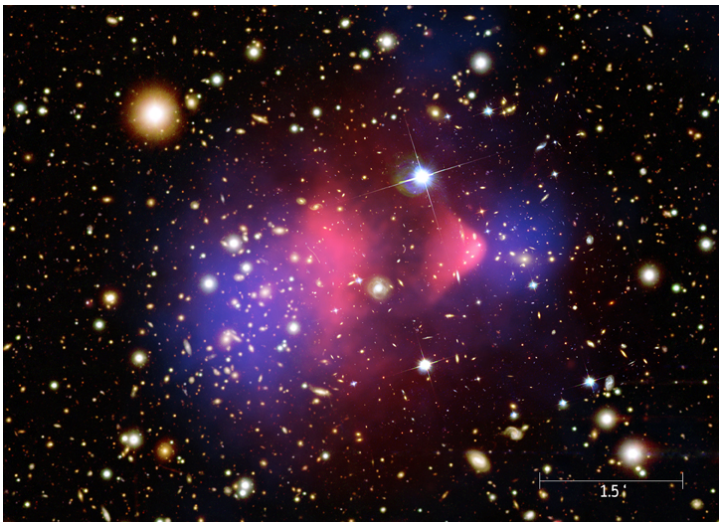

Fig. 2 X-ray image (pink) of the Bullet cluster by Chandra observatory superimposed over a visible light image (galaxies) by Hubble and Magellanic telescope, with matter distribution calculated from gravitational lensing (blue) [59, 58]. Credit: Chandra X-ray observatory

"fudge factor", and one should instead postulate a different field equation for the Newtonian potential $\Phi(r)$.

However, from the point of view of a relativist, this argument does not make so much sense. In an attempt to eliminate an independent and tunable degree of freedom ρ_{DM} by modifying gravity, one always ends up including at least one new independent and tunable degree of freedom in the gravity sector itself. This can be seen from the fact that the Einstein equations do not allow modifications without either adding more derivatives, adding new fields, or violating the conservation of stress-energy [153, 154]. More precisely formulated results of a similar nature come from the considerations of the initial value problem for metric gravity [139, 99]. This is a part of the aforementioned *robustness* of relativity.

Nevertheless, even though the new degree of freedom is a proper degree of freedom, its dynamics can be still set so as to reproduce the relation (1) automatically. Hence many modified relativistic gravities reproducing relations such as (1) were formulated [27, 297, 178, 71, 38, 117]. However, they typically require much more than a single new degree of freedom along with a number of freely tunable parameters or even functions. Additionally, they will often be plagued with various instabilities and pathologies (as could be expected from the diverging mass of the effective dark matter halo (2)).

But still, the strongest hits to the program of explaining dark matter by modified gravity come simply from observations on scales larger than galaxies [30, 85]. Clusters of galaxies do not obey the phenomenology (1), and modified gravities almost always need some amount of dark matter to explain the observations. The power spectrum of the small anisotropies in the

cosmic microwave background also generally require that some degree of freedom behaves essentially as dark matter particles before the cosmological epoch of recombination, and this same fraction of dark matter is consistent with recent cosmological expansion and currently observable large scale structure.

Another, less obvious constraint comes from the recent detection of the merger of neutron stars by the LIGO/Virgo gravitational wave detectors and the follow-up observations of the corresponding electromagnetic signal [5, 4]. This observation is important because many modified gravities predict that gravitational waves will propagate through space at a different speed than light. The fact that we observed the gamma-ray signal traveling for $\sim 10^7$ light-years with a few-second lag after the gravitational-wave merger signal puts very strong constraints on the difference between the speed of light and gravity and thus also on modified gravitational theories [83, 19, 64, 231].

If this is not enough to convince the reader, we may consider the particularly suggestive example of the Bullet cluster, where two galaxy clusters were observed after a relatively recent (on cosmological scales) merger that occurred 150 million years ago [59, 58]. As can be seen in Fig. 2, the gravitational lensing reconstructs the effective gravitating mass of the clusters as clearly separated from the source of X-rays, a feature that suggests the additional gravitating degree of freedom of the modified gravity must be only weakly coupled to the ordinary baryonic mass.

Last but not least, let me also mention a very recently published result testing the so-called *strong equivalence principle*. The strong equivalence principle states that even a strongly gravitating object such as a neutron star or a black hole will follow an orbit that is independent of its composition [198]. Quite surprisingly, almost every modification of GR will violate this principle and by observing orbits of compact astrophysical bodies, we are also able to separate the wheat from chaff. In a recent report, Archibald et al. [15] presented the results of 5 years of observations of a hierarchical stellar triple consisting of a central pulsar and a white-dwarf binary orbiting it. Their observations improve the existing upper bound on the violations of the strong equivalence principle in the strong field by 3 orders of magnitude and by on order of magnitude as compared to the weak-field Solar-system tests.

As a result of all of these observations, essentially all major modified-gravity alternatives to dark matter have been eliminated – and relativity reigns once again. The exposition of the last few pages was not meant as any exhaustive review of which arguments are in favor of Einstein's gravity and which perhaps suggest there are some flaws. Instead, it is supposed to underline the size of the communities approaching the problem from different sides, and the sheer richness of physics and contexts through which we learn about gravity in this day and time.

It was my privilege to work on my Ph. D. in this field at the Center of Applied Space Technology and Microgravity (Zentrum für angewandte Raumfahrttechnologie und Mikrogravitation, ZARM) in Bremen in the wider Research training group *Models of gravity*. In these three years this environment has allowed me to meet down-to-earth engineers designing and realizing precise tests of gravity while employing state of the art technology, but also theorists questioning our every assumption and dreaming of deep mathematical truths in the sky. These and all the others in between have convinced me that it is an exciting time to be a part of the community studying gravitational theory and fundamental physics in general. I hope to channel at least a part of the excitement to the kind reader in the presented dissertation.

Table of contents

List of figures

List of tables

Chapter 1

Black hole fields

The first exact solution of Einstein's gravitational equations was found by Karl Schwarzschild [235] only two months after the publication of the definitive paper on Einstein's general relativity [82], all this while Schwarzschild was stationed at the Russian front as a soldier during the First World War. Quite surprisingly, Schwarzschild's solution was also the first black hole solution. Specifically, it represents the gravitational field of a non-rotating isolated black hole. This fact was recognized neither by Schwarzschild nor by anyone else at that period. Nevertheless, as time progressed, both theoretical relativists and astrophysicists came to a solid and well established understanding of the properties and inevitability of formation of black holes in nature (see the summary of Israel [123] for a historical review).

Black holes are characterized as massive, compact, dark objects with a special boundary at a radius[1] $\sim 1M - 2M$ delineating the edge of the region of outer communication. This boundary is called the *event horizon*.

Unlike many popularly held intuitions of this boundary as some kind of "surface", the event horizon is not locally discernible from any ordinary vacuum region of space-time. In particular, an observer falling into the black hole will not experience passing through the event horizon as any special event. However, once this boundary is passed, any message the unfortunate infalling observer tries to send into the external universe will never reach its destination and will stay within the black hole. On the other hand, from the point of view of a second, external observer watching the infall from afar, the image of the infalling body will freeze upon reaching the horizon, and exponentially quickly dim and redden in the process.

However, the event horizon is not the only feature of a black hole, and key astrophysical observations come from interactions of matter and radiation with its gravitational field well

[1] In this dissertation and unless stated differently, I will consistently use geometrized $G = c = 1$ units, where G is Newton's gravitational constant, and c the speed of light. M as a length in geometrized units would be GM/c^2 in terms of SI units

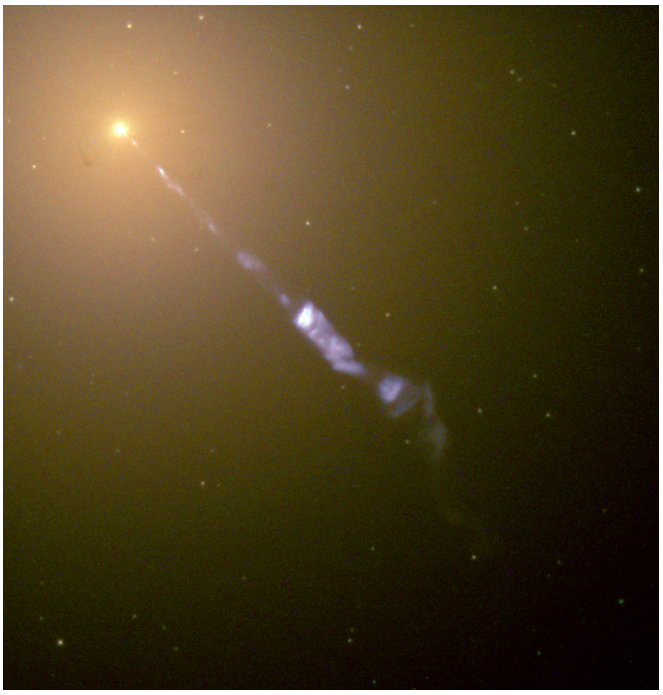

Fig. 1.1 A picture of a jet emerging from the galactic nucleus in the Messier 87 galaxy obtained by combining UV, blue, green, and IR light. The yellow color corresponds to light from stars, whereas the blueish-white color to synchrotron radiation coming from the jet. The jet is about 500 000 light-years ($\sim 150\,\mathrm{kpc}$) long and thus much larger than the host galaxy itself. Credit: NASA and The Hubble Heritage Team.

above it. Before we can discuss such issues, we need to examine the black hole field in more detail. Furthermore, we need to identify the astrophysical contexts where black holes appear. I will start with the latter in the upcoming section, and then work my way to the former in the rest of the sections of this chapter.

1.1 Black holes in space

Astrophysical black holes are formed through different evolutionary channels which means that they are characterized by a vast range of mass scales and locations. The first black holes formed early after the last scattering of photons with ionized matter after the Big Bang. These black holes then acted as focal points of matter halos in the early universe and hierarchically merged to finally form the so-called *supermassive black holes* that we nowadays observe in centers of most galaxies (see [90] for a review). The masses of supermassive black holes are in the range $\sim 10^6 - 10^{10} M_\odot$, where $M_\odot = 2 \times 10^{30}\mathrm{kg}$ is the solar mass.

The presence of supermassive black holes in the core of a galaxy often leads to a high electromagnetic activity in a wide spectrum from radio to X-ray, and the overall luminosity of such cores often outshines the galaxy by many orders of magnitude. Galactic cores of such overwhelming power are called Active galactic nuclei, commonly abbreviated as AGN, and their luminosity is assumed to be sourced by relativistic accretion of the surrounding matter onto the central black hole. A somewhat enigmatic feature of many AGN are powerful, and surprisingly collimated outflows of matter leaving the center at relativistic speeds – the so-called *relativistic jets* (see fig. 1.1).[2] In return, the radiation of the AGN and the jet act on the surrounding matter itself, and the galaxy tends to evolve with the AGN in a correlated manner [136].

Inactive galactic nuclei are also common, and specifically some of the supermassive black holes in our cosmic vicinity are inactive or of a low electromagnetic activity. An important example of such an inactive galactic black hole is the one in the center of our galaxy, the Milky Way. It powers the compact radio source in the Sagittarius constellation known as Sgr A* by very slow accretion of matter [187].

The case of our galactic center is also important because individual stars orbiting it can be resolved in detail (this is not possible in the case of other galactic cores), and we can determine the central black hole mass from its gravitational influence on the orbits as $\approx 4 \times 10^6 M_\odot$ and the distance as[3] $\approx 8\,\mathrm{kpc}$ [100]. There are many more supermassive black holes with good mass estimates, but the case of the black hole in Sgr A* is the most watertight mass measurement for a supermassive black hole we have to date.

Another important class of black holes formed only later in cosmic history as remnants of burnt-out stars with mass at least $M \gtrsim 10M\odot$. When such a star goes through its entire evolution, gradually converting various elements in its interior by nuclear fusion and radiating the heat away, it will eventually run out of nuclear fuel and lack pressure in the core to support itself against gravitation. The violent process that ensues as the star consequently contracts and expands in one last explosion is called a core-collapse supernova. In some cases the leftover remnant is a neutron star and in others a black hole. It is currently not clear what is the exact critical mass of the progenitor of a given composition to form a black hole, but generally it seems that the mass of the progenitor star has to be $\gtrsim 25M_\odot$ for a a very good chance of black hole formation [114, 179].

The estimates of the masses of this population of black holes obtained from electromagnetic radiation is in the range $\sim 2-20M_\odot$ [264], and this is why they are called *stellar-mass black*

[2] *Relativistic* jets are jets emerging at relativistic speeds from accreting black holes. "Normal" jets emerge from a number of other astrophysical objects at non-relativistic speeds. These two classes of jets seem to have different launching mechanisms, and it is thus important to draw a distinction between them in nomenclature.

[3] A parsec (pc) is $\sim 3.1 \times 10^{16} m$ or 3.2 light-years, which puts Sgr A* about 26 thousand light-years away.

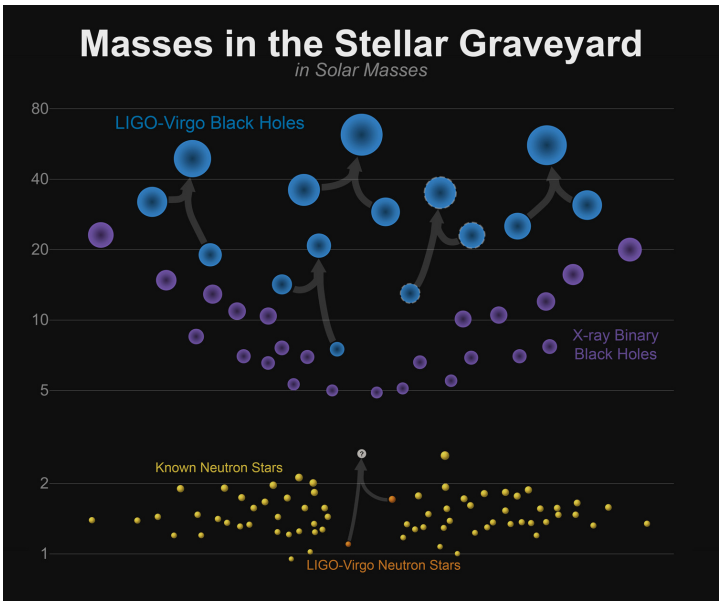

Fig. 1.2 A comparison of the masses of stellar-mass black holes and neutron stars as estimated from gravitational-wave observations with masses of black holes and neutron stars as estimated from orbital dynamics in X-ray binaries. The gray arrows indicate an observed merger. Credit: LIGO-Virgo/Frank Elavsky/Northwestern University

holes. They can be observed as parts of X-ray binaries, that is, binaries of black holes or neutron stars and main-sequence stars that produce strong radiation in the X-ray as well as other bands. The radiation in X-ray binaries comes from the black hole or neutron star accreting matter from the stellar companion.

The matter for the accretion is released either as a stellar wind when the secondary is a heavy $M_* \gtrsim 10M_\odot$ (O,B) star on an orbit of a similar size as that of Mercury in the Solar system ($\sim 10^9$ km), or as direct Roche-lobe overflow when the star is lighter, $M_* \lesssim 10M_\odot$ (spectral type A and higher), and on a tighter orbit.[4] These two types of X-ray binaries classified by the mass of the stellar companion are known as high-mass and low-mass X-ray binaries respectively, and it is this gross classification that tends to influence many of their spectral and variability properties [150]. X-ray binaries have a rich observational phenomenology, there are quasi-periodic oscillations appearing in their luminosity with curious properties [278], and the entire system tends to go through a cycle of states of varying luminosities and spectral characteristics [87].

[4] It is not that other combinations of orbital separations and companion types cannot exist. If a light star is on a wider orbit, it just does not release matter to fall on the black hole, and it is thus essentially impossible for us to identify its companion as a black hole. If a heavy star is on a tighter orbit around a black hole, it will get either stripped of its outer shells, or completely tidally disrupted, which would be classified as a different phenomenon than an X-ray binary. One last note is that X-ray binaries with companions in the range $\sim 1 - 10M_\odot$ are uncommon, this is likely also a consequence of evolutionary and selection effects [150].

Another important venue of observing black holes are gravitational waves. These emerge from binary systems if the orbit is so close that the binary components reach at least mildly relativistic speeds relative to each other. Consequently, only binaries made of compact objects such as neutron stars or black holes can produce appreciable amounts of gravitational waves before colliding or getting tidally disrupted. The gravitational waves then carry angular momentum and energy away from the system, the orbit slowly decays, and the two objects eventually collide and merge. The gradual decay of the orbit is called a *gravitational-wave inspiral*. After generations of work, the gravitational-wave community finally succeeded in detecting the inspiral of two black holes in 2015. This first detection was achieved by the LIGO Scientific collaboration [8], and since then a number of other observations were accomplished also in tandem with the European Virgo detector [8, 6, 7, 9, 11, 10, 5].

The $M \sim 10 - 80 M_\odot$ mass estimates obtained from the gravitational-wave observations could seem in tension with the electromagnetic estimates $2 - 20 M_\odot$ (see fig. 1.2). However, all the black-hole mass estimates from X-ray binaries come from binaries within our galaxy, whereas all of the gravitational-wave signals detected so far are extra-galactic binaries composed of two black holes. One of the likely explanations of the dichotomy between the two populations is the relatively high abundance of heavier elements (metallicity) in our galaxy, which leads to higher mass-loss during the lives of stars and lower masses of the consequent black hole remnants [161, 3].

Last but not least, there is an intriguing gap in the mass range $10^2 - 10^5 M_\odot$ in the observed black hole distribution. Naturally, understanding whether and in which numbers such intermediate-mass black holes exist should clarify the history of growth supermassive black holes. This is because they could be understood as a progenitor of a supermassive black hole, or its early-universe sibling that was "left behind" in terms of mass-accretion. There is currently circumstantial evidence that intermediate-mass black holes exist in the centers of some stellar clusters and dwarf galaxies (see [60, 134] for more possible locations).

Now that I have covered the basic spectrum of astrophysical black holes, let me proceed to the theoretical description of black hole fields.

1.2 The Kerr metric

For this section and for the rest of the dissertation in general, I assume that the reader is acquainted with the basics of General-relativity theory at least on the level of an introductory course (for textbooks, see e.g. [48, 283, 181]). Namely, I assume that the reader knows the Schwarzschild solution and its basic properties and that they are comfortable with terms such as the space-time metric $g_{\mu\nu}$, stress-energy tensor $T^{\mu\nu}$, four-velocity u^μ and others.

As for notation, I will use the geometric $G = c = 1$ units if not stated otherwise, and the $(-+++)$ signature of the metric. Einstein summation is assumed, and Greek letters $\mu, \nu, \kappa...$ as subscript or superscript indices run from 0 to 3 and signify coordinate components of a tensor. Partial derivatives are denoted by an index preceded by a coma, and covariant derivatives by an index preceded by a semi-colon.

The gravitational fields of astrophysical black holes that are not in the process of a gravitational-wave inspiral or merger are well approximated by the Kerr metric [129]. The Kerr metric with parameters M, a represents an uncharged, spinning, isolated, and stationary black hole of mass M and angular momentum $J = aM$. In Boyer Linquist coordinates $t \in \mathbb{R}, \varphi \in [0, 2\pi), r \in (0, \infty), \vartheta \in (0, \pi)$ the metric reads [43]

$$\begin{aligned} \mathrm{d}s^2 = &- \left(1 - \frac{2Mr}{\Sigma}\right) \mathrm{d}t^2 + \frac{\Sigma}{\Delta}\mathrm{d}r^2 + \Sigma \mathrm{d}\vartheta^2 + \sin^2\vartheta \left(r^2 + a^2 + \frac{2Mra^2\sin^2\vartheta}{\Sigma}\right) \mathrm{d}\varphi^2 \\ &- \frac{4Mra\sin^2\vartheta}{\Sigma} \mathrm{d}t\mathrm{d}\varphi\,, \end{aligned} \tag{1.1}$$

where $\Sigma \equiv r^2 + a^2\cos^2\vartheta$ and $\Delta \equiv r^2 - 2Mr + a^2$. The Kerr metric components are independent of φ, t, which makes $\xi^\mu = \delta^\mu_t$ and $\eta^\mu = \delta^\mu_\varphi$ its Killing vectors (see subsection 1.4.2 for more details). The discrete symmetries of the Kerr metric are the reflection $\vartheta \to \pi - \vartheta$, and the time-rotation reversals, which are obtained by combining any two of the following three transforms $a \to -a$, $t \to -t$, and $\varphi \to 2\pi - \varphi$. One last geometric property of the Kerr metric which is often called a "hidden symmetry" is the existence of Killing and Killing-Yano tensors; this property is discussed in section 1.4.

The metric has coordinate singularities at $\Delta = 0$, which are the positions of the event horizons of the black hole. The outermost event horizon is placed at $r_\mathrm{H} = M + \sqrt{M^2 - a^2}$; the structure of the metric at smaller radii is not important for astrophysical purposes because no observer in the external universe will receive any information from that region. Other physically relevant radii are discussed in the upcoming sections.

The horizons vanish whenever $a^2 > M^2$ and the space-time then contains a naked ring singularity. These so-called "over-extremal" Kerr space-times are generally conjectured as unreachable by physical processes. The limit $a^2 \to M^2$ is called the extremal black hole, and the spin $a = \pm M$ is called the maximal spin; this limit is often used in idealized mathematical computations because it conveniently simplifies many problems.

There are many more properties of the Kerr metric that can be discussed in great detail, and for that and references to previous literature I refer the reader to the books of Griffiths and Podolský [102] and Stephani et al. [254].

The inverse metric can be computed using the fact that it has a 2×2 matrix in the $t - \varphi$ sector, and otherwise it is diagonal. The inverse metric coefficients then read

$$g^{rr} = \frac{1}{g_{rr}}, \; g^{\vartheta\vartheta} = \frac{1}{g_{\vartheta\vartheta}}, \tag{1.2}$$

$$g^{tt} = -\frac{g_{\varphi\varphi}}{\rho^2}, \; g^{\varphi\varphi} = -\frac{g_{tt}}{\rho^2}, \tag{1.3}$$

$$g^{t\varphi} = \frac{g_{t\varphi}}{\rho^2}, \tag{1.4}$$

where $\rho^2 \equiv (g_{t\varphi})^2 - g_{tt}g_{\varphi\varphi} = \Delta \sin^2\vartheta$ is minus the determinant of the $t - \varphi$ part of the metric. I write these general formulas for inversion here because they apply generally to any stationary and axisymmetric metric in a quasi-diagonal form. For the Kerr metric we obtain explicitly

$$g^{rr} = \frac{\Delta}{\Sigma}, \; g^{\vartheta\vartheta} = \frac{1}{\Sigma}, \tag{1.5}$$

$$g^{tt} = -\frac{(r^2+a^2)^2 - a^2\Delta\sin^2\vartheta}{\Delta\Sigma}, \; g^{\varphi\varphi} = \frac{\Delta - a^2\sin^2\vartheta}{\Delta\Sigma\sin^2\vartheta}, \tag{1.6}$$

$$g^{t\varphi} = -\frac{2Mra}{\Delta\Sigma}. \tag{1.7}$$

1.3 Dragging effects

The geometry in Einstein equations couples to the whole stress-energy tensor $T^{\mu\nu}$. In particular, in the frame of coordinate observers, the stress-energy tensor has the mass-energy density T^{00}, the *fluxes* of mass-energy T^{0i}, and the internal stresses T^{ij}. Hence, if an object has matter currents in loops that can be characterized by a total angular momentum J, it should leave specific imprints in the surrounding gravitational field. One such effect is *frame dragging*, which, informally stated, is the "forcing" of nearby matter to co-rotate with the body purely by gravitational effects. This results, for instance, in the precession of the orbital plane of particles near such rotating objects, as was historically found by Thirring [267, 268] and Lense and Thirring [148].

The analogy of such effects to the forces an electric current exerts on nearby charged particles also leads to the term *gravitomagnetism* for frame dragging.[5] I will now discuss these effects in the Kerr space-time and generally any stationary and axisymmetric space-time.

[5] In fact, gravitoelectric and gravitomagnetic effects are not sufficient to characterize gravity. Another set of effects that has no analogy in electromagnetism would be called "topogravitic", and they can be identified, e.g., by the Bel decomposition [28].

1.3.1 Zero angular momentum observers

Let us assume a stationary axisymmetric space-time and coordinates where the metric attains a quasi-diagonal form similar to (1.1). Now let us place a set of observers into this space-time whose covariant four-velocity u_μ has the only non-zero component u_t. In particular, the specific angular momentum of the particle u_φ is zero, so we call this family zero-angular-momentum observers (ZAMOs). Then we have

$$u_t = -\frac{1}{\sqrt{-g^{tt}}}\,. \tag{1.8}$$

However, after raising the index to obtain the physical (contravariant) four-velocity $u^\mu \equiv \mathrm{d}x^\mu/\mathrm{d}\tau$, we obtain the non-zero components

$$u^t = \sqrt{-g^{tt}}\,,\; u^\varphi = -\frac{g^{t\varphi}}{\sqrt{-g^{tt}}}\,. \tag{1.9}$$

Specifically, these observers will appear to move with an angular frequency $\omega = u^\varphi/u^t = g^{t\varphi}/g^{tt} = -g_{t\varphi}/g_{\varphi\varphi}$ with respect to coordinate time t.

In the Kerr metric the coordinate time t is the time measured by the set of observers at spatial infinity that are asymptotically inertial and see the black hole as non-moving ("static observers"). These static observers will see the ZAMOs rotating with the frequency ω. This frequency is thus also often called the *dragging frequency*.

1.3.2 Possible circular motions and the ergosphere

Let us use the same assumptions about the space-time as in the last subsection and investigate the general circular orbit with non-zero four-velocity components u^t, u^φ. Let us furthermore define the angular frequency of these orbits as measured by static observers $\Omega \equiv \mathrm{d}\varphi/\mathrm{d}t = u^\varphi/u^t$. Then we obtain from the normalization of four-velocity $u^\mu u_\mu = -1$

$$u^t = \frac{1}{\sqrt{g_{tt} + 2g_{t\varphi}\Omega + g_{\varphi\varphi}\Omega^2}}\,. \tag{1.10}$$

When u^t becomes imaginary, it means that there is no physical observer (or massive particle) that can move at the given angular frequency Ω at that point. This occurs for the two frequencies Ω_+, Ω_- given as

$$\Omega_\pm = \omega \pm \sqrt{\omega^2 - \frac{g_{tt}}{g_{\varphi\varphi}}}\,. \tag{1.11}$$

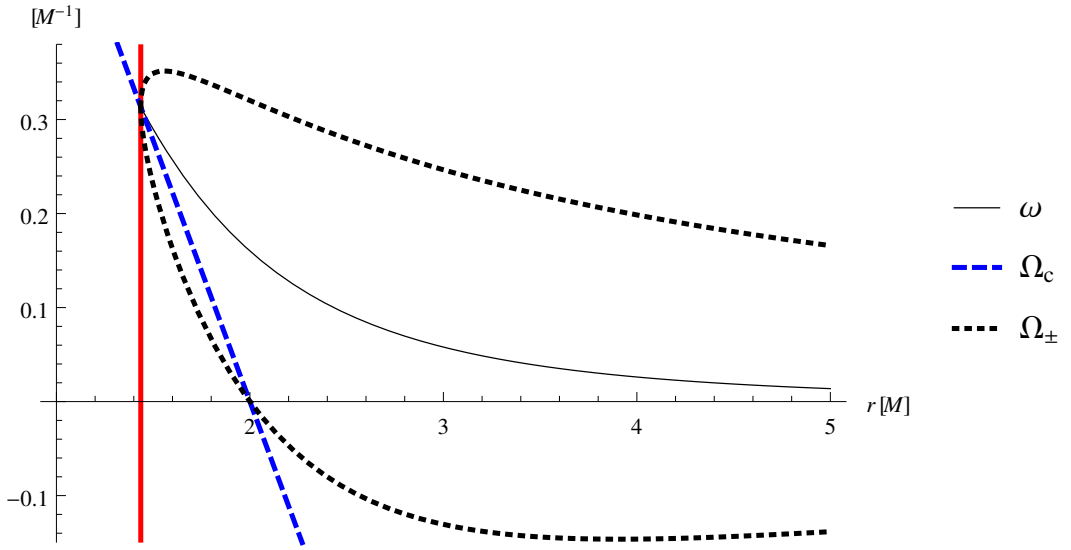

Fig. 1.3 The range of possible angular rotation frequencies of massive test particles near a Kerr black holes delineated by $\Omega_{\pm}$ along with the angular rotation frequency of ZAMO observers ω. The particles underneath the curve $\Omega_{\rm c} = -g_{t\varphi}/g_{tt}$ have negative energy with respect to infinity and allow for energy extraction. The plot is in the equatorial plane ($\vartheta = \pi/2$) and the spin parameter is taken as $a = 0.9M$.

I plotted the maximal and minimal possible angular frequencies $\Omega_{\pm}$ along with the dragging frequency ω in the equatorial plane $\vartheta = \pi/2$ of the Kerr space-time as function of radius in fig. 1.3. We can see in this figure that an important effect happens at the radius $r = 2M$; the lowest possible frequency of motion Ω_{-} crosses zero and all time-like orbits will thus necessarily be rotating with some non-zero angular frequency at smaller radii. The spatial region where this phenomenon occurs is called the *ergosphere* and is given by the condition $g_{tt} > 0$. In Boyer-Lindquist coordinates, the surface of the ergosphere is found at the radii

$$r_{\rm E} = M + \sqrt{M^2 - a^2\cos^2\vartheta}\,. \tag{1.12}$$

We can see that the ergosphere, for $a \neq 0$, is above the horizon in the equatorial plane and touches it at the poles $\vartheta = 0, \pi$. It may seem that the metric is degenerate on the surface of the ergosphere because $g_{tt} = 0$, but this is not necessarily true; the metric becomes degenerate only when the $t - \varphi$ determinant $\rho^2 = \Delta\sin^2\vartheta$ becomes zero. An important property of the ergosphere in the Kerr space-time is that there are physical particles inside it that have negative specific energy, $-u_t < 0$. This happens under the condition

$$\Omega < -\frac{g_{tt}}{g_{t\varphi}}\,. \tag{1.13}$$

A closer comparison with $\Omega_\pm$ shows that this condition can be fulfilled by physical particles only within the ergosphere. The region of negative energy orbits is also shown in fig. 1.3.

Another feature that we observe in fig. 1.3 is that as we approach the horizon, all the frequencies $\omega, \Omega_+, \Omega_-$ meet at a value that is called the horizon rotation frequency, which reads

$$\Omega_{\rm H} = \frac{a}{2M(M+\sqrt{M^2-a^2})}\,. \tag{1.14}$$

Even though the horizon frequency is "only" the frequency of circular photon orbits on the horizon, it is also often loosely considered to be the angular frequency at which the horizon itself is rotating. This viewpoint comes from Newtonian analogies based on observations of the behavior of various matter fields near the horizon, and it is notably summarized by the so-called Membrane paradigm [159, 270, 160, 271].

1.3.3 Penrose, Blandford, Znajek, and energy extraction

The ergosphere causes the particles to co-rotate with the black hole and it is interesting to ask whether this effect can be exploited by some physical process to extract rotational energy from the black hole field. This would have obvious counterparts in other branches of physics, where matter can approach a heavy rotating object, get spun through friction or some other coupling with its surface, and leave with additional kinetic energy. Of course, the question is what should the "surface" and the "friction" be in the case of black holes.

The first example of a mechanism extracting energy from black holes was considered by Penrose [209]. In Penrose's example, a particle is falling into the spinning black hole, decays into two smaller particles inside the ergosphere and one particle escapes while the other falls into the black hole. The total energy balance in the ergosphere is then allowed to be such that the escaping particle has a larger energy than the original particle coming from infinity, and the particle infalling into the black hole has negative energy. In other words, energy was extracted from the black hole.

Various other energy-extraction mechanisms including continuum processes have been considered since, and the general pattern is very much the same as in the Penrose process: One can extract energy from the black hole if a non-linear (momentum-exchanging) process occurs in the ergosphere (see Ref. [146] for details). Going back to the analogy with rotating objects discussed in the beginning of this subsection, the "surface" that needs to be made contact with is the ergosphere (*not* the horizon), and the "friction" is momentum transfer.

Furthermore, Christodoulou [57] showed that it is impossible to reduce the mass-energy of the black hole beyond a certain irreducible mass $M_{\rm ir}$ by such mechanisms, the formula for

which reads

$$M_{\rm ir}^2 = \frac{1}{2}M^2\left(1+\sqrt{1-\frac{a^2}{M^2}}\right). \tag{1.15}$$

In particular, we see that if the black hole has the maximal spin $a = M$, the maximal energy one can extract through a Penrose process is about 29% of the original black hole mass.

In the context of black-hole astrophysics, a prominent version of such a process was proposed by Blandford and Znajek [40] (see also Ruffini and Wilson [224]), and I will now discuss it because of its somewhat controversial role in black hole astrophysics (see [135] for a clear historical review and further references).

In the original version of the Blandford-Znajek (BZ) mechanism, the vacuum near the black hole was assumed to break down due to the presence of very strong magnetic fields supported by external currents. Specifically, the estimate was that the magnetic fields need to be

$$B \gtrsim 20\left(\frac{a}{M}\right)^{3/4}\frac{M}{M_\odot}\mathrm{T}, \tag{1.16}$$

where $M_\odot$ is the solar mass and T is the unit of magnetic field strength Tesla. When such magnetic fields are imposed near the black hole horizon, a positron-electron cascade occurs and the coupled system of the electromagnetic field and the thin, but highly conductive electron-positron medium form a specific dynamical system. Within certain bounds of applicability, the particles can be assumed to quickly react to Lorentz forces on the bulk of the plasma, and rearrange so that the Lorentz forces are essentially immediately canceled. The resulting idealized system is called force-free electrodynamics.

The salient feature of force-free electrodynamics is that, unlike in vacuum electrodynamics, its solutions do not need to be non-stationary or non-axisymmetric (with $\mathrm{e}^{im\varphi}$ and $\mathrm{e}^{i\kappa t}$ factors) in order to carry angular momentum and energy away from the black hole. This is because angular momentum and energy can be implicitly carried by the charged particles supporting the field, or they can be transferred through the magnetic field lines being anchored in a passive sink such as an external accretion disk. Blandford & Znajek were then able to show that the force-free electrodynamics has solutions with Poynting fluxes of electromagnetic energy pointing out of the Kerr black hole horizon. In other words, they found astrophysical means of extracting energy from rotating black holes.

However, even though magnetic fields of sufficient strengths to create a positron-electron cascade are not thought to be uncommon near black holes, it is often misunderstood what is the real significance of the positron-electron plasma in the BZ process. The BZ process as we talk about it here, and as the majority of the astrophysics community does, is the mechanism in

which energy is extracted from the rotation of the black hole by a force-free magnetosphere. The *medium* that supports this magnetosphere can be either the ordinary proton-electron plasma provided by the surrounding accretion disk, or the positron-electron plasma from the broken vacuum – or a mix of both. Then, the energy extracted from the black hole can either enter into a nearby accretion disk through a closed field-line (a line anchored in the disk), or it can escape to infinity as a wind *of either positron-electron or proton-electron composition* traveling along an open field line. Since lines near the equator will be terminated in the disk and open field lines will occur mostly along the rotation axes, the BZ process naturally gives rise to a polar outflow of plasma – a relativistic jet.

On the other hand, this should be contrasted with the proposal of Blandford and Payne [39] that the energy for jets is provided simply by the kinetic and potential energy of the accretion disk near the black hole. There, the medium supporting the outflow is naturally the proton-electron plasma of the accretion disk and none of the power of the jet comes from the black hole spin. However, these jets are *non-relativistic*, their gamma factor is $\gamma \lesssim 2$. They can be launched from black holes even at zero spin [229], and they will emerge even from obviously non-relativistic sources such as young stellar objects [14].

Let us now return to relativistic jets. Numerical simulations of accretion disks have shown that the mechanism of launching relativistic jets from black holes is most probably of the BZ type (with no need for a positron-electron cascade). Magneto-hydrodynamics simulations show that Poynting fluxes are often positive through some parts of the horizon, and in special cases rotational energy is indubitably extracted from the black hole [168]. Furthermore, the structure of the magnetic fields near the rotation axes of the black hole generically exhibit the same qualitative structure as the "split magnetic monopole" field that is the basis of the argumentation of Blandford & Znajek. Last but not least, the BZ formula for jet power $P_{\rm jet} \propto a^2$ holds, at least for small spins [167, 261] and there are some indications that this correlation also holds observationally for the so-called ballistic jets emerging from accreting stellar-mass black holes [188, 249] (see, however, the challenge of these results in [225] and the response in [165]).

For higher spins, the $P_{\rm jet} \propto a^2$ law receives higher-order corrections and becomes largely sensitive on the disk geometry, becoming particularly steep for geometrically thick disks [167, 261]. This is the basis of the proposal of Tchekhovskoy et al. [261] that the observed distinction between the so-called radio-loud and radio-quiet active galactic nuclei is due to differences in the spin parameter of their central black holes. Another ingredient in this proposal is the existence of the so-called magnetically-arrested disks that arise when the black hole is allowed to accumulate large amount of magnetic flux in the accretion process (see subsection 2.2.5 for more details).

In these states, the accretion disk is pushed back by magnetic pressure and allowed to drip only small inflows into the black hole. Additionally, there is a massive outflow that can, for near-extremal spins, return *more* mass-energy than was in the inflow [262]. In other words, the magnetically regulated mass inflow mediates a pure energy extraction from the black hole, and this energy output is carried by a jet. This idea was, in fact, motivated by a series of previous observations suggesting jets that carry a mass-energy outflow comparable *or larger* than the matter-inflow estimate [221, 97, 219, 89, 172], and this disproportion was later also confirmed in recent observational studies of active galactic nuclei [98, 195].

In summary, it seems that observations *force* us to consider Penrose-like processes in modeling jet formation rather than *allowing* us to speculate about them, and the current models give rise to the extraction of rotational energy of the black hole through the dynamics of strongly magnetized matter. The development of this field might become particularly exciting due to the fact that the IceCube collaboration very recently recorded a cosmic neutrino arriving from the direction of a temporarily flaring galactic jet, thus promising a new era of multimessenger study of these enigmatic ouflows [1, 2].

1.4 Geodesics near spinning black holes

It can be argued that the nature of a given solution to the Einstein equations has not been understood until one has studied the structure of its geodesics, the orbits of free structureless test particles steered only by the gravitational field. This is equally true for the Kerr space-time. Let us consider the Lagrangian of a time-like geodesic parametrized by proper time τ

$$\mathscr{L} = \frac{1}{2} m g_{\mu\nu}(x^\kappa)\dot{x}^\mu \dot{x}^\nu \,, \tag{1.17}$$

where $\dot{x}^\mu \equiv u^\mu \equiv \mathrm{d}x^\mu/\mathrm{d}\tau$. This Lagrangian corresponds to four space-time degrees of freedom x^μ and it thus requires four integrals of motion in involution to be fully integrated. One such integral is the four-velocity normalization $u^\mu u_\mu = -1$, and another two correspond to the symmetry of the Kerr metric with respect to translations in coordinate time t and φ-rotations. The corresponding integrals of motion are

$$-E = \frac{\partial L}{\partial \dot{t}} = m g_{t\nu}\dot{x}^\nu = m u_t \,, \tag{1.18}$$

$$L = \frac{\partial L}{\partial \dot{\varphi}} = m g_{\varphi\nu}\dot{x}^\nu = m u_\varphi \,, \tag{1.19}$$

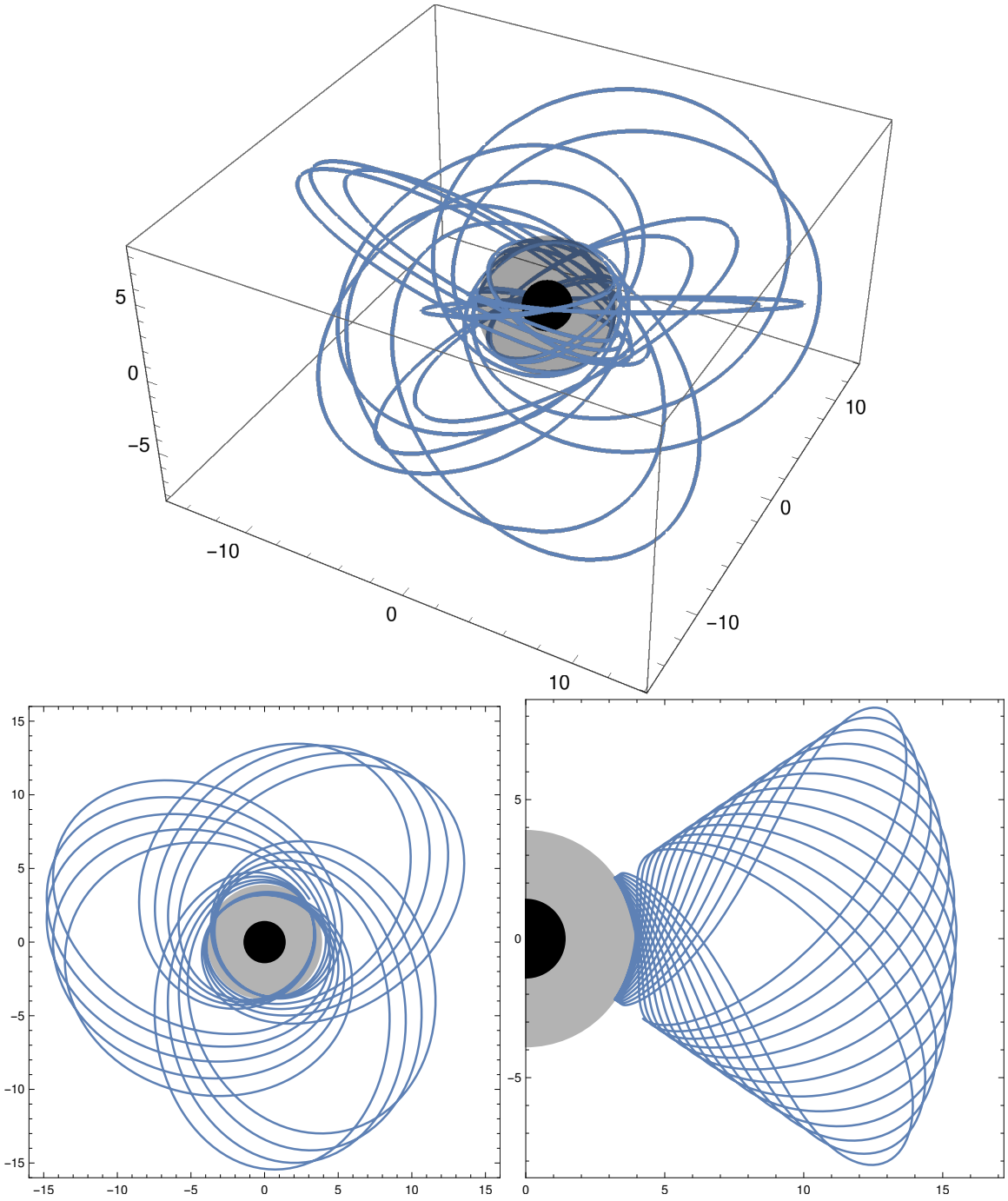

Fig. 1.4 Three visualizations of a generic geodesic near a Kerr black hole with spin $a = 0.9M$. The first two images are representations of the orbit with Boyer-Lindquist coordinates r, ϑ, φ identified with spherical coordinates in flat space, first at a general and the second at a "bird view" angle. The third image is a projection of the orbit into the $r\sin\vartheta, r\cos\vartheta$ plane. The axes are in units of M, and the gray and black circle are the photon sphere and horizon respectively. We see that the orbital plane of this particular geodesic shifts by almost a third of a full angle with every pericenter passage, and that the photon sphere plays the role of an ultimate limit for non-plunging particles. The orbit was computed with the help of the KerrGeodesics Mathematica package [286].

where we define the total energy (that includes an additional m rest mass contribution) so that it is positive.

Nevertheless, there are no other obvious integrals of motion of this Lagrangian. By counting the degrees of freedom, we see that geodesic motion in axisymmetric and stationary fields is not globally integrable and will have parts of phase space that are chaotic. This is in fact the *generic* case, as can be demonstrated by numerous examples in static and axisymmetric space-times [240, 241, 256, 292].

Nevertheless, the Kerr space-time is remarkable in the fact that the geodesics equation is fully integrable in its field. I will show this via the separability of the Hamilton-Jacobi equation as was done by Carter [49]. Then I will discuss the so-called "hidden symmetry" behind this integrability, and also the astrophysically important sub-class of circular geodesics in the equatorial plane. One particular issue that I will not discuss in detail are null geodesics and lensing effects, for that purpose I refer the readers to [211], [101] or [56].

1.4.1 Separability of Hamilton-Jacobi equation

The Hamiltonian for a geodesic obtained by a Legendre transform from (1.17) reads

$$H = \frac{1}{2m} g^{\mu\nu} p_\mu p_\nu \,, \tag{1.20}$$

where $p_\mu = m u_\mu$ is canonically conjugate to x^μ. The on-shell value of the Hamiltonian is $-m/2$ for all massive particles due to the four-velocity normalization. The respective Hamilton-Jacobi equation for the action $S(\tau, x^\kappa)$ reads

$$\frac{\partial S}{\partial \tau} = \frac{1}{2m} g^{\mu\nu} S_{,\mu} S_{,\nu} \,. \tag{1.21}$$

We now assume the action to be separable in Boyer-Lindquist coordinates as $S = -m\tau/2 - Et + L\varphi + S_r(r) + S_\vartheta(\vartheta)$ and the resulting equations separate as

$$\begin{aligned} (S'_\vartheta)^2 + \left(\frac{L}{\sin\vartheta} - aE\sin\vartheta \right)^2 - m^2 a^2 \cos^2\vartheta = \\ -\Delta (S'_r)^2 + \frac{1}{\Delta}\left((r^2+a^2)E - aL \right)^2 - m^2 r^2 \,. \end{aligned} \tag{1.22}$$

Now, the left-hand side of equation (1.22) is only a function of ϑ and the right-hand side only a function of r. This suggests, that both sides must be equal to a constant K independent of r

and ϑ and we obtain the r and ϑ parts of the action as one-dimensional indefinite integrals

$$S_r = \pm \int \frac{1}{\Delta} \sqrt{\left[(r^2+a^2)E - aL\right]^2 - \Delta(K + m^2 r^2)}\,\mathrm{d}r\,, \tag{1.23}$$

$$S_\vartheta = \pm \int \sqrt{K + m^2 a^2 \cos^2\vartheta - \left(\frac{L}{\sin\vartheta} - aE\sin\vartheta\right)^2}\,\mathrm{d}\vartheta\,, \tag{1.24}$$

where the signs of the integrals must be chosen according to the current sign of $\dot{r}, \dot{\vartheta}$ respectively.

More importantly, however, the separable solution of the Hamilton-Jacobi equation also leads to the complete separability of the geodesic equation in the form

$$\frac{\mathrm{d}r}{\mathrm{d}\lambda} = \pm\frac{1}{m}\sqrt{\left[(r^2+a^2)E - aL\right]^2 - \Delta(K + m^2 r^2)}\,, \tag{1.25}$$

$$\frac{\mathrm{d}\vartheta}{\mathrm{d}\lambda} = \pm\frac{1}{m}\sqrt{K + m^2 a^2 \cos^2\vartheta - \left(\frac{L}{\sin\vartheta} - aE\sin\vartheta\right)^2}\,, \tag{1.26}$$

$$\frac{\mathrm{d}\tau}{\mathrm{d}\lambda} = r^2 + a^2\cos^2\vartheta\,, \tag{1.27}$$

$$\frac{\mathrm{d}t}{\mathrm{d}\lambda} = \frac{1}{m}\left[\frac{r^2+a^2}{\Delta}\left[(r^2+a^2)E - aL\right] + a\sin\vartheta\left(\frac{L}{\sin\vartheta} - aE\sin\vartheta\right)\right]\,, \tag{1.28}$$

$$\frac{\mathrm{d}\varphi}{\mathrm{d}\lambda} = \frac{1}{m}\left[\frac{a}{\Delta}\left[(r^2+a^2)E - aL\right] + \frac{1}{\sin\vartheta}\left(\frac{L}{\sin\vartheta} - aE\sin\vartheta\right)\right]\,, \tag{1.29}$$

where a solution in terms of quadratures is obtained hierarchically first by solving for $r(\lambda), \vartheta(\lambda)$ and then for $\tau(\lambda), t(\lambda), \varphi(\lambda)$. The parameter λ is called the Mino parameter [180] and the constant K the Carter constant [49].

A large number of other results on Kerr geodesics were summarized by Chandrasekhar [56] and O'Neill [203]. In particular, the full set of analytically computable properties of bound geodesics in Kerr space-time was given by Fujita and Hikida [95]. Another notable result are the analytical formulas for the large family of the so-called Plebański-Demianski black-hole space-times generalizing the Kerr black hole given by Hackmann and Lämmerzahl [106] (see therein for further references).

The interpretation of the Carter constant is elucidated by considering

$$K = p_\vartheta^2 + \left(\frac{L}{\sin\vartheta} - aE\sin\vartheta\right)^2 - m^2 a^2 \cos^2\vartheta\,. \tag{1.30}$$

Specifically in the case $a = 0$, the expression for the Carter constant is exactly the same as the Newtonian expression for angular momentum squared.

Any physical initial condition x^μ, p_ν will have an associated K, L, E and the corresponding geodesic can be given by the formal solutions above.

It should be noted that many of our intuitions about orbits in gravitational fields as obtained from studying e.g. the Newtonian two-body problem or even geodesics in Schwarzschild space-time are broken in the Kerr field. Orbits in the Kerr field are generically non-planar (apart from equatorial orbits), they generically never close, and the observational signal coming from them will be triperiodic with generally incommensurate periods in the r, ϑ, φ degrees of freedom (see [78] for examples). An illustration of this fact is given in Figure 1.4.

1.4.2 The hidden symmetry

A metric symmetry such as axisymmetry or stationarity can be expressed without reference to any set of coordinates by the fact that there exists a vector field ξ^μ such that

$$\mathscr{L}_\xi g_{\mu\nu} = \xi_{\mu;\nu} + \xi_{\nu;\mu} = 0\,, \tag{1.31}$$

where $\mathscr{L}_\xi$ is a Lie derivative with respect to ξ, a well-defined derivative that compares the values of a tensor along the flow of ξ^μ (see e.g. [115]). The vector field ξ^μ is then called a Killing vector field and the equation $\xi_{(\mu;\nu)} = 0$ the Killing equation. It is then easy to show that $\xi_\mu u^\mu$ is an integral of geodesic motion.

In the case of axisymmetry and stationarity expressed in terms of translations with respect to coordinates t and φ, the Killing vector fields are $\xi^\mu_{(\varphi)} = \delta^\mu_\varphi, \xi^\mu_{(t)} = \delta^\mu_t$, the Killing equations reduce to the criterion that $g_{\mu\nu,\varphi} = 0, g_{\mu\nu,t} = 0$, and the associated integrals of geodesic motion are simply $u_t = -E/m, u_\varphi = L/m$. This provides a link between Killing vectors and the discussion in the beginning of this section.

However, let us consider the following: what kind of condition would be fulfilled by a symmetric tensor $K^{\mu\nu}$ such that $K_{\mu\nu}u^\mu u^\nu$, a *quadratic* function of velocity, is an integral of geodesic motion? By direct computation we get

$$\frac{\mathrm{d}}{\mathrm{d}\tau}(K_{\mu\nu}u^\mu u^\nu) = K_{\mu\nu;\kappa}u^\mu u^\nu u^\kappa + 2K_{\mu\nu}a^\mu u^\nu\,. \tag{1.32}$$

The four-acceleration a^μ vanishes for geodesics, so we only need the first term to vanish. If we want the term to vanish for any choice of u^μ, the gradient $K_{\mu\nu;\kappa}$ must reduce to zero under any such symmetric contraction and we thus obtain

$$K_{(\mu\nu;\kappa)_{\text{cycl.}}} \equiv K_{\mu\nu;\kappa} + K_{\kappa\mu;\nu} + K_{\nu\kappa;\mu} = 0\,. \tag{1.33}$$

The equation (1.33) could be considered as a generalized Killing equation and the tensor fulfilling such a conditions is called a Killing or Stäckel-Killing tensor [246]. I will use the term Stäckel-Killing tensor to make it more distinct from the Killing-Yano tensor to be introduced later.

The expression (1.30) essentially gives the form of the Stäckel-Killing tensor in Kerr space-time since it is quadratic in momenta/velocities (the velocity-independent term must be multiplied by $-g_{\mu\nu}u^\mu u^\mu$ to be assimilated into an expression of the form $K_{\mu\nu}u^\mu u^\nu$). The Killing tensor in Kerr space-time was first investigated by Walker and Penrose [284], and the mechanism by which an integral of motion $K_{\mu\nu}u^\mu u^\nu$ appears as a separation constant in the geodesic Hamilton-Jacobi equation was given by Woodhouse [294].

Let us now investigate another question. Suppose that we want to know under which conditions there is a tensor $\tilde{Y}_{\mu\nu}$ such that $\tilde{L}_\mu \equiv \tilde{Y}_{\mu\nu}u^\nu$ is parallel-transported along geodesics. We obtain

$$\frac{\mathrm{D}}{\mathrm{d}\tau}(\tilde{Y}_{\mu\nu}u^\nu) = \tilde{Y}_{\mu\nu;\kappa}u^\nu u^\kappa + \tilde{Y}_{\mu\nu}a^\nu\,. \tag{1.34}$$

The second term vanishes automatically and the first term vanishes when $\tilde{Y}_{\mu\nu;\kappa} + \tilde{Y}_{\mu\kappa;\nu} = 0$. Now, one of the defining properties of parallel transport is that the product of two parallel-transported vectors does not change. Thus, the tensor defines *two* new integrals of motion $\tilde{L}^\kappa\tilde{L}_\kappa = \tilde{Y}_{\mu\kappa}\tilde{Y}^\kappa_\nu u^\mu u^\nu$ and $u^\kappa\tilde{L}_\kappa = \tilde{Y}_{\mu\nu}u^\mu u^\nu$.

In other words, the symmetric part $\tilde{Y}_{(\mu\nu)}$ is a Stäckel-Killing tensor, and the square $\tilde{Y}_{\mu\kappa}\tilde{Y}^\kappa_\nu$ is a Stäckel-Killing tensor as well. I will call a tensor with such properties a *generalized Killing-Yano tensor*. If we want the generalized Killing-Yano tensor to generate only a single Stäckel-Killing tensor in this way, we have to require that it is either a "partially null" product of the form $\tilde{Y}_{\mu\nu} = l_\mu n_\nu$, $l^\mu l_\mu = 0$, or totally antisymmetric, $\tilde{Y}_{(\mu\nu)} = 0$. Antisymmetric tensors $Y_{(\mu\nu)} = 0$ with likewise antisymmetric gradients $Y_{\mu(\nu;\kappa)} = 0$ are called *Killing-Yano tensors*.

Let us now consider whether a generalized Killing-Yano tensor could exist in Kerr space-time. There is already a sufficient number of integrals of motion in Kerr space-time if we already have a single Stäckel-Killing tensor, and we know that the motion is non-degenerate. One of the two Stäckel-Killing tensors $\tilde{Y}_{(\mu\nu)}, \tilde{Y}_{\mu\kappa}\tilde{Y}^\kappa_\nu$ must thus generate a dependent constant of motion or it must be in the restricted forms given above. It was shown by Floyd [91] (and reported by Penrose [210]) that there is a (non-generalized) Killing-Yano tensor in Kerr space-time whose components are compactly expressed as

$$Y_{\mu\nu}\mathrm{d}x^\mu \wedge \mathrm{d}x^\nu = a\cos\vartheta\,\mathrm{d}r \wedge (\mathrm{d}t - a\sin^2\vartheta\,\mathrm{d}\varphi) + r\sin\vartheta\,\mathrm{d}\vartheta \wedge ((r^2+a^2)\mathrm{d}\varphi - a\mathrm{d}t)\,, \tag{1.35}$$

where $\wedge$ stands for the antisymmetric tensor product. We see that this tensor is independent of the parameter M and it thus indicates a background, gravity-independent structure of the Kerr space-time. Apart from the separability of the geodesic equations, all fundamental wave equations for free quantum particles with half-integer and integer spin are also separable [50, 265, 266, 277, 205, 55, 127] and this can be also linked to the existence of the Stäckel-Killing and Killing-Yano tensors [51, 52, 272, 126]. This vast range of miraculous results in the Kerr geometry is dubbed its "hidden symmetry".

A particular family of the generalized Killing-Yano tensors is given as

$$\tilde{Y}_{\mu\nu} = \alpha g_{\mu\nu} + \beta Y_{\mu\nu}\,, \tag{1.36}$$

where α, β are some constants. The Stäckel-Killing tensor $\tilde{Y}_{(\mu\nu)}$ is just the metric and the associated integral of motion is proportional to four-velocity normalization,. Then, $\tilde{Y}_{\mu\kappa}\tilde{Y}^{\kappa}_{\nu}$ will give the various forms of the non-trivial Killing tensor as they appear in the literature. Quite satisfyingly, the "basic" Killing tensor obtained by the square at $\alpha = 0$ corresponds to an integral of motion identical to the separation constant (1.30).

There is a huge body of other fascinating and deep mathematical results on the hidden symmetry and integrability, especially when the number of space-time dimensions is higher than 4. For details of these topics, I refer the reader to the exhaustive reviews given in the PhD thesis of Kubizňák [138], and by Frolov et al. [94].

1.4.3 Circular orbits

Circular orbits in the equatorial plane represent a family of nested trajectories that do not intersect and have only a stationary shear amongst themselves. Indeed, the dragging effects of the Kerr black hole lead to a torque that forces any bound geodesic to oscillate around the equatorial plane and its average ϑ position will always be $\pi/2$. Hence, circular orbits in the equatorial plane of the Kerr space-time play an important role in a number of astrophysical settings.

Let us consider the solution of the Hamilton-Jacobi equation discussed in subsection 1.4.1 and set $\vartheta = \pi/2$ along with the requirement $p_\vartheta = S'_\vartheta = 0$. From that we obtain $K = (L - aE)^2$. The set of geodesics fulfilling $K = (L - aE)^2$ are thus bound to the equator and oscillating between a radial pericenter and apocenter. For the orbit to be circular, we have to also require $p_r = S'_r = 0$ to obtain

$$0 = \left[(r^2 + a^2)E - aL\right]^2 - \Delta\left[(L - aE)^2 + m^2 r^2\right]\,. \tag{1.37}$$

This expression boils down to a cubic equation of the form

$$0 = (E^2 - m^2)r^3 + 2Mm^2r^2 - \left[L^2 - a^2(E^2 - m^2)\right] r + 2M(L - aE)^2 \,. \tag{1.38}$$

However, this equation will generally have three roots, two physical and one unphysical. The two physical roots corresponds to the turning points (pericentra and apocentra) of the non-circular orbits mentioned above. If we want to obtain a circular orbit, we must require that the cubic equation above has a double root (the pericenter is at the same point as the apocenter), which leads to [25, 56]

$$E_{\rm c}(r) = m\frac{r^{3/2} - 2Mr^{1/2} \pm aM^{1/2}}{\sqrt{r^3 - 3Mr^2 \pm 2aM^{1/2}r^{3/2}}} \,, \tag{1.39}$$

$$L_{\rm c}(r) = m\frac{\pm M^{1/2}(r^2 \mp 2aM^{1/2}r^{1/2} + a^2)}{\sqrt{r^3 - 3Mr^2 \pm 2aM^{1/2}r^{3/2}}} \,, \tag{1.40}$$

where the upper sign will always refer to the co-rotating circular orbits and the lower sign to the counter-rotating circular orbits.

For astrophysical purposes, it is also useful to express the orbital angular frequency as recorded by observers at infinity $\Omega = {\rm d}\varphi/{\rm d}t$, which reduces to the impressively simple form

$$\Omega_{\rm c}(r) = \frac{\pm M^{1/2}}{r^{3/2} \pm aM^{1/2}} \,. \tag{1.41}$$

Formulas for the small oscillations of the circular orbits about their equilibria (epicyclic frequencies) can be found in [25].

I will only note that unlike in the case of a non-rotating black hole, the frequency of the "vertical" oscillation around the equatorial plane does *not* match the orbital frequency Ω when $a \neq 0$. This can be intuitively understood from the fact that, unlike in the Schwarzschild case, the orbital plane of any non-equatorial particle is precessing due to frame dragging, and the frequency of this precession is proportional exactly to the difference between the orbital and vertical-oscillation frequency.

Let us now list some special circular orbits and discuss their meaning (see also [13])

$$r_{\rm ph} = 2M\left[1+\cos\left(\arccos\frac{a}{M}\right)\right], \tag{1.42}$$

$$r_{\rm mb} = 2M - a + 2M\sqrt{M-a}, \tag{1.43}$$

$$r_{\rm ms} = 3M + Z_2 - \sqrt{(3M-Z_1)(3M+Z_1+2Z_2)}, \tag{1.44}$$

$$Z_1 = M + (M-a^2)^{1/3}\left[(M+a)^{1/3}+(M-a)^{1/3}\right], \tag{1.45}$$

$$Z_2 = \sqrt{3a^2+Z_1^2}. \tag{1.46}$$

The radius $r_{\rm ph}$ is the radius where both the energy and angular momentum distributions (1.39) and (1.40) diverge. Consequently, only photons (massless particles) can move on such a circular orbit. This exact radius is also important away form the equatorial plane, it defines the so-called photon sphere where (marginally stable) light-rays keep orbiting for an infinite time. Additionally, the photon sphere plays an important role in distinguishing light-rays that escape to infinity from those plunging in the black hole, and is thus the key element in computing the black hole shadow [211, 101].

Next, the radius $r_{\rm mb}$ is the point at which the circular geodesic has energy $E = m$. Since $E = m$ is also the energy of particles at rest at infinity, this circular orbit will start spiraling out to infinity upon a small perturbation directed outwards from the black hole. On the other hand, if we have non-relativistic particles approaching from infinity ($E \approx m$), they can be captured by the black hole only if they have angular momentum $L < L_{\rm mb} \equiv L(r_{\rm mb})$.

Last but not least, the marginally stable orbit at $r_{\rm ms}$ is at the location of the minimum of the energy and angular momentum distributions, $\mathrm{d}E_{\rm c}/\mathrm{d}r = \mathrm{d}L_{\rm c}/\mathrm{d}r = 0$. Also, it is the divisor between stable and unstable circular orbits. The stable orbits at $r > r_{\rm ms}$ will oscillate around their original position upon small perturbation, whereas the unstable orbits, located at $r < r_{\rm ms}$, will start to either spiral out into a highly eccentric orbit or start plunging into the black hole. The marginally stable orbit is also often called the innermost stable circular orbit (ISCO).

To further illustrate the significance of the marginally stable orbit, consider a particle that is adiabatically loosing energy and angular momentum, which forces it to very slowly descend towards the black hole through almost circular orbits. Any loss of angular momentum and energy at any $r > r_{\rm ms}$ can be compensated by the particle descending on a slightly lower orbit. However, once $r_{\rm ms}$ and thus also the minimum of energy and angular momentum is reached, there is nowhere to descend in the space of circular orbits and the particle suddenly switches to a rapid plunge into the black hole. This is why the ISCO is important not only in accretion disk physics but also, for instance, in gravitational-wave inspirals.

Table 1.1 A list of orbital parameters of circular orbits. The quantities are given in terms of the central mass M. They can be converted into SI units by considering $[M]_{L\mathrm{SI}} = 4.4 \times 10^{11}(M/M_\odot)\mathrm{m}^2\mathrm{s}^{-1}$, $[M]_{r\mathrm{SI}} = 1.5 \times 10^3(M/M_\odot)\mathrm{m}$, $[M]_{t\mathrm{SI}} = 4.9 \times 10^{-6}(M/M_\odot)\mathrm{s}$, where $M_\odot$ is the solar mass.

Orbit	$L/m[M]$	$E/m-1$	$r[M]$	$\Omega[M^{-1}]$
$a=0$ Marg. stable	3.5	-5.7%	6	6.8×10^{-2}
$a=0$ Marg. bound	4	0%	4	1.2×10^{-1}
$a=1$ Marg. stable	1.2	-42%	1	5×10^{-1}
$a=1$ Marg. bound	2	0%	1	5×10^{-1}
Earth vs. Sun	1.0×10^4	-3.7×10^{-10}	1.0×10^8	1.6×10^{-13}

Let me finish this subsection by listing a few important radii, orbital energies, and angular momenta and frequencies in Table 1.1. This provides a basic orientation in the orbital scales of the black hole problem.

1.4.4 Non-geodesic corrections to the motion

Free test structureless particles will move on geodesics in a given space-time. However, this is certainly not exactly true for the motion of real bodies. Real bodies have a finite size, and they back-react on the gravitational field itself. In principle, this would mean that we should evolve the whole continuum of the object orbiting the black hole along with the full set of dynamical Einstein equations, and the analysis given so far in this section would be rendered essentially irrelevant. Fortunately enough, there is a formalism that allows us to approximate the motion of real physical bodies as particle-like motion, and the geodesic motion is the "zeroth-order" approximation in that sense. In the upcoming paragraphs, I briefly discuss how higher-order corrections in this scheme can be in principle obtained.

It turns out that in relativity the problems of sourcing gravity and the equations of motion are coupled. This is because the non-linear Einstein equations *automatically* require that the source fulfills equations of motion given by the conservation of the stress-energy tensor $T^{\mu\nu}{}_{;\nu} = 0$. Hence, both the problem of gravitational back-reaction and finite-size corrections have to be, in some sense, considered at the same time.

In linear field theories such as classical electrodynamics, a source of non-zero density ρ within a region of finite extent viewed from the outside can be mathematically replaced by a singular distribution at a single point x_0^μ. This new singular source could be called a "multipolar particle" and it is defined so that it carries the same set of multipolar moments as the original finite source. Specifically, when the source is spherically symmetric, its external field will be the same as the field of a monopole, "structureless" source, and it can be treated as such in

many computations. A small charge asymmetry between two halves of the source will then lead to an electric dipole, and overall current loops to a *magnetic* dipole. With an increasing number of such multipoles included in our computations, we are able to describe the external field of the body with increasing accuracy.

An interesting question is whether and how this can be extended to general relativity, which is endowed with strong non-linearity. The problem turns out to be rather complex, but direct analogies of the multipolar particle from linear field theories were successfully found and investigated notably by Mathisson [164], Papapetrou [208], and Dixon [74]. In that case, a matter source in the form of a continuous stress-energy tensor $T^{\mu\nu}(x^\kappa)$ is replaced by a distributional tensor concentrated around some representative $x_0^\mu(\tau)$. Then, following the conservation of stress-energy $T^{\mu\nu}_{\ \ ;\nu} = 0$, the so-called Mathisson-Papapetrou-Dixon equations for the motion of the representative particle are uniquely derived (see also [251]).

These multipolar equations carry the information about the finite size of the body along a single particle-like world-line, and by taking a sufficient number of multipoles into account, we get a good approximation of the finite-size effects on the motion. Nevertheless, the gravitational back-reaction does not necessarily simplify with this singular replacement. This is because the singular source carries a singular gravitational perturbation, and that becomes troublesome in the non-linear theory. Fortunately, it turns out that there is a procedure, well-defined to at least second perturbative order, that allows to compute the gravitational perturbation and identify the effective nonsingular metric in which the representative particle is moving (see [216]).

A context in which these techniques become strongly relevant are the slow gravitational-wave inspirals of neutron stars or stellar-mass black holes into supermassive black holes. In that case, both the gravitational back-reaction of the small, stellar-mass objects and the finite-size effects on the orbit are small enough so that a perturbative description of the kind described above is appropriate (see [213, 23] for reviews). In contrast, a full numerical simulation of the Einstein equations would have difficulties to maintain the desired accuracy for the entire lengthy inspiral, and post-Newtonian methods (expansions in $v \ll 1$, where v is the velocity of the orbiting object) would struggle with the large eccentricities and general orientations of the rotation axes of the bodies.

The first and most important correction entering into such inspirals due to the finite size of the bodies is the effect of the "gravitomagnetic dipole", or the so-called spin-curvature coupling. This is an exclusively relativistic effect that occurs due to a gravitomagnetic interaction of a rotating body with its gravitational background. There are many technical issues to be considered when introducing the spin-curvature coupling (see [63]), but one particularly simple

form of the resulting equations of motion reads [143]

$$\frac{\mathrm{D}^2 x_0^\mu}{\mathrm{d}\tau} = -\frac{1}{2m} R^\mu{}_{\nu\kappa\lambda} \dot{x}_0^\nu S^{\kappa\lambda} \,, \tag{1.47}$$

$$\frac{\mathrm{D}S^{\kappa\lambda}}{\mathrm{d}\tau} = 0 \,, \tag{1.48}$$

where $R^\mu{}_{\nu\kappa\lambda}$ is the Riemann curvature tensor, $S^{\kappa\lambda}$ is the angular-momentum ("spin") tensor of the body, and $x_0^\mu(\tau)$ is the representative world-line of the "particle". $\mathrm{D}/\mathrm{d}\tau$ is the covariant time derivative along $x_0^\mu(\tau)$, and the Riemann curvature tensor is also evaluated along $x_0^\mu(\tau)$.

This spin-curvature term in the equations of motion of bodies near black holes, along with the gravitational self-force corrections, lead to equations of motion that are not analytically solvable and generally even chaotic [157]. On the other hand, gravitational-wave inspirals of the type mentioned above are expected to be detectable by the upcoming space-based detector LISA. Currently, considerable effort is being invested in developing efficient models that will meet the needs of the LISA detector [151]. These and related questions are discussed in detail in Chapter 3.

Chapter 2

Basic dynamics of black-hole accretion

In popular context, black holes are often depicted as the ultimate sinks, mercilessly sucking in anything in their surroundings. This, as we have partially seen already in the last section, is a mistaken intuition. Black holes behave as any Newtonian mass attracting with a simple M/r^2 force from afar, which leads to the absolutely same orbits of celestial bodies around them as for any other object – unless the angular momentum of the bodies is very low and the orbit reaches within a very small distance from the black hole (cf. Table 1.1).

Furthermore, the fact that the black holes are extremely compact suggests that they are even more disappointing accretors, since particles randomly occurring near the black hole end up interacting only with a very small effective cross-section. For comparison, the Sun sweeping through a field of matter would hit and potentially accrete everything within its radius of $\sim 10^5$km. On the other hand, a black hole of the same mass has an event horizon of at most the size of ~ 3 km and can thus be naively estimated to "hit" $\sim 10^9$ fewer particles as it sweeps through the same field of matter!

In this chapter, I will show that, in the end, black holes are not as disappointing accretors as these naive discussions might suggest. In fact, black-hole accretion leads to the most energetic stationary sources of radiation in the Universe. I get to this conclusion step by step, by considering various physics that enter the accretion process. Readers who are interested in this topic beyond the brief overview in this chapter are referred to the textbook of Frank et al. [92], or to the technical summaries of Abramowicz and Fragile [13] and Yuan and Narayan [296].

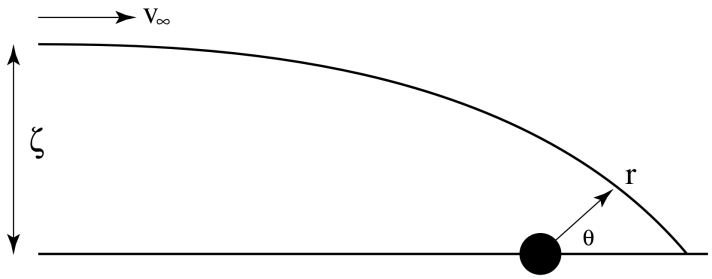

Fig. 2.1 Sketch of stream deflection in Hoyle-Lyttleton accretion. The streams crossing behind the black hole will average their momenta and form a new stream that can sometimes be accreted. Taken from [80].

2.1 Bondi, Hoyle, Lyttleton, and Eddington: gathering mass from afar

2.1.1 Sweeping through a field of dust

Let us make the estimate of the accretion by a black hole flying through some dilute matter field more precise by following the historical model of Hoyle and Lyttleton [119] (see [80] for a review). Let us assume that the black hole is non-spinning, $a = 0$, and moving through a field with density ρ_∞ at non-relativistic speed v_∞. The ∞ subscripts signify that these quantities are actually defined asymptotically far away from the black hole, because the local fields will, of course, be modified by the presence of the gravitating source.

Now, we can compute the amount of directly accreted matter by noticing that the angular momentum is given by $L = m\zeta_\infty v_\infty$, where ζ_∞ is the asymptotic impact parameter of the matter element. Since v_∞ is non-relativistic, we have $E/m \approx 1$ and we see that the black hole will directly accrete all matter with an impact parameter smaller than $\zeta_{\rm mb} = L_{\rm mb}/(mv_\infty)$, where $L_{\rm mb}$ is the angular momentum of the marginally bound orbit fulfilling $L_{\rm mb}/m = 4M$ for non-spinning black holes. The "direct" accretion rate can thus be given as

$$\dot{M}_{\rm direct} = \pi\zeta_{\rm mb}^2\rho_\infty v_\infty = \frac{16\pi M^2\rho_\infty}{v_\infty}\,. \tag{2.1}$$

However, Hoyle and Lyttleton [119] argued that as the gravitating mass deflects matter, it will induce stream crossings behind the black hole that will quickly average out their momentum by collisions so that a new coherent stream emerges (see fig. 2.1).

Then, a part of these reprocessed streams will have too little velocity to escape the black hole and will fall back as part of an almost purely radial accretion flow from behind the black hole. The Newtonian analysis yields that by this process all elements with an impact parameter

smaller than $\zeta_{\rm HL} = 2M/v_\infty^2$ will be accreted, and the Hoyle-Lyttleton accretion rate is

$$\dot{M}_{\rm HL} = \frac{4\pi M^2 \rho_\infty}{v_\infty^3}\,. \tag{2.2}$$

For non-relativistic v_∞, the Hoyle-Lyttleton impact parameter and accretion rate will be of many orders of magnitude larger than the "direct" accretion estimate we come to when ignoring inter-particle collisions. Relativistic corrections will be important when the velocity v_∞ becomes so small that $\zeta_{\rm HL} \sim \zeta_{\rm mb}$. However, in realistic situations other effects will always dominate the relativistic contribution, as we are about to discuss.

2.1.2 Regulating inflow by a pressure barrier

As the black hole slows down to $v_\infty \to 0$, both the direct and Hoyle-Lyttleon accretion rates diverge. This lead Bondi [42] to set $v_\infty = 0$ but to also ask about the influence of pressure, which was neglected in the previous analysis. To illustrate this point in a relativistic setting, consider the accretion of dust of some non-zero ρ_∞ onto a non-spinning black hole.

This field is completely spherically symmetric and so will be the inflow, angular momentum is zero, and the specific energy $E/m = -u_t = 1$ is conserved during the infall. From four-velocity normalization $u^\mu u_\mu = -1$ in the Schwarzschild metric we then obtain

$$u^r = -\sqrt{\frac{2M}{r}}\,. \tag{2.3}$$

On the other hand, if we impose the matter conservation equation $(\rho u^\mu)_{;\mu} = 0$ along with stationarity, we get

$$\dot{M} = 4\pi r^2 \rho u^r = 4\pi\sqrt{2M} r^{3/2}\rho = \text{const.} \tag{2.4}$$

Obviously, if we have ρ_∞ nonzero, then ρ at any finite radius as well as $\dot{M}$ diverge.

However, as the matter starts accelerating towards the black hole in a real physical situation, it starts increasing in density, and eventually builds up a large pressure. This pressure build-up (and specifically the pressure gradient) acts as a barrier against the gravitational acceleration, essentially halts the fluid from proceeding to the black hole, and cures the density divergence by allowing the velocity to only have a $\dot{M}/(4\pi\rho_\infty r^2)$ tail.

On the other hand, once the matter passes through a so-called *sonic point* at a critical radius $r_{\rm s} = 2M/v_{\rm s\infty}^2$, it is clear of the pressure barrier and starts essentially free-streaming into the black hole. One could then write the accretion rate formula as $\dot{M}_{\rm B} \approx 4\pi\sqrt{2M} r_{\rm s}^{3/2}\rho(r_{\rm s})$. However, in terms of asymptotic quantities and for a monatomic ideal gas at non-relativistic

temperatures it can be written as

$$\dot{M}_{\rm B} = \frac{4\pi M^2 \rho_\infty}{v_{\rm s\infty}^3}\,, \tag{2.5}$$

where $v_{\rm s\infty}$ is the sound speed of the gas at infinity.

The treatment of Bondi [42] was only Newtonian, but an analogous computation by Michel [173] in the Schwarzschild space-time yields the same result as long as $v_{\rm s\infty}$ is non-relativistic (which is a very fair astrophysical assumption). By a number of ad-hoc arguments and examples, it can be shown [274, 80] that an approximate formula for the Bondi-Hoyle-Lyttleton accretion of a black hole moving through a pressurized medium reads

$$\dot{M}_{\rm BHL} \approx \frac{4\pi M^2 \rho_\infty}{(v_\infty^2 + v_{\rm s\infty}^2)^{3/2}}\,. \tag{2.6}$$

Formulas such as (2.5) and (2.6) are one of ingredients in estimating accretion rates onto galactic black holes from their galactic enviroment. The sonic-point radius $r_{\rm s} = 2M/v_{\rm s\infty}^2$ is also called the *Bondi radius*, and it serves as a criterion for the resolution in cosmological numerical simulations; if the grid has several points within $r_{\rm s}$, it will simulate the regulation of the accretion by the sonic barrier on its own, but if not, it will overestimate the accretion, and one must instead switch to the Bondi-Hoyle-Lyttleton formula (2.6) to model the sub-grid physics (e.g., [72]).

2.1.3 Blowing gas away by radiation

Nevertheless, the formula (2.6) does not yet include all the important effects that play a role in the accretion process. This is because in the process of accretion, the gas will heat up and radiate. This can, in principle, enhance the accretion because it drains internal energy from the gas and thus also the pressure. However, the effect of opposite nature that will be typically more important is the fact that the escaping radiation will exert a pressure on the infalling particles. This radiation pressure accelerates the exposed matter element as

$$a^\mu = \frac{1}{h}\kappa f^\mu\,, \tag{2.7}$$

where f^μ is the radiation energy flux, κ is the opacity of the material affected, and $h = 1 + \mathcal{O}(k_{\rm B}T/m)$ is the enthalpy per unit rest mass ($k_{\rm B}$ is the Boltzmann constant). I assume non-relativistic temperatures so that $h \approx 1$.

For a spherically symmetric source of radiation, the radial flux will be $f^r = \lambda(r)/(4\pi r^2)$, where $\lambda(r)$ is the total luminosity leaving through r. If, in the far field, we neglect the absorption

of the luminosity by the medium, we have $\lambda(r) \to \lambda_\infty = \text{const.}$, and we see that the matter is subject to the total acceleration

$$\frac{\mathrm{d}^2 r}{\mathrm{d}t^2} = \frac{1}{r^2}\left(\frac{\kappa\lambda_\infty}{4\pi} - M\right) = -\frac{M}{r^2}\left(1 - \frac{\lambda_\infty}{\lambda_\mathrm{E}}\right), \tag{2.8}$$

$$\lambda_\mathrm{E} \equiv \frac{4\pi M}{\kappa}. \tag{2.9}$$

The luminosity λ_E at which the acceleration changes sign is called the *Eddington luminosity* or the *Eddington limit*. We see that when the far-field luminosity of a source is below the Eddington luminosity, then accretion of matter is possible. On the other hand, sources radiating above Eddington luminosity will, at least in spherically symmetric situations, blow away far-away gas and stop the matter supply for accretion.

We can now use the far-field behavior (2.8) to build a rough estimate of an equilibrium accretion rate of a compact body at rest in a large, asymptotically homogeneous cloud of matter. We can assume that the escaping luminosity is some fixed fraction of the mass-energy accreted on the center in the form of gas $\lambda_\infty = \eta\dot{M}$, where η is called the *efficiency* of the accretion process. Now, we also see that, at least in the far field, the "effective attracting mass" is $M(1 - \lambda_\infty/\lambda_E)$. We assume that this far-field mass will also play the role of the mass in the Bondi formula (2.5) up to a dimensionless factor $\gamma \sim 1$, which is set to be constant for now. Then, we obtain the model

$$\dot{M} = \frac{4\pi\gamma\rho_\infty M^2}{v_{\mathrm{s}\infty}^3}\left(1 - \frac{\eta\dot{M}}{\lambda_\mathrm{E}}\right)^2. \tag{2.10}$$

The point is, of course, that this model is essentially just a parametrization if we allow η, γ to be functions of other variables such as $\dot{M}, \rho_\infty, v_{\mathrm{s}\infty}$ or κ. However, one expects $\gamma \approx 1$ if $\lambda(r) \approx \lambda_\infty$ throughout the flow. Of course, this is true only if most radiation is deposited very close to the black hole and the effects of absorption and radiation in the rest of the matter approximately cancel out. On the other hand, the independence of η on other conditions will be fulfilled only in a special "dust-geometric" limit, where the radiated energy per particles is only dependent on the geometry of the flow near the black hole and not, in particular, on any of its internal properties such as density or temperature.

Let us now invert (2.10) for $\dot{M}$, we obtain

$$\dot{M}_\mathrm{eq} = \frac{\lambda_\mathrm{E}\left[8\pi\eta\gamma\rho_\infty M^2 + \lambda_\mathrm{E} v_{\mathrm{s}\infty}^3 - \sqrt{\lambda_\mathrm{E} v_{\mathrm{s}\infty}^3 (16\pi\eta\gamma\rho_\infty M^2 + \lambda_\mathrm{E} v_{\mathrm{s}\infty}^3)}\right]}{8\pi\eta^2\gamma\rho_\infty M^2}. \tag{2.11}$$

This is a rather unwieldy expression, but I show it because it has an elegant limit as $v_{s\infty} \to 0$

$$\lim_{v_{s\infty}\to 0} \dot{M}_{\rm eq} \equiv \dot{M}_{\rm E} = \frac{\lambda_{\rm E}}{\eta}. \tag{2.12}$$

The accretion rate $\dot{M}_{\rm E}$ is often called the *Eddington accretion rate* because it is the rate at which the source radiates at exactly the Eddington limit. Since the typical accreted media are rather cold and dilute, and since the model above already makes a number of other approximation, models of galactic black hole growth often take $\dot{M}_{\rm E}$ as their estimate for cosmological evolution along with $\eta \sim 10\%$ obtained from the standard accretion disk model (see subsection 2.2.1).

Nonetheless, such models of growth apply only if their two foundational assumptions hold: that γ and η are universal constants. In the $v_{s\infty} \to 0$ limit, the dependence on γ will be unimportant as long as η and γ are non-zero. On the other hand, the variations in η will be crucial in deriving the limit $v_{s\infty} \to 0$.

Specifically, as will be discussed in section 2.2.3, the efficiency of the radiation process generally drops when $\dot{M} \ll 10\lambda_{\rm E}$, as well as when $\dot{M} \gtrsim 10\lambda_{\rm E}$. In the specific case of low supplies of gas and very small accretion rates $\dot{M} \ll 10\lambda_{\rm E}$, the Eddington luminosity is by far not reached, the limit $v_{s\infty} \to 0$ is not physically valid, and one resorts to the Bondi formula (2.5). In the case of high gas supply and thus $\dot{M} \gtrsim 10\lambda_{\rm E}$, the Eddington luminosity is approximately reached, and the formula $\dot{M} = \lambda_{\rm E}/\eta(\dot{M})$ approximately holds. However, since $\eta = \eta(\dot{M}) < \eta_{\rm Standard}$, this can possibly lead to *much* higher accretion rates than the standard estimates.

Nonetheless, the "hardest" case is the intermediate $\dot{M} \lesssim 10\lambda_{\rm E}$ which corresponds to radiation at some significant fraction of the Eddington luminosity that is, however, not too close to unity. In that case models such as (2.11) must be used to estimate the accretion rate.

2.1.4 The issue of high redshift gigants

Thus, if one uses the Eddington accretion rate (2.12) along with a constant efficiency $\eta \sim 10\%$, this is by no means consistent. But still, this is what some of the simplest models of cosmological black hole growth do. I have included this discussion because exactly these simple growth models come into problems when faced with observations of "too massive" black holes from the early universe (see e.g. [243, 70] and references therein, and [281] for a brief review).

This is because if we assume the efficiency to be simply constant, then the logarithmic time derivative of the black hole mass is at most $\dot{M}_{\rm E}/M = 4\pi/(\eta\kappa)$ and the mass e-folding time is at least $\tau_{\rm e} = \eta\kappa/(4\pi) \sim 4.5 \times 10^7$ years, where I inserted the opacity of fully ionized hydrogen and $\eta = 10\%$. When we compare this with the fact that some of the supermassive black holes

at redshifts $z \gtrsim 6$ ($\lesssim 10^9$ years after the Big Bang) have mass estimates as high as $M \sim 10^9 M_\odot$, and in some recent shocking examples even $\sim 10^{10} M_\odot$ [295, 269], then we extrapolate the black hole masses to a value M_0 in the interval $10^4 M_\odot \lesssim M_0 \lesssim 10^7 M_\odot$ early in the reionization era. This is at odds with the usual picture in ΛCDM cosmology, where structure formation starts hierarchically from the matter fractured into very small dark matter halos that grow larger only later through mergers; the estimated mass of such early halos constrains the mechanisms by which such massive black hole seeds can form [124].

There are many proposals to resolve this issue, including special scenarios in which such a direct formation of a seed black hole with mass $M_0 \gtrsim 10^5 M_\odot$ truly occurs in the early universe (see [147, 125] and references therein). Another proposal is, however, that the seed masses of black holes are much smaller, and that there is a brief period of super-critical[1] accretion that accounts for their large mass growth [281, 88, 282, 122, 72]. Nevertheless, the early estimates of the $10^{10} M_\odot$ quasars [295, 269] are still challenging and they may be resolved as our observations penetrate deeper into the high-redshift sky. In the meantime, we should study the accretion process to the best of our knowledge and prepare accurate theoretical predictions to be tested in the future.

2.2 Spin up the matter: accretion disks

When the gas a has a small net angular momentum L with respect to the black hole, this will in principle not show in the far-field Bondi formula. This is because $L = mrv^\varphi$, where v^φ is the projection of linear (*not* angular) velocity into the azimuthal direction, and as we take $r \to \infty$ at L constant, we get $v_\varphi \to 0$. Another way to see this is that the centrifugal acceleration in the far field is L^2/r^3 and thus it is a sub-leading contribution to the far-field matter attraction.

On the other hand, as we have discussed in section 2.1, the radial velocity of the gas has to have a leading-order tail $v^r \sim \dot{M}/(4\pi\rho_\infty r^2)$ implying an acceleration of the fluid elements with a tail

$$a^r_{\rm B} \sim \frac{\dot{M}^2}{8\pi^2\rho_\infty^2 r^5}\,. \tag{2.13}$$

[1] Super-critical accretion is sometimes unfortunately coined as "super-Eddington" accretion, because it surpasses $\lambda_{\rm E}/\eta$ with a standard-disk value for η. Nevertheless, it should be understood that the Eddington luminosity is *not* generally breached by super-critical accretion.

The location at which $a^r_{\rm B} \sim L^2/r^3$ then reads

$$r = \frac{\dot{M}}{2\sqrt{2}\pi\rho_\infty L}\,. \tag{2.14}$$

The competition of the Bondi solution with the centrifugal effects will thus start very early on.

Nevertheless, if the angular momentum of the gas is $L < L_{\rm mb}$ and if it smoothly vanishes around the rotation axes, then by studying e.g. dust flows, one can see that the effects of angular momentum do not really influence the qualitative structure of the flow. To my knowledge, there are no analytical solutions of the angular-momentum-modified Bondi accretion, so I will now discuss the numerical results of perfect-fluid simulations by Proga and Begelman [217].

The numerical solutions of Proga & Begelman show that as long as $L < L_{\rm mb}$, the accretion rate will fulfill $\dot{M} \approx \dot{M}_{\rm B}$. Then again, whenever $L > L_{\rm mb}$, a particle infalling from infinity will never plunge into the black hole and this shows also in a hydrodynamical simulation; any matter with $L \gtrsim L_{\rm mb}$ will become a part of a thick disk essentially eternally orbiting the black hole. Then, this disk will block the path of other infalling elements and accretion will only be possible through a funnel along the rotation axes. The accretion rate can then be expressed as

$$\dot{M} \approx \dot{M}_{\rm B}\frac{\Omega_{\rm f}}{4\pi}\,, \tag{2.15}$$

where $\Omega_{\rm f}$ is the solid angle over which the funnel opens and $\dot{M}_{\rm B}$ is the Bondi accretion rate given in (2.5). Furthermore, in the case when most of the mass has $L \gg L_{\rm mb}$, then $\Omega_{\rm f}$ is approximated simply by integrated over the range of angles around the poles at which the matter coming from infinity has $L < L_{\rm mb}$.

Comparing these conclusions with typical angular momenta in astrophysical systems (see Table 1.1) would lead to a rather bleak bleak prospect for the Bondi formula and astrophysical accretion onto black holes in general. The total angular momentum in an isolated system will always stay constant, but there is one loophole. In principle, there can be a process that *passes* angular momentum from one fluid element to another, letting most of the matter accrete while a small fraction of the mass acquires high angular momentum and is pushed outside of the system. The central goal of the theory of accretion disks is to precisely capture and characterize such mechanisms.

In principle, if the matter carries a strong magnetic field whose energy density is larger than the binding-energy density $\sim \rho M/r$, then the anisotropic Maxwell stress $\sim\sim B_r B_\varphi$ could act exactly as the desired angular-momentum transport mechanism, and the accretion would become quasi-spherical again [34, 33]. However, the sign of B_r cannot be uniform throughout the flow, because otherwise magnetic monopoles would be implied, and the Maxwell torques

cannot be assumed to act in a consistent manner. It thus seems inevitable that we need to investigate specific, non-spherical geometries of the flow. The first such model I will discuss it the so-called thin disk.

2.2.1 The thin disk energy budget

When the streams with non-zero L in a Bondi-like inflow reach close to the black hole, they will eventually brake due to the centrifugal barrier and start orbiting the black hole, which will cause stream crossings. In the process of these crossings, the total angular momentum will be conserved, but the flow will eventually collapse into an almost circular motion restricted to a region close to a preferred plane that is aligned with its average angular momentum. In other words – a differentially rotating disk is formed.

Let us now estimate the height of such a disk under the assumption that the height itself is is not large. We choose a set of cylindrical coordinates R, z, φ so that R is the distance from the axis of rotation of the disk, φ the azimuthal angle aligned with the rotation axis, and $z = 0$ in the center of the disk. The z-component of the Euler equation under the assumption of negligible vertical velocities then reads

$$a^z = g^{z\mu}\frac{P_{,\mu}}{h\rho}\,, \tag{2.16}$$

where a^z is the four-acceleration $a^z = \ddot{z} + \Gamma^z_{\mu\nu}u^\mu u^\nu$, P is the pressure, h the enthalpy per unit mass, and ρ the rest mass density of the fluid. Let us now assume that the pressure is at a maximum $P_\mathrm{c}(r)$ in the center of the disk and that the disk is approximately axisymmetric. Then we can write $P(R,z) = P_\mathrm{c}(R)(1 - z^2/H(R)^2)$, where H is the height of the disk. Plugging this expression into (2.16) along with similar assumption for h and ρ and the requirement of a stationary near-circular flow, we obtain the height estimate

$$\sin\vartheta_\mathrm{d} \approx \frac{H(R)}{R} \approx \sqrt{\frac{2RP_\mathrm{c}}{Mh_\mathrm{c}\rho_\mathrm{c}(u^t_\mathrm{c})^2}}\,, \tag{2.17}$$

where I again assume a non-rotating black hole, the "c" subscript denotes quantities evaluated at the center of the disk and ϑ_d is the angle to which the disk subtends in spherical coordinates.

Now, $P/(h\rho)$ is proportional to the temperature of the gas T divided by particle mass m_p, and $M/(2R)$ is approximately the specific binding energy of the orbital element. We then see that the angular extent of the disk will scale as $\sqrt{T/T_\mathrm{v}}$ where $T_\mathrm{v} \equiv m_\mathrm{p}M/(2k_\mathrm{B}R)$ is the so-called *virial temperature*, the temperature at which the internal energy of the gas approximately

matches the binding energy. Consequently, we see that whenever disk height is $H/R \gtrsim 1$, the gas will be weakly bound to the black hole and this can in principle lead to strong outflows.

Let us, however, assume that the temperature of the gas is in fact much smaller than the virial temperature, and that the angular extent of the disk is thus small. This would be called a *thin disk* assumption, and we see that it is identical to the assumption that the disk is *cold*. Let me now pass to the "average" formalism as defined rigorously e.g. by Page and Thorne [206], where the disk is assumed to be almost perfectly axisymmetric, and all quantities are expressed in terms of quantities averaged over z and φ.

Let us also investigate what will the thin-disk assumption imply for the rotation profile. The radial Euler equation will have a $\sim M/R^2$ gravitational, L^2/R^3 centrifugal, and $P_{,R}/(h\rho)$ term. Assuming that the radial variability length-scale of $P(R)$ goes as R (in other words, $P(R)$ is a power-law $\sim 1/R^\alpha$ with $\alpha \sim \mathcal{O}(1)$), we see that the deviations of the angular momentum profile $L(R)$ from a Keplerian law $\sim \sqrt{Mr}$ (or the relativistic geodesic formula eq. (1.40)), will be also small whenever $T \ll T_\mathrm{v}$. In summary, a thin disk will also have a rotation curve close to geodesic, or in astrophysical parlance, the rotation profile of a thin disk will be *almost Keplerian*.

Then again, we see that this will work only up to the innermost stable circular orbit, because, as discussed in subsection 1.4.3, at smaller radii, the various small perturbations would cause the almost geodesic fluid elements to either plunge into the black hole or spiral out. In consequence, beyond the ISCO the disk must be either truncated, or thin-disk assumptions must be violated and the disk significantly pressure-supported – as it turns out, either can be the case in accretion disk models.

So the picture we have here so far is a thin structure eternally rotating around the center almost like a geodesic – something like Saturn's rings of rocks and ice, but in fact made of a thermalized continuum. Let us now assume that somehow there is a stationary flow of matter through the disk towards the center that, nevertheless, is so small that it only negligibly interferes with the almost circular rotation of the disk. By integrating the continuity equation $(\rho u^\mu)_{;\mu} = 0$ we come to the relation between the radial velocity and accretion rate (restricting for now to Schwarzschild space-time)

$$u^R = \frac{\dot{M}}{2\pi\Sigma(R)R}\,, \tag{2.18}$$

where Σ is the surface density of the disk (volume density integrated over the z-extent of the disk). If we want the radial flow velocity not to interfere with the Keplerian rotation profile, we require $u^r \ll 1$ and this will ultimately impose bounds on the range of accretion rates $\dot{M}$ for which our approximations are valid.

Now comes the central piece of the model – the actual mechanism by which the material transfers angular matter to outer layers. Before we do that, I would like to briefly comment on a slightly paradoxical feature of the result. By assuming a strictly stationary situation, independent of the nature of the angular-momentum transfer, there must be an infinite train of elements passing the angular momentum all the way to infinity. In the stationary accretion disk models, this has an even more dazzling property, that at every radius, every element is receiving angular momentum passed from a lower radius, adding some on top, and passing it along. As a result, the local flux of angular momentum per particle through a radius R will diverge as we approach infinity, even though this pathology will not be strictly visible in the solution itself. This can be ameliorated only by embedding the disk into a more complex, usually non-stationary solution.

Nevertheless, let us ignore this issue for the moment and postulate that angular momentum is transferred through some set of anisotropic stresses in the rest-frame of the fluid. This can be modeled as some sort of viscous coupling between the layers. In a stationary situation, the viscous stress energy tensor of a standard Newtonian fluid[2] is an addition on top the usual perfect-fluid tensor given as [145]

$$T_{\mu\nu}|_{\text{visc.}} = -\mu\sigma_{\mu\nu} - \zeta\Theta h_{\mu\nu}\,, \tag{2.19}$$

$$h_{\mu\nu} \equiv g_{\mu\nu} + u_\mu u_\nu\,, \tag{2.20}$$

$$\Theta \equiv u^{\mu}{}_{;\mu}\,, \tag{2.21}$$

$$\sigma_{\mu\nu} \equiv u_{(\kappa;\lambda)} h^{\kappa}{}_{\mu} h^{\lambda}{}_{\nu} - \frac{1}{3}\Theta h_{\mu\nu}\,, \tag{2.22}$$

where Θ the fluid expansion, $\sigma_{\mu\nu}$ the shearing rate inside the fluid, and μ, ζ are effective viscosity coefficients. The expansion Θ will be zero in the almost stationary and circularized flow, but the shearing rate has the components [237]

$$\sigma_{\mu\varphi} = \sigma_{\varphi\mu} = \frac{1}{2}(u^t)^3(g_{t\varphi}^2 - g_{tt}g_{\varphi\varphi})\partial_\mu\Omega\,, \tag{2.23}$$

$$\sigma_{\mu t} = \sigma_{t\mu} = -\Omega\sigma_{\mu\varphi}\,, \tag{2.24}$$

where $\Omega = \mathrm{d}\varphi/\mathrm{d}t$ is the angular frequency of the fluid and the second identity comes from the orthogonalization of the shear with respect to the four-velocity. An important point to consider is that once a rotation profile is assumed, the shearing rate is uniquely determined. For instance,

[2] "Newtonian fluid" does not mean in this particular context a "non-relativistic fluid" but rather, as is standard in fluid mechanics, a fluid that has a viscosity following exactly the linear laws stated in the text.

in Schwarzschild space-time the Keplerian profile yields

$$\sigma^R_\varphi(R,z=0) = -\frac{3\sqrt{M}(R-2M)^2}{4R(R-3M)^{3/2}}\,. \tag{2.25}$$

The quantities $T^R_\varphi|_{\text{visc.}} = -\mu\sigma^R_\varphi$ and $-T^R_t|_{\text{visc.}} = -\Omega\mu\sigma^R_\varphi$ can be shown to be the flux of angular momentum and energy through the $R=$ const. surface. We now see that for near-Keplerian rotation profiles the flux of energy and angular momentum will always go outwards. Transporting angular momentum outside is exactly what we wanted to do, but accretion is in fact an overall flux of mass-energy *inwards*. For that, we need to add the stress-energy tensor of the bulk[3] of the gas itself

$$T^{\mu\nu}|_{\text{bulk}} = \rho h u^\mu u^\nu + P g^{\mu\nu}\,. \tag{2.26}$$

However, in the case of the thin disk assumptions we obtain effectively $T^{\mu\nu}_{\text{bulk}} \approx \rho u^\mu u^\nu$. The fluxes of energy and angular momentum $-T^R_t|_{\text{bulk}} = -\rho u^R u_t$ and $T^R_\varphi|_{\text{bulk}} = \rho u^R u_\varphi$ can then be related due to four-velocity normalization (neglecting $u^r u_r$) as

$$-T^R_t|_{\text{bulk}} = \Omega T^R_\varphi|_{\text{bulk}} - \frac{\rho u^R}{u^t}\,. \tag{2.27}$$

In other words, there is an additional rest-mass contribution as compared to the relation $-T^R_t|_{\text{visc.}} = \Omega T^R_\varphi|_{\text{visc.}}$ that will allow a balance in which mass-energy flows in, while angular momentum is flowing out.

Now, the only thing left to consider is some sort of cooling of the gas of the disk. This is because the viscous processes will not only transfer orbital energy from element to element, but also heat the gas in its rest frame at a rate [145]

$$\frac{\delta Q}{\delta\tau} = \mu\sigma^{\mu\nu}\sigma_{\mu\nu}\,, \tag{2.28}$$

a rate that must be matched by radiative cooling if the disk is to stay thin.

The radiation can be modeled by a simple stress tensor

$$T^{\mu\nu}|_{\text{rad.}} = 2u^{(\mu} f^{\nu)}\,, \tag{2.29}$$

[3]The "bulk" stress energy tensor is defined as the part of the stress-energy tensor that is diagonal in the averaged frame of the particles of the gas. Nevertheless, the division into the viscous and the bulk parts (2.19) and (2.26) has a degree of conventionality to itself, as can be seen e.g. from the differences of the division as defined by Landau and Lifshitz [145] and Eckart [79]. In our case of small thermal motions the two definitions give the same results.

where $f^\mu, f^\mu u_\mu = 0$, is the radiation flux in the rest frame of the gas. This flux will provide not only a drain for the internal energy of the gas, but will also marginally carry away the orbital energy and angular momentum $-u_t, u_\varphi$. The last assumption that we make is that the flux of radiation is purely vertical, i.e. its only non-zero components will be f^z. This corresponds to the situation where in the co-rotating of the fluid, the radiation flux is purely space-like and it is *conventionally* identified only as the part leaving the disk. The time-like component can be absorbed into the internal energy density co-rotating with the fluid, and the radial direction transfers energy into other parts of the disk and can thus be absorbed into the matter-energy flux v^r.

Under these assumptions and approximations, the total evolution equations $T^{\mu\nu}{}_{;\nu} = 0$ and the mass-conservation $(\rho u^\mu)_{;\mu} = 0$ were solved by Novikov and Thorne [199] (see also the careful and general treatment of Page and Thorne [206]) to give an unambiguous expression for $T^r{}_\varphi|_{\text{visc.}}(R)$ and $f^z(R)$ that has to be necessarily fulfilled for the stationary balance to hold. The full relativistic expressions given e.g. in [206] are somewhat cumbersome, but let me at least give the Newtonian formulas that provide good qualitative and quantitative approximations[4] [242]

$$f^z = \frac{3}{8\pi}\dot{M}\frac{GM}{R^3}\left(1-\sqrt{\frac{R_{\text{ms}}}{R}}\right), \tag{2.30}$$

$$T^r{}_\varphi|_{\text{visc.}} = \frac{\dot{M}}{4\pi H}\left(1-\sqrt{\frac{R_{\text{ms}}}{R}}\right). \tag{2.31}$$

The overall luminosity of the disk then is $\lambda = \eta\dot{M}$, where the efficiency η is then simple the binding energy of the last stable orbit $\eta = 1 - E(R_{\text{ms}})/m$.

I have not discussed the effect of the spin of the black hole so far, but it suffices to say that as long as the overall angular momentum of the disk is aligned with the rotation axis of the black hole, then all of the qualitative statements above are also valid with generally small local corrections due to the deformation of the black hole field. However, the global efficiency will then be $\eta = 1 - E(R_{\text{ms}}(a), a)/m$. Specifically, this will make the radiative efficiency of the accretion process vary between 6% for a non-spinning black hole, and 42% for the extremally spinning case. There is no overly mysterious effect behind that; the spin just lets the Keplerian

[4] It is sometimes stated that this stress-radiation budget was first computed by Shakura and Sunyaev [242] in the Newtonian case and later generalized to relativity by Novikov and Thorne [199]. This is obviously not correct, as Shakura and Sunyaev cite the lectures of Novikov and Thorne in their paper. However, one thing Shakura & Sunyaev certainly deserve credit for, is the concrete model built from the α-prescription as discussed later in subsection 2.2.2.

disk move deeper into the gravitational well before it looses stability, and thus it has the chance to radiate more.

This and related effects is one of the only ways the spin is estimated from electromagnetic observations of black holes. Obviously, these are no deeply fundamental estimates, as they can all be easily thrown off by a disk that is allowed to extend to smaller radii by pressure support rather than the spin-deformed geometry.

2.2.2 Turbulent black box – the α parameter

However, let us return to the general discussion of the thin disk. We now see that if there is a mechanism which provides the necessary torques between the layers to establish a stationary accretion rate $\dot{M}$, and if radiation is so efficient that it will essentially immediately drain all the internal energy away from the disk, the luminous profile of the disk is uniquely determined by (2.30). However, the problem is that 1) we do not know if such torques are possible, and 2) what is the spectrum of the disk at every point. We thus do not know if such objects exist in nature and even if we did, we would not know how to recognize them by their overall spectrum.

Let us start with the discussion of the anisotropic stresses. The molecular viscosity is not sufficiently large to drive the accretion process in astrophysical situations of interest. However, the system of fluid equations we have discussed can be understood as a Reynolds-averaged model, that is, a time- and/or space-averaged form of the equations yielding a split into average velocities u^μ and turbulent fluctuations δu^μ. The term $T^{\mu\nu}|_{\text{visc.}}$ is then equal to the mean quadratic fluctuations $\langle \rho \delta u^\mu \delta u^\nu \rangle$ which, in return can be modeled by the Boussinesq eddy-viscosity hypothesis

$$\langle \rho \delta u^\mu \delta u^\nu \rangle = -\mu_\mathrm{t} \sigma^{\mu\nu} + \frac{2}{3} \kappa_\mathrm{t} h_{\mu\nu} \,, \tag{2.32}$$

where μ_t is a "turbulent dynamical viscosity" and κ_t the density of turbulent kinetic energy (see e.g. [214] for more details). The turbulent kinetic energy can be absorbed into the definition of the pressure of the fluid and is assumed to be small in the spirit of the thin-disk approximation. The term $\mu_\mathrm{t}\sigma^{\mu\nu}$, however, adds exactly the viscous-type interaction between the layers of the fluid we have discussed in subsection 2.2.1.

That is all nice, but how does one actually determine μ_t? By observing the dimensionality of the factors in equation (2.32), we see that we need μ_t to be consisted of a matter density, a typical velocity of the fluctuations v_t, and a length scale l, $\mu_\mathrm{t} \propto \rho v_\mathrm{t} l$. The length-scale l, in particular, is the typical size of the turbulent eddies. Shakura and Sunyaev [242] famously argued that the size of the eddies (assuming fully developed, approximately isotropic turbulence), will be of the order of magnitude of the height of the disk. Then, they argued, the turbulent velocities

cannot be supersonic, otherwise the perfect-fluid approximation is essentially broken and a new hot state of the fluid emerges where $v_t < v_s$. At low pressures we have $v_s \approx \sqrt{P/\rho}$ and we see from formula (2.17) that $H \propto v_s/\Omega$. Finally, we can then parametrize the turbulent viscosity as

$$\mu_t = \alpha \frac{\rho v_s^2}{\Omega} = \alpha \frac{P}{\Omega}, \tag{2.33}$$

where α is a free parameter that is generally non-constant and roughly between zero and one. For purposes of closure of the model and the ability to give predictions, one usually sets α as constant. We now see that the energy budget for the thin disk (2.31) dictates

$$\frac{\alpha P}{\Omega} \sigma^R_{\ \varphi} = T^r_{\ \varphi}|_{\text{visc.}} = \frac{\dot{M}}{4\pi H} \left(1 - \sqrt{\frac{R_{\text{ms}}}{R}} \right), \tag{2.34}$$

and that $P(R)$ is then explicitly expressible from this formula. Next, we assume state equations such as

$$P = P_{\text{gas}} + P_{\text{rad.}} = \frac{\rho k_{\text{B}} T}{m_{\text{p}}} + \frac{4}{3}\sigma T^4, \tag{2.35}$$

where σ is the Steffen-Boltzman constant and we assume that the radiation is in perfect thermal equilibrium with the gas in the disk (an optically thick disk). The radiation energy density is then $\varepsilon = \sigma T^4$ which, on the other hand, is related to an estimate of the flux leaving the surface of the disk as

$$\frac{4}{3}\frac{\varepsilon}{\kappa\Sigma} = f^z = \frac{3}{8\pi}\dot{M}\frac{GM}{R^3}\left(1 - \sqrt{\frac{R_{\text{ms}}}{R}} \right), \tag{2.36}$$

where κ is the effective opacity of the material that can in principle be temperature dependent. The solution of these equations will give us the complete set of quantities $T(R), \Sigma(R), u^r(R), H(R)$ and others, parametrized only by the constants $\dot{M}$ and α. Hence, a complete observational prediction for the appearance of the disk can be given[5]. The resulting set of formulas either in the Newtonian [242] or relativistic treatment [199] are nowadays called the *standard accretion disk model*.

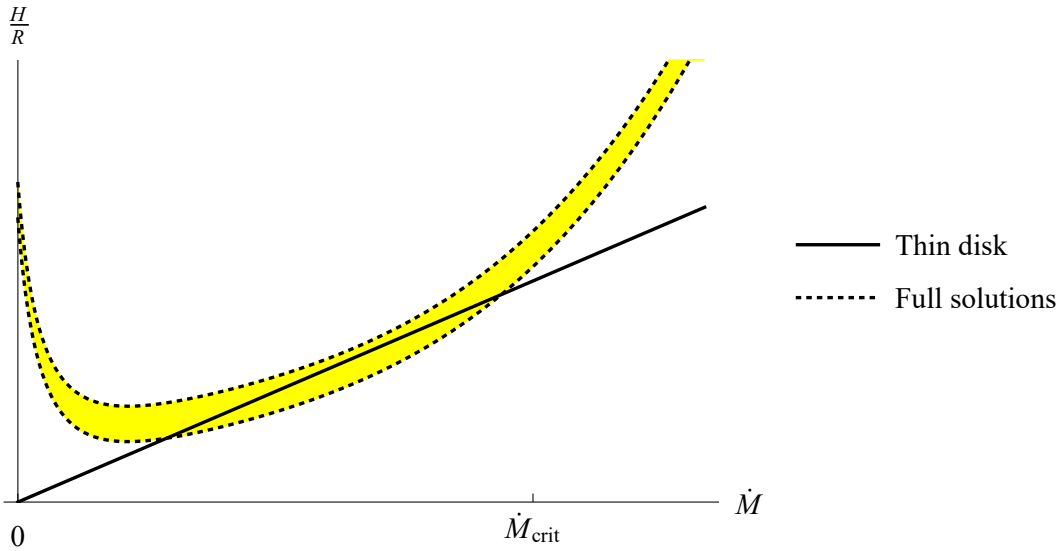

Fig. 2.2 A schematic comparison of the standard thin-disk model and the space of true physical solutions. The thin disk yields a good approximation of the height of the disk and its general properties in an intermediate regime $\dot{M} \sim 0.1\dot{M}_{\rm crit}$ but misrepresents the features of the disk at both higher and lower accretion rates. The theoretical uncertainty in such statements is reflected in the non-zero width of the curve.

2.2.3 Breaking the standard disk and growing thick

To a reader previously unexposed to the thin disk model presented in the last subsection, it might be somewhat confusing as to what is its real physical meaning. We have first only computed the energy budget without solving for any internal thermodynamics (essentially setting them to zero), and later found the internal thermodynamics that fit the budget. Specifically, we did not really allow the internal physics of the gas and radiation to have any proper dynamics and back-reaction on the disk, only evaluating them indirectly.

The way to understand the thin-disk solution is as a *perturbative* solution around an inert pressure-less non-accreting disk *under the assumption that the inert pressure-less disk exists as a limiting point of an analytical family of solutions of the full set of dynamical equations*. If such a family of solutions exists, the first order correction away from the inert disk *must* be the thin disk. Nevertheless, the question still is whether such an analytical family of physical solutions truly exists.

[5] There is a number of other details that come into the modeling of the disk atmosphere and the true spectrum of radiation that comes from it, as was already discussed by Shakura and Sunyaev [242]. I assume these effects are hidden in the effective opacity κ.

Before discussing the results in the literature that attempt to find such solution families, let us first list the effects that need to be included in the full set of dynamical equations and that would "break" the thin disk at second perturbative order:

- The radiation must be first produced in order for the disk to cool (in other words, the thermal radiation equilibrium must be first reached). This comes about as Bremsstrahlung in Coulombic collisions or as synchrotron radiation created mainly by electrons accelerated by magnetic fields in the disk. The rate of collisions is $\propto \rho T^{3/2}$ and both of these factors drop at low accretion rates in the standard disk. This decrease of cooling is felt by the heavy, hard-to-accelerate ions more than the electrons.

- Radiation must be able to leave the disk for cooling. The escape time is $\propto \kappa\Sigma$. When the accretion rate rises, it will naturally increase the immediate density of the disk Σ. However, it will also increase opacity κ due to a temperature increase in the disk. As a result, radiation may become trapped in the gas of the disk for a considerable time.

- Vertical pressure gradients will cause the disk to be of non-zero thickness and the velocities at different heights might be different. The radial pressure gradient will change the balance of forces and take the rotation curve away from a Keplerian profile even in the center of the disk. The inner radius of the disk will not be at R_{ms}.

- The non-zero u^r will also change the rotation curve. Additionally, the flow may take leftover internal energy and other properties of the flow with it, sometimes even all the way into the black hole interior. This is called advection.

We see that there is a large number of effects in question and some of them, such as radiative cooling and radiation trapping show opposite trends with $\dot{M}$; when $\dot{M}$ is low, radiation production drops, when $\dot{M}$ is high, radiation is not able to leave the disk. Then, as it turns out, there is an *intermediate* value of the accretion rate where these two effects are in a good balance to create a state approximately fulfilling the thin-disk assumptions. This is illustrated in fig. 2.2.

The relevant scale for comparison in the "intermediateness" is called the critical accretion rate $\dot{M}_{\mathrm{crit}}$. Let us ask what is the combination of constants characterizing the local properties of the flow that give a physical quantity of the dimension of a mass accretion rate. It should involve opacity κ, and the mass of the black hole M. The only combination giving the correct behaviour is M/κ times some dimensionless factor. We see that this accretion rate is in fact proportional to the Eddington luminosity (2.9) and one can thus conventionally define the critical accretion rate as a multiple thereof.[6] In this text I follow the conventions of Yuan and

[6]Let me pass to SI units for a moment to make this argument clearer. We have $[G] = \mathrm{m}^3\mathrm{kg}^{-1}\mathrm{s}^{-2}$, $[M] = \mathrm{kg}$, $[\kappa] = \mathrm{kg}^{-1}\mathrm{m}^2$, $[c] = \mathrm{m\ s}^{-1}$. We know that M always appears along with a G in the equations. Then the only way

Narayan [296] by defining the critical accretion rate to be equal to the rate at which a process with radiative efficiency 10% radiates at Eddington luminosity

$$\dot{M}_{\rm crit} = \frac{\lambda_{\rm E}}{0.1} = \frac{40\pi M}{\kappa}\,. \tag{2.37}$$

This critical rate and variants thereof are sometimes called the "Eddington" rate. However, the relevance of $\dot{M}_{\rm crit}$ is for the *near field* accretion physics, and it is only by coincidence that it is within an order of magnitude or so from a quantity that is relevant in the far field.

Whenever the accretion rate in the disk is $\dot{M} \lesssim \dot{M}_{\rm crit}$ but not $\dot{M} \ll \dot{M}_{\rm crit}$, the radiation production and release is both at sufficient rates for the thin-disk equations to be approximately true.

However, when $\dot{M} \gtrsim \dot{M}_{\rm crit}$, the accretion disk becomes optically thick and traps the radiation until a part of the thermal energy is advected along the flow and eventually even into the black hole. This super-critical disk is thus thick, extended beyond the last stable orbit, and less radiatively efficient than the thin disk. First numerical solutions to the disk equations in this case were found by Abramowicz et al. [12] in a Newtonian treatment. Abramowicz also coined the term "slim disks" for these disks. A relativistic treatment of the slim disks was then given by Beloborodov [29]. A number of more recent references along with properties of the solutions for a range of parameters can be found in [228].

It is possible to construct super-critical accretion disks that surpass the Eddington luminosity. However, the luminosity from these sources does not escape isotropically, so it is an open question how the far-field matter inflow will be regulated. This is especially true in the case when source of the matter itself is anisotropic, such as in Roche-lobe overflow from an orbiting star companion to the black hole, or from an outright tidal disruption of a star that approached the black hole. In tidal disruptions, the accretion disk formed in its aftermath is, in fact, expected to surpass Eddington luminosity for a certain time, and this could explain some enigmatic ultraluminous X-ray events [204, 229].

On the other hand, whenever $\dot{M} \ll \dot{M}_{\rm crit}$, the ability of the disk to produce radiation to cool itself is quenched by the low densities and thus low collision rates. However, the lighter electrons will be accelerated by the magnetic fields in the disk and this will lead them to produce sufficient amounts of synchrotron radiation for cooling. Then again, not so the ions and that leads to a two-temperature ion-electron gas and a characteristic spectral signature.

Furthermore, since only a small part of the initial energy of the gas is radiated away, the bulk of the gas will have enough energy to launch significant amounts of matter particles to

an accretion rate $\sim$ kg s^{-1} can be assembled from these quantities is $\sim GM/(\kappa c)$. The Eddington luminosity, on the other hand, is $\sim GMc/\kappa$.

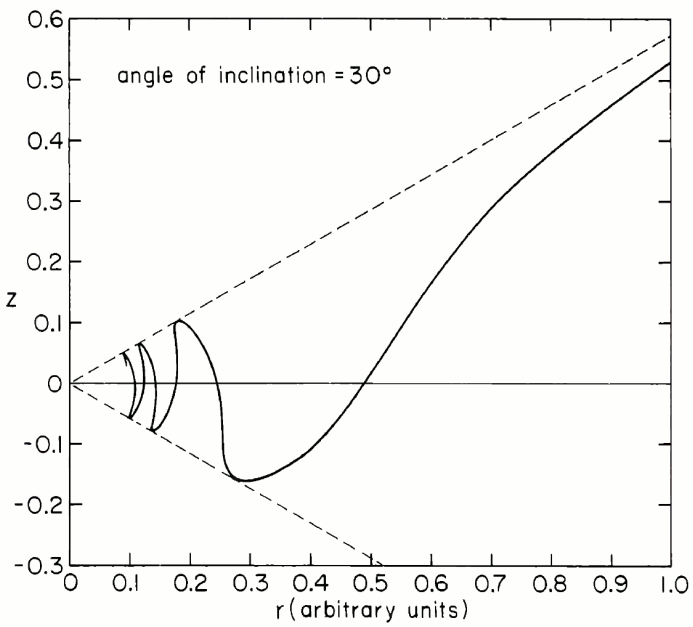

Fig. 2.3 A sketch of a meridional section of a warped disk. Taken from Bardeen and Petterson [26].

infinity in the form of a wind from the disk surface. This means that the formal accretion rate inside the disk $\dot{M}$ becomes a function of R, but also that jets will easily find matter for their formation. Similar to the slim disks, the overall lack of radiative cooling leads to a smaller η and a thick geometry of the disk extending beyond the ISCO.

Early ideas in the direction of these dilute hot disks were presented by Ichimaru [120] and Rees et al. [222] to be left largely neglected until their rediscovery in a series of papers by Narayan and Yi [190, 192, 191]. Recent references and discussion can be found in [296].

In summary, there is no limit in which the solutions of the equations converge to the inert non-accreting disk, and the foundational assumption of the validity of the standard accretion disk is thus broken. This conclusion is largely unsatisfactory to a theorist. On the other hand, the standard accretion disk model proves to be effective in modeling a part of the observed spectrum of accreting sources, and seems to be a reasonable approximation to full numerical solutions of the disk equations in the intermediate $\dot{M} \lesssim \dot{M}_{\rm crit}$ regime, at least at somewhat larger radii [202]. Nevertheless, in any other regime the disk is thick and, in that mode, there are no analytical constructions as complete and self-contained as the standard thin disk.

One last point that I would like to mention before the end of this subsection is the issue of a disk whose angular momentum is misaligned with the spin of the black hole. Even though some correlation between the angular momentum of the infalling matter and the black hole spin is to be expected, it is only reasonable to assume that there will always be *some* misalignment

between the two [132, 131]. Then, whenever the matter of the disk spirals in under a general angle, the gravito-magnetism will cause the local orbital plane of the matter to precess with a frequency $\approx 2Ma\cos\vartheta_{\rm d}/r^3$, where $\vartheta_{\rm d}$ is the local inclination of the disk with respect to the black-hole rotation axis [287]. Since this frequency is differential, the local orbital planes of the matter dephase, and the disk gets "warped" into an intricate non-planar shape (see fig. 2.3).

This effect on the disk was studied for the first time by Bardeen and Petterson [26], who also gave a simple analytical estimate for the properties of the disk in the spirit of Shakura and Sunyaev [242]. However, a more careful analysis by Papaloizou and Pringle [207] showed that the interaction of viscous torques and the non-stationary, non-axisymmetric dynamics of such disks must lead to highly complex behavior not covered by the model of Bardeen and Petterson [26] unless the viscosity is strong and the thickness of the disk small. (Other references and discussion of the analytical equations can be found in [273].)

For example, in other regimes when the disk is thick or viscous torques not very large, the warping of the disk may cause it to have sudden break or completely tear apart in the inner regions (see [194, 193] for references). The sensitivity of the models to the precise dynamics of the internal stresses mean that an α-like prescription is inadequate and one must model the "internal" turbulence directly. Since a trustworthy physical model resolving a highly non-stationary disk up to turbulent scales requires considerable computational power, this line of research has been pursued only very recently [152].

2.2.4 So what is the value of α?

The turbulent transport in the thin accretion disk was estimated essentially by dimensional analysis and its precise dynamics were hidden in the parameter α. The values of α obtained from observational estimates are usually $\alpha \sim 0.1 - 0.4$ [133], which corresponds to very strongly developed turbulence. However, the Keplerian hydrodynamical flows have $\mathrm{d}L/\mathrm{d}R > 0$, which are flows that were known to generally stabilize against turbulence [260, 22]. Furthermore, observations of accretion disks near white dwarfs showed that the parameter α had to vary between states of the disk [244] and the theory with $\alpha = \text{const.}$ is thus useless for dynamical analyses of the accretion disk.

This conundrum is now believed to be resolved by the realization that any differentially rotating conductive plasma is subject to the so-called magneto-rotational instability (MRI). The MRI was first studied by Velikhov [279] and Chandrasekhar [54], but it was rediscovered in the context of accretion disks by Balbus and Hawley [20] (see [21] for an excellent review).

The instability can be characterized as follows. A weak magnetic-field perturbation is frozen into the elements of the conductive plasma, and this introduces an essentially elastic coupling between them. Then, due to the differential rotation of the disk, the distance between

the elements grows and the coupling attempts tries to draw them closer together. However, this elastic effect ends up acting exactly in the opposite way: The element on a higher orbit that lags behind is pulled in the positive φ direction, obtains extra angular momentum, moves to a higher orbit, and slows down even further. In contrast, the element on the lower orbit is pulled in the negative φ direction, looses angular momentum, moves to a lower orbit, and speeds up even more. The result is a runaway process that mixes the fluid layers and amplifies magnetic fields.

Let me now just list some of the essential properties of the MRI. When the plasma is infinitely conductive, the instability can be triggered by infinitely small magnetic fields, even though the wavelength of the fastest-growing disturbance is proportional to B. As a result, magnetic fields in highly conductive disks arise naturally without the need of strong external input.

However, in the case of finite conductivity the MRI needs to be triggered by a finite magnetic field, the magnetic fields dissipate, and some sort of dynamo action must thus be established to keep the MRI in effect. This seems to be possible only if an overall vertical (B_z or $F^{R\varphi}$) magnetic field is present [21] (however, see also the recent results of Guseva et al. [103]). On the other hand, when the magnetic pressure B^2 is larger than the thermodynamic pressure P, the instability is suppressed.

In the case of only partially ionized disks farther from the perfectly conductive state, such as would be the case of galactic molecular discs or protostellar discs, the instability can also occur under the assumption that the collisions between the ions and neutrals are sufficiently frequent [35]. Furthermore, the MRI occurs even in rarefied plasmas where the hydrodynamic approximation is no longer valid [141].

The significance of MRI is mainly to provide a driving for the turbulent cascade and the magnetic dynamo action; the direct angular-momentum transport by MRI will typically be sub-leading. Thus, to deduce the value of α, one needs to either construct a full theory of turbulence in compressible magnetized plasmas, or to use direct numerical simulations at sufficient resolution.

Nevertheless, in the case of turbulence in the compressible magnetized plasma accessible to our direct observations, the solar wind, the fundamental modeling has proven to be highly complex and was able to yield correct predictions only after considerable phenomenological feedback (e.g., [45]). Thus, most astrophysical studies of α and turbulence in accretion disks in general are based on direct numerical simulations (but see also the terrestrial analogue models using liquid metals [248, 247, 236, 104]).

2.2.5 Numerical simulations of magnetized accretion disks

Nevertheless, one problem that universally arises in such simulations is the fact that the effective α parameter is computed to be in the ranges $\alpha \sim 0.01 - 0.02$, and order of magnitude below the observation fits [133, 112, 137]. The theoretical estimates are obtained either in a local "shearing box" simulation or a global simulation.

The shearing box is a clever trick, where the dynamics of a small column from the disk in the range $R \in (R_0, R_0 + \Delta R), \varphi \in (\varphi_0, \varphi_0 + \Delta\varphi)$ is mimicked by identifying the angular boundaries $(R, \varphi_0) \leftrightarrow (R, \varphi_0 + \Delta\varphi)$ (in other words, periodic boundary conditions are imposed in the angular direction), and a "differentially rotating" identification at the radial boundaries $(R_0, \varphi) \leftrightarrow (R_0 + \Delta R, \varphi - \Omega' \Delta R t)$, where $\Omega' = \mathrm{d}\Omega/\mathrm{d}R$ is the gradient of angular velocity. As a result, shearing-box simulations can resolve the smallest turbulent scales at reasonable computational cost. Then again, these simulations are unable to predict various cumulative and global effects in the disk, such as the evolution of the strength of the magnetic fields or the rotation curve of the gas, because these enter the model essentially as external boundary conditions [245].

On the other hand, global simulations could in principle act as universal predictors; just input the physical model, run a full simulation, and get the correct output. Of course, life is not as easy. The proper modeling of the MRI length-scales requires that $l_{\mathrm{MRI}} \sim B/(\sqrt{\rho}\Omega)$ is well resolved [112, 113], where, however, we would like to keep the initial B as small as possible so that the magnetic fields develop spontaneously.

Furthermore, another consistency criterion should be applied: If a simulation already captures the required physics, its results should not change by increasing resolution. This is called *convergence*, and it at least doubles the computational budget if checked consistently. An additional version of convergence would be the dependence on initial conditions: If we have no real physical motivation for different choices of initial conditions of our simulations, then we should explore the entire range and compare the resulting predictions. If the predictions do not match across initial conditions, our model is obviously unpredictive. Many numerical simulations to date fail to fulfill some of the above-listed criteria [112, 245, 113].

For example, the physically motivated initial condition would be to evolve an accretion disk by injecting matter in a Bondi-like scenario from far away, and let it spontaneously establish the quasi-stationary accretion disk. However, the typical time for a fluid element starting from R at Keplerian velocity to spiral onto the black hole is given by the (turbulent-)viscous time-scale $t_{\mathrm{visc}} = \rho R^2/\mu_{\mathrm{t}} = \sqrt{MR}/(\alpha v_s^2)$. If we compare this with the fact that we need to resolve the orbital time-scale near the black hole $T_{\mathrm{orb}} \sim 10M$ with a time step about $\Delta t \sim 0.1M$, we would require astronomically long simulations to track the evolution of the gas from any radius $R \gg M$ ($v_{\mathrm{s}} \sim 10^{-7} - 10^{-5}$ for gases infalling from afar).

To date, there is probably no simulation that would see turbulent transport act over scales larger than a few tens of M (see [189, 230] for $t = 200\,000M$ simulations). Instead, one usually starts with various *Ansätze* for the initial conditions, such as a torus of matter near the black hole. It is currently not clear what the imprints of such a choice will be on the simulation results, but by the comparison of scales, it is reasonable to assume that *local* physics of the accretion flow are well captured by such simulations.

Related question to the initial conditions of the gas distribution are the initial geometry of the magnetic field. These will generally "wash out" by the influence of the MRI up to one property: the overall magnetic flux carried by the matter. This will, in general, accumulate on the black hole during the accretion process and can lead to a state of the accretion disk known as a magnetically arrested disk (MAD) [186, 121, 261, 262, 189, 169, 230]. Once the black hole accumulates a magnetic flux through its horizon $\Phi_{\rm BH} \sim 50 - 60\sqrt{\dot{M}M}$, the magnetic pressure at the horizon is sufficient to stop the flow and push it to larger radii. Accretion then occurs only through slow, thin streams of matter, and the black hole produces powerful Blandford-Znajek jets that can extract even more mass-energy than was present in the inflow (see discussion in Subsec. 1.3.3). It is not far-fetched that a significant fraction of accretion disks in active galactic nuclei are in the MAD state but it is exactly our uncertainty in physical input (initial conditions) that limits the predictivity of such results [186, 230].

One last note to the general discussion of global simulations and the "α-parameter conundrum" is the fact that it is easy to model thick disks either at strongly sub-critical or strongly super-critical accretion rates. In these modes the direct simulation approach seems to yield results generally consistent with observations [182, 184, 183, 229, 226]. In other words, it may be that once we obtain reliable simulations for accretion disks in the intermediate regime and compare *directly* with observations rather than looking at some effective values of α, the discrepancy disappears because the standard thin disk was simply a bad model [233, 234]. However, a sufficiently fundamental treatment of the strong radiation processes in the intermediate regime is out of reach of current simulations.

Before ending this section, let me now give an example of a current state of the art numerical study of accretion disks by describing the recent work of Ryan et al. [226]. In doing so, I hope to illustrate the scale of complexity of realistic simulations, and I pick the study of Ryan et al. [226] mostly because of its advanced physical modeling and recency.

The study aims to model the supermassive black hole in the center of the M87 galaxy in the Virgo cluster. The M87 black hole is at a distance of $\approx 17\,$Mpc [36] and it is estimated to be of the mass $\approx 3 - 6 \times 10^9 M_\odot$ [96, 285]. This makes it, along with the black hole in the center of our galaxy, Sgr A*, one of the two black holes with a shadow just (or barely) large enough to be observed by terrestrial very long baseline interferometry [76, 155]. The black hole is accreting

in a sub-critical, radiatively inefficient regime, has a powerful jet extending over thousands of light years, which, consequently, makes it observable in essentially all electromagnetic bands (see fig. 1.1 in the first chapter). However, the electromagnetic spectrum is not currently understood (but see [183]), and the aim of Ryan et al. [226] was to explain that spectrum by a first-principle computation.[7]

To do so, Ryan et al. implemented non-trivial electron thermodynamics [223], separate prescriptions for ion and electron heating and cooling (including radiation production and absorption) [255, 118], frequency-dependent radiation transport, and radiation-force back-reaction on the plasma [227]. The radiation transport, in particular, introduces large computational costs as it is realized by tracking a probabilistic evolution of $\sim 10^7$ representative "superphotons" [77].

Even under an axisymmetric idealization, every run of these simulations then cost about 1000 CPU hours (which was, obviously, broken up by parallelization). The authors then ran many simulations for four different scenarios for the M87 black hole parameters varying the accretion rate until they matched the 230 GHz radio flux of M87 as obtained by Doeleman et al. [76]. The black hole parameters in these scenarios were the mass $M = 3.3 \times 10^9 M_\odot$; $6.9 \times 10^9 M_\odot$ along with spin $a = 0.5M$; $0.9375M$. Ultimately, the combination $M = 6.2 \times 10^9 M_\odot$ with $a = 0.9375M$ was favored by comparison with the observed spectra and image sizes. However, the limited set of simulations did not probe the MAD states and this is also probably the reason it failed to reproduce the power of the M87 jet.

This underlines the character of numerical simulations in general; complex physics without strong assumptions can be implemented, but ultimately assumptions on another end must be done because of the computations costs. Analytical methods, with their own kinds of simplifications, should interact with this field in a mutually constructive manner, looking out for the blind spots and providing insights for the numerics.

On this note, I would like to conclude the introductory part of the thesis, and pass to my original published investigations, which I briefly comment upon in the next chapter before the papers themselves are presented.

[7] By "first principle" computation I mean a computation that provides a full solution of the dynamical equations without any ad-hoc parameters characterizing the dynamical state and the geometry of the solution such as the α parameter. Nevertheless, there always will free parameters that correspond to true physical input, such as the black hole mass and spin M, a, accretion rate $\dot{M}$, overall magnetization and angular momentum of the infalling matter, and others. Furthermore, the model of Ryan et al. [226] contains implicit or explicit assumptions about how various microscopic process yield closed-form macroscopic dynamics of the fluid.

Chapter 3

Hamiltonians and canonical coordinates for spinning particles in curved space-time

Disclaimer: *Sections 3.1 to 3.5 of this chapter are a close adaptation of the following preprint(short ref.: [293]):*
Witzany, V., Steinhoff, J., & Lukes-Gerakopoulos, G. (2018). Hamiltonians and canonical coordinates for spinning particles in curved space-time. Preprint at arXiv:1808.06582. (In review at Physical Review D.)
This preprint was not allowed to be appended to the the thesis due to the rules of the University of Bremen. (Section 3.6 is a presentation of new, independent results.)

Statement of contributions to original preprint: *I have written the majority of the text, derived all of the original theoretical results in the paper, written the code for the numerical simulations, and prepared the plots. Jan Steinhoff provided me with critical knowledge needed to derive the canonical coordinates presented in the paper, and helped me understand many issues in the formalism. Georgios Lukes-Gerakopoulos found and classified chaotic layers in the Poincaré surfaces of section. All authors were engaged in recomputing and checking the theoretical results, providing references to literature, and forming the discussion and explanations given in the original preprint.*

As was already discussed to a large extent in subsection 1.4.4, the dynamics of real astrophysical objects deviate from geodesics due to finite-size effects and gravitational back-reaction, and these effects can be modeled by multipole-particles.

The multipolar Mathisson-Papapetrou-Dixon equations such as (1.47) and (1.48) were originally stated "as is", without reference to a variational principle. In the paper Witzany et al. [293], we have investigated how the Mathisson-Papapetrou-Dixon equations in the pole-dipole approximation can be cast in a Hamiltonian formalism in various approaches and contexts. This may seem as a formality, but connecting the equations to the powerful Hamiltonian framework allows to implement them in a variety of theoretical settings even beyond the gravitational-wave inspirals mentioned in subsection 1.4.4.

One of the main issues that accompany the Mathisson-Papapetrou-Dixon equations from their very beginning is the choice of the point inside the body at which the representative "particle" is placed. This choice can be uniquely fixed by requiring a so-called supplementary spin condition along with the fundamental Mathisson-Papapetrou-Dixon equation.

In [293] we found Hamiltonians for all commonly employed "comoving" supplementary spin conditions, that is, conditions that only use the local dynamical state of the body and no background tensors in their statement. Additionally, we constructed canonical coordinates for the phase space of the problem. We used these coordinates to integrate the equations with high efficiency and accuracy for the case of a spinning particle moving in the equatorial plane of the Schwarzschild space-time; we found the motion to be weakly chaotic. Apart from a minor contribution to the picture of non-integrability of the Mathisson-Papapetrou-Dixon equations near black holes, the paper represents a major leap in the understanding of their Hamiltonian form, and it unlocks the path to many future applications both in analytical theory and numerics. I restate these results in the following Chapter.

In section 3.2 I review the so-called Mathisson-Papapetrou-Dixon (MPD) equations under various supplementary conditions. Then, I proceed to the Hamiltonian formalism in section 3.3, where I present the Poisson brackets and various sets of variables that can be used during the evolution, and Hamiltonians for all the usual "comoving" supplementary conditions both in proper-time and coordinate-time parametrizations. Next, in section 3.4, I also give a set of canonical coordinates covering the spin tensor, which is useful for the numerical integration of the MPD equations. Finally, in section 3.5, I demonstrate the power of the new coordinates and Hamiltonian formalism by numerically studying spinning particles moving in the equatorial plane of a Schwarzschild black hole. A new development of this formalism that was not given in [293] is the formulation of a Hamilton-Jacobi problem along with a perturbative solution in Kerr space-time as given in section 3.6.

In Appendix A at the end of the thesis I provide context to the presented results and details of the derivations mentioned in this chapter.

My convention for the Riemann tensor $R^{\mu}{}_{\nu\alpha\beta}$ is such that $2a_{\mu;[\alpha\beta]} = R^{\nu}{}_{\mu\alpha\beta}a_{\nu}$ for a generic a_{μ}, or explicitly $R^{\mu}{}_{\nu\alpha\beta} = 2\Gamma^{\mu}{}_{\rho[\alpha}\Gamma^{\rho}{}_{\beta]\nu} - 2\Gamma^{\mu}{}_{\nu[\alpha,\beta]}$. An additional convention contrasting with the rest of this thesis is that covariant time derivatives $\mathrm{D}/\mathrm{d}\tau$ are now denoted by a simple overdot.

3.1 Importance of spin-curvature coupling for gravitational waves

The gravitational-wave detections made by the terrestrial detectors LIGO and Virgo were in the $\sim$10-100 Hz frequency band and always corresponded to inspiraling binaries of comparable mass. Upcoming space-based missions such as LISA should be able to probe the gravitational-wave spectrum in lower frequency ranges than the terrestrial detectors, approximately $\sim 10^{-4} - 10^{-1}$ Hz. Consequently, LISA will ideally allow to study the dynamics of many other types of sources of gravitational radiation [151]. One such class of sources are the so-called extreme-mass-ratio inspirals (EMRIs); during these stellar-mass compact objects spiral into massive black holes, which have masses at least five orders of magnitude higher than the solar mass [18].

Independent of the ratio of masses between the components of the system, neither the primary nor the secondary objects of the binary can be modeled as point particles in a sufficiently accurate treatment of the inspiral – effects of the finite size of both of the bodies must be taken into account. This is clear when both of the components of the binary are of comparable size and mass, but in the case of EMRIs we need to provide a somewhat more careful argumentation.

Let us denote the mass of the primary massive black hole by M, and the mass of the secondary, stellar-mass object as m. Then the mass ratio in EMRIs is approximately $q \equiv m/M \sim 10^{-4} - 10^{-7}$ and, as partially discussed in section 1.4.4, one can describe the gravitational field of the secondary as a perturbation of the gravitational field of the primary. As a result, the secondary is conventionally described as moving on the original unperturbed background while being subject to a self-force whose relative size with respect to the Christoffel-connection terms is of the order $\mathscr{O}(q)$ (see [213, 23] for recent reviews and references).

Let us now consider the effects of the finite size of the secondary component of the binary. If the secondary is rotating at relativistic rates, a matter element near its surface will feel a relative acceleration with respect to the center of mass proportional to the speed of the surface v, the radius of the object r, and the local space-time curvature R. Under the assumption of a balance of forces inside the body, this results in a "spin force" $\sim mvrR$ acting on its center of mass. Additionally, let us assume that the binary orbital separation is within a few horizon radii of the primary, and that the secondary is either a maximally spinning black hole, a few-millisecond

pulsar, or a few-second pulsar. For the maximally rotating black hole we obtain $vrR \sim 1q/M$ and for the millisecond and few second pulsar we get, under the canonical assumption of $r \sim 10$km, $vrR \sim 10^{-1}q/M, 10^{-4}q/M$ respectively. When we consider that the Christoffel symbol terms in the equations of motion scale as $\sim 1/M$, we see that the relative size of the acceleration caused by the spin-force is then generally $\mathscr{O}(q)$, the same as the gravitational self-force.

The influence of the self-force and the spin-force on the orbit will thus scale as $\mathscr{O}(q)$. It is clear that it would be close to impossible to distinguish such a perturbed orbit from a geodesic when using observables collected over just a few orbital cycles. Nevertheless, the orbit will only decay over $\mathscr{O}(1/q)$ full periods, and the small deviations amount to secular effects in the phase of the orbit. The final orbital phase $\phi_{\rm f}$ can then be schematically written as a sum of terms of the form [116]

$$\begin{aligned}
\phi_f = \phi^{(1)}_{\rm avg} & \qquad \mathscr{O}(q^{-1}) & (3.1)\\
+ \phi^{(1)}_{\rm osc} + \phi^{(2)}_{\rm avg} + \phi_{\rm spin} & \qquad \mathscr{O}(1) & (3.2)\\
+ \phi^{(2)}_{\rm osc} + \phi^{(3)}_{\rm avg} + \phi_{\rm quad} & \qquad \mathscr{O}(q) & (3.3)\\
+ \ldots & \qquad \mathscr{O}(q^2)\,, & (3.4)
\end{aligned}$$

where "avg" and "osc" denote respectively contributions from the averaged dissipative, and oscillating dissipative and conservative parts of the self-force computed from the metric perturbations of order (n) in the mass ratio. Now we see that at the contribution of the spin force appears at the same order as the first-order conservative piece of the self-force. Both the $\mathscr{O}(q^{-1})$ and the $\mathscr{O}(1)$ terms must eventually be taken into account if sub-radian precision is to be achieved in the EMRI wave-form modeling.

Let me also briefly discuss the higher-order corrections to the motion. The $\mathscr{O}(q)$ terms in the phase contain the contribution of the next-to-leading effect of the finite size of the secondary, the quadrupolar coupling. Specifically, this will include the spin-induced quadrupole that scales as $\sim S^2$ for neutron stars and black holes [108, 144, 250], where $S \sim mrv$ is called the spin magnitude. Tidal deformation of the body also formally appears in the quadrupole; however, the magnitude of the tidal deformation itself is proportional to the local curvature, which makes the tidal effects enter the equations of motion at relative order $\mathscr{O}(q^4)$ [67, 32, 252]. Consequently, these effects enter the phase only at $\mathscr{O}(q^3)$ for conservative effects and perhaps at $\mathscr{O}(q^2)$ if the dissipative tidal effects contribute to the orbital decay time.

In summary, we see that the spin-curvature coupling considered at least to linear order is a necessary piece of any EMRI model. Additionally, the spin-curvature coupling plays an important role in the post-Newtonian (weak-field and slow-motion) description of binaries of

comparable mass [37, 232]; the current state-of-the-art models include conservative effects of the spin to fourth post-Newtonian order [149]. Nevertheless, it is also desirable to build unified models that capture the inspiral dynamics of the whole range of mass ratios from extreme to comparable.

One challenging problem in the intermediate mass-ratio range is an inspiral of a neutron star into a relatively heavy stellar mass black hole, which implies $q \lesssim 0.1$. Inspirals in this regime are relatively difficult to capture in full numerical relativity simulations because of the relatively large number of cycles before the final merger. On the other hand, in the perturbative EMRI-like approach the convergence can be questioned because of the relatively large size of q. One of the goals of the so-called effective-one-body (EOB) models [46, 41, 185, 47, 69] is to interpolate through this gap.

The central piece of the EOB models are Hamiltonians coupling a representative "test particle" to an effective curved dynamical background. The dynamics of this effective test particle then encode the dynamics of the real binary. One of the flavours of the EOB models uses a Hamiltonian for a *spinning* test particle [24, 41] coupled to a curved background, and this means that it captures the spin-force in the EMRI limit automatically (see also the progress of the other EOB flavor in Refs. [68, 111, 128, 31]). Hence, exploring simplified or alternative Hamiltonians for spinning particles appears to be crucial in this context as well.

3.2 The MPD equations

The equations of motion of massive bodies in a gravitational field are among the most basic topics in Newtonian mechanics, and a surprisingly difficult problem in general relativity. However, by assuming that the stress-energy tensor is replaced by some distributional equivalent, and by imposing the covariant conservation of the stress-energy tensor, we obtain the general-relativistic equations of motion in the celebrated MPD form. The MPD equations to pole-dipole order read [164, 208, 74]

$$\dot{P}^{\mu} = -\frac{1}{2} R^{\mu}{}_{\nu\kappa\lambda} \dot{x}^{\nu} S^{\kappa\lambda} \,, \tag{3.5a}$$

$$\dot{S}^{\kappa\lambda} = P^{\kappa}\dot{x}^{\lambda} - P^{\lambda}\dot{x}^{\kappa} \,, \tag{3.5b}$$

where $x^{\mu}(\tau)$ is the position of some representative point from within the rotating body, $S^{\kappa\lambda}$ the spin tensor, and P^{μ} the momentum (flux of stress-energy) of the body. Here τ is the proper time, $\dot{x}^{\mu}\dot{x}_{\mu} = -1$. However, it is noteworthy that the MPD equations are invariant under affine reparametrizations of the world-line, at least to pole-dipole order.

The relation between $\dot{x}^\nu$ and P^ν is not fully determined and has to be derived from an additional relation, the supplementary spin condition. A supplementary spin condition is usually given in the form $S^{\mu\nu}V_\nu = 0$, where V_ν is some time-like direction. The physical interpretation of this supplementary condition is that V^ν is the observer frame in which the momenta of the stress-energy tensor P^μ and $S^{\nu\kappa}$ are computed. The position of the referential world-line $x^\mu(\tau)$ is then the center of mass of the spinning body in this frame [63].

The MPD equations as given here do not include the contributions from the quadrupole and higher-order mass moments of the body. One reason why studying this system has far-reaching consequences is the fact that the pole-dipole equations are *universal*, i.e., independent of the internal structure of the body. Among other effects, and as already mentioned in the previous section, one expects the rotation to flatten the body and thus to produce a structure-dependent quadrupole moment that scales as S^2. The character of the pole-dipole equations is thus inherently perturbative and one often resorts to various expansions in powers of S in the description.

Some identities useful independent of the supplementary condition read

$$\dot{x}^{(\mu}\dot{S}^{\nu\kappa)_{\text{cycl.}}} = 0\,, \tag{3.6}$$

$$P^\mu = m\dot{x}^\mu + \dot{x}_\gamma \dot{S}^{\gamma\mu}\,, \tag{3.7}$$

$$m \equiv -P^\mu \dot{x}^\mu\,. \tag{3.8}$$

A number of other useful identities along with a short historical review of the MPD equations can be found in Ref. [238].

Let me also define the spin vector s^μ, the spin magnitude S, and a mass-like quantity $\mathscr{M}$ as

$$s^\mu \equiv -\frac{1}{2\sqrt{-V^\alpha V_\alpha}}\varepsilon^{\mu\nu\kappa\lambda}V_\nu S_{\kappa\lambda} = -\frac{1}{\sqrt{-V^\alpha V_\alpha}}\star S^{\mu\nu}V_\nu\,, \tag{3.9}$$

$$S \equiv \sqrt{\frac{S^{\kappa\lambda}S_{\kappa\lambda}}{2}} = \sqrt{s^\mu s_\mu}\,, \tag{3.10}$$

$$\mathscr{M} \equiv \sqrt{-P^\alpha P_\alpha}\,, \tag{3.11}$$

where $\star S^{\mu\nu} = \varepsilon^{\mu\nu\kappa\lambda}S_{\kappa\lambda}/2$ is the dual spin tensor. It is important to remember that the definition of s^μ will be different whenever a different supplementary condition is chosen. Now we see that $S^{\kappa\lambda}s_\lambda = 0$ and it is possible to build a projector on the sub-space orthogonal to V_μ, s_ν as

$$h^\mu_\nu = \frac{1}{S^2}S^{\mu\kappa}S_{\nu\kappa} = \left(\delta^\mu_\nu + \frac{V^\mu V_\nu}{(-V^\alpha V_\alpha)} - \frac{s^\mu s_\nu}{S^2}\right). \tag{3.12}$$

It should also be noted that this projector is of zeroth order in the spin, even though higher powers of the spin magnitude and the spin tensor were used in its definition.

Now, the question is which supplementary spin condition should be used to close the system of MPD equations. However, all observer frames in relativity are equivalent and there is no strict criterion for this choice. Hence, in the rest of this section, I will review the various commonly employed choices for the supplementary spin conditions and the aesthetic and practical advantages they offer.

3.2.1 The KS condition

Eq. (3.7) indicates that the momentum P^μ can be generally linearly independent of the time derivative of the referential position $\dot{x}^\mu$. Kyrian and Semerák [143] (KS) asked the question which supplementary condition eliminates this linear independence and makes the two proportional, $P^\mu = m\dot{x}^\mu$, and found that this holds when we assume the existence of a time-like vector w_μ such that $S^{\mu\nu}w_\nu = 0$ and $\dot{w}_\nu = 0$. We also set $w_\alpha w^\alpha = -1$ for simplicity of the resulting expressions. The MPD equations then simplify into the form

$$P^\mu = m\dot{x}^\mu\,, \tag{3.13a}$$

$$\dot{m} = 0\,, \tag{3.13b}$$

$$\ddot{x}^\mu = -\frac{1}{2m}R^\mu{}_{\nu\kappa\lambda}\dot{x}^\nu S^{\kappa\lambda}\,, \tag{3.13c}$$

$$\dot{S}^{\kappa\lambda} = 0\,. \tag{3.13d}$$

This is probably the simplest and most elegant form of the MPD equations one can acquire. This form of the MPD equations can in fact be generated by a large set of other supplementary conditions, which is discussed in Appendix A.1.

In terms of variables that need to be evolved during a numerical integration, the system of equations (3.13) is characterized by a phase space $(x^\mu, \dot{x}^\nu, S^{\kappa\lambda})$. An important point is to realize that once an initial condition with some vanishing direction of the spin tensor is chosen, $S^{\mu\nu}w_\nu|_{\tau=\tau_0} = 0$, then the equations of motion (3.13) will evolve with two vanishing directions. The first of these directions is proportional to w^μ, and the second one is proportional to s^μ. We can always choose the time-like direction to fulfill $\dot{w}^\mu = 0$. In other words, once the initial condition is set up with a degenerate spin tensor, the set of equations (3.13) can be evolved "as is" without further reference to the auxiliary vector w^μ.

Nonetheless, the equations of motion can also be re-expressed using w_ν and s_μ as

$$\ddot{x}^\mu = \frac{1}{m} \star R^\mu{}_{\nu\kappa\lambda} \dot{x}^\nu s^\kappa w^\lambda \,, \tag{3.14a}$$

$$\dot{w}^\kappa = \dot{s}^\lambda = 0 \,, \tag{3.14b}$$

where $\star R_{\mu\nu\kappa\lambda} \equiv R_{\mu\nu\gamma\delta}\varepsilon^{\gamma\delta}{}_{\kappa\lambda}/2$. In this case the phase space is $(x^\mu, \dot{x}^\nu, s^\lambda, w^\kappa)$, i.e., it consists of the coordinate position, its first time derivative, the spin vector, and the auxiliary time-like vector w^λ.

3.2.2 The MP condition

Another supplementary spin condition proposed independently by various authors [93, 164, 212] is $S^{\mu\nu}\dot{x}_\nu = 0$. I call it here the Mathisson-Pirani (MP) spin condition due to the pioneering works using this condition in the context of curved space-time [164, 212]. In the context of flat space-time, it is often called the Frenkel spin condition due to the earlier work of Frenkel [93]. The physical interpretation of this spin condition is that the multipole momenta are chosen in a frame in which the center of mass itself is at rest.

Under this supplementary condition, the MPD equations are simply the equations (3.5) with the substitution of the following relation in place of $\dot{x}^\mu$ [62]

$$\dot{x}^\mu = \frac{1}{m} P^\nu \left(\delta^\mu_\nu - \frac{1}{S^2} S^{\mu\kappa} S_{\nu\kappa} \right) = P^\nu \left(\delta^\mu_\nu - h^\mu_\nu \right) . \tag{3.15}$$

Once again, in this representation the phase space needed for numerical evolution is $(x^\mu, P^\nu, S^{\kappa\lambda})$, the identical variables as for the KS condition. Another interesting fact is that in this representation it is sufficient to choose the initial data with the spin tensor having *some* degenerate time-like direction, and the relation (3.15) will always make the four-velocity fulfill $S^{\kappa\lambda}\dot{x}_\lambda = 0$.

Another representation of the phase space can be obtained through the spin vector and higher order time derivatives of the position:

$$\dddot{x}^\mu = f^\mu(x^\nu, \dot{x}^\lambda, \ddot{x}^\kappa, s^\gamma) \,, \tag{3.16}$$

$$\dot{s}^\lambda = s^\nu \ddot{x}_\nu \dot{x}^\lambda \,, \tag{3.17}$$

where f^μ is derived in Appendix A.2 and its explicit form is given in equation (A.9). In other words, the phase space in this approach consists of $(x^\mu, \dot{x}^\nu, \ddot{x}^\kappa, s^\lambda)$. When one compares these variables with that of the KS condition, it can be seen that even though no auxiliary w^λ is evolved, there is, nevertheless, additional data stored and evolved in the acceleration vector $\ddot{x}^\lambda$.

A recent discussion of this degeneracy of the MP supplementary condition was given by Costa et al. [62].

3.2.3 The TD condition

The Tulczyjew-Dixon supplementary spin condition [275, 75], also sometimes referred to as the "covariant" supplementary spin condition, is given as $S^{\mu\nu}P_\nu = 0$. Its physical interpretation is clear: it corresponds to a frame in which the fluxes of energy-momentum vanish.

The TD conditions results in MPD equations of motion that are closed by substituting for $\dot{x}^\mu$ as [81, 200]

$$\dot{x}^\mu = \frac{m}{\mathscr{M}^2}\left(P^\mu + \frac{2S^{\mu\nu}R_{\nu\gamma\kappa\lambda}P^\gamma S^{\kappa\lambda}}{4\mathscr{M}^2 + R_{\chi\eta\omega\xi}S^{\chi\eta}S^{\omega\xi}}\right), \tag{3.18}$$

where $\mathscr{M}$ is now an integral of motion, $\dot{\mathscr{M}} = 0$. The other mass m is not conserved during the evolution, and it can be easily expressed as a function of $P^\mu, S^{\kappa\lambda}, R_{\alpha\beta\gamma\delta}$ from $\dot{x}^\mu \dot{x}_\mu = -1$ as

$$m = \frac{\mathscr{A}\mathscr{M}^2}{\sqrt{\mathscr{A}^2\mathscr{M}^2 - \mathscr{B}S^2}}, \tag{3.19}$$

$$\mathscr{A} = 4\mathscr{M}^2 + R_{\alpha\beta\gamma\delta}S^{\alpha\beta}S^{\gamma\delta}, \tag{3.20}$$

$$\mathscr{B} = 4h^{\kappa\eta}R_{\kappa\iota\lambda\mu}P^\iota S^{\lambda\mu}R_{\eta\nu\omega\pi}P^\nu S^{\omega\pi}. \tag{3.21}$$

The phase space is then again expressible as $(x^\mu, P^\nu, S^{\kappa\lambda})$.

However, we will now see that the TD condition in fact eliminates some degrees of freedom as compared to the KS and MP conditions. Once again, there is the possibility to transform to a spin vector which leads to [cf. 257]

$$\dot{P}^\mu = \frac{1}{\mathscr{M}}\star R^\mu{}_{\nu\kappa\lambda}\dot{x}^\nu s^\kappa P^\lambda, \tag{3.22}$$

$$\dot{s}^\mu = \frac{1}{\mathscr{M}^3}\star R_{\gamma\nu\kappa\lambda}s^\gamma \dot{x}^\nu s^\kappa P^\lambda P^\mu, \tag{3.23}$$

where we use the substitution (3.18) whenever $\dot{x}^\nu$ appears. This set of equations is non-linear and complicated, but the phase space now consists only of (x^μ, P^ν, s^κ), which is one vector less as compared to the KS and MP conditions and also probably the most economic set of variables possible for the MPD system.

3.2.4 The CP and NW conditions

All of the previously stated supplementary conditions only used the "internal" state of the body in choosing the frame in which the averaging is done (even though this somehow implicitly refers to the background curvature), or at least some "comoving" structure in the case of the KS condition. The Corinaldesi-Papapetrou (CP) [61] and Newton-Wigner (NW) [218, 196] conditions, on the other hand, employ an external time-like vector field $\xi^\mu(x^\nu)$. The conditions read

$$S^{\mu\nu}\left(\xi_\nu + \alpha\frac{P_\nu}{\mathscr{M}}\right) = 0\,, \tag{3.24}$$

where $\alpha = 0$ corresponds to the CP and $\alpha = 1$ to the NW condition.

The physical meaning of the CP condition is clear; it foliates the worldtube of the body by a "lab frame" $\xi^n u$, and computes the center of mass and all the other quantities in such a frame. In this sense, the world-line it describes is closest to a point of view of an observer registering the orbit from infinity, at least if ξ^μ is chosen to correspond to a time-foliation established by such observers. On the other hand, the Newton-Wigner condition has no clear interpretation and was chosen for purely technical reason.

The convenience of these supplementary conditions lies in the fact that one can recast the evolution for the spin tensor in terms of a tetrad basis $S^{AB} = e^A_\mu e^B_\nu S^{\mu\nu}$, and by choosing $e^0_\mu = \xi_\mu$ one can eliminate three of the six independent spin-tensor components $S^{0I}, I = 1,2,3$ as

$$S^{0I} = -\frac{\alpha}{\mathscr{M} + \alpha P_0} P_J S^{JI}\,,\ J = 1,2,3\,. \tag{3.25}$$

The equations of motion for the spin tensor are then obtained with the use of (3.6) as

$$\dot{S}^{\mu\nu} = 2S^{\kappa[\mu}\dot{x}^{\nu]}\frac{(\mathscr{M}\xi_{\kappa;\lambda} - \alpha R_{\hat{\kappa}\lambda\gamma\delta}S^{\gamma\delta}/2)\dot{x}^\lambda}{(\mathscr{M}\xi_\chi + \alpha P_\chi)\dot{x}^\chi}\,, \tag{3.26}$$

where the notation $\hat{\kappa}$ in the curvature tensor denoted the part orthogonal to the momentum P^ν.

The relation between momentum and velocity then attains the following implicit form

$$m\dot{x}^\mu = P^\mu - (S^{\kappa\mu} + S^{\kappa\omega}\dot{x}_\omega\dot{x}^\mu)\frac{(\mathscr{M}\xi_{\kappa;\lambda} - \alpha R_{\hat{\kappa}\lambda\gamma\delta}S^{\gamma\delta}/2)\dot{x}^\lambda}{(\mathscr{M}\xi_\chi + \alpha P_\chi)\dot{x}^\chi}\,. \tag{3.27}$$

This equation cannot be explicitly inverted into a $\dot{x}^\mu(P_\nu)$ or $P_\nu(\dot{x}^\mu)$ formula in the general case, and the CP/NW condition often does not yield a set of evolution equations in strictly closed form.

Nonetheless, it is possible to iterate the momentum-velocity relation by starting from $\dot{x}^\mu = P^\mu/m + \mathscr{O}(S)$ to obtain results of higher and higher precision with respect to powers of S. The first iteration leads to

$$m\dot{x}^\mu = P^\mu - \left(S^{\kappa\mu} + \frac{1}{m^2}S^{\kappa\omega}P_\omega P^\mu\right)\frac{\xi_{\kappa;\lambda}P^\lambda}{(m\xi_\chi + \alpha P_\chi)P^\chi} + \mathscr{O}(S^2)\,. \tag{3.28}$$

Equations such as the one above inserted into the MPD equations along with the assumption that (3.25) is exactly true at all times lead to closed-form evolution equations with the phase space (x^μ, P_ν, S^{IJ}).

Again, by counting the variables, we see that the NW and CP conditions lead to systems with the same "minimal" number of degrees of freedom as the TD+MPD equations. One other reason the NW condition received heightened attention in the recent years is the fact that it is possible to formulate it as a Hamiltonian system with the canonical $SO(3)$ commutation relations for the spin vector [110, 24, 280].

3.2.5 Equivalence of the supplementary conditions

It is obvious that it should be possible to transform the descriptions induced by various supplementary conditions into each other by shifting the world-line $x^\mu(\tau)$ to a different representative point inside the body and transforming the quantities $P^\mu, S^{\mu\nu}$. Details of such procedures were given for instance by Kyrian and Semerák [143] and Vines et al. [280]. These transformations are truncated at spin-squared order. Alternatively, the different supplementary conditions can be understood as describing bodies with the same internal angular momenta, but different *quadrupole* momenta (see [280]). In practice, this leads to a rather fast divergence of equivalent evolutions under various supplementary conditions [143].

There is another way equivalence between the KS, MP, and TD conditions can be established, at least to linear order in spin and for a short time. Take any initial data $(x^\mu_0, P^\nu_0, S^{\kappa\lambda}_0)$ such that $S^{\kappa\lambda}_0 P_{0\lambda} = 0$. Then it is obvious from the discussion of the previous subsections that this data can be used to evolve the system of MPD equations under either the KS,MP, or TD equations. Furthermore, we will have initially $\dot{x}^\mu = P^\mu/m + \mathscr{O}(S^2)$ and also $\ddot{x}^\mu = -R^\mu_{\nu\kappa\lambda}\dot{x}^\nu S^{\kappa\lambda}/(2m) + \mathscr{O}(S^2)$, $\dot{S}^{\kappa\lambda} = \mathscr{O}(S^2)$. Hence, on this subclass of initial data and for short times, the KS,MP, and TD conditions are also approximately equivalent. Then again, on longer time scales the evolutions under different supplementary conditions will accumulate differences that cause $\mathscr{O}(S)$ differences even at the level of equations of motion. Furthermore, in the case of the NW/CP conditions and for general ξ^μ such an equivalence cannot be reached even at linear order in spin and for any time period.

3.3 Hamiltonians for spinning particles

3.3.1 Poisson brackets

Before we can discuss Hamiltonians, we need to set up the stage in the form of a phase space endowed with a symplectic structure, postulated here through a Poisson bracket. Consider the set of non-zero Poisson brackets for the phase-space coordinates $x^\mu, P_\nu, S^{\gamma\kappa}$

$$\{x^\mu, P_\nu\} = \delta^\mu_\nu\,, \tag{3.29a}$$

$$\{P_\mu, P_\nu\} = -\frac{1}{2}R_{\mu\nu\kappa\lambda}S^{\kappa\lambda}\,, \tag{3.29b}$$

$$\{S^{\mu\nu}, P_\kappa\} = -\Gamma^\mu_{\lambda\kappa}S^{\lambda\nu} - \Gamma^\nu_{\lambda\kappa}S^{\mu\lambda}\,, \tag{3.29c}$$

$$\{S^{\mu\nu}, S^{\kappa\lambda}\} = g^{\mu\kappa}S^{\nu\lambda} - g^{\mu\lambda}S^{\nu\kappa} + g^{\nu\lambda}S^{\mu\kappa} - g^{\nu\kappa}S^{\mu\lambda}\,. \tag{3.29d}$$

This set of brackets arises in many models for spinning-particle dynamics [142, 86, 259, 130, 24, 220, 66] and I present our own motivation from field theory in Appendix A.3. Furthermore, it is easy to prove that the Poisson brackets follow from the generic effective action used in Refs. [253, 250, 280] (see Appendix A.5).

The Poisson brackets (3.29) can be partially canonicalized by choosing an orthonormal tetrad e^A_μ, $e^A_\mu e^{\mu B} = \eta^{AB}$ (= Minkowski metric), and adopting a set of variables [86, 259, 130]

$$S^{AB} = S^{\mu\nu}e^A_\mu e^B_\nu\,, \tag{3.30}$$

$$p_\mu = P_\mu + \frac{1}{2}e_{\nu A;\mu}e^\nu_B S^{AB} = P_\mu - \frac{1}{2}\Gamma_{\nu\kappa\mu}S^{\nu\kappa}\,. \tag{3.31}$$

Under this change of variables the only non-zero brackets read

$$\{x^\mu, p_\nu\} = \delta^\mu_\nu\,, \tag{3.32a}$$

$$\{S^{AB}, S^{CD}\} = \eta^{AC}S^{BD} - \eta^{AD}S^{BC} + \eta^{BD}S^{AC} - \eta^{BC}S^{AD}\,. \tag{3.32b}$$

In this coordinate basis it is clear that S^{AB} and its commutation relations are a representation of the generators of the Lorentz group. Additionally, we see that $2S^2 = S^{AB}S_{AB} = S^{\mu\nu}S_{\mu\nu}$ and $2(S^*)^2 \equiv S^{AB}S^{CD}\varepsilon_{ABCD} = S^{\mu\nu}S^{\kappa\lambda}\varepsilon_{\mu\nu\kappa\lambda}$ are Casimir elements of this algebra. That is, the spin magnitudes S, S^* commute with all the phase-space coordinates and will always be integrals of motion independent of the Hamiltonian.

However, if we compare with the MPD equations (3.5), we see that

$$\frac{\mathrm{d}}{\mathrm{d}\tau}(S^2) = S_{\mu\nu}\dot{S}^{\mu\nu} = 2S_{\mu\nu}P^\mu\dot{x}^\nu\,. \tag{3.33}$$

In other words, for conditions such as NW/CP that have $\dot{S} \neq 0$, the herein presented bracket will either not have any corresponding Hamiltonian, or the Hamiltonian dynamics will describe the NW/CP+MPD system indirectly through some deformed (non-MPD) set of variables.

3.3.2 Hamilton's equations of motion

We have now prepared everything needed in order to study the equations of motion for a general Hamiltonian $H = H(x^\mu, P_\nu, S^{\kappa\lambda})$ with the Poisson brackets (3.29). We obtain

$$\frac{\mathrm{d}x^\mu}{\mathrm{d}\lambda} = \frac{\partial H}{\partial P_\mu}\,, \tag{3.34a}$$

$$\frac{\mathrm{d}P_\nu}{\mathrm{d}\lambda} + \frac{\partial H}{\partial x^\nu} - \frac{\partial H}{\partial S^{\mu\kappa}}(\Gamma^\mu_{\nu\gamma} S^{\gamma\kappa} + \Gamma^\kappa_{\nu\gamma} S^{\mu\gamma}) = -\frac{1}{2} R_{\nu\omega\lambda\chi} \frac{\partial H}{\partial P_\omega} S^{\lambda\chi}\,, \tag{3.34b}$$

$$\begin{aligned}&\frac{\mathrm{d}S^{\gamma\kappa}}{\mathrm{d}\lambda} + \Gamma^\gamma_{\nu\lambda} \frac{\partial H}{\partial P_\nu} S^{\lambda\kappa} + \Gamma^\kappa_{\nu\lambda} \frac{\partial H}{\partial P_\nu} S^{\gamma\lambda} = \\ &\frac{\partial H}{\partial S^{\mu\nu}}(g^{\gamma\mu} S^{\kappa\nu} - g^{\gamma\nu} S^{\kappa\mu} + g^{\kappa\nu} S^{\gamma\mu} - g^{\kappa\mu} S^{\gamma\nu})\,,\end{aligned} \tag{3.34c}$$

where λ is some parameter along the trajectory. These equations cannot be expected to make any sense on the full phase space, but only on the part where some supplementary condition $S^{\mu\nu} V_\nu = 0$ holds.

By comparison with equations (3.5), the equations (3.34) will be the MPD equations when the following equalities are fulfilled

$$\frac{\partial H}{\partial S^{\mu\nu}}(g^{\gamma\mu} S^{\kappa\nu} + \text{perm.}) \cong P^\kappa \frac{\partial H}{\partial P_\gamma} - P^\gamma \frac{\partial H}{\partial P_\kappa}\,, \tag{3.35}$$

$$\frac{\partial H}{\partial x^\nu} - \frac{\partial H}{\partial S^{\mu\kappa}}(\Gamma^\mu_{\nu\gamma} S^{\gamma\kappa} + \Gamma^\kappa_{\nu\gamma} S^{\mu\gamma}) \cong -\Gamma^\alpha_{\beta\nu} \frac{\partial H}{\partial P_\beta} P_\alpha\,, \tag{3.36}$$

where $\cong$ means that the equalities need to hold only on a certain "on-shell" part of the phase space where conditions such as $S^{\mu\nu} V_\nu = 0$ hold. The fact that the equalities are $\cong$ makes them impractical to solve directly and we resort to heuristic approaches.

3.3.3 Hamiltonian for KS condition

Khriplovich [130], inspired by field theory on curved background, postulated the following Hamiltonian for semi-classical spinning particles which is supposed to be used along the

Poisson brackets (3.29) (see also d'Ambrosi et al. [66])

$$H_{\mathrm{KS}} = \frac{1}{2m} g^{\mu\nu} P_\mu P_\nu \cong -\frac{m}{2}. \tag{3.37}$$

However, at the time of the publication of this Hamiltonian it was not clear what is the relation of the generated set of equations with the MPD equations. Nevertheless, we can now compare the generated equations of motion (3.34) with those corresponding to the relatively recently discovered KS supplementary spin condition (3.13) to see that the two sets of equation agree.

In other words, the Hamiltonian (3.37) generates the MPD equations of motion under the KS spin condition. The only condition that needs to be met by the initial condition apart from four-velocity normalization is for $S^{\mu\nu}$ to have some vanishing time-like direction w^ν, $S^{\mu\nu} w_\nu = 0$.

3.3.4 Hamiltonian for TD condition

The basis of our heuristic approach is to first reproduce the momentum-velocity relation under the TD condition and see whether this is sufficient to determine the correct Hamiltonian. We take the velocity-momentum relation (3.18) and combine it with equation (3.34a) to obtain

$$\frac{\partial H}{\partial P_\nu} \cong \frac{m}{\mathscr{M}^2} \left(P^\nu + \frac{2 S^{\nu\mu} R_{\mu\gamma\kappa\lambda} P^\gamma S^{\kappa\lambda}}{4\mathscr{M}^2 + R_{\chi\eta\omega\xi} S^{\chi\eta} S^{\omega\xi}} \right). \tag{3.38}$$

Now let us assume that the equations of motion hold under the on-shell conditions $\mathscr{M} = \sqrt{-P^\alpha P_\alpha}$, $S^{\mu\nu} P_\nu = 0$ where $\mathscr{M}$ is now some chosen constant independent of phase-space coordinates. Then the following holds

$$\frac{\partial}{\partial P_\omega} \left[(g^{\mu\nu} P_\mu P_\nu + \mathscr{M}^2) F \right] \cong 2 F P^\omega, \tag{3.39}$$

$$\frac{\partial}{\partial P_\omega} \left(G_\mu S^{\mu\nu} P_\nu \right) \cong G_\mu S^{\mu\omega}, \tag{3.40}$$

where F, G_μ are arbitrary functions of the phase-space coordinates $x^\kappa, P_\lambda, S^{\gamma\delta}$. By choosing appropriate F, G_μ, we are able to reproduce all the terms on the right hand side of (3.38) and thus obtain the Hamiltonian

$$H_{\mathrm{TD}} = \frac{m}{2\mathscr{M}^2} \left[\left(g^{\mu\nu} - \frac{4 S^{\nu\gamma} R^{\mu}{}_{\gamma\kappa\lambda} S^{\kappa\lambda}}{4\mathscr{M}^2 + R_{\chi\eta\omega\xi} S^{\chi\eta} S^{\omega\xi}} \right) P_\mu P_\nu + \mathscr{M}^2 \right] \cong 0, \tag{3.41}$$

where we substitute the expression (3.19) for m. A straight-forward computation of Hamilton's equations of motion then shows that they agree with the MPD equations of motion under the TD supplementary condition.

An interesting result discussed in Appendix A.4 is that the Hamiltonian (for a different time parametrization, $\lambda \neq \tau$) can be obtained by applying $S^{\mu\nu}P_\nu = 0$ as a Hamiltonian constraint of the Khriplovich Hamiltonian (3.37). However, this procedure does not seem to work for any other supplementary condition.

3.3.5 Hamiltonian for MP condition

Similarly to the heuristic approach of the previous subsection, we are now trying to derive a Hamiltonian that generates the MP momentum-velocity relation (3.15)

$$\frac{\partial H}{\partial P_\mu} \cong \frac{1}{m} P^\nu \left(\delta^\mu_\nu - \frac{1}{S^2} S^{\mu\kappa} S_{\nu\kappa} \right) . \tag{3.42}$$

We can compose it from the single on-shell condition $P_\mu P_\nu (g^{\mu\nu} - S^{\mu\kappa} S^\nu_{\ \kappa}/S^2) = -m^2$ similarly to the previous section (m is now a fixed number independent of the phase-space variables) to obtain

$$H_{\mathrm{MP}} = \frac{1}{2m} \left(g^{\mu\nu} - \frac{1}{S^2} S^{\mu\kappa} S^\nu_{\ \kappa} \right) P_\mu P_\nu \cong -\frac{m}{2} . \tag{3.43}$$

Once again, the computation of the equations of motion shows that they are identical to the MPD equations under the MP condition.

3.3.6 Hamiltonians for CP and NW conditions?

Let us now attempt to reproduce the linearized NW/CP momentum-velocity relation (3.28)

$$m \frac{\partial H}{\partial P_\mu} = P^\mu - \left(S^{\kappa\mu} + \frac{1}{m^2} S^{\kappa\omega} P_\omega P^\mu \right) \frac{\xi_{\kappa;\lambda} P^\lambda}{(m\xi_\chi + \alpha P_\chi) P^\chi} . \tag{3.44}$$

We use the on-shell condition $P^\mu P_\mu = -m^2 + \mathcal{O}(S^2)$ and $S^{\kappa\mu}(\alpha P_\mu/m + \xi_\mu) = 0$ to build the unique Hamiltonian that reproduces the relation above

$$H_{\mathrm{NW/CP?}} = \frac{1}{2m} g^{\mu\nu} P_\mu P_\nu - \frac{1}{\alpha} \frac{\xi_{\kappa;\lambda} P^\lambda}{(m\xi_\chi + \alpha P_\chi) P^\chi} S^{\kappa\mu} \left(\alpha \frac{P_\mu}{m} + \xi_\mu \right) . \tag{3.45}$$

However, the computation of Hamilton's equations related to this Hamiltonian show that they are *not* a set of MPD equations of the form (3.5). It is thus probably possible to cast the NW/CP+MPD system into Hamiltonian form only through a more sophisticated set of variables such as in Refs. [110, 215, 24, 280].

3.3.7 Coordinate-time parametrization

All of the Hamiltonians derived in the previous subsections generate motion parametrized by proper time τ. It is possible to generalize them to any time parametrization λ with $\mathrm{d}\lambda/\mathrm{d}\tau$ an arbitrary function of any variables by exploiting the fact that the Hamiltonians have a constant value for any trajectory. We can then get the new λ-Hamiltonians as

$$H_\lambda = \left(\frac{\mathrm{d}\lambda}{\mathrm{d}\tau}\right)^{-1}(H_\tau - H_0)\,. \tag{3.46}$$

The constant H_0 is $-m/2$ for the KS and MP Hamiltonians (3.37) and (3.43), and 0 for the TD Hamiltonian (3.41). These Hamiltonians evolve the full set of variables $x^\mu, P_\nu, S^{\gamma\kappa}$.

Alternatively, it is also possible to use the component of "non-covariant" momentum p_t from eq. (3.31) expressed as a function of the other variables to generate the equations of motion parametrized by coordinate time t. To show this in the simplest possible way, we pass to the coordinates p_μ, S^{AB} defined in equations (3.30) and (3.31). We compute

$$\frac{\mathrm{d}p_i}{\mathrm{d}t} = -\frac{\partial H}{\partial x^i}\left(\frac{\partial H}{\partial p_t}\right)^{-1} = -\frac{\partial(-p_t)}{\partial x^i}\Big|_{H=\text{const.}}, \tag{3.47}$$

$$\frac{\mathrm{d}x^i}{\mathrm{d}t} = \frac{\partial H}{\partial p_i}\left(\frac{\partial H}{\partial p_t}\right)^{-1} = \frac{\partial(-p_t)}{\partial p_i}\Big|_{H=\text{const.}}, \tag{3.48}$$

$$\begin{aligned}\frac{\mathrm{d}S^{AB}}{\mathrm{d}t} &= \{S^{AB}, S^{CD}\}\frac{\partial H}{\partial S^{CD}}\left(\frac{\partial H}{\partial p_t}\right)^{-1} \\ &= \{S^{AB}, S^{CD}\}\frac{\partial(-p_t)}{\partial S^{CD}}\Big|_{H=\text{const.}},\end{aligned} \tag{3.49}$$

where we have used the implicit function theorem. In other words, for any phase-space function $F(x^i, P_i, S^{AB})$

$$\frac{\mathrm{d}F}{\mathrm{d}t} = \{F, -p_t\Big|_{H=const.}\}\,. \tag{3.50}$$

We now list the respective Hamiltonians $H_t = -p_t|_{H=const.}$ for the KS, TD, and MP spin conditions, given here in terms of the phase-space coordinates $P_\mu, S^{\kappa\lambda}$

$$H_{t\mathrm{KS}} = -P_i\omega^i + \sqrt{\alpha^2 m^2 + \gamma^{ij}P_iP_j} + \frac{1}{2}\Gamma_{\nu\kappa t}S^{\nu\kappa}, \tag{3.51}$$

$$\omega^i \equiv -\frac{g^{ti}}{g^{tt}}, \ \alpha \equiv \frac{1}{\sqrt{-g^{tt}}}, \ \gamma^{ij} = -\frac{g^{ij}}{g^{tt}} + \omega^i\omega^j, \tag{3.52}$$

$$H_{t\mathrm{TD}} = -P_i\tilde{\omega}^i + \sqrt{\tilde{\alpha}^2\mathscr{M}^2 + \tilde{\gamma}^{ij}P_iP_j} + \frac{1}{2}\Gamma_{\nu\kappa t}S^{\nu\kappa}, \tag{3.53}$$

$$\tilde{g}^{\mu\nu} \equiv g^{\mu\nu} + \frac{4S^{\gamma(\nu}R^{\mu)}{}_{\gamma\kappa\lambda}S^{\kappa\lambda}}{4\mathscr{M}^2 + R_{\chi\eta\omega\xi}S^{\chi\eta}S^{\omega\xi}}, \tag{3.54}$$

$$\tilde{\omega}^i \equiv -\frac{\tilde{g}^{ti}}{\tilde{g}^{tt}}, \ \tilde{\alpha} \equiv \frac{1}{\sqrt{-\tilde{g}^{tt}}}, \ \tilde{\gamma}^{ij} = -\frac{\tilde{g}^{ij}}{\tilde{g}^{tt}} + \tilde{\omega}^i\tilde{\omega}^j, \tag{3.55}$$

$$H_{t\mathrm{MP}} = -P_i\bar{\omega}^i + \sqrt{\bar{\alpha}^2 m^2 + \bar{\gamma}^{ij}P_iP_j} + \frac{1}{2}\Gamma_{\nu\kappa t}S^{\nu\kappa}, \tag{3.56}$$

$$\bar{g}^{\mu\nu} \equiv g^{\mu\nu} - \frac{1}{S^2}S^{\mu\kappa}S^{\nu}{}_{\kappa}, \tag{3.57}$$

$$\bar{\omega}^i \equiv -\frac{\bar{g}^{ti}}{\bar{g}^{tt}}, \ \bar{\alpha} \equiv \frac{1}{\sqrt{-\bar{g}^{tt}}}, \ \bar{\gamma}^{ij} = -\frac{\bar{g}^{ij}}{\bar{g}^{tt}} + \bar{\omega}^i\bar{\omega}^j, \tag{3.58}$$

where we have chosen roots of p_t corresponding to particles traveling forward in time.

Now the reduced set of variables, to be evolved by the spatial part of the Poisson brackets (3.29) and the Hamiltonians above, is $x^i, P_j, S^{\mu\kappa}$. Alternatively, one can rewrite the Hamiltonians using the variables x^i, p_j, S^{AB} and use the spatial part of the brackets (3.32).

3.4 Canonical coordinates for numerical integration

In this section I discuss further details about the structure of the phase space. Constraints such as the supplementary spind conditions define sub-manifolds in this phase space, and the correct way to "project" the Poisson brackets on this sub-manifold is called the Dirac constraint procedure [73, 109]. On the other hand, independent of whether the Poisson bracket has or has not been "projected", we know that we can always construct local coordinates on the phase space that put the bracket into canonical form. These two topics are discussed in the upcoming two subsections in respective order.

3.4.1 Importance of canonical coordinates and Dirac brackets

Let us assume that we have a set of constraints $\Phi^a = 0$, where a, b are some labelling indices, and that the constraint algebra $C^{ab} = \{\Phi^a, \Phi^b\}$ with C^{ab} is a non-degenerate matrix with an inverse C^{-1}_{ab}. Then it is possible to define a new constrained Poisson bracket [73, 109]

$$\{A,B\}' = \{A,B\} - \{A,\Phi^a\} C^{-1}_{ab} \{\Phi^b, B\} \,. \tag{3.59}$$

The bracket $\{,\}'$ is often called the Dirac or Dirac-Poisson bracket. If we have a Hamiltonian that fulfills $\{\Phi^a, H\} \cong 0$, then the equations of motion generated by $\{,\}'$ and H are the same as with $\{,\}$ and H. The bracket-constraining procedure was originally devised for the purposes of canonical quantization. Nonetheless, it is also useful for classical Hamiltonian dynamics.

When we want to study the evolution of a classical Hamiltonian system at high accuracy over a large number of periods (such as would be the case of EMRIs), it is highly advantageous to use symplectic integration [see e.g. 107]. Most symplectic integrators require that the equations are formulated in terms of pairs of canonical coordinates, i.e. a colection of phase-space coordinates χ^i, π_i, with i some labelling index, such that $\{\chi^i, \pi_j\} = \delta^i_j$ (however, there do exist symplectic integrators for special classes of systems that require no such coordinates [171, 170]).

The importance of the constrained bracket $\{,\}'$ in these considerations can be twofold. First, it may be easier to find canonical coordinates for $\{,\}'$ rather than $\{,\}$. Second, the constraints $\Phi^a = 0$ are only integrals of motion with respect to the dynamical system evolved by the unconstrained bracket $\{,\}$, and they cannot be forced to be zero during integration, otherwise the advantageous properties of the symplectic algorithm are broken. On the other hand, in the case of the bracket $\{,\}'$, the constraints Φ^a commute with any phase-space variable. In return, they are effectively promoted to a "phase-space identity" and can be used to reduce the number of variables in a numerical integrator symplectic with respect to $\{,\}'$.

For instance, Barausse et al. [24] applied the NW supplementary spin condition as a constraint to the bracket (3.32) (along with brackets and constraints for auxilliary variables) to obtain, at least at linear order in spin, a simplified bracket for the reduced number of variables p_μ, x^ν, S^{IJ} (see subsection 3.2.4). This system was then easy to cover by approximate canonical coordinates and thus to study by symplectic integration [158].

Concerning the possibility to reduce the variables in the case of other supplementary conditions, the TD condition $S^{\mu\nu}P_\nu = 0$ applied as a constraint leads to a very complicated Dirac bracket that mixes the spin and momentum degrees of freedom. As a result, it is very difficult to find the canonical coordinate basis for the TD-constrained bracket.

Then again, as discussed in subsections 3.2.1 and 3.2.2, the KS and MP condition in fact do not allow to reduce the number of evolved variables to the same extent as the TD and NW/CP conditions. A closer inspection shows that the KS and MP conditions cannot even be formulated as a constraint on the phase space p_μ, x^ν, S^{AB}, and the Poisson bracket will thus always be (3.32). Hence, for the purposes of the TD, KS, and MP conditions we have decided to find the canonical coordinates covering the full phase-space p_μ, x^ν, S^{AB} for the unconstrained bracket (3.32).

3.4.2 Canonical coordinates on the spin sector

The p_μ, x^ν part of the phase-space coordinates is already canonical, so we are looking for canonical coordinates covering the spin tensor S^{AB}. To find the canonical coordinates, we mimic the procedure of Tessmer et al. [263] by expressing S^{AB} as a simple constant tensor $S^{\hat{A}\hat{B}}$ in some "body-fixed frame" plus a Lorentz transformation $\Lambda^A{}_{\hat{A}}$ into the "background frame" e^A_μ. The parameters of the transformation, when chosen appropriately, then turn out to be canonically conjugate pairs of coordinates.

The details of the procedure are described in Appendix A.5, and I only summarize here the resulting coordinates

$$A = S^{12} - \sqrt{(S^{12})^2 + (S^{23})^2 + (S^{31})^2}\,, \tag{3.60a}$$

$$B = \sqrt{(S^{12})^2 + (S^{23})^2 + (S^{31})^2} - S\,, \tag{3.60b}$$

$$\phi = \arctan\left(\frac{S^{31}}{S^{23}}\right)\,, \tag{3.60c}$$

$$\psi = \arctan\left(\frac{S^{31}}{S^{23}}\right) - \arccos\left(S^{03}\sqrt{\mathscr{C}}\right)\,, \tag{3.60d}$$

$$\mathscr{C} = \frac{(S^{12})^2 + (S^{23})^2 + (S^{31})^2}{[(S^{13})^2 + (S^{23})^2]\,[(S^{01})^2 + (S^{02})^2 + (S^{03})^2]}\,. \tag{3.60e}$$

Even though the construction in Appendix A.5 provides the derivation of these coordinates, one may simply compute their Poisson brackets directly. The brackets then are $\{\phi, A\} = \{\psi, B\} = 1$ and 0 otherwise.

The inverse transformations from the canonical coordinates to the spin tensor read

$$S^{01} = \mathscr{D}\left[A\cos(2\phi-\psi)+(A+2B+2S)\cos\psi\right], \tag{3.61a}$$
$$S^{02} = \mathscr{D}\left[A\sin(2\phi-\psi)+(A+2B+2S)\sin\psi\right], \tag{3.61b}$$
$$S^{03} = -2\mathscr{D}\mathscr{E}\cos(\phi-\psi), \tag{3.61c}$$
$$S^{12} = A+B+S, \tag{3.61d}$$
$$S^{23} = -\mathscr{E}\cos\phi, \tag{3.61e}$$
$$S^{31} = \mathscr{E}\sin\phi, \tag{3.61f}$$
$$\mathscr{D} = -\frac{\sqrt{B(B+2S)}}{2(B+S)}, \tag{3.61g}$$
$$\mathscr{E} = \sqrt{-A(A+2B+2S)}. \tag{3.61h}$$

The coordinates cover the space of general antisymmetric tensors with a degenerate time-like direction and a closer consideration reveals a number of similarities with hyperspherical coordinates in $\mathbb{R}^4$.

The canonical coordinates have singularities at $B=0$ and $A=0,-2(B+S)$, which have the character similar to those of the singularities at $r=0$ and $\cos(\vartheta)=1,-1$ in spherical coordinates in $\mathbb{R}^3$. As a result, the physical coordinate ranges then are $B\in(0,\infty)$ and $A\in(-2(B+S),0)$. The coordinates ϕ,ψ are simple angular coordinates similar to the azimuthal angle φ in spherical coordinates in $\mathbb{R}^3$, and they both run in the $[0,2\pi)$ interval. More details about the coordinate singularities are discussed in Appendix A.5.

One last remark I would like to draw attention to is that the coordinates ϕ,ψ are dimensionless and have finite limits as $S\to 0$, whereas A,B have the dimension of the spin and should generally go to zero when $S\to 0$. However, if we keep $a\equiv A/S, b\equiv B/S$ finite, then the evolution of the coordinates a,b,ϕ,ψ can be used to track the evolution of a "test spin", i.e. an intrinsic spin of the particle that is transported along the trajectory while not exerting any back-reaction on the orbit itself.

There is a special limiting case when A,B can remain finite while $S\to 0$, and that corresponds to the body-fixed frame being infinitely boosted with respect to the background frame and the vanishing direction of the spin tensor becoming light-like. This particular limit may be useful for the description of massless particles with spin but we consider it to be physically meaningless for the current context of massive bodies.

3.5 Special planar motion

I will now present the results of a small showcase study we conducted in [293] that allows to demonstrate the power and character of the canonical coordinates. We considered motion in the equatorial plane of the Schwarzschild space-time under the KS condition. Then we required that both the four-velocity and the spin tensor are initially vanishing in the ϑ direction, $S^{\mu\vartheta} = 0, = \dot{\vartheta} = 0$. One can then easily compute that

$$\frac{\mathrm{d}^2\vartheta}{\mathrm{d}\tau^2} = 0\,, \tag{3.62}$$

$$\frac{\mathrm{d}S^{\mu\vartheta}}{\mathrm{d}\tau} = 0\,. \tag{3.63}$$

In other words, the conditions $S^{\mu\vartheta} = 0$, $\dot{\vartheta} = 0$ are satisfied throughout the motion.

A similar system restricted to the equatorial plane can be formulated by requiring $P_\vartheta = S^{\mu\vartheta} = 0$ also for the MP and TD conditions, and, furthermore, the background could be generalized to the Kerr space-time. However, we chose to study the special planar problem only in the KS incarnation and in the Schwarzschild space-time because of its simplicity.

It should also be noted that this system is *more general* than the motion of a particle with the spin vector aligned in a normal direction to the equatorial plane; such motion can be acquired from the system described below by setting $B = 0$. However, for $B \neq 0$ the motion is different from the aligned-spin case. The spin vector undergoes nutations and exerts non-uniform torques on the orbit that, nonetheless, never push the worldline out of the equatorial plane.

3.5.1 The Hamiltonian

For our computations, we chose the coordinate-aligned tetrad in the usual Schwarzschild coordinates t, φ, r, ϑ: $e^0_\mu = \sqrt{-g_{tt}}\delta^t_\mu$, $e^1_\mu = \sqrt{g_{\varphi\varphi}}\delta^\varphi_\mu$, $e^2_\mu = \sqrt{g_{rr}}\delta^r_\mu$, $e^3_\mu = \sqrt{g_{\vartheta\vartheta}}\delta^\vartheta_\mu$. The choice of the tetrad and even the order of the legs are important for the final form of the Hamiltonian and the physical interpretation of the quantities appearing in it. However, the choice of the tetrad never matters for the real physical evolution of the KS, TD, or MP conditions (unlike in the case of the NW/CP condition where the choice $\sim \xi^\mu \sim e^\mu_0$ is crucial [140]).

The condition $S^{\vartheta\mu} = 0$ then means either $A = 0$ or $A = -2(B+S)$ for $S^{12} > 0$ and $S^{12} < 0$ respectively. Here we chose $S^{12} > 0$, and ϕ thus becomes a redundant coordinate (see more details in Appendix A.5). In a typical right-hand-oriented interpretation and for an orbit with positive $\dot{\varphi}$, this corresponds to a spin vector counter-aligned to the orbital angular-momentum vector.

Finally, the Hamiltonian (3.37) expressed in canonical coordinates in the case of the special planar motion reads

$$H_{\mathrm{SP}} = \frac{1}{2m}\left[\frac{-1}{1-2M/r}\left(p_t - \frac{M\sqrt{B(B+2S)}\sin\psi}{r^2}\right)^2 + \left(1-\frac{2M}{r}\right)p_r^2 + \frac{1}{r^2}\left(p_\varphi - \sqrt{1-\frac{2M}{r}}(B+S)\right)^2\right]. \tag{3.64}$$

The system has two obvious integrals of motion p_φ, p_t, since the coordinates t, φ are cyclic. However, it should be noted that the orbital angular momentum and energy will generally vary during the evolution since they relate to the phase-space coordinates as

$$u_t = \frac{1}{m}\left(p_t - \frac{M\sqrt{B(B+2S)}\sin\psi}{r^2}\right), \tag{3.65}$$

$$u_\varphi = \frac{1}{m}\left(p_\varphi - \frac{r^{5/2}(B+S)}{\sqrt{r-2M}}\right). \tag{3.66}$$

3.5.2 Poincaré surfaces of section

We constructed the special planar problem so that only two degrees of freedom become dynamically important, r, p_r, and ψ, B. Since the trajectory is also constrained by four-velocity normalization, all the phase-space trajectories of a given p_φ, p_t are then confined to a 3-dimensional hypersurface. We made a natural Poincaré surface of section through this hypersurface by sampling this set of trajectories and recording the phase-space variables every time ψ finishes a 2π cycle. Thanks to this construction, we obtained well-defined 2D Poincaré surface of section, whereas in the general case the surface of section becomes higher-dimensional and new methods need to be employed for visualization [see 157].

We integrated the trajectories using the 6-th order Gauss collocation scheme with a fixed-point iteration of the collocation points [see, e.g., 107]. Additionally, we exploited the parametrization invariance of the trajectory by using a time parameter λ such that

$$\frac{\mathrm{d}\lambda}{\mathrm{d}\tau} = \frac{r_0^2}{r(r-2M)}\frac{S}{\sqrt{B(B+2S)}+\varepsilon}, \tag{3.67}$$

where ε, r_0 are constants we set to $10^{-4}, 10M$ respectively. This effective time-stepping does not spoil the symplecticity of the integrator because the respective equations of motion can be generated by a Hamiltonian of the form (3.46).

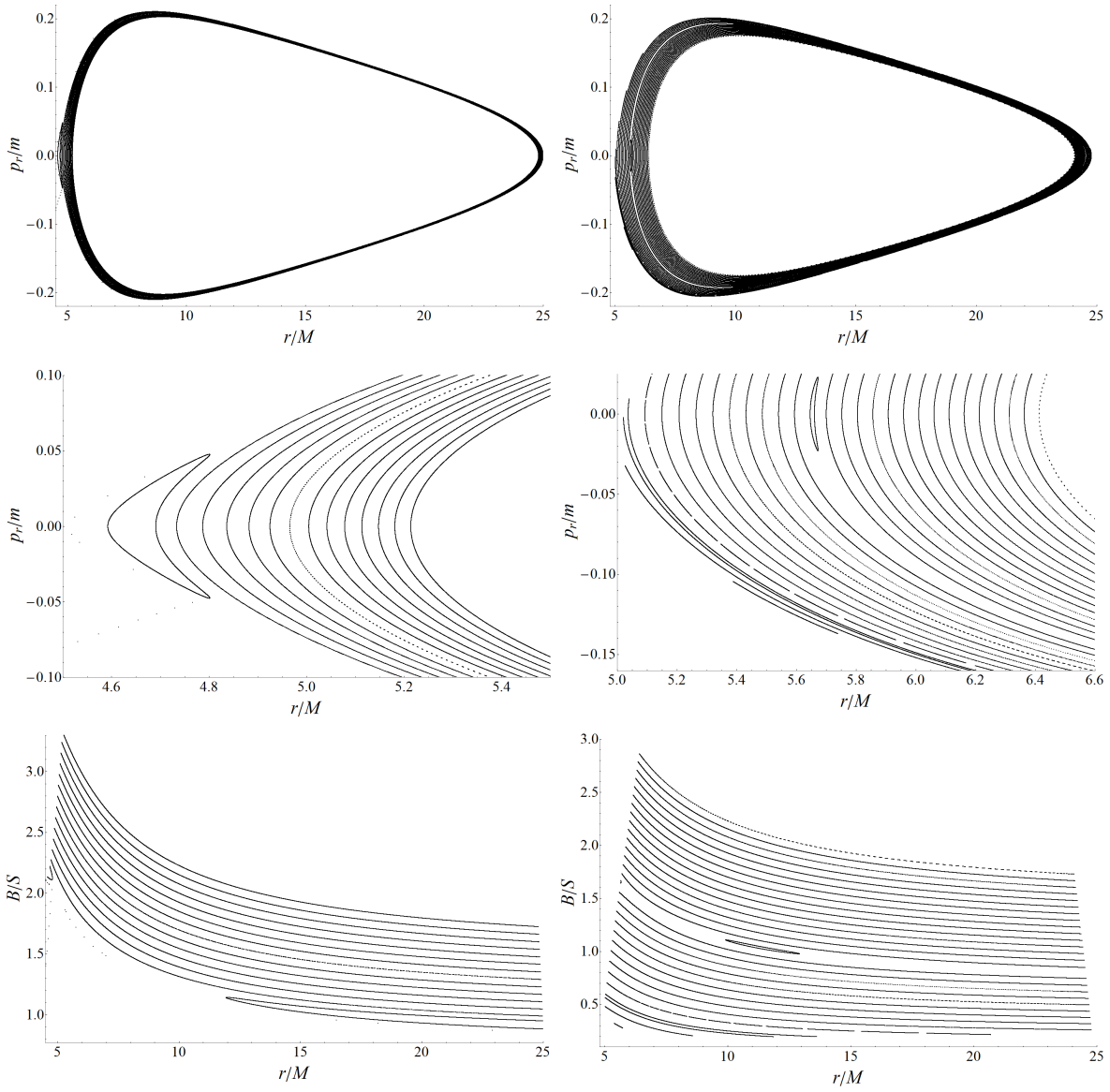

Fig. 3.1 Poincaré surfaces of section for the special planar problem at $p_t/m = -0.97, p_\varphi/m = 3.7M$ created by snapshots after every 2π-cycle in the spin-angle ψ. The left column corresponds to $S/m = 0.05M$ and the right column to $S/m = 0.1M$. The outer parts of the nested sections correspond to small B/S whereas the inner parts to growing B/S. The left column features a smaller number of orbits because the "outer" orbits are not bound and plunging into the black hole.

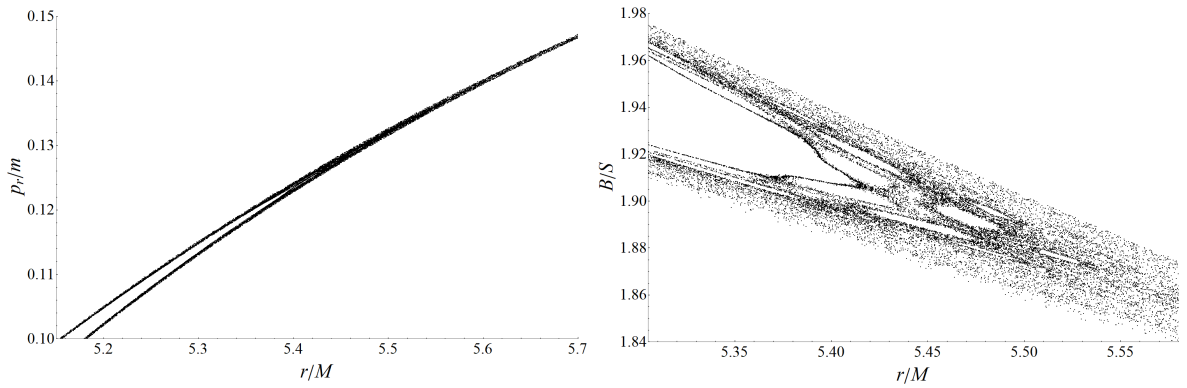

Fig. 3.2 Detail of a Poincaré surface of section of a single chaotic trajectory at $p_t/m = -0.97, p_\varphi/m = 3.7M, S/m = 0.05M$ (compare with left column of fig. 3.1). The trajectory was integrated over $\sim 10^5$ spin cycles ($\sim 10^4$ orbital cycles). For more than a half of that time the orbit would stay in the "darker" fractal layer around the resonance to be later released into the general separatrix chaos.

With this theoretical construction in place and by using a standard single-thread computation in C++, we were able to integrate through 10^4 spin cycles within minutes at a relative error less than 10^{-12} in the four-velocity normalization. Of course, such efficiency and long-term accuracy would hardly be possible without the canonical coordinates and geometrical integration. This is an important point of the present section.

Generally speaking, the dimensionless parameter $S/(Mm)$ can be understood as a perturbation strength non-linearly coupling two exactly integrable systems, the geodesic motion in Schwarzschild space-time, and the parallel transport of the "test spin" on top of that geodesic. As such, the dependence of the phase portrait of the special planar problem on the particle spin should have the same characteristics as any weakly non-integrable system [e.g. 16]: The originally smooth phase-space foliation by regular oscillations of the trajectories should now feature occasional "breaks" in the form of resonances and thin chaotic layers.

In order to show and demonstrate the presence of such structures, we probed values of p_t, p_φ so that phase-space trajectories in the studied congruence are near unstable circular orbits in the original geodesic flow. This is because the neighboring phase space also contains the "homoclinic" infinite whirl-zoom orbits that are well known to act as "seeds of chaos" in perturbed black hole space-times [see, e.g., 240, 241, 256, 292]. However, as can be seen from equations (3.65) and (3.66), the variations of S also have the unfortunate effect of shifting the meaning of p_t, p_φ, and this easily pushes us into the phase-space regions of orbits plunging into the black hole.

As already discussed in section 3.1, we should be already imposing self-force effects along with the spin-force even for the smallest values of $S/(mM)$ in a self-consistent physical model. Thus, it does not make sense to study the influence of the spin beyond perturbation-like values and we chose to study only $S/(mM) \leq 0.1$.

In addition, the ratio B/S is equal to $\gamma - 1$, where γ is the usual gamma factor of the Lorentz boost from the body-fixed frame to the background frame (see Appendix A.5). The unconstrained nature of the KS condition allows this γ to be arbitrary, but we believe that if it becomes too large, the world-line becomes shifted outside of the interior of the real physical body, and the system of equations instead obtains the character of some sort of perturbed geodesic-deviation equation. Hence, we only allow $B/S \lesssim 5$ in our initial conditions.

I show two Poincaré surfaces of section in the relevant ranges in fig. 3.1. In these sections, we were able to find resonances corresponding to ratios as low as $1:1$ or $1:2$ in the spin-orbital frequencies. Additionally, small chaotic layers can be found near the saddle points of the resonant chains (see fig. 3.2).

As we went to smaller values of $S/(mM) \lesssim 0.01$, the resonances became extremely thin, and most of the chaotic structure had to be disqualified based on the criterion $B/S \lesssim 5$. If we were to ignore the B/S criterion and allowed $B/S \gtrsim 10$, we could find chaos up to $S/(mM) \sim 10^{-3}$.

3.5.3 Comparison with previous results

Let me now briefly compare these results with the study of Lukes-Gerakopoulos et al. [157], who studied the chaotization of general orbits of spinning particles in Kerr space-time while using the NW-condition Hamiltonian of Barausse et al. [24]. The motion of non-planar orbits with general spin orientations leads to richer dynamics, as an additional degree of freedom enters the interactions. Consequently, Lukes-Gerakopoulos et al. found chaotic motion in the phase space until $S/(mM) = 10^{-3}$.

At face value, it might not be obvious whether our findings are in tension or in agreement with those of Lukes-Gerakopoulos et al. [157]. As discussed in subsection 3.2.4, the NW condition constrains one more degree of freedom than the KS condition. Consequently, an analogous special planar motion $P^\vartheta = \dot{x}^\vartheta = S^{\mu\vartheta} = 0$ would in fact have only a single active degree of freedom under the NW condition and would thus be integrable at any value of spin. Additionally, even the non-planar motion under the NW Hamiltonian of Barausse et al. [24] is integrable to linear order in S in Schwarzschild space-time, at least under the right choice of ξ^μ [140].

In this sense, our study added a result to this chain of research by showing that the KS+MPD system is not integrable in Schwarzschild space-time even in the planar case. Hence, one should be cautious in issuing general statements about the (non)-integrability and chaos in MPD

equations near black holes, because such statements seem to be dependent on the context and approximations made.

It is difficult to study weakly chaotic systems in a systematic manner, but it would be interesting to see whether we can identify for each supplementary condition to which perturbation order the non-integrability corresponds. For instance, if the system is non-integrable at linear-in-spin order, then the resonant layers should grow as $\sim \sqrt{S/(mM)}$. On the other hand, if it is integrable to that order and integrability is broken only at quadratic order, the resonances should grow as $\sim S/(mM)$. A well designed survey of these properties could help clarify the questions of integrability and non-integrability for spinning particles near black holes, and I suggest this as a possibility for future studies.

3.6 Hamilton-Jacobi equation for spinning particles

Having a set of canonical coordinates in hand, it is possible to formulate a Hamilton-Jacobi equation. We simply need to postulate an action $W(x^\mu, \psi, \phi)$, insert its gradients in place of the respective momenta in any of the Hamiltonians (3.37), (3.41) or (3.43), and solve the resulting partial differential equation. In this section, I present how to do so perturbatively in the Kerr space-time.

3.6.1 Perturbative problem

Let us now compute the first perturbation to the Hamilton-Jacobi equation for an action $W(r,t,\varphi,\vartheta,\psi,\phi)$ corresponding to either the Hamiltonian (3.37) or (3.41). Note that the action is also dependent on the coordinates ϕ, ψ, and $A = W_{,\phi}, B = W_{,\psi}$. The spin-tensor components are then given functions of these variables as given in equations (3.61).

The zeroth iteration of the Hamilton-Jacobi equation neglects all spin-dependent terms and we obtain

$$g^{\mu\nu} W^{(0)}_{,\mu} W^{(0)}_{,\nu} = -1\,, \tag{3.68}$$

which is just the geodesic problem with the well-known solution by Carter [49] presented in section 1.4.

Let us now iterate the Hamilton Jacobi equation with a new action that is assumed to fulfill $W^{(1)} = W^{(0)} + \mathscr{O}(S^\alpha)$ with some $\alpha > 0$. If we then allow only for the lowest-order correction to the Hamilton-Jacobi equation coming either from the TD Hamiltonian (3.41) or the KS

Hamiltonian (3.37), we obtain

$$g^{\mu\nu}W^{(1)}_{,\mu}W^{(1)}_{,\nu} - e_{A\kappa}e^{\kappa}_{B;\nu}S^{AB}W^{(0),\nu} = -1 \tag{3.69}$$

Now it appears that the choice of the tetrad e^{μ}_{A} and thus also implicitly the orientation of the canonical coordinates on the spin tensor will be crucial to the separability of the problem.

3.6.2 Adapted tetrad

Let us construct a special "geodesic-adapted" tetrad which turns out to be identical to that of Marck [162]. We take a geodesic congruence $u^{\mu}_{\rm c} = W_{(0),\mu}$ with Carter constant $K_{\rm c}$, azimuthal specific angular momentum $L_{\rm c}$ and specific energy $E_{\rm c}$. The zeroth leg of the tetrad is then defined as the geodesic four-velocity $e^{\mu}_{0} = u_{{\rm c}\mu}$, the third leg as $e^{3}_{\mu} = Y_{\mu\nu}u^{\nu}_{\rm c}/\sqrt{K_{\rm c}}$, where $Y_{\mu\nu}$ is the Killing-Yano tensor in the Kerr metric, and the two other legs read

$$e^{1}_{\mu} = \frac{1}{\sqrt{K^{(2)}_{\rm c} + K^{2}_{\rm c}}}\left(K_{\mu\nu} + K_{\rm c}g_{\mu\nu}\right)u^{\nu}_{\rm c}\,, \tag{3.70}$$

$$e^{2}_{\mu} = \frac{1}{\sqrt{K^{(3)}_{\rm c} - (K^{(2)}_{\rm c})^{2}/K_{\rm c}}}\left(K_{\mu\nu} - \frac{K^{(2)}_{\rm c}}{K_{\rm c}}g_{\mu\nu}\right)Y^{\nu}_{\ \kappa}u^{\kappa}_{\rm c}\,, \tag{3.71}$$

$$K^{(2)}_{\rm c} = K_{\mu\nu}K^{\nu}_{\ \kappa}u^{\mu}_{\rm c}u^{\kappa}_{\rm c}\,, \tag{3.72}$$

$$K^{(3)}_{\rm c} = K_{\mu\nu}K^{\nu}_{\ \kappa}K^{\kappa}_{\ \gamma}u^{\mu}_{\rm c}u^{\gamma}_{\rm c}\,. \tag{3.73}$$

$$\tag{3.74}$$

Thanks to this construction a number of projections of the spin connection components into the four-velocity vanish as $e^{0}_{\mu;\nu}u^{\mu}_{\rm c} = e^{3}_{\mu;\nu}u^{\mu}_{\rm c} = 0$.The only nonzero components of $e_{A\kappa}e^{\kappa}_{B;\nu}W^{(0),\nu}$ then are $e_{1\kappa}e^{\kappa}_{2;\nu}W^{(0),\nu} = -e_{2\kappa}e^{\kappa}_{1;\nu}W^{(0),\nu}$ and one can obtain with the strong assistance of computer algebra

$$e_{1\kappa}e^{\kappa}_{2;\nu}W^{(0),\nu} = \frac{\sqrt{K_{\rm c}}}{\Sigma}\left(\frac{E_{\rm c}(r^2+a^2) - aL_{\rm c}}{r^2 + K_{\rm c}} - a\frac{L_{\rm c} - aE_{\rm c}\sin^2\vartheta}{K_{\rm c} - a^2\cos^2\vartheta} + \frac{2a(L_{\rm c} - aE_{\rm c})}{K_{\rm c}}\right). \tag{3.75}$$

It should be noted that the original formula of Marck [162] for the same quantity contains a mistake.

3.6.3 Separable solution

When we insert the adapted tetrad into equation (3.69) we see that it does not contain any reference to ψ, ϕ, and A, B are thus constants of motion in the perturbed problem.

By assuming a separable action $W^{(1)} = E_{\rm so}t + L_{\rm so}\varphi + \phi B + \psi A + W_r(r) + W_\vartheta(\vartheta)$ we then obtain

$$\begin{aligned}(W'_\vartheta)^2 =& K_{\rm so} - \left(\frac{L_{\rm so}}{\sin\vartheta} - aE_{\rm so}\sin\vartheta\right)^2 - a^2\cos^2\vartheta \\ &- 2aS^{12}\sqrt{K_{\rm c}}\frac{L_{\rm c} - aE_{\rm c}\sin^2\vartheta}{K_{\rm c} - a^2\cos^2\vartheta}\,,\end{aligned} \tag{3.76}$$

$$\begin{aligned}\Delta(W'_r)^2 =& -K_{\rm so} + \frac{1}{\Delta}\left(E_{\rm so}(r^2+a^2) - aL_{\rm so}\right)^2 - r^2 \\ &- 2S^{12}\sqrt{K_{\rm c}}\frac{E_{\rm c}(r^2+a^2) - aL_{\rm c}}{r^2 + K_{\rm c}}\,,\end{aligned} \tag{3.77}$$

where $K_{\rm so}$ is a separation constant similar to the Carter constant and $S^{12} = A + B + S$. The spin-orbital integrals of motion $K_{\rm so}, E_{\rm so}, L_{\rm so}$ have to be chosen as equal to their background congruence counter-parts $K_{\rm c}, E_{\rm c}, L_{\rm c}$ only up to $\mathscr{O}(S)$ corrections. Furthermore, these corrections can be chosen as free functions of constants of motion.

Let us compare the integrals of motion with the now non-constant orbital functions defined as

$$E_{\rm o} \equiv -u_t \tag{3.78}$$

$$L_{\rm o} \equiv u_\varphi \tag{3.79}$$

$$K_{\rm o} \equiv (u_\vartheta)^2 - \left(\frac{L_{\rm o}}{\sin\vartheta} - aE_{\rm o}\sin\vartheta\right)^2 + a^2\cos^2\vartheta\,. \tag{3.80}$$

Recall that $u_\mu = W_{,\mu} - e_{A\kappa}e^{\kappa}_{B;\mu}S^{AB}/2$. The true integrals of motion of the spin-orbital system can then be related to the orbital functions defined above as

$$E_{\rm so} = E_{\rm o} + \frac{1}{2}\Gamma_{ABt}S^{AB}\,, \tag{3.81}$$

$$L_{\rm so} = L_{\rm o} - \frac{1}{2}\Gamma_{AB\varphi}S^{AB}\,, \tag{3.82}$$

$$\begin{aligned}K_{\rm so} =& K_{\rm o} - e_{A\kappa}e^{\kappa}_{B;\vartheta}u_\vartheta S^{AB} + \left(\frac{L_{\rm o}}{\sin\vartheta} - aE_{\rm o}\sin\vartheta\right)\left(\frac{\Gamma_{AB\varphi}}{\sin\vartheta} + a\sin\vartheta\Gamma_{ABt}\right)S^{AB} \\ &- a\sqrt{K_{\rm c}}\frac{L_{\rm c} - aE_{\rm c}\sin^2\vartheta}{K_{\rm c} - a^2\cos^2\vartheta}S^{12}\,,\end{aligned} \tag{3.83}$$

where we have used the fact that the tetrad is independent of t, φ and $\Gamma_{AB\kappa} \equiv \Gamma_{\mu\nu\kappa} e^{\mu}_{A} e^{\nu}_{B}$. We have also discarded $\mathcal{O}(S^2)$ terms.

We can now see that the four-velocity will mostly be $\mathcal{O}(S)$ close to the geodesic velocity with orbital parameters $K_{\rm o}, E_{\rm o}, L_{\rm o}$. However, at turning points or for planar and purely radial orbits, the spin effects induce an $\mathcal{O}(\sqrt{S})$ deviation from the geodesic four-velocity. This is only an artifact of the non-smoothness of the coordinates x^{μ}, p_{μ} for the description of the trajectory around turning points; in action-angle coordinates the $\mathcal{O}(\sqrt{S})$ shifts should transform to $\mathcal{O}(S)$ corrections.

3.6.4 Integration of orbits

The equations for the (r, ϑ) orbital shape in Mino time read

$$\frac{\mathrm{d}r}{\mathrm{d}\lambda} = \Delta \left(W'_r - \frac{1}{2} e_{A\kappa} e^{\kappa}_{B;r} S^{AB} \right) , \tag{3.84a}$$

$$\frac{\mathrm{d}\vartheta}{\mathrm{d}\lambda} = W'_{\vartheta} - \frac{1}{2} e_{A\kappa} e^{\kappa}_{B;\vartheta} S^{AB} . \tag{3.84b}$$

These are not separable, which can be easily see e.g. from the appearance of terms involving $\sin(\psi)$ or $\cos(\psi)$ in S^{AB}. However, already at this level we see that the system reduces to two first-order non-linear differential equations which, due to the Darboux theorem, cannot be chaotic.

We can rewrite the equations as

$$\frac{\mathrm{d}r}{\mathrm{d}\lambda} = \bar{R}(r) - \frac{1}{2}\delta\gamma_r , \tag{3.85}$$

$$\frac{\mathrm{d}\vartheta}{\mathrm{d}\lambda} = \bar{\Theta}(\vartheta) - \frac{1}{2}\delta\gamma_{\vartheta} , \tag{3.86}$$

$$\gamma_{\mu} \equiv e_{A\kappa} e^{\kappa}_{B;\mu} S^{AB} , \tag{3.87}$$

$$\bar{R}(r) \equiv \Delta W'_r + \frac{\int_0^{2\pi} \int \gamma_r / W'_{\vartheta} \mathrm{d}\vartheta \mathrm{d}\psi}{2\pi \int 1/W'_{\vartheta} \mathrm{d}\vartheta} , \tag{3.88}$$

$$\bar{\Theta}(\vartheta) \equiv W'_{\vartheta} + \frac{\int_0^{2\pi} \int \gamma_{\vartheta} / (\Delta W'_r) \mathrm{d}r \mathrm{d}\psi}{2\pi \int 1/(\Delta W'_r) \mathrm{d}r} , \tag{3.89}$$

$$\delta\gamma_r \equiv \gamma_r - \frac{\int_0^{2\pi} \int \gamma_r / W'_{\vartheta} \mathrm{d}\vartheta \mathrm{d}\psi}{2\pi \int 1/W'_{\vartheta} \mathrm{d}\vartheta} , \tag{3.90}$$

$$\delta\gamma_{\vartheta} \equiv \gamma_{\vartheta} - \frac{\int_0^{2\pi} \int \gamma_{\vartheta} / (\Delta W'_r) \mathrm{d}r \mathrm{d}\psi}{2\pi \int 1/(\Delta W'_r) \mathrm{d}r} , \tag{3.91}$$

where the integration bounds in the definition of $\bar{R}$ and $\bar{\Theta}$ are between the zeros of W'_ϑ, W'_r respectively.

Now consider a transformation to a set of deformed local coordinates given as $\tilde{r} = r + S\bar{R}\chi_r(r,\vartheta), \tilde{\vartheta} = \vartheta + S\bar{\Theta}\chi_\vartheta(r,\vartheta)$ such that

$$\chi_{r,r}\bar{R} + \chi_{r,\vartheta}\bar{\Theta} = \frac{1}{2S\bar{R}}\delta\gamma_r\,, \tag{3.92}$$

$$\chi_{\vartheta,r}\bar{R} + \chi_{\vartheta,\vartheta}\bar{\Theta} = \frac{1}{2S\bar{\Theta}}\delta\gamma_\vartheta\,. \tag{3.93}$$

Then it is easy show that up to $\mathcal{O}(S^2)$ terms the equations of motion transform into

$$\frac{\mathrm{d}\tilde{r}}{\mathrm{d}\lambda} = \bar{R}(\tilde{r})\,, \tag{3.94}$$

$$\frac{\mathrm{d}\tilde{\vartheta}}{\mathrm{d}\lambda} = \bar{\Theta}(\tilde{\vartheta})\,, \tag{3.95}$$

$$\tag{3.96}$$

To obtain the real orbital shape, we must integrate χ_r, χ_ϑ. For that we notice that the left-hand sides of equations (3.92) and (3.93) can be rewritten with $\mathrm{d}/\mathrm{d}\lambda$ and at the given order of approximation we obtain

$$\frac{\mathrm{d}\chi_r}{\mathrm{d}\lambda} = \frac{1}{2S\bar{R}(\tilde{r})}\delta\gamma_r(\tilde{r},\tilde{\vartheta})\,,\,, \tag{3.97}$$

$$\frac{\mathrm{d}\chi_\vartheta}{\mathrm{d}\lambda} = \frac{1}{2S\bar{\Theta}(\tilde{\vartheta})}\delta\gamma_\vartheta(\tilde{r},\tilde{\vartheta})\,, \tag{3.98}$$

If we have a quasi-periodic trajectory, then by averaging and by the construction of $\delta\gamma_\mu$ we see that the long-term secular growth of the shift functions χ_μ will be zero. If we then set $\chi_\mu = 0$ initially, we see that the average of χ_μ will also be zero, and the coordinates r, ϑ and $\tilde{r}, \tilde{\vartheta}$ stay close at all times.

I hope that I have convinced the dear reader of the power of the Hamiltonian approach to spinning particles. On the other hand, I believe that it is also clear that more work needs to be done to fully exhaust its potential. On this note, I would like to pass to the next Chapter, where the other works of my PhD are introduced and commented upon.

Chapter 4

Context and results of the appended papers

I now provide a few comments to the appended papers that might serve as an "extended introduction" for readers not strictly acquainted with the respective sub-fields. To facilitate the reading of the thesis, I also summarized the most important results. Additionally, each section has a *Statement of contribution to paper* at the very end, where I specify the contributions of the individual authors. These comments are slightly less formal, and the reader is expected to read the papers for more complete discussion and lists of references.

I append the four published papers as downloaded from the respective journal websites. The fifth paper that I wrote during my PhD and which is currently in review was not allowed to be appended due to the rules of the University of Bremen. The kind reader can find the preprint at arXiv:1808.06582, and its results restated in Chapter 3.

4.1 Pseudo-Newtonian Equations for Evolution of Particles and Fluids in Stationary Space-times

Full reference (short ref.: [291]): Witzany, V., & Lämmerzahl, C. (2017). Pseudo-Newtonian Equations for Evolution of Particles and Fluids in Stationary Space-times. *The Astrophysical Journal*, 841(2), 105. Preprint at arXiv:1601.01034.

A preliminary advertisement of our work was given in the proceedings [290].

Context: Consider the Bondi flow discussed in subsection 2.1.2. We see that the key interactions happen at the Bondi radius $r_{\rm B} = 2M/v_{\rm s\infty}$, where the speed of sound in the faraway

gas is realistically $v_{s\infty} \ll 1$, and the relativistic corrections to the Newtonian picture come with a characteristic length-scale $r_g = 2M$. Considering all the other approximations such as spherical symmetry, stationarity, and perfect-fluid evolution, it is only natural to absolutely ignore relativistic corrections to the far-field regulation of accretion.

Let us now approach the black hole a little bit closer and examine the formulas for the Keplerian rotation in the Newtonian and relativistic case (assuming non-spinning black hole)

$$\Omega_{\text{Newt.}} = \sqrt{\frac{M}{r^3}}\,,\ \Omega_{\text{Rel.}} = \sqrt{\frac{M}{r^3}}\,, \tag{4.1}$$

$$L_{\text{Newt.}} = m\sqrt{Mr}\,,\ L_{\text{Rel.}} = m\sqrt{\frac{Mr}{1-3M/r}}\,, \tag{4.2}$$

$$E_{\text{Newt.}} = m\left(1-\frac{M}{2r}\right)\,,\ E_{\text{Rel.}} = m\frac{1-2M/r}{\sqrt{1-3M/r}}\,, \tag{4.3}$$

$$\tag{4.4}$$

where I have tentatively included the rest-mass term into the Newtonian expression for energy. Of course, there is the issue of identifying the Schwarzschild radius r with the flat Euclidean radius, but as long as we allow for that identification, we see that the rotation frequencies in a Keplerian disk are absolutely identical in the Newtonian and relativistic case. On the other hand, the angular-momentum and the binding energy at the inner edge of the disk at $r_{\text{ms}} = 6M$ would be predicted by the Newtonian formulas with a relative error of 40% and 10% respectively.

Considering the systematic errors common in astronomy and astrophysics, this would not necessarily be a major issue for first-approximation models (especially the binding energy defining the overall luminosity of the disk is almost correct). However, the bigger issue with the Newtonian gravity is that the circular orbits are stable up to the very point $r = 0$ and the disk will simply not have an inner edge at $r = 6M$. Nevertheless, it is easy to write simple Newtonian potentials that will have circular orbits becoming unstable at $6M$. These are the so-called pseudo-Newtonian potentials, and they were used in some important accretion studies such as that of Proga and Begelman [217] and Abramowicz et al. [12] mentioned in the previous chapter. Our study Witzany and Lämmerzahl [291] explores this topic in a somewhat more systematic manner.

Summary of results: We gave a universal prescription for a pseudo-Newtonian potential in any given stationary space-time. This prescription exactly reproduces all the orbital shapes in the given space-time, albeit under a different time parametrization – all that without beforehand knowledge of the structure of the orbits. The prescription yields closed and highly useful

formulas in *static* space-times, such as the Schwarzschild space-time, but in the general *stationary* space-times such as Kerr with $a \neq 0$, the gravitomagnetic terms in the metric make the formalism complicated.

Statement of contributions to paper: I derived the entire theoretical formalism, researched the literature, created the plots, and wrote the majority of the text of the paper. Claus Lämmerzahl wrote parts of the Introduction of the paper, and was responsible for critical revisions of the writing, explanations, and organization of the paper.

4.2 Conservation laws and evolution schemes in geodesic, hydrodynamic, and magnetohydrodynamic flows

Full reference (short ref.: [163]): Markakis, C., Uryū, K., Gourgoulhon, E., Nicolas, J. P., Andersson, N., Pouri, A., & Witzany, V. (2017). Conservation laws and evolution schemes in geodesic, hydrodynamic, and magnetohydrodynamic flows. *Physical Review D*, 96(6), 064019. Preprint at arXiv:1612.09308.

Context: The geometrical approach to fluid equations is a fascinating topic already on the level of Newtonian mechanics. For instance, an elegant result of this approach is Kelvin's circulation theorem that states that when we choose any co-moving loop within a perfect fluid, then the integrated projection of the velocity of the fluid on the loop will never change. The investigation of these topics in relativistic fluid and magnetofluid dynamics is of high importance to their analytical theory and computer simulations. In astrophysics, this is relevant both for the magnetized plasma in accretion-disk physics, but also for the dense environment of magnetized neutron stars.

The purpose of our paper with Markakis et al. [163] was to generalize such theorems to relativistic hydrodynamics and magneto-hydrodynamics, or to even find non-trivial extensions not obvious outside of the relativistic formalism.

Summary of results: The main result of the paper is casting the dynamics of an ideally conductive magneto-fluid in a variational principle along its stream-lines. This allows a version of the Kelvin theorem valid for magnetofluids to be naturally derived from the respective Hamiltonian theory and its Poincaré invariants. Other results include re-expressing the stream-lines as geodesics in Finsler metrics, and constructing the equations of magnetofluids in a "comoving" hyperbolic form.

Statement of contributions to paper: The major part of the writing and theoretical derivations are due to the other authors of Markakis et al. [163]. My direct contributions, in particular, were to sections B.5 on the generalization of the Carter constant in fluids, section C.1 on Hamiltonians for fluid streamlines, section D.7 on the Bekenstein-Oron formulation of magneto-hydrodynamics, and Appendix C on Hamiltonians for various parametrizations of the streamlines.

4.3 Exploiting the hidden symmetry of spinning black holes: conservation laws and numerical tests

Full reference (short ref.: [288]): Witzany, V. (2017). Exploiting the hidden symmetry of spinning black holes: conservation laws and numerical tests. *Monthly Notices of the Royal Astronomical Society*, 473(2), 2434-2440. Preprint at arXiv:1709.03330.

Context: Current astrophysical simulations are built with only the axi-symmetry and stationarity of the Kerr metric in mind. In particular, the hidden symmetry of the Kerr space-time (discussed in subsection 1.4.2) is left completely unused in modern numerical computations. In Witzany [288], my aim was to investigate whether this can be changed. In principle, if there were identities and additional "hidden" conservation laws that could be used on top of usual conservation of mass-energy and angular-momentum fluxes, we would potentially obtain a great tool both for theoretical and numerical computations.

Summary of results: I showed that any continuum that can be understood as an ensemble of particles with occasional collisions will not conserve its sum of Carter constants. In other words, it is unlikely that a hidden conservation law for general, nonlinearly interacting matter fields will exist. Despite this no-go result, I found expressions that can be understood as "weak" conservation laws, and I demonstrated that they can be, in principle, used to test numerical simulations beyond what can be achieved with commonly employed checks of angular-momentum and energy conservation.

Statement of contributions to paper: As the single author, I have full credit for every aspect of the paper.

4.4 New closed analytical solutions for geometrically thick fluid tori around black holes

Full reference (short ref.: [289]): Witzany, V., & Jefremov, P. (2018). New closed analytical solutions for geometrically thick fluid tori around black holes – Numerical evolution and the onset of the magneto-rotational instability. *Astronomy & Astrophysics*, 614, A75. Preprint at arXiv:1711.09241.

Context: As discussed in subsection 2.2.5, numerical simulations of accretion disks are typically initialized by fluid tori in equilibrium around the black holes. The point of having the tori in equilibrium is that if the state is in fact very far from equilibrium, its evolution will be very abrupt and the simulations would require very careful and computationally expensive treatment to be convergent (see subsection 2.2.5). In Witzany and Jefremov [289], we have summarized our efforts of finding new closed formulas for such initial conditions.

Summary of results: The tori we have found considerably widen the landscape of closed formulas that can be used in accretion-disk simulations. As a showcase study, we have also implemented the tori in the publicly available general-relativistic magneto-hydrodynamics code HARM, and evolved them numerically. We documented the onset of the magneto-rotational instability, accretion from the torus, and various other properties. The results of our simulations are not of direct physical importance, but the irregular dependence of certain aspects of the accretion flow on the initial data challenge the predictivity of current numerical studies.

Statement of contributions to paper: I researched the relevant literature, wrote the majority of the text of the paper, implemented the initial conditions in the HARM code, and ran the simulations on the ZARM computer clusters. The analytical derivations, analysis and discussion of the simulation results, and preparation of the plots were joint efforts with Pavel Jefremov.

References

[1] Aartsen, M. G. et al. (2018a). Multimessenger observations of a flaring blazar coincident with high-energy neutrino IceCube-170922A. *Science*, 361(6398):eaat1378.

[2] Aartsen, M. G. et al. (2018b). Neutrino emission from the direction of the blazar TXS 0506+056 prior to the IceCube-170922A alert. *Science*, 361(6398):147–151.

[3] Abbott, B., Abbott, R., Abbott, T., Abernathy, M., Acernese, F., Ackley, K., Adams, C., Adams, T., Addesso, P., Adhikari, R., et al. (2016a). Astrophysical implications of the binary black hole merger GW150914. *Astrophys. J. Lett.*, 818(2):L22.

[4] Abbott, B., Abbott, R., Abbott, T., Acernese, F., Ackley, K., Adams, C., Adams, T., Addesso, P., Adhikari, R., Adya, V., et al. (2017a). Gravitational waves and gamma-rays from a binary neutron star merger: GW170817 and GRB 170817a. *Astrophys. J. Lett.*, 848(2):L13.

[5] Abbott, B. et al. (2017b). GW170817: Observation of Gravitational Waves from a Binary Neutron Star Inspiral. *Phys. Rev. Lett.*, 119(16):161101.

[6] Abbott, B. P. et al. (2016b). Binary Black Hole Mergers in the first Advanced LIGO Observing Run. *Phys. Rev.*, X6(4):041015.

[7] Abbott, B. P. et al. (2016c). GW151226: Observation of Gravitational Waves from a 22-Solar-Mass Binary Black Hole Coalescence. *Phys. Rev. Lett.*, 116(24):241103.

[8] Abbott, B. P. et al. (2016d). Observation of Gravitational Waves from a Binary Black Hole Merger. *Phys. Rev. Lett.*, 116(6):061102.

[9] Abbott, B. P. et al. (2017c). GW170104: Observation of a 50-Solar-Mass Binary Black Hole Coalescence at Redshift 0.2. *Phys. Rev. Lett.*, 118(22):221101.

[10] Abbott, B. P. et al. (2017d). GW170608: Observation of a 19-solar-mass Binary Black Hole Coalescence. *Astrophys. J.*, 851(2):L35.

[11] Abbott, B. P. et al. (2017e). GW170814: A Three-Detector Observation of Gravitational Waves from a Binary Black Hole Coalescence. *Phys. Rev. Lett.*, 119(14):141101.

[12] Abramowicz, M., Czerny, B., Lasota, J., and Szuszkiewicz, E. (1988). Slim accretion disks. *Astrophys. J.*, 332:646–658.

[13] Abramowicz, M. A. and Fragile, P. C. (2013). Foundations of black hole accretion disk theory. *Living Rev. Relativ.*, 16(1):1.

[14] Anglada, G., Rodríguez, L. F., and Carrasco-González, C. (2018). Radio jets from young stellar objects. *Astron. Astrophys. Rev.*, 26(1):3.

[15] Archibald, A. M., Gusinskaia, N. V., Hessels, J. W., Deller, A. T., Kaplan, D. L., Lorimer, D. R., Lynch, R. S., Ransom, S. M., and Stairs, I. H. (2018). Universality of free fall from the orbital motion of a pulsar in a stellar triple system. *Nature*, 559(7712):73.

[16] Arnold, V. I., Kozlov, V. V., and Neishtadt, A. I. (2007). *Mathematical aspects of classical and celestial mechanics*, volume 3. Springer Science & Business Media.

[17] Audretsch, J. (1981). Trajectories and Spin Motion of Massive Spin 1/2 Particles in Gravitational Fields. *J. Phys.*, A14:411–422.

[18] Babak, S., Gair, J., Sesana, A., Barausse, E., Sopuerta, C. F., Berry, C. P. L., Berti, E., Amaro-Seoane, P., Petiteau, A., and Klein, A. (2017). Science with the space-based interferometer LISA. V: Extreme mass-ratio inspirals. *Phys. Rev.*, D95(10):103012.

[19] Baker, T., Bellini, E., Ferreira, P. G., Lagos, M., Noller, J., and Sawicki, I. (2017). Strong constraints on cosmological gravity from GW170817 and GRB 170817a. *Phys. Rev. Lett.*, 119(25):251301.

[20] Balbus, S. A. and Hawley, J. F. (1991). A powerful local shear instability in weakly magnetized disks. I-linear analysis. II-nonlinear evolution. *Astrophys. J.*, 376:214–233.

[21] Balbus, S. A. and Hawley, J. F. (1998). Instability, turbulence, and enhanced transport in accretion disks. *Rev. Mod. Phys.*, 70(1):1.

[22] Balbus, S. A., Hawley, J. F., and Stone, J. M. (1996). Nonlinear Stability, Hydrodynamical Turbulence, and Transport in Disks. *Astrophys. J.*, 467:76.

[23] Barack, L. and Pound, A. (2018). Self-force and radiation reaction in general relativity.

[24] Barausse, E., Racine, E., and Buonanno, A. (2009). Hamiltonian of a spinning test particle in curved spacetime. *Phys. Rev.*, D80:104025. [Erratum: Phys. Rev.D85,069904(2012)].

[25] Bardeen, J. M. (1970). Stability of circular orbits in stationary, axisymmetric space-times. *Astrophys. J.*, 161:103.

[26] Bardeen, J. M. and Petterson, J. A. (1975). The Lense-Thirring effect and accretion disks around Kerr black holes. *Astrophys. J.*, 195:L65.

[27] Bekenstein, J. D. (2004). Relativistic gravitation theory for the MOND paradigm. *Phys. Rev.*, D70:083509. [Erratum: Phys. Rev.D71,069901(2005)].

[28] Bel, L. (1958). Définition d'une densité d'énergie et d'un état de radiation totale généralisée. *C. R. Acad. Sci. Paris*, 246:3015.

[29] Beloborodov, A. M. (1998). Super-Eddington accretion discs around Kerr black holes. *Mon. Notices Royal Astron. Soc.*, 297(3):739–746.

[30] Bertone, G. and Hooper, D. (2016). A History of Dark Matter. *arXiv preprint arXiv:1605.04909*.

[31] Bini, D., Damour, T., and Geralico, A. (2018). Spin-orbit precession along eccentric orbits: improving the knowledge of self-force corrections and of their effective-one-body counterparts. *Phys. Rev.*, D97(10):104046.

[32] Binnington, T. and Poisson, E. (2009). Relativistic theory of tidal Love numbers. *Phys. Rev.*, D80:084018.

[33] Bisnovatyi-Kogan, G. and Ruzmaikin, A. (1974). The accretion of matter by a collapsing star in the presence of a magnetic field. *Astrophys. Space Sci.*, 28(1):45–59.

[34] Bisnovatyi-Kogan, G. S. and Syunyaev, R. A. (1971). Galaxy Nuclei and Quasars as Infrared Emission Sources. *Astroph. Zh.*, 48:881.

[35] Blaes, O. M. and Balbus, S. A. (1994). Local shear instabilities in weakly ionized, weakly magnetized disks. *Astrophys. J.*, 421:163–177.

[36] Blakeslee, J. P., Jordán, A., Mei, S., Côté, P., Ferrarese, L., Infante, L., Peng, E. W., Tonry, J. L., and West, M. J. (2009). The ACS Fornax cluster survey. V. Measurement and recalibration of surface brightness fluctuations and a precise value of the Fornax-Virgo relative distance. *Astrophys. J.*, 694(1):556.

[37] Blanchet, L. (2014). Gravitational Radiation from Post-Newtonian Sources and Inspiralling Compact Binaries. *Living Rev. Rel.*, 17:2.

[38] Blanchet, L. and Heisenberg, L. (2015). Dipolar Dark Matter with Massive Bigravity. *JCAP*, 1512(12):026.

[39] Blandford, R. D. and Payne, D. G. (1982). Hydromagnetic flows from accretion discs and the production of radio jets. *Mon. Not. Roy. Astron. Soc.*, 199:883.

[40] Blandford, R. D. and Znajek, R. L. (1977). Electromagnetic extractions of energy from Kerr black holes. *Mon. Not. Roy. Astron. Soc.*, 179:433–456.

[41] Bohé, A. et al. (2017). Improved effective-one-body model of spinning, nonprecessing binary black holes for the era of gravitational-wave astrophysics with advanced detectors. *Phys. Rev.*, D95(4):044028.

[42] Bondi, H. (1952). On spherically symmetrical accretion. *Mon. Notices Royal Astron. Soc.*, 112(2):195–204.

[43] Boyer, R. H. and Lindquist, R. W. (1967). Maximal analytic extension of the Kerr metric. *J. Math. Phys.*, 8(2):265–281.

[44] Brink, L., Deser, S., Zumino, B., Di Vecchia, P., and Howe, P. S. (1976). Local Supersymmetry for Spinning Particles. *Phys. Lett.*, B64:435. [Erratum: Phys. Lett.68B,488(1977)].

[45] Bruno, R. and Carbone, V. (2013). The solar wind as a turbulence laboratory. *Living Rev. in Solar Physics*, 10(1):2.

[46] Buonanno, A. and Damour, T. (1999). Effective one-body approach to general relativistic two-body dynamics. *Phys. Rev.*, D59:084006.

[47] Buonanno, A. and Sathyaprakash, B. (2014). Sources of gravitational waves: Theory and observations. In *General Relativity and Gravitation: A Centennial Perspective*, pages 287–346. University Press.

[48] Carroll, S. M. (2004). *Spacetime and geometry: An introduction to general relativity*.

[49] Carter, B. (1968a). Global structure of the Kerr family of gravitational fields. *Phys. Rev.*, 174(5):1559.

[50] Carter, B. (1968b). Hamilton-Jacobi and Schrödinger separable solutions of Einstein's equations. *Commun. Math. Phys.*, 10(4):280–310.

[51] Carter, B. (1977). Killing tensor quantum numbers and conserved currents in curved space. *Phys. Rev. D*, 16(12):3395.

[52] Carter, B. and McLenaghan, R. G. (1979). Generalized total angular momentum operator for the Dirac equation in curved space-time. *Phys. Rev. D*, 19(4):1093.

[53] Casalbuoni, R. (1976). Relativity and Supersymmetries. *Phys. Lett.*, 62B:49–50.

[54] Chandrasekhar, S. (1960). The stability of non-dissipative Couette flow in hydromagnetics. *Proc. Natl. Acad. Sci. U.S.A*, 46(2):253–257.

[55] Chandrasekhar, S. (1976). The solution of Dirac's equation in Kerr geometry. *Proc. R. Soc. Lond. A*, 349(1659):571–575.

[56] Chandrasekhar, S. (1983). *The mathematical theory of black holes*. Oxford, UK: Clarendon.

[57] Christodoulou, D. (1970). Reversible and irreversible transformations in black hole physics. *Phys. Rev. Lett.*, 25:1596–1597.

[58] Clowe, D., Bradač, M., Gonzalez, A. H., Markevitch, M., Randall, S. W., Jones, C., and Zaritsky, D. (2006). A direct empirical proof of the existence of dark matter. *Astrophys. J. Lett.*, 648(2):L109.

[59] Clowe, D., Gonzalez, A., and Markevitch, M. (2004). Weak-lensing mass reconstruction of the interacting cluster 1e 0657–558: Direct evidence for the existence of dark matter. *Astrophys. J.*, 604(2):596.

[60] Coleman Miller, M. and Colbert, E. J. (2004). Intermediate-mass black holes. *Int. J. Mod. Phys. D*, 13(01):1–64.

[61] Corinaldesi, E. and Papapetrou, A. (1951). Spinning test particles in general relativity. II. *Proc. Roy. Soc. Lond.*, A209:259–268.

[62] Costa, L. F. O., Lukes-Gerakopoulos, G., and Semerák, O. (2018). On spinning particles in general relativity: momentum-velocity relation for the Mathisson-Pirani spin condition. *Phys. Rev.*, D97(8):084023.

[63] Costa, L. F. O. and Natário, J. (2015). Center of mass, spin supplementary conditions, and the momentum of spinning particles. In *Equations of Motion in Relativistic Gravity*, pages 215–258. Springer.

[64] Creminelli, P. and Vernizzi, F. (2017). Dark energy after GW170817 and GRB170817a. *Phys. Rev. Lett.*, 119(25):251302.

[65] d'Ambrosi, G., Satish Kumar, S., van de Vis, J., and van Holten, J. W. (2016). Spinning bodies in curved spacetime. *Phys. Rev.*, D93(4):044051.

[66] d'Ambrosi, G., Satish Kumar, S., and van Holten, J. W. (2015). Covariant Hamiltonian spin dynamics in curved space–time. *Phys. Lett.*, B743:478–483.

[67] Damour, T. and Nagar, A. (2009). Relativistic tidal properties of neutron stars. *Phys. Rev.*, D80:084035.

[68] Damour, T. and Nagar, A. (2014). New effective-one-body description of coalescing nonprecessing spinning black-hole binaries. *Phys. Rev. D*, 90(4):044018.

[69] Damour, T. and Nagar, A. (2016). The Effective-One-Body Approach to the General Relativistic Two Body Problem. *Lect. Notes Phys.*, 905:273–312.

[70] De Rosa, G., Venemans, B. P., Decarli, R., Gennaro, M., Simcoe, R. A., Dietrich, M., Peterson, B. M., Walter, F., Frank, S., McMahon, R. G., Hewett, P. C., Mortlock, D. J., and Simpson, C. (2014). Black Hole Mass Estimates and Emission-line Properties of a Sample of Redshift z < 6.5 Quasars. *Astrophys. J.*, 790:145.

[71] Deffayet, C., Esposito-Farese, G., and Woodard, R. P. (2011). Nonlocal metric formulations of MOND with sufficient lensing. *Phys. Rev.*, D84:124054.

[72] Di Matteo, T., Croft, R. A., Feng, Y., Waters, D., and Wilkins, S. (2017). The origin of the most massive black holes at high-z: Bluetides and the next quasar frontier. *Mon. Notices Royal Astron. Soc.*, 467(4):4243–4251.

[73] Dirac, P. A. M. (1966). *Lectures on quantum field theory*. Yeshiva Univ.

[74] Dixon, W. (1964). A covariant multipole formalism for extended test bodies in general relativity. *Il Nuovo Cimento (1955-1965)*, 34(2):317–339.

[75] Dixon, W. G. (1970). Dynamics of extended bodies in general relativity. I. Momentum and angular momentum. *Proc. Roy. Soc. Lond.*, A314:499–527.

[76] Doeleman, S. S., Fish, V. L., Schenck, D. E., Beaudoin, C., Blundell, R., Bower, G. C., Broderick, A. E., Chamberlin, R., Freund, R., Friberg, P., et al. (2012). Jet-launching structure resolved near the supermassive black hole in M87. *Science*, 338(6105):355–358.

[77] Dolence, J. C., Gammie, C. F., Mościbrodzka, M., and Leung, P. K. (2009). grmonty: A Monte Carlo code for relativistic radiative transport. *Astrophys. J. Suppl.*, 184(2):387.

[78] Drasco, S. and Hughes, S. A. (2006). Gravitational wave snapshots of generic extreme mass ratio inspirals. *Phys. Rev. D*, 73(2):024027.

[79] Eckart, C. (1940). The thermodynamics of irreversible processes. III. Relativistic theory of the simple fluid. *Phys. Rev.*, 58(10):919.

[80] Edgar, R. (2004). A review of Bondi–Hoyle–Lyttleton accretion. *New Astron. Rev.*, 48(10):843–859.

[81] Ehlers, J. and Rudolph, E. (1977). Dynamics of extended bodies in general relativity center-of-mass description and quasirigidity. *General Relativity and Gravitation*, 8(3):197–217.

[82] Einstein, A. (1915). Die Feldgleichungen der Gravitation. *Sitzungsberichte der Königlich Preußischen Akademie der Wissenschaften (Berlin), Seite 844-847.*

[83] Ezquiaga, J. M. and Zumalacárregui, M. (2017). Dark energy after GW170817: dead ends and the road ahead. *Phys. Rev. Lett.*, 119(25):251304.

[84] Faber, S. M. and Jackson, R. E. (1976). Velocity dispersions and mass to light ratios for elliptical galaxies. *Astrophys. J.*, 204:668.

[85] Famaey, B. and McGaugh, S. (2012). Modified Newtonian Dynamics (MOND): Observational Phenomenology and Relativistic Extensions. *Living Rev. Rel.*, 15:10.

[86] Feldman, Y. and Tauber, G. E. (1980). The internal state of a gas of particles with spin. *Gen. Rel. Grav.*, 12(10):837–856.

[87] Fender, R. and Belloni, T. (2012). Stellar-mass black holes and ultraluminous X-ray sources. *Science*, 337(6094):540–544.

[88] Feng, Y., Di Matteo, T., Croft, R., and Khandai, N. (2014). High-redshift supermassive black holes: accretion through cold flows. *Mon. Notices Royal Astron. Soc.*, 440(2):1865–1879.

[89] Fernandes, C. A. C., Jarvis, M. J., Rawlings, S., Martinez-Sansigre, A., Hatziminaoglou, E., Lacy, M., Page, M. J., Stevens, J. A., and Vardoulaki, E. (2011). Evidence for a maximum jet efficiency for the most powerful radio galaxies. *Mon. Not. Roy. Astron. Soc.*, 411:1909.

[90] Ferrarese, L. and Ford, H. (2005). Supermassive black holes in galactic nuclei: past, present and future research. *Space Sci. Rev.*, 116(3-4):523–624.

[91] Floyd, R. (1973). *The Dynamics of Kerr Fields*. PhD thesis, London Univ., London, England.

[92] Frank, J., King, A., and Raine, D. (2002). *Accretion power in astrophysics*. Cambridge university press.

[93] Frenkel, J. (1926). Die Elektrodynamik des rotierenden Elektrons. *Z. Phys.*, 37:243–262.

[94] Frolov, V., Krtouš, P., and Kubizňák, D. (2017). Black holes, hidden symmetries, and complete integrability. *Living Rev. Rel.*, 20(1):6.

[95] Fujita, R. and Hikida, W. (2009). Analytical solutions of bound timelike geodesic orbits in Kerr spacetime. *Class. Quantum Grav.*, 26(13):135002.

[96] Gebhardt, K., Adams, J., Richstone, D., Lauer, T. R., Faber, S., Gültekin, K., Murphy, J., and Tremaine, S. (2011). The black hole mass in M87 from gemini/nifs adaptive optics observations. *Astrophys. J.*, 729(2):119.

[97] Ghisellini, G., Tavecchio, F., Foschini, L., Ghirlanda, G., Maraschi, L., and Celotti, A. (2010). General physical properties of bright Fermi blazars. *Mon. Not. Roy. Astron. Soc.*, 402:497.

[98] Ghisellini, G., Tavecchio, F., Maraschi, L., Celotti, A., and Sbarrato, T. (2014). The power of relativistic jets is larger than the luminosity of their accretion disks. *Nature*, 515:376.

[99] Giesel, K., Schuller, F. P., Witte, C., and Wohlfarth, M. N. (2012). Gravitational dynamics for all tensorial spacetimes carrying predictive, interpretable, and quantizable matter. *Phys. Rev. D*, 85(10):104042.

[100] Gillessen, S., Plewa, P., Eisenhauer, F., Sari, R., Waisberg, I., Habibi, M., Pfuhl, O., George, E., Dexter, J., von Fellenberg, S., et al. (2017). An update on monitoring stellar orbits in the galactic center. *Astrophys. J.*, 837(1):30.

[101] Grenzebach, A. (2016). *The Shadow of Black Holes*. Springer.

[102] Griffiths, J. B. and Podolský, J. (2009). *Exact space-times in Einstein's general relativity*. Cambridge University Press.

[103] Guseva, A., Hollerbach, R., Willis, A. P., and Avila, M. (2017). Dynamo action in a quasi-Keplerian Taylor-Couette flow. *Phys. Rev. Lett.*, 119(16):164501.

[104] Guseva, A., Willis, A., Hollerbach, R., and Avila, M. (2015). Transition to magnetorotational turbulence in Taylor–Couette flow with imposed azimuthal magnetic field. *New J. Phys.*, 17(9):093018.

[105] Guzmán Ramírez, W., Deriglazov, A. A., and Pupasov-Maksimov, A. M. (2014). Frenkel electron and a spinning body in a curved background. *JHEP*, 03:109.

[106] Hackmann, E. and Lämmerzahl, C. (2012). Observables for bound orbital motion in axially symmetric space-times. *Phys. Rev. D*, 85(4):044049.

[107] Hairer, E., Lubich, C., and Wanner, G. (2006). *Geometric numerical integration: structure-preserving algorithms for ordinary differential equations*, volume 31. Springer Science & Business Media.

[108] Hansen, R. O. (1974). Multipole moments of stationary space-times. *J. Math. Phys.*, 15:46–52.

[109] Hanson, A., Regge, T., and Teitelboim, C. (1976). *Constrained Hamiltonian systems*. Accademia Nazionale dei Lincei.

[110] Hanson, A. J. and Regge, T. (1974). The Relativistic Spherical Top. *Annals Phys.*, 87:498.

[111] Harms, E., Lukes-Gerakopoulos, G., Bernuzzi, S., and Nagar, A. (2016). Spinning test body orbiting around a Schwarzschild black hole: Circular dynamics and gravitational-wave fluxes. *Phys. Rev. D*, 94(10):104010.

[112] Hawley, J. F., Guan, X., and Krolik, J. H. (2011). Assessing Quantitative Results in Accretion Simulations: From Local to Global. *Astrophys. J.*, 738:84.

[113] Hawley, J. F., Richers, S. A., Guan, X., and Krolik, J. H. (2013). Testing convergence for global accretion disks. *Astrophys. J.*, 772(2):102.

[114] Heger, A., Fryer, C., Woosley, S., Langer, N., and Hartmann, D. H. (2003). How massive single stars end their life. *Astrophys. J.*, 591(1):288.

[115] Helgason, S. (2001). *Differential geometry and symmetric spaces*, volume 341. American Mathematical Soc.

[116] Hinderer, T. and Flanagan, E. E. (2008). Two timescale analysis of extreme mass ratio inspirals in Kerr. I. Orbital Motion. *Phys. Rev.*, D78:064028.

[117] Hossenfelder, S. (2017). Covariant version of Verlinde's emergent gravity. *Phys. Rev.*, D95(12):124018.

[118] Howes, G. G. (2010). A prescription for the turbulent heating of astrophysical plasmas. *Mon. Notices Royal Astron. Soc. Lett.*, 409(1):L104–L108.

[119] Hoyle, F. and Lyttleton, R. A. (1939). The effect of interstellar matter on climatic variation. In *Math. Proc. Camb. Philos. Soc.*, volume 35, pages 405–415. Cambridge University Press.

[120] Ichimaru, S. (1977). Bimodal behavior of accretion disks-theory and application to Cygnus X-1 transitions. *Astrophys. J.*, 214:840–855.

[121] Igumenshchev, I. V., Narayan, R., and Abramowicz, M. A. (2003). Three-dimensional magnetohydrodynamic simulations of radiatively inefficient accretion flows. *Astrophys. J.*, 592(2):1042.

[122] Inayoshi, K., Haiman, Z., and Ostriker, J. P. (2016). Hyper-Eddington accretion flows on to massive black holes. *Mon. Notices Royal Astron. Soc.*, 459(4):3738–3755.

[123] Israel, W. (1987). Dark stars: the evolution of an idea. *Three hundred years of gravitation*, pages 199–276.

[124] Johnson, J. L., Whalen, D. J., Fryer, C. L., and Li, H. (2012). The growth of the stellar seeds of supermassive black holes. *Astrophys. J.*, 750(1):66.

[125] Johnson, J. L., Whalen, D. J., Li, H., and Holz, D. E. (2013). Supermassive seeds for supermassive black holes. *Astrophys. J.*, 771(2):116.

[126] Kalnins, E. G., Williams, G., and Miller Jr, W. (1996). Intrinsic characterization of the separation constant for spin one and gravitational perturbations in Kerr geometry. *Proc. R. Soc. Lond. A*, 452(1948):997–1006.

[127] Kamran, N. (1985). Separation of variables for the Rarita–Schwinger equation on all type D vacuum backgrounds. *J. Math. Phys.*, 26(7):1740–1742.

[128] Kavanagh, C., Bini, D., Damour, T., Hopper, S., Ottewill, A. C., and Wardell, B. (2017). Spin-orbit precession along eccentric orbits for extreme mass ratio black hole binaries and its effective-one-body transcription. *Phys. Rev.*, D96(6):064012.

[129] Kerr, R. P. (1963). Gravitational field of a spinning mass as an example of algebraically special metrics. *Phys. Rev. Lett.*, 11(5):237.

[130] Khriplovich, I. (1989). Spinning particle in a gravitational field. *Sov. Phys. JETP*, 69:217.

[131] King, A. and Nixon, C. (2016). Black holes in stellar-mass binary systems: expiating original spin? *Mon. Notices Royal Astron. Soc.*, 462(1):464–467.

[132] King, A. R. and Pringle, J. (2006). Growing supermassive black holes by chaotic accretion. *Mon. Notices Royal Astron. Soc.: Lett.*, 373(1):L90–L92.

[133] King, A. R., Pringle, J., and Livio, M. (2007). Accretion disc viscosity: how big is alpha? *Mon. Notices Royal Astron. Soc.*, 376(4):1740–1746.

[134] Kızıltan, B., Baumgardt, H., and Loeb, A. (2017). An intermediate-mass black hole in the centre of the globular cluster 47 Tucanae. *Nature*, 542(7640):203.

[135] Komissarov, S. S. (2004). Electrodynamics of black hole magnetospheres. *Mon. Not. Roy. Astron. Soc.*, 350:407.

[136] Kormendy, J. and Ho, L. C. (2013). Coevolution (or not) of supermassive black holes and host galaxies. *Annu. Rev. Astron. Astrophys.*, 51:511–653.

[137] Kotko, I. and Lasota, J.-P. (2012). The viscosity parameter α and the properties of accretion disc outbursts in close binaries. *Astron. Astrophys.*, 545:A115.

[138] Kubizňák, D. (2008). *Hidden Symmetries of Higher-Dimensional Rotating Black Holes*. PhD thesis, Alberta U.

[139] Kuchař, K. (1974). Geometrodynamics regained: A Lagrangian approach. *J. Math. Phys.*, 15(6):708–715.

[140] Kunst, D., Ledvinka, T., Lukes-Gerakopoulos, G., and Seyrich, J. (2016). Comparing Hamiltonians of a spinning test particle for different tetrad fields. *Phys. Rev.*, D93(4):044004.

[141] Kunz, M. W., Stone, J. M., and Quataert, E. (2016). Magnetorotational turbulence and dynamo in a collisionless plasma. *Phys. Rev. Lett.*, 117(23):235101.

[142] Künzle, H. P. (1972). Canonical dynamics of spinning particles in gravitational and electromagnetic fields. *J. Math. Phys.*, 13:739–744.

[143] Kyrian, K. and Semerák, O. (2007). Spinning test particles in a Kerr field–ii. *Mon. Not. Roy. Astron. Soc.*, 382:1922.

[144] Laarakkers, W. G. and Poisson, E. (1999). Quadrupole moments of rotating neutron stars. *Astrophys. J.*, 512:282–287.

[145] Landau, L. and Lifshitz, E. (1959). *Course of theoretical physics. vol. 6: Fluid mechanics*. London.

[146] Lasota, J. P., Gourgoulhon, E., Abramowicz, M., Tchekhovskoy, A., and Narayan, R. (2014). Extracting black-hole rotational energy: The generalized Penrose process. *Phys. Rev.*, D89(2):024041.

[147] Latif, M., Schleicher, D., Schmidt, W., and Niemeyer, J. (2013). Black hole formation in the early universe. *Mon. Notices Royal Astron. Soc.*, 433(2):1607–1618.

[148] Lense, J. and Thirring, H. (1918). Über den Einfluß der Eigenrotation der Zentralkörper auf die Bewegung der Planeten und Monde nach der Einsteinschen Gravitationstheorie. *Physikalische Zeitschrift*, 19.

[149] Levi, M. and Steinhoff, J. (2016). Complete conservative dynamics for inspiralling compact binaries with spins at fourth post-Newtonian order.

[150] Lewin, W. and Van der Klis, M. (2006). *Compact stellar X-ray sources*, volume 39. Cambridge University Press.

[151] LISA Consortium (2017). LISA: Laser interferometer space antenna.

[152] Liska, M., Hesp, C., Tchekhovskoy, A., Ingram, A., van der Klis, M., and Markoff, S. (2017). Formation of precessing jets by tilted black hole discs in 3d general relativistic mhd simulations. *Mon. Notices Royal Astron. Soc.: Lett.*, 474(1):L81–L85.

[153] Lovelock, D. (1971). The Einstein tensor and its generalizations. *J. Math. Phys.*, 12(3):498–501.

[154] Lovelock, D. (1972). The four-dimensionality of space and the Einstein tensor. *J. Math. Phys.*, 13(6):874–876.

[155] Lu, R.-S., Broderick, A. E., Baron, F., Monnier, J. D., Fish, V. L., Doeleman, S. S., and Pankratius, V. (2014). Imaging the supermassive black hole shadow and jet base of M87 with the event horizon telescope. *Astrophys. J.*, 788(2):120.

[156] Lukes-Gerakopoulos, G. (2017). Time parameterizations and spin supplementary conditions of the Mathisson-Papapetrou-Dixon equations. *Phys. Rev.*, D96(10):104023.

[157] Lukes-Gerakopoulos, G., Katsanikas, M., Patsis, P. A., and Seyrich, J. (2016). The dynamics of a spinning particle in a linear in spin Hamiltonian approximation. *Phys. Rev.*, D94(2):024024.

[158] Lukes-Gerakopoulos, G., Seyrich, J., and Kunst, D. (2014). Investigating spinning test particles: spin supplementary conditions and the Hamiltonian formalism. *Phys. Rev.*, D90(10):104019.

[159] MacDonald, D. and Thorne, K. S. (1982). Black-hole electrodynamics: an absolute-space/universal-time formulation. *Mon. Notices Royal Astron. Soc.*, 198(2):345–382.

[160] Macdonald, D. A. and Suen, W.-M. (1985). Membrane viewpoint on black holes: Dynamical electromagnetic fields near the horizon. *Phys. Rev. D*, 32(4):848.

[161] Maeder, A. (1992). Stellar yields as a function of initial metallicity and mass limit for black hole formation. *Astron. Astrophys.*, 264:105–120.

[162] Marck, J.-A. (1983). Solution to the equations of parallel transport in Kerr geometry; tidal tensor. *Proc. R. Soc. Lond. A*, 385(1789):431–438.

[163] Markakis, C., Uryū, K., Gourgoulhon, E., Nicolas, J.-P., Andersson, N., Pouri, A., and Witzany, V. (2017). Conservation laws and evolution schemes in geodesic, hydrodynamic, and magnetohydrodynamic flows. *Phys. Rev. D*, 96(6):064019.

[164] Mathisson, M. (1937). Neue mechanik materieller systemes. *Acta Phys. Polon.*, 6:163–2900.

[165] McClintock, J. E., Narayan, R., and Steiner, J. F. (2014). Black Hole Spin via Continuum Fitting and the Role of Spin in Powering Transient Jets. *Space Sci. Rev.*, 183:295–322.

[166] McGaugh, S. S., Lelli, F., and Schombert, J. M. (2016). Radial acceleration relation in rotationally supported galaxies. *Phys. Rev. Lett.*, 117(20):201101.

[167] McKinney, J. C. (2005). Total and Jet Blandford-Znajek Power in Presence of Accretion Disk. *Astrophys. J.*, 630:L5–L8.

[168] McKinney, J. C. and Gammie, C. F. (2004). A Measurement of the electromagnetic luminosity of a Kerr black hole. *Astrophys. J.*, 611:977–995.

[169] McKinney, J. C., Tchekhovskoy, A., and Blandford, R. D. (2013). Alignment of Magnetized Accretion Disks and Relativistic Jets with Spinning Black Holes. *Science*, 339:49.

[170] McLachlan, R., Modin, K., and Verdier, O. (2017). A minimal-variable symplectic integrator on spheres. *Mathematics of Computation*, 86(307):2325–2344.

[171] McLachlan, R. I., Modin, K., and Verdier, O. (2014). Symplectic integrators for spin systems. *Physical Review E*, 89(6):061301.

[172] McNamara, B. R., Rohanizadegan, M., and Nulsen, P. E. J. (2011). Are Radio AGN Powered by Accretion or Black Hole Spin? *Astrophys. J.*, 727:39.

[173] Michel, F. C. (1972). Accretion of matter by condensed objects. *Astrophys. Space Sci.*, 15(1):153–160.

[174] Milgrom, M. (1983a). A Modification of the Newtonian dynamics as a possible alternative to the hidden mass hypothesis. *Astrophys. J.*, 270:365–370.

[175] Milgrom, M. (1983b). A Modification of the Newtonian dynamics: Implications for galaxies. *Astrophys. J.*, 270:371–383.

[176] Milgrom, M. (1983c). A modification of the Newtonian dynamics: implications for galaxy systems. *Astrophys. J.*, 270:384–389.

[177] Milgrom, M. (1983d). A modification of the Newtonian dynamics as a possible alternative to the hidden mass hypothesis. *Astrophys. J.*, 270:365–370.

[178] Milgrom, M. (2009). Bimetric MOND gravity. *Phys. Rev.*, D80:123536.

[179] Miller, M. C. and Miller, J. M. (2015). The masses and spins of neutron stars and stellar-mass black holes. *Phys. Rep.*, 548:1–34.

[180] Mino, Y. (2003). Perturbative approach to an orbital evolution around a supermassive black hole. *Phys. Rev.*, D67:084027.

[181] Misner, C. W., Thorne, K. S., and Wheeler, J. A. (1973). *Gravitation*. W. H. Freeman, San Francisco.

[182] Mościbrodzka, M. and Falcke, H. (2013). Coupled jet-disk model for Sagittarius A*: explaining the flat-spectrum radio core with GRMHD simulations of jets. *Astron. Astroph.*, 559:L3.

[183] Mościbrodzka, M., Falcke, H., and Shiokawa, H. (2016). General relativistic magneto-hydrodynamical simulations of the jet in M87. *Astron. Astrophys.*, 586:A38.

[184] Mościbrodzka, M., Falcke, H., Shiokawa, H., and Gammie, C. F. (2014). Observational appearance of inefficient accretion flows and jets in 3D GRMHD simulations: Application to Sagittarius A*. *Astron. Astroph.*, 570:A7.

[185] Nagar, A. et al. (2018). Time-domain effective-one-body gravitational waveforms for coalescing compact binaries with nonprecessing spins, tides and self-spin effects.

[186] Narayan, R., Igumenshchev, I. V., and Abramowicz, M. A. (2003). Magnetically arrested disk: an energetically efficient accretion flow. *Publ. Astron. Soc. Jpn*, 55(6):L69–L72.

[187] Narayan, R. and McClintock, J. E. (2008). Advection-dominated accretion and the black hole event horizon. *New Astron. Rev.*, 51(10):733–751.

[188] Narayan, R. and McClintock, J. E. (2012). Observational Evidence for a Correlation Between Jet Power and Black Hole Spin. *Mon. Not. Roy. Astron. Soc.*, 419:L69–L73.

[189] Narayan, R., SÄ dowski, A., Penna, R. F., and Kulkarni, A. K. (2012). GRMHD simulations of magnetized advection-dominated accretion on a non-spinning black hole: role of outflows. *Mon. Notices Royal Astron. Soc.*, 426:3241–3259.

[190] Narayan, R. and Yi, I. (1994). Advection-dominated accretion: A self-similar solution. *Astrophys. J. Lett.*, 428:L13–L16.

[191] Narayan, R. and Yi, I. (1995a). Advection-dominated accretion: Self-similarity and bipolar outflows. *Astrophys. J.*, 444:231–243.

[192] Narayan, R. and Yi, I. (1995b). Advection-dominated Accretion: Underfed Black Holes and Neutron Stars. *Astrophys. J.*, 452:710.

[193] Nealon, R., Nixon, C., Price, D. J., and King, A. (2015a). Apsidal precession, disc breaking and viscosity in warped discs. *Mon. Notices Royal Astron. Soc. Lett.*, 455(1):L62–L66.

[194] Nealon, R., Price, D. J., and Nixon, C. J. (2015b). On the Bardeen-Petterson effect in black hole accretion discs. *Mon. Notices Royal Astron. Soc.*, 448(2):1526–1540.

[195] Nemmen, R. S. and Tchekhovskoy, A. (2015). On The Efficiency of Jet Production in Radio Galaxies. *Mon. Not. Roy. Astron. Soc.*, 449(1):316–327.

[196] Newton, T. D. and Wigner, E. P. (1949). Localized States for Elementary Systems. *Rev. Mod. Phys.*, 21:400–406.

[197] Nordström, G. (1913). Träge und schwere Masse in der Relativitätsmechanik. *Ann. Phys. (Berl.)*, 345(5):856–878.

[198] Nordtvedt, K. (1968). Equivalence Principle for Massive Bodies. 1. Phenomenology. *Phys. Rev.*, 169:1014–1016.

[199] Novikov, I. D. and Thorne, K. S. (1973). Astrophysics of black holes. In Dewitt, C. and Dewitt, B. S., editors, *Black Holes (Les Astres Occlus)*, pages 343–450.

[200] Obukhov, Y. N. and Puetzfeld, D. (2011). Dynamics of test bodies with spin in de Sitter spacetime. *Phys. Rev.*, D83:044024.

[201] Ohashi, A. (2003). Multipole particle in relativity. *Phys. Rev.*, D68:044009.

[202] Ohsuga, K. and Mineshige, S. (2011). Global structure of three distinct accretion flows and outflows around black holes from two-dimensional radiation-magnetohydrodynamic simulations. *Astrophys. J.*, 736(1):2.

[203] O'Neill, B. (2014). *The geometry of Kerr black holes*. Courier Corporation.

[204] Paczynsky, B. and Wiita, P. J. (1980). Thick accretion disks and supercritical luminosities. *Astron. Astrophys.*, 88:23–31.

[205] Page, D. N. (1976). Dirac equation around a charged, rotating black hole. *Phys. Rev. D*, 14(6):1509.

[206] Page, D. N. and Thorne, K. S. (1974). Disk-accretion onto a black hole. time-averaged structure of accretion disk. *Astrophys. J.*, 191:499–506.

[207] Papaloizou, J. and Pringle, J. (1983). The time-dependence of non-planar accretion discs. *Mon. Notices Royal Astron. Soc.*, 202(4):1181–1194.

[208] Papapetrou, A. (1951). Spinning test-particles in general relativity. i. *Proc. Roy. Soc. Lond.*, A209:248–258.

[209] Penrose, R. (1969). Gravitational Collapse: the Role of General Relativity. *Nuovo Cimento Rivista Serie*, 1.

[210] Penrose, R. (1973). Naked singularities. *Ann. N. Y. Acad. Sci.*, 224(1):125–134.

[211] Perlick, V. (2004). Gravitational lensing from a spacetime perspective. *Living Rev. Rel.*, 7:9.

[212] Pirani, F. A. E. (1956). On the Physical significance of the Riemann tensor. *Acta Physica Polonica*, 15:389–405.

[213] Poisson, E., Pound, A., and Vega, I. (2011). The Motion of point particles in curved spacetime. *Living Rev. Rel.*, 14:7.

[214] Pope, S. B. (2000). *Turbulent Flows*. Cambridge University Press.

[215] Porto, R. A. (2006). Post-newtonian corrections to the motion of spinning bodies in nonrelativistic general relativity. *Phys. Rev.*, D73:104031.

[216] Pound, A. (2017). Nonlinear gravitational self-force: second-order equation of motion. *Phys. Rev. D*, 95(10):104056.

[217] Proga, D. and Begelman, M. C. (2003). Accretion of low angular momentum material onto black holes: Two-dimensional hydrodynamical inviscid case. *Astrophys. J.*, 582(1):69.

[218] Pryce, M. H. L. (1948). The Mass center in the restricted theory of relativity and its connection with the quantum theory of elementary particles. *Proc. Roy. Soc. Lond.*, A195:62–81.

[219] Punsly, B. (2011). High Jet Efficiency and Simulations of Black Hole Magnetospheres. *Astrophys. J.*, 728:L17.

[220] Ramírez, W. G. and Deriglazov, A. A. (2015). Lagrangian formulation for Mathisson-Papapetrou-Tulczyjew-dixon equations. *Phys. Rev.*, D92:124017.

[221] Rawlings, S. and Saunders, R. (1991). Evidence for a common central-engine mechanism in all extragalactic radio sources. *Nature*, 349:138–140.

[222] Rees, M., Begelman, M., Blandford, R., and Phinney, E. (1982). Ion-supported tori and the origin of radio jets. *Nature*, 295(5844):17.

[223] Ressler, S. M., Tchekhovskoy, A., Quataert, E., Chandra, M., and Gammie, C. F. (2015). Electron thermodynamics in GRMHD simulations of low-luminosity black hole accretion. *Mon. Notices Royal Astron. Soc.*, 454(2):1848–1870.

[224] Ruffini, R. and Wilson, J. R. (1975). Relativistic Magnetohydrodynamical Effects of Plasma Accreting Into a Black Hole. *Phys. Rev.*, D12:2959.

[225] Russell, D. M., Gallo, E., and Fender, R. P. (2013). Observational constraints on the powering mechanism of transient relativistic jets. *Mon. Not. Roy. Astron. Soc.*, 431:405.

[226] Ryan, B. R., Ressler, S. M., Dolence, J. C., Gammie, C. F., and Quataert, E. (2018). Two-temperature GRRMHD simulations of M87. *arXiv preprint arXiv:1808.01958*.

[227] Ryan, B. R., Ressler, S. M., Dolence, J. C., Tchekhovskoy, A., Gammie, C., and Quataert, E. (2017). The radiative efficiency and spectra of slowly accreting black holes from two-temperature GRRMHD simulations. *Astrophys. J. Lett.*, 844(2):L24.

[228] Sądowski, A. (2009). Slim disks around Kerr black holes revisited. *Astrophys. J. Suppl.*, 183(2):171.

[229] Sądowski, A. and Narayan, R. (2015). Powerful radiative jets in supercritical accretion discs around non-spinning black holes. *Mon. Notices Royal Astron. Soc.*, 453(3):3213–3221.

[230] Sądowski, A., Narayan, R., Penna, R., and Zhu, Y. (2013). Energy, momentum and mass outflows and feedback from thick accretion discs around rotating black holes. *Mon. Notices Royal Astron. Soc.*, 436(4):3856–3874.

[231] Sakstein, J. and Jain, B. (2017). Implications of the neutron star merger GW170817 for cosmological scalar-tensor theories. *Phys. Rev. Lett.*, 119(25):251303.

[232] Schäfer, G. and Jaranowski, P. (2018). Hamiltonian formulation of general relativity and post-Newtonian dynamics of compact binaries.

[233] Schnittman, J. D., Krolik, J. H., and Noble, S. C. (2013). X-ray spectra from magnetohydrodynamic simulations of accreting black holes. *Astrophys. J.*, 769(2):156.

[234] Schnittman, J. D., Krolik, J. H., and Noble, S. C. (2016). Disk emission from magnetohydrodynamic simulations of spinning black holes. *Astrophys. J.*, 819(1):48.

[235] Schwarzschild, K. (1916). Über das Gravitationsfeld eines Massenpunktes nach der Einsteinschen Theorie. *Sitzungsberichte der Königlich Preußischen Akademie der Wissenschaften (Berlin), 1916, Seite 189-196*.

[236] Seilmayer, M., Galindo, V., Gerbeth, G., Gundrum, T., Stefani, F., Gellert, M., Rüdiger, G., Schultz, M., and Hollerbach, R. (2014). Experimental evidence for nonaxisymmetric magnetorotational instability in a rotating liquid metal exposed to an azimuthal magnetic field. *Phys. Rev. Lett.*, 113(2):024505.

[237] Semerák, O. (1998). Circular orbits in stationary axisymmetric spacetimes. *Gen. Rel. Gravit.*, 30(8):1203–1215.

[238] Semerák, O. (1999). Spinning test particles in a Kerr field—i. *Monthly Notices of the Royal Astronomical Society*, 308(3):863–875.

[239] Semerák, O. and Šrámek, M. (2015). Spinning particles in vacuum spacetimes of different curvature types. *Phys. Rev.*, D92(6):064032.

[240] Semerák, O. and Suková, P. (2010). Free motion around black holes with discs or rings: between integrability and chaos - I. *Mon. Not. Roy. Astron. Soc.*, 404:545–574.

[241] Semerák, O. and Suková, P. (2012). Free motion around black holes with discs or rings: between integrability and chaos - II. *Mon. Not. Roy. Astron. Soc.*, 425:2455–2476.

[242] Shakura, N. I. and Sunyaev, R. A. (1973). Black holes in binary systems. observational appearance. *Astron. Astrophys.*, 24:337–355.

[243] Shen, Y. (2013). The mass of quasars. *Bull. Astron. Soc. India*, 41:61–115.

[244] Smak, J. (1984). Accretion in cataclysmic binaries. IV - Accretion disks in dwarf novae. *Acta Astron.*, 34:161–189.

[245] Sorathia, K. A., Reynolds, C. S., Stone, J. M., and Beckwith, K. (2012). Global Simulations of Accretion Disks. I. Convergence and Comparisons with Local Models. *Astrophys. J.*, 749:189.

[246] Stäckel, P. (1891). *Über die Integration der Hamilton-Jacobischen Differentialgleichung mittelst Separation der Variabeln...* Teubner. digital version at archiv.ub.uni-heidelberg.de/volltextserver/12758/.

[247] Stefani, F., Gerbeth, G., Gundrum, T., Hollerbach, R., Priede, J., Rüdiger, G., and Szklarski, J. (2009). Helical magnetorotational instability in a Taylor-Couette flow with strongly reduced Ekman pumping. *Phys. Rev. E*, 80(6):066303.

[248] Stefani, F., Gundrum, T., Gerbeth, G., Rüdiger, G., Schultz, M., Szklarski, J., and Hollerbach, R. (2006). Experimental evidence for magnetorotational instability in a Taylor-Couette flow under the influence of a helical magnetic field. *Phys. Rev. Lett.*, 97(18):184502.

[249] Steiner, J. F., McClintock, J. E., and Narayan, R. (2013). Jet Power and Black Hole Spin: Testing an Empirical Relationship and Using it to Predict the Spins of Six Black Holes. *Astrophys. J.*, 762:104.

[250] Steinhoff, J. (2015). Spin and quadrupole contributions to the motion of astrophysical binaries. In *Equations of Motion in Relativistic Gravity*, volume 179, pages 615–649.

[251] Steinhoff, J. and Puetzfeld, D. (2010). Multipolar equations of motion for extended test bodies in general relativity. *Physical Review D*, 81(4):044019.

[252] Steinhoff, J. and Puetzfeld, D. (2012). Influence of internal structure on the motion of test bodies in extreme mass ratio situations. *Phys. Rev.*, D86:044033.

[253] Steinhoff, J. and Schäfer, G. (2009). Canonical formulation of self-gravitating spinning-object systems. *EPL*, 87(5):50004.

[254] Stephani, H., Kramer, D., MacCallum, M., Hoenselaers, C., and Herlt, E. (2009). *Exact solutions of Einstein's field equations*. Cambridge University Press.

[255] Stepney, S. (1983). Two-body relaxation in relativistic thermal plasmas. *Mon. Notices Royal Astron. Soc.*, 202(2):467–481.

[256] Suková, P. and Semerák, O. (2013). Free motion around black holes with discs or rings: between integrability and chaos - III. *Mon. Not. Roy. Astron. Soc.*, 436:978–996.

[257] Suzuki, S. and Maeda, K.-i. (1997). Chaos in Schwarzschild space-time: The motion of a spinning particle. *Phys. Rev.*, D55:4848–4859.

[258] Synge, J. L. (1960). *Relativity: The general theory*. North-Holand Publishing Co., Amsterdam.

[259] Tauber, G. E. (1988). Canonical formalism and equations of motion for a spinning particle in general relativity. *Int. J. Theor. Phys.*, 27:335.

[260] Taylor, G. I. (1923). Stability of a Viscous Liquid Contained between Two Rotating Cylinders. *Philosophical Transactions of the Royal Society of London Series A*, 223:289–343.

[261] Tchekhovskoy, A., Narayan, R., and McKinney, J. C. (2010). Black Hole Spin and the Radio Loud/Quiet Dichotomy of Active Galactic Nuclei. *Astrophys. J.*, 711:50–63.

[262] Tchekhovskoy, A., Narayan, R., and McKinney, J. C. (2011). Efficient Generation of Jets from Magnetically Arrested Accretion on a Rapidly Spinning Black Hole. *Mon. Not. Roy. Astron. Soc.*, 418:L79–L83.

[263] Tessmer, M., Steinhoff, J., and Schäfer, G. (2013). Canonical angles in a compact binary star system with spinning components: Approximative solution through next-to-leading-order spin-orbit interaction for circular orbits. *Phys. Rev.*, D87(6):064035.

[264] Tetarenko, B., Sivakoff, G., Heinke, C., and Gladstone, J. (2016). Watchdog: a comprehensive all-sky database of galactic black hole X-ray binaries. *Astrophys. J. Suppl.*, 222(2):15.

[265] Teukolsky, S. A. (1972). Rotating black holes: Separable wave equations for gravitational and electromagnetic perturbations. *Phys. Rev. Lett.*, 29(16):1114.

[266] Teukolsky, S. A. (1973). Perturbations of a rotating black hole. 1. fundamental equations for gravitational electromagnetic and neutrino field perturbations. *Astrophys. J.*, 185:635–647.

[267] Thirring, H. (1918). Über die Wirkung rotierender ferner Massen in der Einsteinschen Gravitationstheorie. *Phys. Z.*, 19.

[268] Thirring, H. (1921). Berichtigung zu meiner Arbeit: "Über die Wirkung rotierender Massen in der Einsteinschen Gravitationstheorie". *Physikalische Zeitschrift*, 22.

[269] Thomas, J., Ma, C.-P., McConnell, N. J., Greene, J. E., Blakeslee, J. P., and Janish, R. (2016). A 17-billion-solar-mass black hole in a group galaxy with a diffuse core. *Nature*, 532(7599):340.

[270] Thorne, K. S. and Macdonald, D. (1982). Electrodynamics in curved spacetime: 3+ 1 formulation. *Mon. Notices Royal Astron. Soc.*, 198(2):339–343.

[271] Thorne, K. S., Price, R. H., and MacDonald, D. A. (1986). *Black holes: the membrane paradigm*. Yale university press.

[272] Torres del Castillo, G. (1988). The separability of Maxwell's equations in type-D backgrounds. *J. Math. Phys.*, 29(4):971–977.

[273] Tremaine, S. and Davis, S. W. (2014). Dynamics of warped accretion discs. *Mon. Notices Royal Astron. Soc.*, 441(2):1408–1434.

[274] Treves, A., Maraschi, L., and Abramowicz, M. (1988). Basic elements of the theory of accretion. *Publ. Astron. Soc. Pac.*, 100(626):427.

[275] Tulczyjew, W. (1959). Motion of multipole particles in general relativity theory. *Acta Phys. Pol.*, 18:393.

[276] Tully, R. B. and Fisher, J. R. (1977). A New method of determining distances to galaxies. *Astron. Astrophys.*, 54:661–673.

[277] Unruh, W. (1973). Separability of the neutrino equations in a Kerr background. *Phys. Rev. Lett.*, 31(20):1265.

[278] Van Der Klis, M. (2006). *Rapid X-ray variability*, volume 39, pages 39–112.

[279] Velikhov, E. (1959). Stability of an ideally conducting liquid flowing between cylinders rotating in a magnetic field. *Sov. Phys. JETP*, 36(9):995–998.

[280] Vines, J., Kunst, D., Steinhoff, J., and Hinderer, T. (2016). Canonical Hamiltonian for an extended test body in curved spacetime: To quadratic order in spin. *Phys. Rev.*, D93(10):103008.

[281] Volonteri, M. (2012). The formation and evolution of massive black holes. *Science*, 337(6094):544–547.

[282] Volonteri, M., Silk, J., and Dubus, G. (2015). The case for supercritical accretion onto massive black holes at high redshift. *Astrophys. J.*, 804(2):148.

[283] Wald, R. M. (1984). *General Relativity*. Chicago Univ. Pr., Chicago, USA.

[284] Walker, M. and Penrose, R. (1970). On quadratic first integrals of the geodesic equations for type $\{22\}$ spacetimes. *Commun. Math. Phys.*, 18(4):265–274.

[285] Walsh, J. L., Barth, A. J., Ho, L. C., and Sarzi, M. (2013). The M87 black hole mass from gas-dynamical models of space telescope imaging spectrograph observations. *Astrophys. J.*, 770(2):86.

[286] Warburton, N. and van de Meent, M. (2017-2018). KerrGeodesics Mathematica package. http://bhptoolkit.org/{K}errGeodesics/.

[287] Wilkins, D. C. (1972). Bound geodesics in the Kerr metric. *Phys. Rev. D*, 5(4):814.

[288] Witzany, V. (2017). Exploiting the hidden symmetry of spinning black holes: conservation laws and numerical tests. *Mon. Notices Royal Astron. Soc.*, 473(2):2434–2440.

[289] Witzany, V. and Jefremov, P. (2018). New closed analytical solutions for geometrically thick fluid tori around black holes-numerical evolution and the onset of the magneto-rotational instability. *Astron. Astrophys.*, 614:A75.

[290] Witzany, V. and Lämmerzahl, C. (2016). A pseudo-Newtonian description of any stationary space-time. *Proc. Int. Astron. Union*, 12(S324):45–46.

[291] Witzany, V. and Lämmerzahl, C. (2017). Pseudo-Newtonian equations for evolution of particles and fluids in stationary space-times. *Astrophys. J.*, 841(2):105.

[292] Witzany, V., Semerák, O., and Suková, P. (2015). Free motion around black holes with discs or rings: between integrability and chaos – IV. *Mon. Not. Roy. Astron. Soc.*, 451(2):1770–1794.

[293] Witzany, V., Steinhoff, J., and Lukes-Gerakopoulos, G. (2018). Hamiltonians and canonical coordinates for spinning particles in curved space-time. *arXiv preprint arXiv:1808.06582*. In review at Phys. Rev. D.

[294] Woodhouse, N. (1975). Killing tensors and the separation of the Hamilton-Jacobi equation. *Commun. Math. Phys.*, 44(1):9–38.

[295] Wu, X.-B., Wang, F., Fan, X., Yi, W., Zuo, W., Bian, F., Jiang, L., McGreer, I. D., Wang, R., Yang, J., et al. (2015). An ultraluminous quasar with a twelve-billion-solar-mass black hole at redshift 6.30. *Nature*, 518(7540):512.

[296] Yuan, F. and Narayan, R. (2014). Hot accretion flows around black holes. *Annu. Rev. Astron. Astrophys.*, 52:529–588.

[297] Zlosnik, T. G., Ferreira, P. G., and Starkman, G. D. (2007). Modifying gravity with the Aether: An alternative to Dark Matter. *Phys. Rev.*, D75:044017.

Appendix A

Derivations for Hamiltonians for spinning particles

A.1 The generalized KS conditions

The sole condition that we need to be fulfilled for $\dot{S}^{\kappa\lambda} = 0$ to hold is that $\dot{S}^{\mu\nu} w_\nu = 0$ for some time-like w^ν. From equation (3.6) projected into w^ν we then get

$$w^\nu \dot{x}_\nu \dot{S}^{\kappa\lambda} = 0\,. \tag{A.1}$$

Since the product of any two time-like vectors is non-zero, we then get simply $\dot{S}^{\kappa\lambda} = 0$. The supplementary condition can thus be of the form $S^{\mu\nu} w_\nu = m^\mu$ with

$$S^{\mu\nu} \dot{w}_\nu = \dot{m}^\mu\,, \tag{A.2}$$

because then we will have $\dot{S}^{\mu\nu} w_\nu = 0$. The meaning of m^μ is the mass dipole moment in the frame w^μ. In other words, whenever $m^\mu \neq 0$, $x^\mu(\tau)$ does not describe the center of mass in the w^μ frame but a slightly shifted position.

In the case when $m^\mu = 0$, we get that $\dot{w}_\nu$ must lay in the degenerate directions of the spin tensor, $\dot{w}_\nu = \alpha w_\nu + \beta s_\nu$ with α, β arbitrary functions of any variables [239]. Nonetheless, we may generally set $m^\mu \neq 0$ and then the only condition on the evolution is Eq. (A.2). One particular option is $\dot{w}^\mu = \dot{m}^\mu = 0$.

However, it should be noted that only the initial choices of w^μ, m^ν matter. This can be seen from the fact that if the equations of motion are expressed in terms of $S^{\mu\nu}$, we need no reference to $\dot{w}^\mu, \dot{m}^\nu$ as long as equation (A.2) is satisfied.

In conclusion, once we allow for $m^\mu \neq 0$, the initial conditions for $S^{\mu\nu}$ are completely unconstrained. The study of d'Ambrosi et al. [65] can be understood as conducted exactly in the $m^\mu \neq 0$ generalized KS condition.

One last remark is that the vector m^μ represents a mass dipole in the frame w^μ, and by setting its dynamics to fulfill different evolution equations than in Eq. (A.2), we can in fact obtain other supplementary conditions [201].

A.2 The expression for $\dddot{x}^\mu$ under MP condition

Take equations (3.5) and (3.7) to obtain

$$(m\dot{x}^\mu + \dot{x}_\gamma \dot{S}^{\gamma\mu})^\cdot = -\frac{1}{2} R^\mu{}_{\nu\kappa\lambda} \dot{x}^\nu S^{\kappa\lambda} \,. \tag{A.3}$$

Now use $S^{\mu\nu}\dot{x}_\nu = 0$ along with its time-derivatives and the fact that $\dot{x}_\gamma \ddot{x}^\gamma = 0$, $\dot{x}_\gamma \dot{P}^\gamma = 0$ to obtain [212]

$$m\ddot{x}^\mu - \dddot{x}_\gamma S^{\gamma\mu} = -\frac{1}{2} R^\mu{}_{\nu\kappa\lambda} \dot{x}^\nu S^{\kappa\lambda} \,. \tag{A.4}$$

We now contract the expression above with $S_{\nu\mu}/S^2$ and partially re-express the result using the spin vector s^λ to obtain

$$\dddot{x}^\kappa \left(\delta^\nu_\kappa + \dot{x}_\kappa \dot{x}^\nu - \frac{s_\kappa s^\nu}{S^2} \right) = \frac{m}{S^2} \ddot{x}^\mu S^\nu_\mu + \frac{1}{2S^2} R_{\mu\lambda\kappa\gamma} \dot{x}^\lambda S^{\nu\mu} S^{\kappa\gamma} \,. \tag{A.5}$$

In other words, we now have the expression for the jerk $\dddot{x}^\nu$ on the subspace orthogonal to $s^\lambda, \dot{x}^\kappa$. The projection of the jerk into velocity can be computed from the second derivative of four-velocity normalization as $\dddot{x}^\mu \dot{x}_\mu = -\ddot{x}^\mu \ddot{x}_\mu$. For the projection of the jerk into the spin vector, we use the Fermi-transport property $\dot{s}^\mu = -\dot{s}^\nu \dot{x}_\nu \dot{x}^\mu$ to express $\dot{s}^\nu \ddot{x}_\nu = 0$. This allows us rewrite the projection as

$$s^\mu \dddot{x}_\mu = \frac{\mathrm{D}}{\mathrm{d}\tau} (s^\mu \ddot{x}_\mu) \,. \tag{A.6}$$

Hence, let us project Eq. (A.4) into s^μ to obtain

$$s^\mu \ddot{x}_\mu = -\frac{1}{2m} R_{\mu\nu\kappa\lambda} s^\mu \dot{x}^\nu S^{\kappa\lambda} \,. \tag{A.7}$$

We now see that the time-derivative of $\ddot{x}^\mu s_\mu$ can be completely expressed by known functions of $x^\mu, \dot{x}^\nu, \ddot{x}^\kappa, s^\lambda$.

From that, it is now easy to compose the complete prescription for the jerk only in terms of the variables $\dot{x}^\mu, \ddot{x}^\lambda, s^\gamma$ as

$$\dddot{x}^\nu = \frac{1}{S^2}\left(m\ddot{x}_\mu - \star R_{\mu\lambda\kappa\gamma}\dot{x}^\lambda s^\kappa \dot{x}^\gamma\right)\varepsilon^{\nu\mu\sigma\tau}\dot{x}_\sigma s_\tau + \ddot{x}^\kappa \ddot{x}_\kappa \dot{x}^\nu + \frac{1}{mS^2}\left(\star R_{\mu\lambda\kappa\gamma;\sigma}s^\mu \dot{x}^\lambda s^\kappa \dot{x}^\gamma \dot{x}^\sigma + 2\star R_{\mu\lambda\kappa\gamma}s^\mu s^\kappa \dot{x}^{(\lambda}\ddot{x}^{\gamma)}\right)s^\nu . \tag{A.8}$$

A.3 Field-theoretic motivation for Poisson brackets

Let us assume a fixed 3+1 split of space-time which consists of a family of non-intersecting spatial hypersurfaces Σ_t (we will suppress the t in the following) with coordinates x^i and induced metric d_{ij}, volume element $\mathrm{d}\Sigma = \sqrt{d}\,\mathrm{d}^3x$. This means that our time parametrization is fixed and what we expect to find is not strictly the parametrization-invariant Poisson bracket (3.29), but rather a constrained bracket with new terms in the temporal sector [see 110, 109, for more details].

We can now take a Lagrangian density $\mathscr{L} = \tilde{\mathscr{L}}\sqrt{-g}$ ($\tilde{\mathscr{L}}$ is the Lagrangian scalar) and obtain a Hamiltonian density using the usual Legendre transformation

$$\pi_a = \frac{\partial \mathscr{L}}{\partial(\partial_t \phi^a)}, \rightarrow \partial_t \phi_a = f(\pi_b, \phi^b, ...), \tag{A.9}$$

$$\mathscr{H}(\pi_b, \phi^b, ...) = \frac{\partial \mathscr{L}}{\partial(\partial_t \phi^a)}\partial_t \phi^a - \mathscr{L}, \tag{A.10}$$

where ϕ^a stands for a generic collection of fields. Note that π_a is a density on Σ (*not* in the whole space-time). In the following we will always assume that all the fields and momenta vanish smoothly at the boundary of Σ (spatial infinity).

This system of fields and momentum densities then has the non-zero local Poisson brackets (meaningful only when evaluated for fields at the same t)

$$\{\phi^a(x^i,t), \pi_b(y^i,t)\} = \delta^a_b \delta^{(3)}(x^i - y^i), \tag{A.11}$$

where we can generate brackets for gradients by commuting the gradient with the bracket. It can be shown that this generates a Poisson bracket for functionals

$$A(t)[\pi,\phi] = \int \mathscr{A}(\pi_a, \pi_{a,i}, \phi, \phi^a_{,i}, x^i, t)\mathrm{d}^3x\,, \tag{A.12}$$

$$B(t)[\pi,\phi] = \int \mathscr{B}(\pi_a, \pi_{a,i}, \phi, \phi^a_{,i}, x^i, t)\mathrm{d}^3x\,, \tag{A.13}$$

$$\{A(t), B(t)\} = \int \frac{\delta\mathscr{A}}{\delta\phi^a}\frac{\delta\mathscr{B}}{\delta\pi_a} - \frac{\delta\mathscr{B}}{\delta\phi^a}\frac{\delta\mathscr{A}}{\delta\pi_a}\mathrm{d}^3x\,, \tag{A.14}$$

where $\mathscr{A}, \mathscr{B}$ are densities on Σ and $\delta\mathscr{F}/\delta f$ is the variational derivative

$$\frac{\delta\mathscr{F}}{\delta f} = \frac{\partial\mathscr{F}}{\partial f} - \frac{\partial}{\partial x^i}\frac{\partial\mathscr{F}}{\partial(f_{,i})}\,, \tag{A.15}$$

where we have assumed that $\mathscr{F}$ is dependent only on f and its first-order gradients (for higher order gradients we get a series of analogous terms of varying sign).

A.3.1 Total momentum

Let us now define a particular momentum quantity Π_μ that will play an analogous role as the covariant momentum P_μ

$$\Pi_\mu(t) \equiv -\int_\Sigma T^\nu_\mu n_\nu \mathrm{d}\Sigma\,, \tag{A.16}$$

where n_ν is the unit normal to Σ.

For this expression, we choose the canonical stress-energy tensor generated by diffeomorphism invariance rather than the Hilbert stress-energy tensor

$$T^\nu_\mu = \frac{\partial\tilde{\mathscr{L}}}{\partial(\phi^a_{,\nu})}\phi^a_{;\mu} - \delta^\nu_\mu\tilde{\mathscr{L}}\,. \tag{A.17}$$

The momentum can then be rewritten as

$$\Pi_\mu(t) = -\int \pi_a\phi^a_{;\mu} - \delta^t_\mu\mathscr{L}\mathrm{d}^3x\,. \tag{A.18}$$

Namely, we have

$$\Pi_t = -\int \mathscr{H} + \gamma^a_{tb}\pi_a\phi^b\mathrm{d}^3x\,, \tag{A.19}$$

where $\gamma^a_{\mu b}$ are some connection coefficients for the covariant derivative of the fields ϕ^a, $\phi^a_{;\mu} = \phi^a_{,\mu} + \gamma^a_{\mu b}\phi^b$.

We require that $(\phi^a\pi_a)_{,\mu} = (\phi^a\pi_a)_{;\mu}$ and the validity of the Leibniz rule, which leads us to the definition of the pseudo-covariant derivative of π_a as $\pi_{a;\mu} = \pi_{a,\mu} - \gamma^b_{\mu a}\pi_b$. This convention is at odds with the usual convention for the covariant gradient of a density; its intuitive meaning is that $\pi_{a;\mu}$ is rather some kind of "total density variation" of π_a.

Since $\{\phi^a(x^i,t), \mathscr{H}(y^i,t)\} = \partial_t\phi(x^i,t)\delta^{(3)}(x^i-y^i)$ then we get

$$\{\phi^a(x^i,t), \Pi_t\} = -\phi^a_{,t} - \gamma^a_{tb}\phi^b = -\phi^a_{;t}(x^i,t)\,. \tag{A.20}$$

For the spatial part we obtain similarly

$$\{\phi^a(x^j,t), \Pi_i\} = -\int\{\phi^a, \pi_b\phi^b_{;i}\}\mathrm{d}^3x = -\phi^a_{;i}(x^j,t)\,. \tag{A.21}$$

For the momenta we obtain analogously

$$\{\pi_a(x^i,t), \Pi_\mu\} = -\pi_{a,\mu} + \gamma^b_{\mu a}\pi_b = -\pi_{a;\mu}(x^i,t)\,. \tag{A.22}$$

That is, at least for functions of fields and momenta which do not involve their gradients, $\{\cdot, \Pi_\mu\}$ is minus the covariant gradient operator.

A.3.2 Mutual momentum brackets

We start by computing the bracket $\{\Pi_\mu, \Pi_\nu\}$. First we compute

$$\begin{aligned}\{\Pi_i, \Pi_t\} &= \iint\{\pi_c(\phi^c_{,i} + \gamma^c_{id}\phi^d), \mathscr{H} + \gamma^a_{tb}\pi_a\phi^b\}\,\mathrm{d}^3x\,\mathrm{d}^3y \\ &= -2\int\pi_{c;[i}\phi^c_{;t]}\mathrm{d}^3x\,.\end{aligned} \tag{A.23}$$

The spatial brackets then yield

$$\begin{aligned}\{\Pi_i, \Pi_j\} &= \iint\{\pi_c(\phi^c_{,i} + \gamma^c_{id}\phi^d), \pi_a(\phi^a_{,i} + \gamma^a_{id}\phi^b)\}\,\mathrm{d}^3x\,\mathrm{d}^3y \\ &= -2\int\pi_{c;[i}\phi^c_{;j]}\mathrm{d}^3x\,.\end{aligned} \tag{A.24}$$

In summary $\{\Pi_\mu, \Pi_\nu\} = -2\int\pi_{c[;\mu}\phi^c_{;\nu]}\mathrm{d}^3x$. On the other hand, in the brackets (3.29) we have $\{P_\mu, P_\nu\} = -R_{\alpha\beta\mu\nu}S^{\alpha\beta}/2$.

We try to simplify the brackets further, starting with $\{\Pi_i, \Pi_j\}$. To do that we reexpress

$$\pi_{c;i}\phi^c_{;j} = (\pi_c\phi^c_{;j})_{,i} - \pi_c\phi^c_{|ji}\,, \tag{A.25}$$

$$\begin{aligned}\phi^c_{|ji} &\equiv \phi^c_{,ji} + \gamma^c_{ib}\phi^b_{,j} + \gamma^c_{jb}\phi^b_{,i} + \gamma^c_{jb,i}\phi^b + \gamma^c_{jb}\gamma^b_{ia}\phi^a \\ &= \phi^c_{;ji} - \Gamma^k_{\ ji}\phi^c_{,k}\,,\end{aligned} \tag{A.26}$$

Although $\phi^c_{|ij}$ is missing a part to be fully covariant with respect to the background space-time, its antisymmetric part is in fact covariant and yields

$$\phi^c_{|ji} - \phi^c_{|ij} = R^c_{\ bji}\phi^b\,. \tag{A.27}$$

We then assume that the field vanishes at the boundaries of Σ and obtain

$$\{\Pi_i, \Pi_j\} = \int \pi_{c;j}\phi^c_{;i} - \pi_{c;i}\phi^c_{;j}\mathrm{d}^3x = -\int R^a_{\ bij}\pi_a\phi^b\mathrm{d}^3x\,. \tag{A.28}$$

For the $\{\Pi_t, \Pi_i\}$ bracket we can use a similar trick but some of the gradients will be with respect to t and do not integrate out to boundary terms. As a result, we obtain

$$\{\Pi_i, \Pi_t\} = -\int R^a_{\ bit}\pi_a\phi^b\mathrm{d}^3x + \int (\pi_c\phi^c_{;i})_{,t}\mathrm{d}^3x\,. \tag{A.29}$$

In summary

$$\{\Pi_\mu, \Pi_\nu\} = -\int R^a_{\ b\mu\nu}\pi_a\phi^b\mathrm{d}^3x + \delta^t_\mu\frac{\mathrm{d}\Pi_\nu}{\mathrm{d}t} - \delta^t_\nu\frac{\mathrm{d}\Pi_\mu}{\mathrm{d}t}\,. \tag{A.30}$$

This is an *exact* relation for an arbitrary collection of fields vanishing at infinity and an arbitrary 3+1 split. Note that for a single scalar field the first term vanishes and we probably cannot get anything resembling the Poisson brackets (3.29). In the next Section we briefly describe a formal expansion of this relation.

A.3.3 "Monopole" approximation

Let us assume that the fields ϕ^a, π_b are non-vanishing only over a small volume as compared to the variability length of the curvature. Then we can expand the integral from the $\{\Pi_\mu, \Pi_\nu\}$

bracket as

$$\begin{aligned}\int R^a_{b\mu\nu}\pi_a\phi^b\mathrm{d}^3x =& R^a_{b\mu\nu}(x^i_{\mathrm{W}},t)\int \pi_a\phi^b\mathrm{d}^3x \\ &+ R^a_{b\mu\nu;k}(x^i_{\mathrm{W}},t)\int X^k\pi_a\phi^b\mathrm{d}^3x \\ &+\dots,\end{aligned} \tag{A.31}$$

where x^i_{W} is some referential point inside the volume where the fields are non-vanishing, and the vector field $X^k(x^i,x^i_{\mathrm{W}},t)$ can be constructed, e.g., as the gradient of Synge's world function around x^i_{W} [258]. If we take only the first term of this expansion, we obtain

$$\begin{aligned}\{\Pi_\mu(t),\Pi_\nu(t)\} =& -\frac{1}{2}R^a_{b\mu\nu}(x^i_{\mathrm{W}},t)\mathscr{S}_a{}^b \\ &+\delta^t_\mu\frac{\mathrm{d}\Pi_\nu}{\mathrm{d}t}-\delta^t_\nu\frac{\mathrm{d}\Pi_\mu}{\mathrm{d}t}+\dots,\end{aligned} \tag{A.32}$$

$$\mathscr{S}_a{}^b \equiv 2\int \pi_a\phi^b\mathrm{d}^3x, \tag{A.33}$$

where the spin tensor S^{AB} corresponds to the antisymmetric part of $\mathscr{S}_a{}^b$ drawn into tetrad components.

A.3.4 $\{\mathscr{S}_a{}^b,\Pi_\mu\}$ bracket

Let us first compute the spatial part,

$$\begin{aligned}\{\mathscr{S}_a{}^b,\Pi_i\} &= -2\iint\{\pi_a\phi^b,\pi_c\phi^c_{;i}\}\mathrm{d}^3x\,\mathrm{d}^3y \\ &= -2\int \pi_a\phi^b_{;i}+\pi_{a;i}\phi^b\mathrm{d}^3x \\ &= -2\int(\pi_a\phi^b)_{,i}+\gamma^b_{id}\pi_a\phi^d-\gamma^c_{ia}\pi_c\phi^b\mathrm{d}^3x.\end{aligned} \tag{A.34}$$

The temporal part reads

$$\begin{aligned}\{\mathscr{S}_a{}^b,\Pi_t\} &= -2\iint\{\pi_a\phi^b,\mathscr{H}+\gamma^c_{td}\pi_c\phi^d\}\mathrm{d}^3x\,\mathrm{d}^3y \\ &= -2\int(\pi_a\phi^b)_{,t}+\gamma^b_{td}\pi_a\phi^d-\gamma^c_{ta}\pi_c\phi^b\mathrm{d}^3x.\end{aligned} \tag{A.35}$$

The first term in the last line can be rewritten as $\mathrm{d}\mathscr{S}_a{}^b/\mathrm{d}t$.

Assuming again a leading-order expansion of the integrals we obtain

$$\{\mathscr{S}_a{}^b,\Pi_\mu\} = -\gamma^b_{\mu d}\mathscr{S}_a{}^d + \gamma^c_{\mu a}\mathscr{S}_c{}^b + \delta^t_\mu \frac{\mathrm{d}\mathscr{S}_a{}^b}{\mathrm{d}t} + \dots . \tag{A.36}$$

This is in good correspondence to the respective Poisson bracket in (3.29).

A.3.5 $\{\mathscr{S}_a{}^b,\mathscr{S}_c{}^d\}$ bracket

$$\{\mathscr{S}_a{}^b,\mathscr{S}_c{}^d\} = \iint \{\pi_a\phi^b,\pi_c\phi^d\}\mathrm{d}^3x\mathrm{d}^3y = \delta_c{}^b\mathscr{S}_a{}^d - \delta_a{}^d\mathscr{S}_c{}^b . \tag{A.37}$$

The corresponding Poisson bracket in (3.29) contains additional terms that follow once we anti-symmetrize $\mathscr{S}_a{}^b$.

A.3.6 The world-line coordinate

The representative point for the "monopole" approximation defined above can be constructed as

$$x^i_{\mathrm{W}} \equiv \frac{\int x^i f(\phi^a\pi_a)\mathrm{d}^3x}{\int f(\phi^a\pi_a)\mathrm{d}^3x} \tag{A.38}$$

With f an arbitrary differentiable, positive definite function of its argument. Then we can compute

$$\begin{aligned}\{x^j_{\mathrm{W}},\Pi_i\} =& -\frac{\int x^j f'(\phi^a\pi_a)(\phi^a\pi_a)_{,i}\mathrm{d}^3x}{\int f(\phi^a\pi_a)\mathrm{d}^3x} + \frac{\int x^j f(\phi^a\pi_a)\mathrm{d}^3x}{\int f(\phi^a\pi_a)\mathrm{d}^3x}\frac{\int f'(\phi^a\pi_a)(\phi^a\pi_a)_{,i}\mathrm{d}^3x}{\int f(\phi^a\pi_a)\mathrm{d}^3x} \\ =& \frac{\int (x^j)_{,i} f(\phi^a\pi_a)\mathrm{d}^3x}{\int f(\phi^a\pi_a)\mathrm{d}^3x} = \delta_i{}^j .\end{aligned} \tag{A.39}$$

That is, this is exactly the canonically conjugate coordinate we are looking for.

Quite naturally, the time coordinate t_{W} is just t. In principle, we can then write the commutation relation in a unified form that emphasizes the similarity with the other brackets and thus the terms coming from the time-parametrization constraint

$$\{x^\mu_{\mathrm{W}},\Pi_\nu\} = \delta^\mu_\nu - \delta^t_\nu \frac{\mathrm{d}x^\mu_{\mathrm{W}}}{\mathrm{d}t} . \tag{A.40}$$

A.3.7 Discussion of field-theoretic motivation of Poisson bracket

A peculiar feature of the derivation given above is that the spin structure of the brackets comes from the internal field structure already in a monopole, rather than a pole-dipole approximation. However, for instance a perfect fluid can be described only by a set of scalar fields and would

not generate these "spin dynamics". Hence, the present derivation of the Poisson brackets is not a fundamental reasoning as to why such a set of brackets should apply to the motion of compact astrophysical objects. We thus understand the procedure given in this Appendix merely as one of the possible motivations for the Poisson brackets (3.29). The procedure above also provides an interesting field-theoretic background for the spinor and vector-based models of classical particles with spin [53, 44, 17, 105, 220].

When I tried to derive brackets for higher-order multipoles, the attempt broke down as inelegant non-covariant terms started mixing into the expressions. I am convinced that for a generalization of the procedure above to higher multipoles, a more careful construction of the multipolar expansion must be given. Namely, definitions of "vector-like" quantities such as Π_μ are not covariant even with respect to coordinate changes on Σ and covariant definitions with similar properties must be found.

A.4 Constraining the Khriplovich Hamiltonian

A.4.1 Constraint theory

Let me first recapitulate some elements of Dirac-Bergmann constraint theory as presented for example by Dirac [73], Hanson et al. [109].

Let $\Phi^a = 0$ be a set of constraints on phase space we want to impose on the system, with a some index labeling the constraints. Let us further assume that the matrix $C^{ab} \equiv \{\Phi^a, \Phi^b\}$ is non-degenerate and we can thus find an inverse matrix C^{-1}_{ab}. The goal is to find a Hamiltonian H' which fulfills $\{\Phi^a, H'\} = \dot{\Phi}^a \cong 0$, where $\cong$ denotes an equality which is fulfilled under the condition that all the constraints $\Phi^a = 0$ hold. Such a Hamiltonian can be obtained from the original one as

$$H' = H - \{H, \Phi^a\} C^{-1}_{ab} \Phi^b \,. \tag{A.41}$$

In the herein considered case we will be imposing the constraints of the form $S^{\mu\nu}V_\nu = 0$. By counting the components of the constraint, we might be tempted to state that there are a total of 4 constraints imposed on the system. However, two components of the constraint are satisfied trivially due to the identities $S^{\mu\nu}V_\nu V_\mu = 0$ and $S^{\mu\nu}V_\nu \star S_{\mu\kappa}V^\kappa = 0$. As a consequence, the matrix $C^{\mu\lambda} \equiv \{S^{\mu\nu}V_\nu, S^{\lambda\kappa}V_\kappa\}$ will be degenerate on subspaces corresponding to these trivial constraints. However, it can be easily seen that if we find any pseudo-inverse $C^\dagger_{\mu\lambda}$, then the following Hamiltonian will conserve the non-trivial parts of the constraint and thus also the

whole set $S^{\mu\nu}V_\nu = 0$

$$H' = H - \{H, S^{\mu\nu}V_\nu\} C^\dagger_{\mu\lambda} S^{\lambda\kappa} V_\kappa \,. \tag{A.42}$$

The last remark to this procedure is that in the following we never constrain the Poisson algebra; in other words, the Poisson brackets are always those given in (3.29). More details about this topic are discussed in the main text in Section 3.4.

A.4.2 Obtaining the TD Hamiltonian

The first constraint that I apply to the Hamiltonian (3.37) is $S^{\mu\nu}P_\nu = 0$. The constraint algebra yields

$$\{S^{\mu\nu}P_\nu, S^{\kappa\lambda}P_\lambda\} \cong -\tilde{\mathscr{M}}^2 S^{\mu\kappa} \,, \tag{A.43}$$

$$\tilde{\mathscr{M}}^2 \equiv -g^{\mu\nu}P_\mu P_\nu + \frac{1}{4} R_{\mu\nu\kappa\lambda} S^{\mu\nu} S^{\kappa\lambda} \,. \tag{A.44}$$

The pseudo-inverse of $S^{\mu\kappa}$ on the constrained phase space is $-S_{\nu\mu}/S^2$ (cf. eq. (3.12)). The last bracket that needs to be evaluated is

$$\{H_{\mathrm{KS}}, S^{\kappa\lambda}P_\lambda\} \cong \frac{1}{2m} R_{\mu\nu\gamma\chi} S^{\kappa\mu} P^\nu S^{\gamma\chi} \,. \tag{A.45}$$

The constrained Hamiltonian then reads

$$\begin{aligned} H_{\mathrm{TD}} &= \frac{1}{2\mu} g^{\mu\nu} P_\mu P_\nu + \{H_{\mathrm{KS}}, S^{\kappa\lambda}P_\lambda\} \frac{1}{\tilde{\mathscr{M}}^2 S^2} S_{\mu\kappa} S^{\mu\nu} P_\nu \\ &= \frac{1}{2\mu} \left(g^{\mu\nu} + \frac{1}{\tilde{\mathscr{M}}^2} R^\mu{}_{\chi\xi\zeta} S^{\chi\nu} S^{\xi\zeta} \right) P_\mu P_\nu \,, \end{aligned} \tag{A.46}$$

where it is possible to apply $\cong$ equalities for expressions multiplied by the constraint $S^{\mu\nu}P_\nu$ without changing the resulting equations of motion. I also changed the notation $m \to \mu$ because as we will see, the meaning of the parameter μ is different from the definition (3.8). This Hamiltonian generates the equations of motion parametrized by some parameter λ which does not need to be equal to proper time τ. The equations of motion read

$$x'^{\mu} \cong \frac{1}{\mu}\left(g^{\mu\nu} + \frac{1}{2\tilde{\mathscr{M}}^2} R^{\nu}{}_{\chi\xi\zeta} S^{\chi\mu} S^{\xi\zeta}\right) P_{\nu}\,, \tag{A.47}$$

$$P'^{\mu} \cong -\frac{1}{2} R^{\mu}{}_{\nu\kappa\lambda} x'^{\nu} S^{\kappa\lambda}\,, \tag{A.48}$$

$$S'^{\mu\nu} \cong P^{\mu} x'^{\nu} - P^{\nu} x'^{\nu}\,, \tag{A.49}$$

where we denote the derivatives $\mathrm{D}/\mathrm{d}\lambda$ by primes. By comparing the equations above with the MPD equations of motion under the TD supplementary condition (3.18) we see that the parameter λ fulfills

$$\frac{\mathrm{d}\lambda}{\mathrm{d}\tau} = \frac{\mu m}{\mathscr{M}^2}\,, \tag{A.50}$$

where we have to substitute Eq. (3.19) for m. Another way to characterize the parametrization under the condition that $P^{\alpha}P_{\alpha} = -\mathscr{M}^2 = -\mu^2$ is that it holds that $P^{\alpha}x'_{\alpha}/\mathscr{M} = -1$. This is exactly the parametrization introduced by Dixon [75] and vouched for by Ehlers and Rudolph [81] (see also [156]). The Hamiltonian for world-lines parametrized by proper time is discussed in the main text in Subsection 3.3.4. One should compare the above-given constraint procedure with the analogous constraint procedure in the vector-variable model of Ramírez and Deriglazov [220].

A.4.3 Other attempts

I also attempted to use the MP momentum-velocity relation (3.15) and thus to apply the constraint $S^{\mu\nu}(\delta^{\kappa}_{\nu} + S^{\kappa\lambda}S_{\lambda\nu}/S^2)P^{\nu} = 0$. The problem is, however, that once the spin tensor is degenerate, the identity $S^{\mu\nu}(\delta^{\kappa}_{\nu} + S^{\kappa\lambda}S_{\lambda\nu}/S^2) = 0$ holds automatically and has no time derivative under the Kriplovich Hamiltonian. In other words, the MP condition expressed in terms of momenta is satisfied by any degenerate spin tensor and it cannot be used in the constraint procedure.

The Corinaldesi-Papapetrou condition $S^{\mu\nu}\xi_{\nu} = 0$, where $\xi^{\nu}(x^{\mu})$ is now some fixed vector field, can be applied as a constraint to yield the Hamiltonian

$$H = \frac{1}{2m} g^{\mu\nu} P_{\mu} P_{\nu} + \frac{1}{m\xi^2} \xi_{\nu;\gamma} P^{\gamma} S^{\nu\kappa} \xi_{\kappa}\,. \tag{A.51}$$

Yielding the equations of motion

$$x''^{\mu} = -\frac{1}{2m}R^{\mu}{}_{\nu\kappa\lambda}x'^{\nu}S^{\kappa\lambda} - \frac{1}{\xi^2}\xi_{\nu;\gamma}x'^{\gamma}S^{\nu\kappa}\xi_{\kappa}{}^{;\mu}\,, \tag{A.52}$$

$$S'^{\nu\kappa} = -\frac{1}{\xi^2}\xi_{\lambda;\gamma}x'^{\gamma}(S^{\lambda\nu}\xi^{\kappa} - S^{\kappa\lambda}\xi^{\nu})\,. \tag{A.53}$$

Nevertheless, this set of equations are not the MPD equations under the Corinaldesi-Papapetrou condition.

A.5 Construction of canonical coordinates

Le us now consider the effective action for spinning bodies given by Steinhoff and Schäfer [253]:

$$\mathscr{S} = \int p_{\mu}\dot{x}^{\mu} + \frac{1}{2}S_{AB}\Omega^{AB} - H\mathrm{d}\tau\,, \tag{A.54}$$

where $\Omega^{AB} \equiv \Lambda^{A}{}_{\hat{A}}\frac{\mathrm{d}\Lambda^{B\hat{A}}}{\mathrm{d}\tau}$ and $\Lambda^{A}{}_{\hat{A}}$ are the components of the "body-fixed frame" with respect to the background tetrad e^{A}_{μ}. The body-fixed frame is defined by the property that the spin tensor is constant in it, $S^{\hat{A}\hat{B}} = \text{const.}$, and $\Lambda^{A}{}_{\hat{A}}$ thus in fact carry the dynamical state of the spin tensor along with gauge degrees of freedom.

I further assume here, unlike in Refs. [253, 250, 280], that the Hamiltonian H is only a function of the gauge-independent p_{μ}, x^{ν}, S^{AB}. It is then easy to show that the equations of motion following from $\delta\mathscr{S} = 0$, where $p_{\mu}, x^{\nu}, \Lambda^{A}{}_{\hat{A}}, S^{AB}$ are varied independently, imply

$$\frac{\mathrm{d}f}{\mathrm{d}\tau} = \{f, H\}\,, \tag{A.55}$$

where f is any function of p_{μ}, x^{ν}, S^{AB} and the bracket is given as in Eq. (3.32). In this sense, our Hamiltonian-based approach can be understood, up to the discarding of the $\Lambda^{A}{}_{\hat{A}}$ variables, as equivalent to the action-based approach of Refs. [253, 250, 280].

We now realize that if the term $S_{AB}\Omega^{AB}/2$ can be transformed into the form $\sum_i \rho_i\dot{\chi}^i$ with ρ_i, χ^i some dynamical variables, then ρ_i, χ^i are the desired pairs of canonically conjugate coordinates on the phase space. To do so, I mimicked the approach presented in Tessmer et al. [263] and re-expressed

$$\frac{1}{2}S_{AB}\Omega^{AB} = \frac{1}{2}S_{\hat{A}\hat{B}}\Lambda_{A}{}^{\hat{A}}\Lambda_{B}{}^{\hat{B}}\Omega^{AB} = \frac{1}{2}S_{\hat{A}\hat{B}}\Lambda_{A}{}^{\hat{A}}\frac{\mathrm{d}\Lambda^{A\hat{B}}}{\mathrm{d}\tau}\,. \tag{A.56}$$

In other words, we are now looking at the dynamics of the spin tensor purely from the perspective of a Lorentz transformation $\Lambda^{A}_{\hat{A}}$ from the body-fixed frame into the referential tetrad.

Let me now choose the spin tensor in the body-fixed frame to have one degenerate time-like direction and one non-degenerate space-like direction; conventionally $S_{\hat{1}\hat{2}} = -S_{\hat{2}\hat{1}} = S$ and other components zero. Note that this assumes that the spin tensor will eventually fulfill a supplementary spin conditions of the form $S^{\mu\nu}V_{\nu} = 0$; non-degenerate spin tensors will thus not be possible to express in terms of the coordinates that we give in the following paragraphs.

To facilitate an intuitive discussion, let us further identify the legs $\Lambda^{A}_{\hat{1}}, \Lambda^{B}_{\hat{2}}, \Lambda^{C}_{\hat{3}}$ with the x,y,z-axes in Cartesian coordinates, and the $\Lambda^{D}_{\hat{0}}$ with the time axis. Then, by finding the dual of the spatial part of the spin tensor, we see that it is a vector of magnitude S pointing purely in the z-direction.

In this picture, the spin tensor is invariant with respect to rotations around the z-axis, and with respect to boosts in the z direction. Out of the total 6 parameters of a general Lorentz transform $\Lambda^{A}_{\hat{A}}$, 2 will be gauge degrees of freedom of the body-fixed tetrad. In order to not mix the gauge degrees of freedom and the true dynamical degrees of freedom, we parametrize the general Lorentz transform as

$$\Lambda = R(\alpha, \vec{n}_z) B(v_z, \vec{n}_z) B(u, \vec{n}_\psi) R(-\theta, \vec{n}_\phi)\,, \tag{A.57}$$

where $R(\zeta, \vec{n})$ stands for a rotation by angle ζ around $\vec{n}$, and $B(v, \vec{n})$ a boost in the $\vec{n}$ direction. The variables $\alpha, v_z, u, \psi, \theta, \phi$ are then generally time-dependent parameters of the transformation, and the vectors $\vec{n}_\psi, \vec{n}_\phi$ are given as

$$\vec{n}_\psi = (-\sin\psi, \cos\psi, 0)\,, \tag{A.58}$$

$$\vec{n}_\phi = (-\sin\phi, \cos\phi, 0)\,. \tag{A.59}$$

When the dust settles, this transformation yields

$$\begin{aligned} \frac{1}{2} S_{AB}\Omega^{AB} &= S\Lambda_A^{\hat{1}} \frac{\mathrm{d}\Lambda^{A\hat{2}}}{\mathrm{d}\tau} \\ &= -S\dot{\alpha} + S\frac{\cos\theta - 1}{\sqrt{1-u^2}}\dot{\phi} + S\left(\frac{1}{\sqrt{1-u^2}} - 1\right)\dot{\psi}\,. \end{aligned} \tag{A.60}$$

The $-S\dot{\alpha}$ term is a total time derivative and so it will not contribute to the equations of motion. From the other terms we see that we have two canonical momenta A and B conjugate to ϕ and

ψ respectively defined through the parameters of the Lorentz transformation as

$$A = S\frac{\cos\theta - 1}{\sqrt{1-u^2}}\,, \tag{A.61}$$

$$B = S\left(\frac{1}{\sqrt{1-u^2}} - 1\right). \tag{A.62}$$

Expressions for these coordinates in terms of the components of the spin tensor are given in Chapter 3 in equation (3.60). The expressions for the spin tensor components in terms of A, B, ϕ, ψ are then similarly given in equation (3.61).

A.5.1 Coordinate singularities and the special-planar Hamiltonian

To facilitate the discussion of the singularities and their treatment, let us consider a simple example that should be familiar to every physics student. Imagine a particle moving along $x = 0$ and $y = 0$ in Cartesian coordinates in Euclidean space, and make the usual transform to spherical coordinates r, ϑ, φ. In principle, the coordinate $\varphi = \arctan(x/y)$ is not defined, and we are at $\vartheta = 0$ or $\vartheta = \pi$ depending on the sign of z. By a limiting procedure $x \to 0, y \to 0$, we are able to obtain any value between 0 and 2π for φ at the pole.

On the other hand, it is clear to us from the point of view of the more fundamental Cartesian coordinates that nothing is wrong, as the value of φ is of no consequence for them at $\vartheta = 0$. Similarly, $\dot{\varphi}$ is not defined at the pole, and by taking the azimuthal angular momentum along with ϑ to zero, we obtain any value for $\dot{\varphi}$ between $-\infty$ and $+\infty$; again, this is of no physical consequence and evolving φ is redundant.

The singularity at the pole of spatial spherical coordinates discussed above is similar to the singularity of the canonical coordinates for the spin tensor at $S^{A3} = 0$. By inspecting the transformation laws (3.60) we see that the coordinate $\phi = -\arctan(S^{23}/S^{31})$ is undefined and we are either at $A = 0$ or $A = -2(B+S)$ depending on the sign of S^{12}.

When $A = 0$ ($S^{12} > 0$), we see from the parametrization of the spin tensor (3.61) that the value of ϕ will in fact be of no consequence to the spin tensor. These conclusions can then be easily applied to an evolution that fulfills $S^{A3} = \text{const.} = 0$ to reduce the number of variables we need to evolve.

On the other hand, when $A = -2(B+S)$ ($S^{12} < 0$), the situations is somewhat more complicated. If we have an evolution that keeps $S^{A3} = \text{const.} = 0$, we will also have $\dot{S}^{A3} = 0$. This, however, leads only to $\dot{A} = -2\dot{B}$, and it is in fact the combination $2\phi - \psi$ that uniquely parametrizes the spin tensor. For practical purposes, it then useful to define new canonical coordinates $D \equiv A/2 - B, E \equiv A/2 + B, \delta \equiv 2\phi - \psi, \varepsilon \equiv 2\phi + \psi$ so that D, δ and E, ε are

conjugate respectively. The equation $\dot{S}^{A3} = 0$ with $S^{12} < 0$ leads to $\dot{E} = 0$ and the redundance of the coordinate ε.

In the case of the special planar problem presented in sec. 3.5, we chose $S^{12} > 0$ for simplicity. A trick that can be eventually used to avoid the redefinitions of coordinates is simply to permute the definition of the tetrad elements $1 \leftrightarrow 2$, which will lead to a change of the physical meaning of the sign of S^{12}.

Another coordinate singularity is at $S^{A0} = 0$ which unambiguously leads to $B = 0$ and ψ undefined. Once again, we see in (3.61) that the value of ψ is inconsequential in that case. An interesting fact is that if we have an evolution such that $S^{A0} = \text{const.} = 0$, then the coordinates A, ϕ reduce just to the canonical coordinates for the $SO(3)$ Poisson algebra [e.g. 158].

The Astrophysical Journal, 841:105 (14pp), 2017 June 1 https://doi.org/10.3847/1538-4357/aa71a5

Pseudo-Newtonian Equations for Evolution of Particles and Fluids in Stationary Space-times

Vojtěch Witzany[1,2] and Claus Lämmerzahl[1,3]
[1] ZARM, Universität Bremen, Am Fallturm, D-28359 Bremen, Germany; vojtech.witzany@zarm.uni-bremen.de
[2] Institute of Theoretical Physics, Faculty of Mathematics and Physics, Charles University in Prague, Prague, Czech Republic
[3] Institut für Physik, Universität Oldenburg, D-26111 Oldenburg, Germany; claus.laemmerzahl@zarm.uni-bremen.de
Received 2017 February 16; revised 2017 May 2; accepted 2017 May 6; published 2017 May 31

Abstract

Pseudo-Newtonian potentials are a tool often used in theoretical astrophysics to capture some key features of a black hole space-time in a Newtonian framework. As a result, one can use Newtonian numerical codes, and Newtonian formalism, in general, in an effective description of important astrophysical processes such as accretion onto black holes. In this paper, we develop a general pseudo-Newtonian formalism, which pertains to the motion of particles, light, and fluids in stationary space-times. In return, we are able to assess the applicability of the pseudo-Newtonian scheme. The simplest and most elegant formulas are obtained in space-times without gravitomagnetic effects, such as the Schwarzschild rather than the Kerr space-time; the quantitative errors are smallest for motion with low binding energy. Included is a ready-to-use set of fluid equations in Schwarzschild space-time in Cartesian and radial coordinates.

Key words: accretion, accretion disks – black hole physics – gravitation – methods: analytical – methods: numerical

1. Introduction

Until now, all gravity related observations could be fully described within general relativity (GR). There is no single gravitational phenomenon that is in contradiction to GR. Within GR, the gravitational field is given by the Einstein field equations which are highly complicated and can be solved exactly only for a few highly symmetric configurations. Even for the two body system, no exact solution can be found, contrary to the situation in Newtonian gravity. In order to cope with more complicated situations, various analytic approximation schemes have been developed.

The earliest and most prominent approximation scheme, used already by Einstein for the first computation of the perihelion shift of Mercury, is the post-Newtonian approach (see, e.g., Blanchet 2006). This approach is essentially characterized as a formal expansion of the field equations and the equations of motion in terms of orders of the "slowness" of the system v/c, where v is some characteristic velocity of the system. A second prominent approximation scheme is the post-Minkowski approach, which is a weak field approximation expanding in terms of deviations from the flat space-time background and is applicable to any velocity of the constituents of the systems.

However, for bound motion, such as the case of binary stars, the deviation from the flat background and the typical velocity of the objects are intimately related. In the case of a test body in a circular orbit of the radial Schwarzschild coordinate r_c around a Schwarzschild black hole, the test body's velocity is $v/c = \sqrt{GM/(c^2 r_c)}$ and the deviation from the flat background at r_c can be expanded in terms of $GM/(c^2 r_c)$. Hence, a post-Minkowski expansion naturally leads to a post-Newtonian one and vice versa (see, e.g., Sasaki & Tagoshi 2003). Thus, both the post-Newtonian and the post-Minkowski expansion schemes applied to bound motion are weak-field approximations and are not suited to describe bound motion in the very vicinity of a black hole, or more generally, in the strong gravity regime.

Nevertheless, astrophysicists often have to describe, e.g., an accretion disk extending in terms of its inner radius up to the innermost stable circular orbit (ISCO) $r_{\rm ISCO} = 6GM/c^2$ of the black hole, or even the photon sphere $r_{\rm ps} = 3GM/c^2$ (see, e.g., Abramowicz & Fragile 2013). It is obvious that only an extremely careful and laborious post-Newtonian or post-Minkowski expansion would provide a satisfactory description of the motion in the very vicinity of the black hole. On the other hand, the outer radius of the accretion disk often extends up to hundreds of GM/c^2, where relativistic effects become completely negligible.

In other words, the largest part of the accretion process is governed by Newtonian physics and only in the very last few percents of accretion the behavior of the accreted matter as a test field on a strongly curved general-relativistic background becomes important. However, these last stages are essential for the global structure of a steady accretion disk, because of the instability of the disk beyond the ISCO and the precise energetics near the black hole determining the amount of energy radiated away during the accretion process.

Hence, to model accretion on a black hole, we would ideally like a dynamical description, which is mostly Newtonian but reproduces some of the characteristic features of motion near the black hole. Precisely this kind of model was given first by Paczyński & Wiita (1980) by placing the fully Newtonian accretion disk into a non-physical gravitational field with the potential

$$\Phi_{\rm PW} = -\frac{GM}{r - 2GM/c^2}. \tag{1}$$

Obviously, this potential very quickly obtains the Newtonian asymptotics $\sim -GM/r$ as $r \gg GM/c^2$ but a quick computation of its Laplacian shows that it would have to be generated by infinite densities of negative matter. On the other hand, it has an ISCO at $r = 6GM/c^2$ with specific binding energy $\tilde{E} = 1 - \sqrt{8/9}$. Since these are the same values of the

coordinate radius and of the binding energy of the ISCO as in the Schwarzschild space-time, this so-called Paczyński–Wiita potential can be used as an effective model of the static black hole field (see Abramowicz 2009 for a review of other properties).

Since the publication of the Paczyński–Wiita potential, the approach of reproducing some of the characteristic features of a selected class of orbits within an ad hoc Newtonian framework has been called the "pseudo-Newtonian" (pN) approach (see the Introduction of Tejeda & Rosswog 2013 or Artemova et al. 1996 for a review).

Even though pN potentials have been proposed for over 35 years (Paczyński & Wiita 1980; Nowak & Wagoner 1991; Artemova et al. 1996; Semerák & Karas 1999; Mukhopadhyay 2002; Mukhopadhyay & Misra 2003; Chakrabarti & Mondal 2006; Ghosh & Mukhopadhyay 2007; Wegg 2012; Tejeda & Rosswog 2013; Ghosh et al. 2014; Sarkar et al. 2014; Tejeda & Rosswog 2014; Witzany et al. 2015), until recently, the potentials were not able to accurately reproduce properties of general orbits or to accurately describe the field of a rapidly spinning black hole. However, Tejeda & Rosswog (2013, 2014) proposed a class of generalized (velocity-dependent) pN potentials accurately describing the motion of quite general test-particles in the Schwarzschild and generally any spherically symmetric space-time (the same result on spherically symmetric space-times was almost simultaneously given by Sarkar et al. 2014). The pattern in the formulation is remarkably simple, the pN Lagrangians of Tejeda & Rosswog (2013, 2014) and Sarkar et al. (2014) can all be given within a single formula

$$L = \frac{1}{2}\left(\frac{\dot{r}^2}{f(r)^2} + \frac{\dot{\vartheta}^2 + \sin^2\vartheta\,\dot{\varphi}^2}{f(r)}\right) + \frac{1}{2}f(r), \tag{2}$$

where $f(r) = -g_{tt} = 1/g_{rr}$ and t, r, φ, ϑ are Schwarzschild-like spherical coordinates. The key step in the derivation of these pN Lagrangians always seems to be the assumption that the specific energy of the test particle $-u_t$ is approximately 1. Additionally, all the derivations have been done for massive particles. As a result, these Lagrangians give exactly the position of the ISCO, the marginally bound ($-u_t = 1$) circular orbit, the formal angular momentum distribution over circular orbits and a general quantitative agreement with the exact relativistic case.

However, this pattern does not include spinning black holes, i.e., the Kerr metric. For the Kerr space-time, a number of proposals exist, usually fitting the potential by the behavior of some set of orbits or by "reading off" a potential from the equations of motion or the metric (Semerák & Karas 1999; Mukhopadhyay 2002; Mukhopadhyay & Misra 2003; Chakrabarti & Mondal 2006; Ghosh & Mukhopadhyay 2007).

The only proposal for a pN description of spinning black holes, which some how follows the line of reasoning of Tejeda & Rosswog (2013), is that of Ghosh et al. (2014), where the authors derived a generalized pN potential for test-particles in the equatorial plane of a slowly spinning Kerr black hole by utilizing a "low-energy limit" in one of the steps of the derivation. The restriction of the particles in the equatorial plane seems to mainly play the role of convenience during the derivation but the limit on spin of the black hole is set because of emergent singular behavior of important circular orbits, namely the marginally bound and marginally stable orbit (see Section 6.4 for more details).

Even though the development of pN potentials is oriented toward magneto-hydrodynamics of a plasma near a black hole, none of the papers (Tejeda & Rosswog 2013, 2014; Ghosh et al. 2014; Sarkar et al. 2014) have discussed the applicability of their framework in this context.

To conclude our discussion, we give a set of questions that have not been addressed so far in the literature. Are the new velocity-dependent potentials also applicable for null geodesics, i.e., computations of gravitational lensing or black hole shadows? How does this formalism implement additional forces such as electromagnetism? Is it correct to use these Newtonian-like Lagrangians (2) along with non-modified Newtonian fluid dynamics, as was done e.g., by Bonnerot et al. (2016)? Is there a deeper pattern in the way the Lagrangians are formulated and can we perhaps extrapolate it to highly spinning black holes and off-equatorial particles near them? This paper partially resolves these questions.

In Section 2, we derive a general pN Hamiltonian valid in any stationary space-time and specify the exact relationship the corresponding trajectories have with relativistic geodesics in the original space-time. In Section 3, we focus on its properties in the most elegant and simple case of static space-times, and, in Section 4, we show that the herein presented Hamiltonian encompasses all the recently published velocity-dependent pN potentials (2).

As far as concerns new applications of this work, Section 5 gives also a pN Hamiltonian for charged particles and derives pN fluid equations in static space-times. Section 6 then discusses the properties of the pN Hamiltonian for spinning black holes.

2. pN Hamiltonian

We use the $G = c = 1$ geometrized units and the $-+++$ signature of the metric. Space-time coordinates are labeled by Greek letters, spatial coordinates by roman letters. At certain instants, we will switch to SI units and indicate so.

2.1. Flat Space-time

Consider the Lagrangian and respective Hamiltonian of the motion of a test particle in flat space-time in Cartesian coordinates

$$L = \frac{1}{2}\eta_{\mu\nu}u^\mu u^\nu, \tag{3}$$

$$H = \frac{1}{2}\eta^{\mu\nu}u_\mu u_\nu, \tag{4}$$

where $u^\mu \equiv dx^\mu/d\tau$ is the four-velocity of the particle and u_μ is canonically conjugate to x^μ. This description gives the trajectory as parametrized by proper time τ rather than the time in the laboratory frame $t = x^0$. However, since both the Lagrangian and Hamiltonian have the same on-shell value $H = L = -1/2$ for any massive particle, we can obtain a Hamiltonian for trajectories parametrized by time in the laboratory frame instead of proper time

$$H_t = -u_t = \sqrt{1 + \sum_i (u_i)^2}, \tag{5}$$

where we have used the well-known fact that one can use minus the conjugate momentum of a coordinate as a new Hamiltonian to reparametrize the motion via that given

coordinate (see, e.g., Guckenheimer & Holmes 1983). However, we can also use a "pN" Hamiltonian of the form $H_{\rm pN} = (u_t^2 - 1)/2$ to obtain

$$H_{\rm pN} = \frac{1}{2}\sum_i (u_i)^2. \tag{6}$$

This Hamiltonian formally resembles the Hamiltonian of a free Newtonian particle and will give the correct motion of particles parametrized, however, by a pseudo-time $\tilde{t}$ given as

$$\frac{du_i}{d\tilde{t}} = -\frac{\partial H_{\rm pN}}{\partial x^i} = u_t \frac{\partial(-u_t)}{\partial x^i} = -u_t \frac{du_i}{dt}, \tag{7}$$

$$\frac{dx^i}{d\tilde{t}} = \frac{\partial H_{\rm pN}}{\partial u^i} = -u_t \frac{\partial(-u_t)}{\partial u_i} = -u_t \frac{dx^i}{dt}. \tag{8}$$

Thus, we can conclude that this pseudo-time $\tilde{t}$ is related to the lab time on a particle-to-particle basis as $d\tilde{t} = dt/(-u_t)$ (for particles traveling forward in time, $-u_t$ is positive and has the meaning of specific energy of the particle). There is, however, a very important distinction between a truly Newtonian evolution of particles and this pN Ansatz; in Newtonian physics, the time parameter corresponding to $\tilde{t}$ is a globally valid lab-frame time coordinate; here, the parameter $\tilde{t}$ is valid only as a parameter along a single trajectory and cannot be directly tied to a global time coordinate.

2.2. General Stationary Space-time

The point of this whole paper is to exploit the formal Ansatz discussed in the last subsection in the following way. We find a Hamiltonian reproducing exactly the coordinate shapes of relativistic orbits that has a formally Newton-like form, albeit reparametrizing the orbits by some trajectory-specific pseudo-time. Then, we postulate this Ansatz Hamiltonian as a new pN Hamiltonian to be used in fully Newtonian calculations, where the pseudo-time $\tilde{t}$ is elevated to a globally valid time coordinate. This means that for every relativistic geodesic in the original space-time we will have some pN trajectory of identical coordinate shape, even though with a scrambled and rescaled time.

Consider a general stationary space-time with the metric $g_{\mu\nu}$ and a set of coordinates in which the metric is stationary with respect to the coordinate $t = x^0$. This condition usually specifies the coordinate t uniquely but otherwise our computations are covariant with respect to arbitrary coordinate transformations on the spatial hypersurface (coordinates x^i). We can then, analogously to the derivations above, find that the motion of particles parametrized by t will be given by the Hamiltonian

$$\begin{aligned} H_t &= -u_t \\ &= \omega^i u_i - \sqrt{(\omega^i u_i)^2 - (g^{ij}u_i u_j + \kappa)/g^{00}}, \end{aligned} \tag{9}$$

where $\omega^i \equiv g^{0i}/g^{00}$, and we have also introduced the constant κ to account for both massive $\kappa = 1$ and massless particles $\kappa = 0$. We can now again define a pN Hamiltonian $H_{\rm pN} = (u_t^2 - 1)/2$ to obtain

$$H_{\rm pN} = -\frac{1}{2}\frac{g^{ij}}{g^{00}}u_i u_j - \frac{1}{2}\left(\frac{\kappa}{g^{00}} + 1\right) + \omega^i u_i(\omega^i u_i - \sqrt{\mathcal{D}}), \tag{10}$$

where $\mathcal{D} = (\omega^i u_i)^2 - (g^{ij}u_i u_j + \kappa)/g^{00}$. By an identical derivation as in (7) and (8), we obtain that this Hamiltonian generates trajectory evolution reparametrized by a pseudo-time $\tilde{t}$ such that $d\tilde{t} = dt/(-u_t)$. We now postulate this pN Hamiltonian as an effective Hamiltonian for Newtonian computations.

As can be verified by direct computation, the Hamiltonian (10) seamlessly reduces to the Hamiltonian (6) in flat regions of the space-time. Furthermore, if we switch to SI units and use the weak-field metric $g^{ij} = \delta^{ij}(1 + 2\Phi/c^2)$, $g^{00} = -(1 - 2\Phi/c^2)$, we obtain the Hamiltonian (10) to linear order in c^{-2} as

$$H_{\rm pN} = \frac{1}{2}\left(1 + \frac{4\Phi}{c^2}\right)\sum_i (u_i)^2 + \kappa\left(\Phi + \frac{2\Phi^2}{c^2}\right), \tag{11}$$

where we have shifted the Hamiltonian by a dynamically unimportant constant. In the case of massless particles ($\kappa = 0$), we obtain the well-known equations for the deviation of a light-ray in a gravitational field. For massive particles ($\kappa = 1$), the zeroth order in $1/c^2$ gives simply the Newtonian Hamiltonian of a particle in a gravitational field, and the first $1/c^2$ order gives a post-Newtonian correction of first order. This gives us the confidence to call the Hamiltonian (10) a pN one.

We would like to use this opportunity to stress again that the idea of post-Newtonian and pN descriptions is very different and the example above is probably the only point where a connection can be made. The post-Newtonian approximation is an iterative scheme reducing the error of computation at every order, whereas the pN Hamiltonian is in a sense always "exact" with the reservation that it introduces a time-reparametrization as detailed in (7) and (8) (we discuss the implications in the next paragraph).

2.3. Deviations from Relativity

The conclusion of this section so far is that, provided that we give the same initial momenta u_i as in the exact relativistic case, we are able to reproduce the exact shapes of relativistic trajectories via a fully Newtonian framework and the Hamiltonian (10). Two things will be different, however, and both stem from the fact that the Newtonian trajectory is reparametrized with respect to the relativistic one.

First, the coordinate velocities at the same points of the trajectory will be different in the relativistic and the pN case due to the different time parametrization. Consider the following example: we want to compare whether we obtain the same orbit in the relativistic and pN description. Hence, we choose a coordinate point x^i and a coordinate velocity v^i as initial conditions for our comparison. Then, we evolve a particle with an initial condition $dx^i/dt = v^i$ in the relativistic case, and $dx^i/d\tilde{t} = v^i$ in the pN case. It is obvious that by this procedure we will obtain a particle on a different coordinate orbit in each case.

In this sense, the initial velocities leading to the same coordinate orbits are rescaled in the pN case by the total specific energy $-u_t$. On the other hand, the correspondence between the relativistic and pN case in terms of initial momenta and coordinate positions u_i, x^i is always exact.

The second deviation of the pN case with respect to the relativistic one can be best illustrated on circular orbits. As follows from the previous discussion, if there is a set of circular

orbits in the relativistic space-time with some (canonical) angular momentum distribution, then this set of circular orbits along with the angular momentum distribution will be exactly reproduced in the pN description. However, the coordinate frequencies of these circular orbits will be deformed as

$$\Omega_{\rm pN} = \frac{d\varphi}{d\tilde{t}} = -u_t \frac{d\varphi}{dt} = -u_t \Omega, \tag{12}$$

where $\Omega_{\rm pN}$ is the frequency along the orbit in the pN case, Ω the original relativistic angular frequency, and φ some angular coordinate.

The relative error in the frequency η_Ω can then be easily derived as

$$\eta_\Omega \equiv \frac{\Omega_{\rm pN} - \Omega}{\Omega} = -(1 + u_t) \equiv -\mathcal{E}, \tag{13}$$

where we have defined a new quantity $\mathcal{E}$ as the specific binding energy of the particle. (I.e., in an asymptotically flat space-time, $\mathcal{E}$ will be positive if the particle is bound and will represent the energy per unit mass needed to transport the particle to infinity.)

Other important deviations we obtain are the different energies of the particles. Since the Hamiltonian (10) is conserved and reduces to Newtonian energy in weak fields, it is also natural to interpret it as a pN specific energy. In the convention we choose, $H_{\rm pN}$ is zero for a particle at rest in a flat part of the space-time and as such it is equal to minus the pN binding energy $H_{\rm pN} = -\mathcal{E}_{\rm pN} = (u_t^2 - 1)/2$. Then, we can easily derive that the relative error of the specific binding energy will be equal to

$$\eta_\mathcal{E} \equiv \frac{\mathcal{E}_{\rm pN} - \mathcal{E}}{\mathcal{E}} = -\frac{\mathcal{E}}{2}. \tag{14}$$

For instance, in the case of the Schwarzschild space-time, the tightest bound circular orbit (with maximal $\mathcal{E}$) is the ISCO with $\mathcal{E} = 1 - \sqrt{8/9} \approx 0.06$. For example, in the Schwarzschild space-time, the maximal error in binding energy and angular orbital frequency of circular orbits as predicted by the pN Hamiltonian (10) will be 3% and 6% respectively.

2.4. Massless Particles

We would also like to point out that in the special case of massless particles ($\kappa = 0$), the Hamiltonian (10) can reproduce trajectories parametrized exactly by coordinate time t.

The trick enabling us to do this lies in two facts. First, the shape of a null geodesic is completely insensitive to the rescalings of four-velocity $u^\mu \to \lambda u^\mu$, where λ is some constant. Second, if a vector v^μ satisfies four-velocity normalization for a massless particle $g^{\mu\nu} v_\mu v_\nu = 0$, so does another vector $u^\mu = \lambda v^\mu$.

As a result, we can always take an initial condition for the trajectory of a massless particle and rescale it so that $u_t = -1$ and thus $d\tilde{t} = dt$. Since u_t is an integral of motion in stationary space-times, this property will be true along the whole trajectory and we will simply have $t = \tilde{t}$.

3. Static Space-times

We now investigate the pN Hamiltonian from the previous section in the class of metrics for which $g^{0i} = \omega^i = 0$. Considered along with the assumption of stationarity with respect to the time coordinate $t = x^0$, this class of space-times is easily recognized as static space-times.

For these, Equation (10) gives (we use the fact that in static metrics $g_{00} = 1/g^{00}$)

$$H_{\rm pN} = -\frac{1}{2} g_{00} g^{ij} u_i u_j - \frac{\kappa}{2}(g_{00} + 1). \tag{15}$$

In the case of static space-times, it is easy to execute a Legendre transform of the Hamiltonian (15) (this is not possible to do in closed form for a general $\omega^i \neq 0$). We first obtain the relationship between momenta and pN velocities $\dot{x} \equiv dx^i/d\tilde{t} = dx^i/dt\,(1 + \mathcal{E})$:

$$\dot{x}^i = \frac{\partial H}{\partial u_i} = -g_{00} g^{ij} u_i, \tag{16}$$

$$u_i = -\frac{g_{ij}}{g_{00}} \dot{x}^j, \tag{17}$$

where we have used the fact that thanks to $g^{0i} = g_{0i} = 0$ the matrix g_{ij} is the inverse of g^{ij}. It is then easy to see that the resulting Lagrangian $L = u_i \dot{x}^i - H$ reads

$$L_{\rm pN} = -\frac{1}{2} \frac{g_{ij}}{g_{00}} \dot{x}^i \dot{x}^j + \frac{\kappa}{2}(g_{00} + 1). \tag{18}$$

It is also obvious from (17) that

$$\frac{dx^i}{d\tilde{t}} = (-u_t) \frac{dx^i}{dt} = -g_{00} \frac{dx^i}{d\tau}, \tag{19}$$

a fact we will use extensively in the analysis of fluid equations in Section 5.

3.1. Geometrical Interpretation of Equations of Motion

The equations of motion corresponding to Lagrangian (18) can be put in a very elegant form

$$\ddot{x}^k = -\gamma^k_{\ jl} \dot{x}^j \dot{x}^l - \frac{\kappa}{2} \frac{g^{ik}}{g^{00}} g_{00,k}, \tag{20}$$

where $\gamma^k_{\ jl}$ are the Christoffel symbols corresponding to the three-dimensional Riemannian metric $s_{ij} \equiv -g_{ij}/g_{00}$ known also as the optical or Fermat metric (see e.g., Abramowicz et al. 1988)

$$\gamma^k_{\ jl} = \frac{1}{2} s^{ki} (s_{ij,l} + s_{il,j} - s_{jl,i}), \tag{21}$$

where $s^{ij} = -g^{ij}/g^{00}$ is the inverse of s_{ij}. In other words, the motion of a relativistic massive particle ($\kappa = 1$) in a static space-time can be, upon reparametrization, formulated as the motion of a geodesic in curved three-dimensional space in a potential field, and the motion of light ($\kappa = 0$) corresponds simply to the motion of a geodesic in that deformed space.

This notion has already been explored by Abramowicz et al. (1997) where the authors arrive at the same conclusion through fitting the Binet formula of a Newtonian particle in curved space so as to yield the same orbit shapes as in Schwarzschild space-time. Our work clarifies the general possibility of this "shape reproduction" of orbits via the language of reparametrization.

We would like to point out the fact that even in the case of massive particles it is possible to describe their motion on the spatial hyperslice as a geodesic of a Riemannian metric. This

metric is known as the Jacobi metric and it is energy dependent. The derivation of the Jacobi metric in static space-times and relation to previous results in the literature are discussed in Appendix A.

3.2. pN Potentials

Let us now interpret the Lagrangian (18) strictly as a Lagrangian of a Newtonian particle moving in Euclidean space. A part of the Lagrangian then must be the specific kinetic energy of the particle and the rest is a particular pseudo-gravitational potential. However, the Fermat metric s_{ij} is generally not flat and we cannot interpret $s_{ij}\dot{x}^i\dot{x}^j/2$ as the specific kinetic energy of a particle in the flat Euclidean space of Newtonian physics. As a consequence, a part of s_{ij} must be absorbed into the potential, thus forming a "generalized," velocity-dependent gravitational potential.

The first step in identifying this velocity-dependent pN gravitational potential $\Phi_{\rm pN}$ is to interpret the coordinates in which we are working as some set of coordinates in Euclidean space. Then, using the Euclidean metric d_{ij} in these coordinates, we obtain the split of the Lagrangian as

$$L_{\rm pN} = \frac{1}{2}d_{ij}\dot{x}^i\dot{x}^j - \Phi_{\rm pN}(x^i, \dot{x}^i), \tag{22}$$

$$\Phi_{\rm pN} = -\frac{\kappa}{2}(g_{00}+1) - \frac{1}{2}(s_{ij}-d_{ij})\dot{x}^i\dot{x}^j. \tag{23}$$

The part $s_{ij} - d_{ij}$ is then the "non-flat deviation" of the Fermat metric inducing the extra effects that cannot be captured in a simple velocity-independent potential.

In the case of an asymptotically flat space-time the pseudo-gravitational potential $\Phi_{\rm pN}$ goes asymptotically to zero if $g_{00} \to -1$ and $s_{ij} = -g_{ij}/g_{00} \to d_{ij}$. (An explicit example of d_{ij} and $\Phi_{\rm pN}$ for the Schwarzschild space-time is given in Section 4.)

4. Spherically Symmetric Space-times

The most prominent example to demonstrate the results of the last section is the Schwarzschild metric. The formula for the pN Lagrangian (18) applied to the Schwarzschild space-time expressed in Schwarzschild coordinates t, r, ϑ, φ gives

$$L_{\rm TR} = \frac{1}{2}\left(\frac{\dot{r}^2}{(1-2M/r)^2} + \frac{r^2(\sin^2\vartheta\,\dot{\varphi}^2 + \dot{\vartheta}^2)}{1-2M/r}\right) + \kappa\frac{M}{r}, \tag{24}$$

which for $\kappa = 1$ coincides with the Lagrangian derived from the equations of motion in the Schwarzschild space-time by Tejeda & Rosswog (2013). (The $\kappa = 0$ case, giving exact light-rays, is only proposed here.) Similarly, one obtains the same formula as in Tejeda & Rosswog (2014) and Sarkar et al. (2014; Equation (2)) once applying formula (18), $\kappa = 1$ to spherically symmetric space-times.

4.1. Extracting pN Potentials

To obtain the pN potential $\Phi_{\rm pN}$ from the Lagrangian (24), we must first identify the "natural metric" d_{ij}. In the case of the Schwarzschild space-time in Schwarzschild coordinates, this "natural metric" is of course the Euclidean metric in spherical coordinates r, ϑ, φ, i.e.,

$$d_{rr} = 1,\ \ d_{\vartheta\vartheta} = r^2,\ \ d_{\varphi\varphi} = r^2\sin^2\vartheta. \tag{25}$$

This way the Tejeda–Rosswog Lagrangian reorganizes as follows (compare to Equations (22), (23), and (25))

$$L_{\rm TR} = \frac{1}{2}(\dot{r}^2 + r^2(\sin^2\vartheta\,\dot{\varphi}^2 + \dot{\vartheta}^2)) - \Phi_{\rm pNS}, \tag{26}$$

where

$$\Phi_{\rm pNS} = -\kappa\frac{M}{r} - \frac{2M(r-M)}{(r-2M)^2}\dot{r}^2 + \frac{2M}{r-2M}r^2(\dot{\varphi}^2\sin^2\vartheta + \dot{\vartheta}^2). \tag{27}$$

This is also in concordance with the results in Tejeda & Rosswog (2013).

However, we would also like to demonstrate that this "split" of the Lagrangian is not unique. Consider for instance the Schwarzschild metric expressed using the isotropic radius R for which $r = R(1+M/2R)^2$

$$ds^2 = -\left(\frac{1-\frac{M}{2R}}{1+\frac{M}{2R}}\right)^2 dt^2 + \left(1+\frac{M}{2R}\right)^4(dR^2 + R^2 d\Omega^2), \tag{28}$$

where $d\Omega^2 \equiv d\vartheta^2 + \sin^2\vartheta\, d\varphi^2$. From the perspective of these coordinates, the "natural flat metric" is

$$d_{RR} = 1,\ \ d_{\vartheta\vartheta} = R^2,\ \ d_{\varphi\varphi} = R^2\sin^2\vartheta, \tag{29}$$

which, in return, leads to the reorganization of the Tejeda–Rosswog Lagrangian as

$$L_{\rm TR} = \frac{1}{2}(\dot{R}^2 + R^2(\sin^2\vartheta\,\dot{\varphi}^2 + \dot{\vartheta}^2)) - \Phi_{\rm pNI}, \tag{30}$$

where

$$\Phi_{\rm pNI} = -\kappa\frac{4MR}{(M+2R)^2} + \left(\frac{16R^4(M-2R)^2}{(M+2R)^6} - 1\right)(\dot{R}^2 + R^2(\dot{\varphi}^2\sin^2\vartheta + \dot{\vartheta}^2)). \tag{31}$$

Hence, the split into a "usual Newtonian kinetic energy" and the "pN potential" is conventional and relies heavily on what we think is the "natural flat metric" or the "natural Newtonian interpretation of coordinates" in the curved space-time. Furthermore, the pN potentials cannot be simply combined with other external potentials because they are subject to the full nonlinearity of relativistic source superposition.

Nevertheless, as already mentioned, the pN Lagrangian (18) is, as a whole, in fact invariant with respect to transformations of the spatial coordinates (not with respect to transformations involving the time coordinate). In other words, the whole Lagrangian $L_{\rm pN}$ is uniquely defined by the choice of the time coordinate and we will obtain covariantly the same physical behavior no matter which coordinate system or formal reorganization of the terms we use.

5. Charged Particles and Perfect Fluids

Since the development of a pN description is ultimately aimed at modeling a fluid in an accretion process, we now take the first steps toward a formulation of pN magneto-hydrodynamics.

To do that, we first generalize the pN Hamiltonian to charged particles in electromagnetic fields in Section 5.1. Then, in Section 5.2, we proceed to give hydrodynamic equations for a perfect fluid in the pN gravitational field. The inclusion of all the relevant physics to ultimately give a set of equations for, e.g., pN radiative magneto-hydrodynamics near a black hole is out of the scope of the current paper.

5.1. Charged Particle Motion

The relativistic Hamiltonian of the trajectory of a charged particle with specific charge q in an electromagnetic field A^μ reads

$$H_{\mathrm{EM}\tau} = \frac{1}{2} g^{\mu\nu}(\pi_\mu - qA_\mu)(\pi_\nu - qA_\nu), \tag{32}$$

where $\pi_\mu = u_\mu + qA_\mu$ is canonically conjugate to x^μ. Analogously to Section 2, we invert the expression for the constant value of the Hamiltonian $H_{\mathrm{EM}\tau} = -\kappa/2$ to get a Hamiltonian of an electro-geodesic parametrized by coordinate time

$$\begin{aligned} H_{\mathrm{EM}t} &= -\pi_t \\ &= \omega^i u_i - \sqrt{(\omega^i u_i)^2 - (g^{ij}u_i u_j + \kappa)/g^{00}} + qA_0, \end{aligned} \tag{33}$$

with the important substitution $u_i = \pi_i - qA_i$.

Now it is easy to postulate the pN electromagnetic Hamiltonian H_{pNEM} as

$$H_{\mathrm{pNEM}} \equiv \frac{\pi_t^2 - 1}{2}, \tag{34}$$

where we again have to assume the stationarity of the space-time metric $g_{\mu\nu}$ with respect to $t = x^0$, but also stationarity of the electromagnetic potential A_μ because we would have problems with relating the t-dependence to the pseudo-time $\tilde{t}$-dependence of the field. We can formulate this assumption differently to make its gauge-dependence clear; we assume that the Maxwell tensor $F^{\mu\nu}$ is time-independent and we choose a gauge such that A_μ is also globally time-independent.

The Hamiltonian (34) will, similarly to the Hamiltonian H_{pN} in Equation (10), reproduce exact electrogeodesics parametrized by a new pseudo-time $d\tilde{t} = -dt/\pi_t$. Nevertheless, we do not give the explicit expression for H_{pNEM} in the general case because they are very long and can be easily evaluated using (33) and (34).

The only case in which H_{pNEM} reduces to an elegant expression with an easy Legendre transform is the case where the space-time is static and the A_0 component of the electromagnetic field vanishes. That is, for charged particle motion in static space-times with static magnetic fields, we obtain the pN Hamiltonian

$$H_{\mathrm{pNEM}} = -\frac{1}{2} g_{00} g^{ij}(\pi_i - qA_i)(\pi_j - qA_j) - \frac{\kappa}{2}(g_{00} + 1), \tag{35}$$

and the respective Lagrangian L_{pNEM} reads

$$L_{\mathrm{pNEM}} = -\frac{1}{2}\frac{g_{ij}}{g_{00}}\dot{x}^i\dot{x}^j + \frac{\kappa}{2}(g_{00} + 1) + qA_j\dot{x}^j. \tag{36}$$

That is, at least in this special case of static magnetic fields and static space-times, the charged particle dynamics can be obtained along the lines of the usual minimal coupling.

5.2. Perfect-fluid Equations

It is possible to derive pN fluid equations from first principles by starting from the Boltzmann equation governing the motion of particles on pN trajectories, and then finding its zeroth and first moment to obtain the continuity and Euler equation. We have tried this approach but it does not yield equations that fit well with their corresponding relativistic counterparts.

Hence, we adopt an ad hoc approach where the relevant equations are derived as a "pseudo-Newtonization" of the exact relativistic equations. Furthermore, we restrict ourselves only to the case of static metrics, because, as mentioned in Sections 2.2 and 5.1, it is impossible to invert the pN equations of motion so as to feature explicitly the velocities rather than canonical momenta in the general case.

Consider the relativistic particle-conservation equation in coordinate time t

$$\left.\frac{dn}{dt}\right|_{\mathrm{rel}} = -\frac{n}{u^t\sqrt{-g}}[(w^i u^t\sqrt{-g})_{,i} + (u^t\sqrt{-g})_{,t}], \tag{37}$$

where $w^i = dx^i/dt$ is the coordinate velocity, n is the particle-number density, and $dn/dt = \partial n/\partial t + \partial n/\partial x^i w^i$ is the material derivative with respect to t. We will now need the following identity

$$w^i u^t\sqrt{-g} = v^i\sqrt{d}, \tag{38}$$

where $v^i = dx^i/d\tilde{t}$ and $d = -\det(g_{ij})/g_{00}$. We can then reparametrize the continity equation using pseudo-time $\tilde{t}$ to obtain the exact particle-conservation equation as

$$\left.\frac{dn}{d\tilde{t}}\right|_{\mathrm{rel}} = -\frac{n}{\sqrt{d}}[(v^i\sqrt{d})_{,i} + (u_t\sqrt{d})_{,t}]. \tag{39}$$

The term $\sim(u_t\sqrt{d})_{,t}$ is a special-relativistic term, which survives in flat space-time and spoils our otherwise very Newtonian form of the particle-conservation equation. Let us write it out explicitly:

$$-\frac{n}{\sqrt{d}}(u_t\sqrt{d})_{,t} = -\frac{n}{u_t}\frac{g_{ij}}{g_{00}}\frac{\partial v^i}{\partial t}v^j, \tag{40}$$

which, in SI units, attains a factor of c^{-2} relative to the other terms. If we then assume the velocities of the fluid and their variability are non-relativistic in the pN frame v/c, $v_{,t}/c \ll 1$, we can neglect this term. The assumption that $dx^i/d\tilde{t}$ is small is to leading order equivalent to the assumption that dx^i/dt is small so this criterion can also be given in terms of the usual coordinate velocities.

Thus, we postulate the approximate, pN particle-conservation equation as

$$\left.\frac{dn}{d\tilde{t}}\right|_{\rm pN} = -\frac{n}{\sqrt{d}}(v^i\sqrt{d})_{,i}. \tag{41}$$

This pN equation will have a conserved particle number of the form

$$\mathcal{N} = \int n(x^i)\sqrt{d}\; d^3x, \quad \frac{d\mathcal{N}}{d\tilde{t}} = 0. \tag{42}$$

Let us now consider the exact relativistic Euler equation in coordinate time in static space-times (see, e.g., Tejeda et al. 2017 for the case of a general metric)

$$\left.\frac{d^2x^i}{dt^2}\right|_{\rm rel} = -(\Gamma^i{}_{00} + \Gamma^i{}_{jk}w^jw^k) - \frac{1}{(u^t)^2(\varepsilon+P)}(P_{,j}g^{ij} - P_{,t}g^{00}w^i), \tag{43}$$

where ε is the total energy density in the gas and P is the pressure. We can again reparametrize this equation by $\tilde{t}$ to obtain

$$\left.\frac{d^2x^i}{d\tilde{t}^2}\right|_{\rm rel} = -\Gamma^i{}_{00}(u_t)^2 - \Gamma^i{}_{jk}v^jv^k + \frac{g_{00,k}}{g_{00}}v^kv^i - \frac{1}{(\varepsilon+P)}[(g_{00})^2P_{,j}g^{ij} + P_{,t}u_tv^i]. \tag{44}$$

With the use of $(u_t)^2 = -g_{ij}v^iv^j/g_{00} - g_{00}$ we can re-express the gravitational terms as

$$-\Gamma^i_{00}(u_t)^2 - \Gamma^i{}_{jk}v^jv^k + \frac{g_{00,k}}{g_{00}}v^kv^i = -\frac{1}{2}s^{ij}g_{00,j} - \gamma^i{}_{jk}v^jv^k. \tag{45}$$

As expected, the gravitational part of the acceleration of the fluid element is exactly equal to the acceleration of a pN particle (20).

Since the gravitational part of (44) is already pseudo-Newtonized, let us examine the hydrodynamic part. We assume (1) that the gas does not reach relativistic temperatures, in SI units $k_{\rm B}T \ll mc^2$, and (2) that the gas does not reach relativistic velocities in the pN frame, in SI units $v^2 \ll c^2$. Furthermore, we can estimate $P_{,t} \sim P_{,k}c_{\rm s}$, where $c_{\rm s}$ is the local sound speed (which is smaller than the speed of light). Hence, if we neglect terms from Equation (44) that are small in this approximation, we obtain the pN Euler equation as

$$\left.\frac{d^2x^i}{d\tilde{t}^2}\right|_{\rm pN} = -\frac{1}{2}s^{ij}g_{00,j} - \gamma^i{}_{jk}v^jv^k - \frac{1}{\rho}(g_{00})^2P_{,j}g^{ij}. \tag{46}$$

We can see that this Euler equation converges to the Newtonian limit automatically in the weak field without any additional special-relativistic terms. Additionally, it will reproduce most of the strong-field effects of its exact relativistic counterpart (44).

To conclude, by using the reparametrization method and making assumptions that are reasonable for astrophysical applications, one is able to obtain a full set of pN fluid equations, which are pN in the sense of automatically reducing to Newtonian equations in flat regions of space-time.

However, one must keep in mind the more subtle approximation introduced by the time-reparametrization. By evolving the elements of the fluid from some $\tilde{t}_0$ to some $\tilde{t}_0 + \delta\tilde{t}$, we are in fact evolving each element by $\delta t = -u_t\delta\tilde{t}$. This means that the elements in the pN evolution fall slightly out of sync as compared with the exact relativistic situation. This relative error does not show up in a single step but accumulates at a rate that is proportional to the relative differences of $-u_t$ between neighboring elements and also to the strength with which they interact.

Hence, for the validity of the pN fluid evolution, we also have to require that the length scale of the $-u_t$ variability is at all times much larger than the hydrodynamic interaction length scale

$$\frac{(u_t)_{,i}}{u_t} \ll \frac{P_{,i}}{P}. \tag{47}$$

In SI units and the weak-field limit, this criterion is to leading order in c^{-1}

$$\frac{1}{c^2}\left(\frac{1}{2}(v^2) + \Phi\right)_{,i} \ll \frac{P_{,i}}{P}, \tag{48}$$

which is a criterion fulfilled in most physical applications.

For illustration and further applications, we have computed the pN Euler and particle-conservation equations explicitly in the Schwarzschild space-time in the usual radial Schwarzschild coordinates and Cartesian isotropic coordinates and include them in Appendix B. The Cartesian isotropic coordinates, based on the isotropic rather than the usual Schwarzschild radius, correspond to a pN metric, which is isotropic at every space-time point. This set of coordinates could be useful in numerical schemes such as smoothed-particle hydrodynamics, because the smoothing kernel of the particles can be entirely isotropic there as long as the smoothing length is much shorter than the curvature scale of the space-time (compare, e.g., with Laguna et al. 1993).

Of course, simply weighing the order of magnitude of the terms in the relativistic Euler and particle-conservation equations is not sufficient to fully asses the applicability of the set of pN fluid equations. However, the full investigation and testing of this set of equations by either numerical or analytical means is out of the scope of the current paper. Hence, one should understand Equations (41) and (46) as a proposal of which the usefulness can be shown by future work. On the other hand, we are confident that this set of equations will result in better results than naively implementing the gravitational accelerations (20) into Newtonian hydrodynamics without any other modification.

Namely, in situations where densities and pressures are high enough to steer the motion of the fluid elements far away from free test-particle motion, we expect the additional strong-field coupling to the hydrodynamical degrees of freedom to become very important. For instance in the case of the circularized perfect-fluid equilibria in Schwarzschild space-time known as Polish doughnuts (Abramowicz et al. 1978), a simple computation shows that, up to some rescalings of density and angular momentum, our structural equations will yield the same structures of the doughnuts as the exact relativistic equations. If, however, we omit the $(g_{00})^2g^{ij}$ factor in the pressure term in

the Euler equation, one obtains radically different solutions such as equilibria extending to the horizon while being held by finite pressure gradients. Thus, including the strong-field factor in the pressure term is absolutely necessary for a good description of highly pressurized flows near the horizon.

6. The Kerr Space-time

One of the most interesting goals in formulating pN frameworks is a satisfactory description of motion in the Kerr space-time at high values of the spin parameter a. By giving a useful description of highly spinning black holes one would extend the applicability of the pN framework to the vast majority of astrophysical black holes.

The pN Hamiltonian given in Section 2 will describe the motion in the Kerr space-time almost perfectly, and will lag with respect to the exact relativistic case only for large binding energy $\mathcal{E} = 1 + u_t$. However, giving a full description of motion of a fluid near a Kerr black hole has some difficulties as already described in Section 5.2 and is thus out of the scope of the current paper. Hence, we will demonstrate the properties of the pN Hamiltonian in the Kerr space-time only on the motion of individual massive test particles and specifically on circular orbits and their close oscillations.

In Boyer–Lindquist coordinates t, r, ϑ, φ, we have the non-zero inverse metric components of the Kerr metric (e.g., Weinberg 1972; Misner et al. 1973; Griffiths & Podolský 2009)

$$\begin{aligned} g^{tt} &= -\frac{\mathcal{A}}{\Delta\Sigma}, \\ g^{rr} &= \frac{\Delta}{\Sigma},\ g^{\vartheta\vartheta} = \frac{1}{\Sigma}, \\ g^{\varphi\varphi} &= \frac{\Delta - a^2\sin^2\vartheta}{\Delta\Sigma\sin^2\vartheta}, \\ g^{t\varphi} &= \frac{2Mra}{\Delta\Sigma}, \end{aligned} \tag{49}$$

where $\Sigma = r^2 + a^2\cos^2\vartheta$, $\Delta = r^2 - 2Mr + a^2$, and $\mathcal{A} = (r^2 + a^2)^2 - a^2\Delta\sin^2\vartheta$. The corresponding pN Hamiltonian (10) for massive particles $\kappa = 1$ then reads

$$\begin{aligned} H_{\mathrm{pNK}} = &\frac{1}{2\mathcal{A}}\left(\Delta^2 u_r^2 + \Delta u_\vartheta^2 + \frac{\Delta - a^2\sin^2\vartheta}{\sin^2\vartheta}u_\varphi^2\right) \\ &+ \frac{1}{2}\left(\frac{\Delta\Sigma}{\mathcal{A}} + 1\right) + \omega u_\varphi(\omega u_\varphi - \sqrt{\mathcal{D}}), \end{aligned} \tag{50}$$

where $\omega \equiv g^{t\varphi}/g^{tt} = -2Mra/\mathcal{A}$ and

$$\begin{aligned} \mathcal{D} = &(\omega u_\varphi)^2 + \frac{1}{\mathcal{A}}\left(\Delta^2 u_r^2 + \Delta u_\vartheta^2 + \frac{\Delta - a^2\sin^2\vartheta}{\sin^2\vartheta}u_\varphi^2\right) \\ &+ \frac{\Delta\Sigma}{\mathcal{A}}. \end{aligned} \tag{51}$$

The Hamiltonian (50) is formally very complicated. On the other hand, as described in Section 2 and particularly Section 2.3, H_{pNK} provides

1. an angular momentum distribution over circular orbits exactly equal to the Kerr case,
2. absolutely exact behavior of the marginally bound ($H_{\mathrm{pNK}} = 0$, $\mathcal{E} = 0$) circular orbit as compared to the Kerr case including both the radius and rotation frequency, and
3. an easily tractable upper error estimate for all bound circular orbits based on the binding energy of the ISCO and (14) and (13).

We will now discuss the errors induced to circular orbits and close oscillations around them. Furthermore, we will compare our Hamiltonian with the Lagrangian of Ghosh et al. (2014) and offer a few remarks.

6.1. Circular Orbits

The condition for a circular orbit is $\partial H_{\mathrm{pNK}}/\partial r = 0$ with $u_r = u_\vartheta = 0$, $\vartheta = \pi/2$ and some r, u_φ to be determined. As described in Section 2, this condition will be fulfilled for exactly same pairs of r, u_φ for H_{pNK} as for the exact relativistic case of a Kerr black hole. Hence, the formal angular momentum distribution $u_{\varphi\mathrm{c}}(r)$ over circular orbits is the same in both cases and reads (Bardeen et al. 1972)

$$u_{\varphi\mathrm{Kc}}(r) = \frac{\pm M^{1/2}(r^2 \mp 2aM^{1/2}r^{1/2} + a^2)}{\sqrt{r^3 - 3Mr^2 \pm 2aM^{1/2}r^{3/2}}}, \tag{52}$$

where the upper sign will always refer to the co-rotating circular orbits and the lower sign to the counter-rotating circular orbits.

Using the formula for the pN Hamiltonian (10) and the definition of binding energy discussed in Section 2.3, we can find the expression for pN binding energy in terms of the original relativistic one as $\mathcal{E}_{\mathrm{pN}} = \mathcal{E} - \mathcal{E}^2/2$. That means that bound circular orbits will always have a lower energy in the pN case and, since the efficiency of accretion disks is estimated by the binding energy of the ISCO, the accretion disks in the pN fields will generally have lower efficiency than the ones in the corresponding relativistic space-times.

Also, since we know that all time rates such as the rotation frequency along a circular orbit will be rescaled by the factor $-u_t$ in the pN case and that $-u_t \in (0, 1)$ for bound orbits, then the pN rotation frequencies of bound circular orbits will always be smaller than in the exact Kerr case. On the other hand, from the marginally bound orbit inward to the black hole, we have unbound orbits, $-u_t > 1$, and there the pN frequencies will be higher than in the exact Kerr case.

Furthermore, as we approach the photon sphere, the energy of circular orbits diverges and both the time and energy scales become vastly different from the relativistic case. Hence, for accretion disk modeling, we must cut off the dynamics somewhere between the radius of the marginally bound orbit and the photon orbit.

Let us now give a few more explicit expressions for the behavior of the circular orbits. The specific binding energy $\mathcal{E}_{\mathrm{Kc}}$ of circular orbits in the relativistic case reads

$$\mathcal{E}_{\mathrm{Kc}}(r) = 1 - \frac{r^{3/2} - 2Mr^{1/2} \pm aM^{1/2}}{\sqrt{r^3 - 3Mr^2 \pm 2aM^{1/2}r^{3/2}}}. \tag{53}$$

On the other hand, the specific binding energy $\mathcal{E}_{\mathrm{pNKc}}$ of circular orbits in the pN case yields

$$\mathcal{E}_{\mathrm{pNKc}}(r) = \frac{1}{2}\left[1 - \frac{(r^{3/2} - 2Mr^{1/2} \pm aM^{1/2})^2}{r^3 - 3Mr^2 \pm 2aM^{1/2}r^{3/2}}\right]. \tag{54}$$

The position of the marginally bound circular orbit is given by solving $\mathcal{E}_{\rm Kc} = \mathcal{E}_{\rm pNKc} = 0$, which gives

$$r_{\rm Kmb} = 2M - a + 2\sqrt{M(M-a)}. \tag{55}$$

As already stated in Section 2.3, for the circular orbit of radius $r_{\rm Kmb}$, the correspondence between the pN and relativistic case is perfect both in energy and frequency.

The angular rotation frequency $\Omega_{\rm Kc} \equiv d\varphi/dt$ of circular orbits in the relativistic case reads

$$\Omega_{\rm Kc}(r) = \frac{\pm M^{1/2}}{r^{3/2} \pm aM^{1/2}}. \tag{56}$$

In the pN case, we just have the analogous angular rotation frequency given as $\Omega_{\rm pNKc} \equiv d\varphi/d\tilde{t} = (1 - \mathcal{E}_{\rm Kc})\Omega_{\rm Kc}$, which gives

$$\Omega_{\rm pNKc}(r) = \frac{\pm M^{1/2}(r^{3/2} - 2Mr^{1/2} \pm aM^{1/2})}{(r^{3/2} \pm aM^{1/2})\sqrt{r^3 - 3Mr^2 \pm 2aM^{1/2}r^{3/2}}}. \tag{57}$$

Using the expressions above, we can easily plot the properties of the circular orbits in both models for a black hole with any spin a and compare them.

6.2. Innermost Stable Circular Orbit

The most important estimate of accretion disk behavior comes from studying the properties of the ISCO. For instance, the binding energy of the ISCO is equal to the efficiency of the accretion process in a radiatively efficient thin accretion disk (Abramowicz & Fragile 2013). In other cases, the orbital frequency of the ISCO is proposed to distinguish between black hole candidates and neutron stars (Psaltis 2008). Also, as has already been mentioned, the binding energy of the ISCO gives an upper error estimate for various deviations of the pN description from the relativistic case and can thus serve as an overall indicator of the applicability of the pN Hamiltonian (50).

The radius of the ISCO is (Bardeen et al. 1972)

$$r_{\rm ISCO} = M[3 + Z_2 - \sqrt{(2 - Z_1)(4 + Z_1 + 2Z_2)}], \tag{58}$$

$$Z_1 = (1 - a^2/M^2)[(1 - a^2/M^2) + (1 + a^2/M^2)], \tag{59}$$

$$Z_2 = \sqrt{3a^2/M^2 + 1 + Z_1^2}. \tag{60}$$

It is quite obvious that the substitution of $r_{\rm ISCO}$ into the expressions for energy or frequency gives very complicated formulas. Hence, we only compare the relations $\mathcal{E}_{\rm ISCO}(a)$ in Figure 1 and the angular frequencies of the ISCO in Figure 2.

As we go to higher spins of the black hole, the relativistic binding energy $\mathcal{E}_{\rm ISCO}$ grows and thus also the relative errors in the pN values of binding energy and frequency of circular orbits. For instance, if we want the relative error of the binding energy of the ISCO to be less than 10% in the pN model, we can only use the Hamiltonian (50) for spins $a < 0.96M$, which is a reasonable bound. However, if we set the tolerance in the relative error of ISCO binding energy to 5%, we can only use the pN Hamiltonian for spins $a < 0.68M$, which is rather restrictive. Either way, it is not very reasonable to use the pN Hamiltonian all the way up to the extremal $a = M$ black holes because there we have the relativistic ISCO binding energy $\mathcal{E}_{\rm ISCO} = 1 - 1/\sqrt{3} \approx 0.42$, and thus the relative error of the binding energy of the ISCO about 21%.

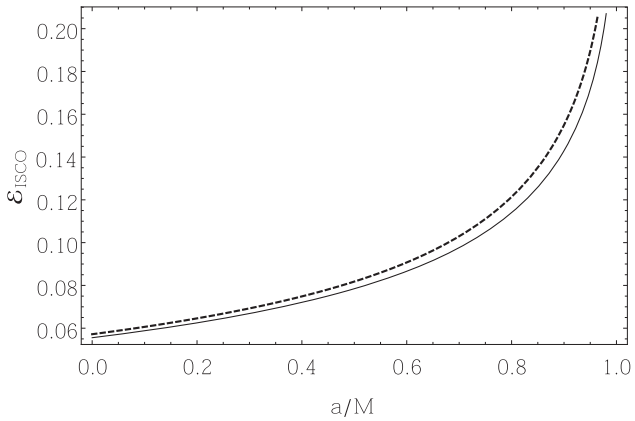

Figure 1. Specific binding energy of the ISCO $\mathcal{E}_{\rm ISCO}$ in the Kerr space-time (dashed) and the pseudo-Newtonian counterpart (full line).

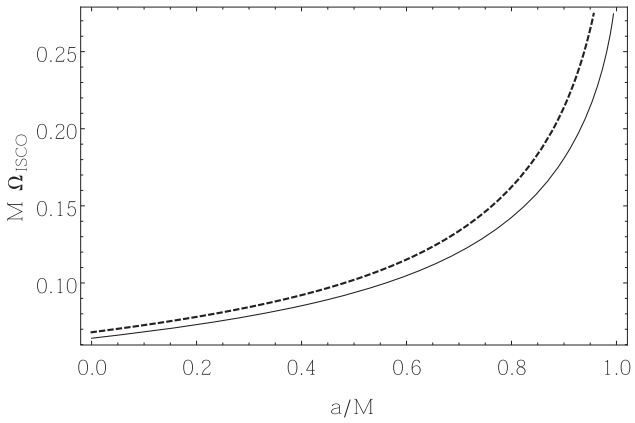

Figure 2. Angular rotation frequency $\Omega_{\rm ISCO}$ of the ISCO in the Kerr space-time (dashed) and the pseudo-Newtonian counterpart (full line). The frequency is given in units of M^{-1} ($G^{-1}\,M^{-1}\,c^3$ in SI units) so that the result is scalable with respect to the mass of the black hole.

6.3. Small Perturbations of Circular Orbits

Let δr, δu_r, $\delta\vartheta$, δu_ϑ be small deviations from a circular orbit. At the point of reflectional symmetry $\vartheta = \pi/2$ all the first $\partial/\partial\vartheta$ derivatives of the Hamiltonian vanish. Additionally for $u_\vartheta = 0$, the first $\partial/\partial u_\vartheta$ derivatives are also zero. Hence, the linearized equations of motion for the small deviations decouple into two sectors corresponding to the purely radial (epicyclic) and purely vertical oscillations around the circular orbit. The equations for the purely radial oscillations in matrix form read

$$\begin{pmatrix} 0 & -\frac{\partial^2 H_{\rm pNK}}{\partial r^2} \\ \frac{\partial^2 H_{\rm pNK}}{\partial u_r^2} & 0 \end{pmatrix} \begin{pmatrix} \delta u_r \\ \delta r \end{pmatrix} = \begin{pmatrix} \delta\dot{u}_r \\ \delta\dot{r} \end{pmatrix}. \tag{61}$$

Because we are considering perturbations around $u_r = 0$, the diagonal terms corresponding to first $\partial/\partial u_r$ derivatives of the Hamiltonian are also zero. The solution for δu_r, δr is an oscillating solution with a frequency

$$\omega_{r\rm pNK} = \left(\frac{\partial^2 H_{\rm pNK}}{\partial u_r^2} \frac{\partial^2 H_{\rm pNK}}{\partial r^2} \right)^{1/2}, \tag{62}$$

where the expression is evaluated at $\vartheta = \pi/2$, $u_r = u_\vartheta = 0$, $u_\varphi = u_{\varphi c}(r)$. Similarly, for the purely vertical oscillations,

we obtain the vertical oscillation frequency

$$\omega_{\vartheta\mathrm{pNK}} = \left(\frac{\partial^2 H_{\mathrm{pNK}}}{\partial u_\vartheta^2}\frac{\partial^2 H_{\mathrm{pNK}}}{\partial \vartheta^2}\right)^{1/2}. \tag{63}$$

Expressions (62) and (63) along with the substitution of $u_{\varphi\mathrm{c}}$ from Equation (52) give the pN oscillation frequencies as cumbersome analytical expressions.

Nevertheless, we can find a workaround by considering that the pN Hamiltonian H_{pNK} is equal to $H_{\mathrm{pNK}} = (u_t^2 - 1)/2 = (H_t^2 - 1)/2$, where H_t is the Hamiltonian generating exact relativistic motion parametrized by coordinate time. The frequencies are thus given as

$$\omega_{r\mathrm{pNK}} = -u_t\left(\frac{\partial^2 H_t}{\partial u_r^2}\frac{\partial^2 H_t}{\partial r^2}\right)^{1/2} = -u_t\omega_r, \tag{64}$$

$$\omega_{\vartheta\mathrm{pNK}} = -u_t\left(\frac{\partial^2 H_t}{\partial u_\vartheta^2}\frac{\partial^2 H_t}{\partial \vartheta^2}\right)^{1/2} = -u_t\omega_\vartheta, \tag{65}$$

where ω_r, ω_ϑ are the exact oscillation frequencies in Kerr space-time. However, these are well known (see, e.g., Abramowicz & Fragile 2013)

$$\omega_r = \Omega_{\mathrm{Kc}}\sqrt{1 - 6rM^{-1} + 8ar^{-3/2}M^{1/2} - 3a^2r^{-2}}, \tag{66}$$

$$\omega_\vartheta = \Omega_{\mathrm{Kc}}\sqrt{1 - 4ar^{-3/2}M^{1/2} + 3a^2r^{-2}}. \tag{67}$$

As a result, we see that once again the relative difference between the relativistic and pN frequencies will be equal to the binding energy of the circular orbit

$$\eta_{\omega\alpha} \equiv \frac{\omega_{\alpha\mathrm{pNK}} - \omega_\alpha}{\omega_{\alpha\mathrm{pNK}}} = \mathcal{E}_{\mathrm{c}}, \tag{68}$$

where $\alpha = r, \vartheta$. This means, in particular, that the maximum error in the oscillation frequencies will be once again given by the binding energy of the ISCO as given in Figure 1. Hence, the pN model is useful in a similar range as discussed in the previous Section 6.2 even for accretion models where the disk oscillations are relevant. For illustration, we plot the oscillation frequencies for a number of values of the spin parameter in Figure 3.

6.4. Remarks on the Ghosh–Sarkar–Bhadra Lagrangian

Ghosh et al. (2014) derived a Lagrangian (the GSB Lagrangian) for the motion of test particles in the equatorial plane, which naturally offers itself for comparison with the herein presented Hamiltonian (50). We point out the differences of the approach of Ghosh et al. (2014) and a few non-trivial facts about the GSB Lagrangian.

Instead of covariant velocity components u_i, the GSB Lagrangian is constructed by a series of Ansatzes using the contravariant (canonically non-conjugate) components u^i. As a consequence, the dynamics are restricted only to the equatorial plane (the pseudo-Kerr Hamiltonian (50) presented in this paper applies to any ϑ) and it seems that there is no simple characterization of the GSB Lagrangian in terms of reparametrized geodesics.

The Ghosh–Sarkar–Bhadra Lagrangian reads

$$L_{\mathrm{GSB}} = \frac{1}{2(r-2M)^2(1+\gamma\dot{\varphi})}\left(\frac{r^3(r-2M)}{\Delta}\dot{r}^2 + \Delta r^2\dot{\varphi}^2\right) + \frac{M}{r}(1-\gamma\dot{\varphi}), \tag{69}$$

where $\gamma = 2Ma/(r-2M)$. It is interesting that the GSB Lagrangian (69) has an impractical *Hamiltonian* counterpart, whereas the herein presented pseudo-Kerr Hamiltonian (50) has a *Lagrangian* counterpart complicated beyond usefulness. Complications associated with either the forward or backward Legendre transform seem to be a general feature of Lagrangians and Hamiltonians modeling the gravitomagnetic effects in the Kerr space-time.

The GSB Lagrangian has certain problems with the angular momentum distribution of circular orbits connected to the singularities of the effective potential. For the angular momenta of circular orbits λ_{GSBc} it holds that

$$\lambda_{\mathrm{GSBc}} = \frac{-Q \pm \sqrt{Q^2 - 4R}}{2},$$
$$Q = \frac{4a^3rM - 6Mar(r^2+a^2)}{a^2r(r-2M) - r(r-3M)(r^2+a^2)},$$
$$R = \frac{M(r^2+a^2)[r(r^3+3a^2) - 2a^2r]}{a^2r(r-2M) - r(r-3M)(r^2+a^2)}. \tag{70}$$

What was not clearly stated or shown in the original paper is the fact that this angular momentum distribution has a singularity at a radius r_{s} given by

$$a^2(r_{\mathrm{s}} - 2M) - (r_{\mathrm{s}} - 3M)(r_{\mathrm{s}}^2 + a^2) = 0, \tag{71}$$

for which the solution varies quite uniformly from $r_{\mathrm{s}} = 3M$ for $a = 0$ to $r_{\mathrm{s}} \approx 3.1M$ for $a = M$.

Even though the authors state that the marginally bound ($\mathcal{E} = 0$) circular orbit exists up to $a \approx 0.7M$ and that the potential is thus useful up to such values, there is a possible issue with the marginally bound orbit; the angular momentum distribution (70) crosses the singularity (71) before reaching the radius of the marginally bound orbit already for $a \gtrsim 0.45M$. Among other things, this means that the Keplerian circular orbits have a "singular pause" before reaching the marginally bound orbit and the matter density of a stationary accretion disk would almost certainly exhibit non-physical behavior at the singular $r = r_{\mathrm{s}}$.

Hence, the GSB Lagrangian should be considered as useful only for $r \gtrsim 3.1M$, and if the marginally bound orbit is important in the given model, only $a \lesssim 0.45M$ should be considered. The point where even the ISCO collides with this singularity is $a \approx 0.7M$ (which is the reason why Ghosh et al. 2014 were not able to find the ISCO beyond that spin). Among other things, this means that for a near-Keplerian accretion disk near a black hole with spin $a \approx 0.7M$ the singularity (71) is very near its edge and exotic effects might ensue. Thus, it seems commendable to use the Lagrangian (69) only for spins well below $a \approx 0.7M$.

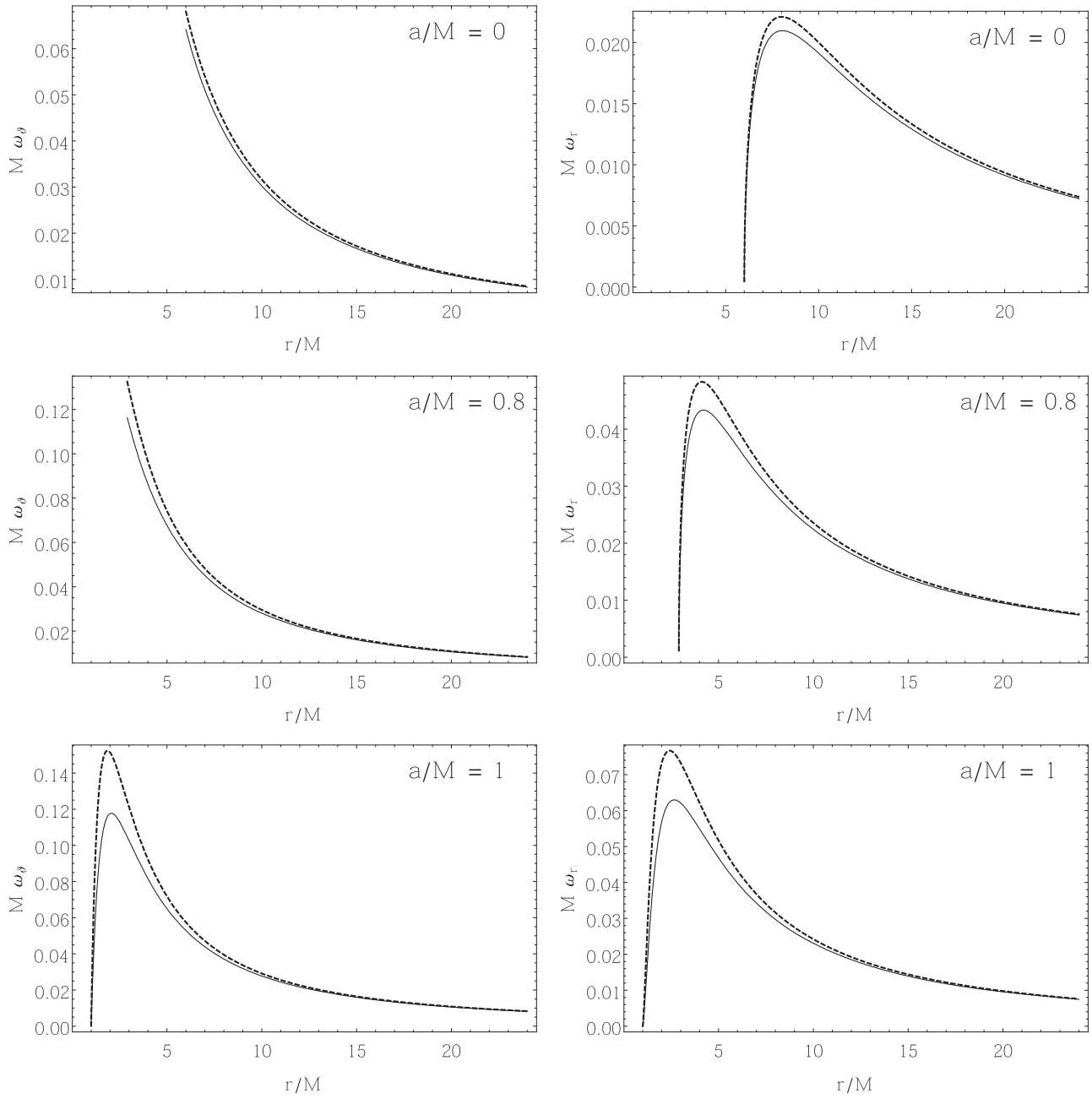

Figure 3. Comparison of vertical (left) and radial (right) oscillation frequencies of perturbed circular orbits between the exact Kerr values (dashed) and the values obtained with the pseudo-Newtonian Hamiltonian (50) (full). The r plot ranges are fixed for all plots while the ω-ranges are individually adjusted and only values up to the ISCO are plotted. It is not entirely obvious that the highest relative errors between the frequencies is always in the left-most part of the individual plots (at the ISCO) but we have verified this fact both by analytical and numerical means.

7. Conclusion

We have developed and studied a generalized pN formalism appropriate for particles, light, and fluids in stationary space-times. In the case of static, spherically symmetric space-times, our formalism coincides with previous results in the literature (Tejeda & Rosswog 2013, 2014; Sarkar et al. 2014). In general static space-times (without gravitomagnetic terms in the metric), this formalism has elegant geometric interpretations and allows for the full explicit development of fluid equations, which can be understood as a particular kinematic limit of the fully relativistic equations. Additionally, we have included electromagnetic fields influencing the motion in the case of particles with charge.

As already stated in Section 5.2, the presented pN fluid equations should be further investigated by comparing their numerical and analytical solutions with relativistic counterparts so that their proper applicability is fully understood. The undeniable point of our analysis is that a naive implementation of the pN acceleration of individual particles into a Newtonian code necessarily neglects further coupling of the strong gravitational field to the hydrodynamical degrees of freedom and may lead to pathological behavior of the fluid near the black hole horizon.

The herein presented pN framework is exceptional in its clear and direct derivation from the space-time that we want to mimic. As a result, we have obtained explicit bounds on the various errors our pN formalism introduces. The general conclusion is that the various relative errors in this description grow linearly with the specific binding energy of the motion in question.

This has consequences for the applicability of Newtonian numerical codes used along with the pN equations of motion. We have derived that, for stationary structures near non-rotating black holes, we can expect the result of a pN computation to be accurate within a few percent of relative error in temporal and energetic quantities, and this error then nonlinearly grows with the spin of the black hole up to a few tens of percent.

One particular shortcoming of the formalism is the fact that in space-times that are stationary but not static (with dragging or gravitomagnetic terms in the metric), it is not possible to express particle Lagrangians in a closed form and we are constrained to Hamiltonian formalism. Similarly, the corresponding fluid equations would be expressed in some set of canonical momenta rather than velocities, which is incompatible with common numerical codes. This means that pN fluid evolution near a spinning black hole probably has to be approached in a different manner.

It is easy to include electromagnetic terms into the pN Euler Equation (46), albeit only in the non-physical case when (1) the fluid is composed exclusively of charged particles of a single value of charge and the current thus proportional to the velocity of the fluid, and (2) the currents in the fluid have no backreaction to the static, externally imposed fields. In the actuallly physically relevant case of a quasi-neutral fluid with the current deviating from the velocity and back-reacting to the electromagnetic field, the equations become very complicated, and the separation of strong-field, "kinematically non-relativistic," and Newtonian terms become much more subtle. Hence, we leave the question of pN magneto-hydrodynamics as a possibility for future work.

We would like to thank Emilio Tejeda, Oldřich Semerák, and Volker Perlick for useful discussions on the preliminary versions of the paper. We would also like to thank the anonymous reviewer for many useful remarks on the paper. V.W. is grateful for support from grants GAUK-2000314 and SVV-260211 and a PhD grant of the German Research Foundation within its Research Training Group 1620 *Models of Gravity*.

Appendix A
Jacobi Metric in Static Space-times

It is a well-known result in the theory of classical mechanics that for a time-independent Lagrangian given in the form

$$L = \frac{1}{2} d_{ij} \dot{x}^i \dot{x}^j - V(x), \tag{72}$$

one can define an energy-dependent metric called the Jacobi metric as

$$j_{ij} = (E - V) d_{ij}, \tag{73}$$

where $E = d_{ij}\dot{x}^i\dot{x}^j/2 + V$ is the energy integral of motion. Then, if $E > V$, the trajectories corresponding to the Lagrangian (72) on a fixed hypersurface $E = \text{const.}$ will be, up to a reparametrization, geodesics corresponding to the metric j_{ij} (see, e.g., Pettini 2007 for more details). Hence, following this pattern, we identify s_{ij} as the analogy of d_{ij}, $\kappa(g_{00} + 1)/2$ as $-V$, and the value of the Hamiltonian $\tilde{E} = H_{\mathrm{pN}} = ((u_t)^2 - 1)/2$ as the energy integral. When the dust settles, we obtain the Jacobi metric

$$j_{ij} = -\frac{(u_t)^2 + \kappa g_{00}}{2} \frac{g_{ij}}{g_{00}}. \tag{74}$$

To summarize, on constant u_t ($\tilde{E}$) hypersurfaces and in static space-times, the full four-dimensional geodesics can always be described as three-dimensional geodesics on the spatial hypersurface with the Jacobi metric (74). This result has recently been given by Gibbons (2015) by considering the action of a geodesic in static space-times; the formalism here provides a connection between the result of Gibbons (2015) and the usual notion of the Jacobi metric known from classical mechanics.

Appendix B
Evolution Equations for a Perfect Fluid near a Black Hole in Various Coordinates

B.1. Cartesian Isotropic Coordinates

The most simple Cartesian-like expression of the Schwarzschild metric is given by a transformation to the isotropic radial coordinate $r = (M + 2R)^2/(4R)$ (introduced already in Section 4.1, for a thorough discussion of the coordinates, see Misner et al. 1973) and then transforming to a set of coordinates $x^{(1)}$, $x^{(2)}$, $x^{(3)}$

$$x^{(1)} = R \sin\vartheta \cos\varphi, \tag{75}$$

$$x^{(2)} = R \sin\vartheta \sin\varphi, \tag{76}$$

$$x^{(3)} = R \cos\vartheta, \tag{77}$$

$$R = \sqrt{\sum_{i=1}^{3} (x^{(i)})^2}. \tag{78}$$

The metric then takes the form

$$ds^2 = -\left(\frac{2R - M}{2R + M}\right)^2 dt^2 + \frac{(2R + M)^4}{16R^4} \sum_{i=1}^{3} (dx^{(i)})^2. \tag{79}$$

An important property of the isotropic coordinates is that they regularize the spatial part of the metric at the horizon, while preserving the $g_{0i} = g^{0i} = 0$ structure of the metric essential to the elegance of the pN formalism. Other sets of "horizon-penetrating" coordinates, which make even the temporal part of the metric regular at the horizon exist (see, for example, Font et al. 1998), but they necessarily violate the $g_{0i} = g^{0i} = 0$ condition. That is, the pN metric $s_{ij} \equiv g_{ij}/g_{00}$ will always be singular at the horizon and the singularity can only be "softened" by a set of coordinates such as the isotropic ones.

Either way, we know from the discussion in Section 2.3 that circularized motion at the location of the photon orbit will always have very large errors as compared to the exact relativistic case, so we should beware of extending the simulation up to there for circularized flows. On the other hand, circular motion at the marginally bound orbit is expected to exactly reproduce the relativistic features. Thus, we recommend to cut off a simulation of an accretion flow somewhere between the marginally bound circular orbit

$r_{\rm mb} = 4M \rightarrow R_{\rm mb} = (3 + 2\sqrt{2})M/2$ and the photon sphere $r_{\rm ps} = 3M \rightarrow R_{\rm ps} = (2 + \sqrt{3})M/2$.

The pN metric $s_{(i)(j)} = -g_{(i)(j)}/g_{00}$ obtains the form

$$s_{(i)(j)} = \frac{(2R+M)^6}{16R^4(2R-M)^2}\delta_{ij}, \tag{80}$$

where δ_{ij} is the Cronecker delta. The pN Christoffel symbols corresponding to this metric then have the simple form

$$\gamma^{(i)}_{(j)(k)} = -\frac{2M}{R^2(4R+M)}(\delta_{ij}x^{(k)} + \delta_{ik}x^{(j)} - \delta_{jk}x^{(i)}). \tag{81}$$

We can thus easily express the respective pN equations of motion for a single particle (20) as

$$\begin{aligned}\ddot{x}^{(i)} = &\frac{4M}{R^2(4R+M)}\sum_{k=1}^{3}(\dot{x}^{(i)}\dot{x}^{(k)}x^{(k)} - \frac{1}{2}\dot{x}^{(k)}\dot{x}^{(k)}x^{(i)}) \\ &- \frac{64M(2R-M)^3R^3}{(2R+M)^9}x^{(i)}.\end{aligned} \tag{82}$$

The factor figuring in the particle-conservation equation then is

$$\sqrt{d} = \frac{(2R+M)^7}{64R^6(2R-M)} \tag{83}$$

and the particle-conservation equation reads

$$\dot{n} = -n\sum_{i=1}^{3}\left(\frac{\partial v^{(i)}}{\partial x^{(i)}} + \frac{2M(3M-8R)}{R^2(2R-M)(2R+M)}x^{(i)}v^{(i)}\right), \tag{84}$$

which corresponds to a conserved total particle number of the form

$$\mathcal{N} = \int n(x^{(i)})\frac{(2R+M)^7}{64R^6(2R-M)}d^3x. \tag{85}$$

The Euler equation for a fluid differs from the single-particle acceleration only by the $-P_{,j}g^{ij}g_{00}^2/\rho$ term and thus takes the form

$$\begin{aligned}\ddot{x}^{(i)} = &\frac{4M}{R^2(4R+M)}\sum_{k=1}^{3}(\dot{x}^{(i)}\dot{x}^{(k)}x^{(k)} - \frac{1}{2}\dot{x}^{(k)}\dot{x}^{(k)}x^{(i)}) \\ &- \frac{64M(2R-M)^3R^3}{(2R+M)^9}x^{(i)} - \frac{P_{,(i)}}{\rho}\frac{16R^4(2R-M)^4}{(2R+M)^8}.\end{aligned} \tag{86}$$

B.2. Schwarzschild Radial Coordinates

In Schwarzschild coordinates r, φ, ϑ the non-zero components of the metric s_{ij} read

$$\begin{aligned}s_{rr} &= \frac{1}{(1-2M/r)^2}, \quad s_{\vartheta\vartheta} = \frac{r^2}{1-2M/r}, \\ s_{\varphi\varphi} &= \frac{r^2\sin^2\vartheta}{1-2M/r}.\end{aligned} \tag{87}$$

From that, we compute the non-zero coefficients γ^{i}_{jk} as

$$\begin{aligned}\gamma^{r}_{rr} &= -\frac{2M}{r(r-2M)}, \quad \gamma^{r}_{\vartheta\vartheta} = -(r-3M), \\ \gamma^{r}_{\varphi\varphi} &= -(r-3M)\sin^2\vartheta,\end{aligned} \tag{88}$$

$$\gamma^{\varphi}_{\varphi r} = \gamma^{\varphi}_{r\varphi} = \frac{r-3M}{r(r-2M)}, \quad \gamma^{\varphi}_{\varphi\vartheta} = \gamma^{\varphi}_{\vartheta\varphi} = \cot\vartheta, \tag{89}$$

$$\gamma^{\vartheta}_{\vartheta r} = \gamma^{\vartheta}_{r\vartheta} = \frac{r-3M}{r(r-2M)}, \quad \gamma^{\vartheta}_{\varphi\varphi} = -\sin\vartheta\cos\vartheta. \tag{90}$$

The corresponding gravitational accelerations of individual particles are then easy to find by direct computation or in Tejeda & Rosswog (2013).

The volume density factor is $\sqrt{d} = r^2\sin\vartheta/(1-2M/r)$ and the particle-conservation equation reads

$$\dot{n} = -n\left(\frac{\partial\dot{r}}{\partial r} + \frac{\partial\dot{\vartheta}}{\partial\vartheta} + \frac{\partial\dot{\varphi}}{\partial\varphi} + \frac{2(r-3M)}{r(r-2M)}\dot{r} + \cot\vartheta\,\dot{\vartheta}\right), \tag{91}$$

which corresponds to a conserved total particle number

$$\mathcal{N} = \int_0^\infty\int_0^\pi\int_0^{2\pi}\frac{n\,r^2\sin\vartheta}{1-2M/r}\,dr\,d\vartheta\,d\varphi. \tag{92}$$

The Euler equations in Schwarzschild coordinates then read

$$\begin{aligned}\ddot{r} = &\frac{2M}{r(r-2M)}\dot{r}^2 + (r-3M)[\dot{\vartheta}^2 + \sin^2\vartheta\,\dot{\varphi}^2] \\ &- \frac{1}{\rho}\left(1-\frac{2M}{r}\right)^3\frac{\partial P}{\partial r} - \frac{M}{r^2}\left(1-\frac{2M}{r}\right)^2,\end{aligned} \tag{93}$$

$$\begin{aligned}\ddot{\varphi} = &-\frac{2(r-3M)}{r(r-2M)}\dot{r}\dot{\varphi} - 2\cot\vartheta\,\dot{\vartheta}\dot{\varphi} \\ &+ -\frac{1}{\rho\,r^2\sin^2\vartheta}\left(1-\frac{2M}{r}\right)^2\frac{\partial P}{\partial\varphi},\end{aligned} \tag{94}$$

$$\begin{aligned}\ddot{\vartheta} = &-\frac{2(r-3M)}{r(r-2M)}\dot{r}\dot{\vartheta} - 2\sin\vartheta\cos\vartheta\,\dot{\varphi}^2 \\ &- \frac{1}{\rho r^2}\left(1-\frac{2M}{r}\right)^2\frac{\partial P}{\partial\vartheta},\end{aligned} \tag{95}$$

Following the pattern of this Appendix, one should be able to derive the fluid equations in any set of coordinates.

References

Abramowicz, M., Jaroszynski, M., & Sikora, M. 1978, A&A, 63, 221
Abramowicz, M. A. 2009, A&A, 500, 213
Abramowicz, M. A., Carter, B., & Lasota, J.-P. 1988, GReGr, 20, 1173
Abramowicz, M. A., & Fragile, P. C. 2013, LRR, 16, 1
Abramowicz, M. A., Lanza, A., Miller, J. C., & Sonego, S. 1997, GReGr, 29, 1585
Artemova, I. V., Björnsson, G., & Novikov, I. D. 1996, ApJ, 461, 565
Bardeen, J. M., Press, W. H., & Teukolsky, S. A. 1972, ApJ, 178, 347
Blanchet, L. 2006, LRR, 9, 4
Bonnerot, C., Rossi, E. M., Lodato, G., & Price, D. J. 2016, MNRAS, 455, 2253
Chakrabarti, S. K., & Mondal, S. 2006, MNRAS, 369, 976
Einstein, A. 1915, Sitzungsberichte der Preußischen Akademie der Wissenschaften, 2, 831
Font, J. A., Ibánez, J. M., & Papadopoulos, P. 1998, ApJL, 507, L67
Ghosh, S., & Mukhopadhyay, B. 2007, ApJ, 667, 367
Ghosh, S., Sarkar, T., & Bhadra, A. 2014, MNRAS, 445, 4463
Gibbons, G. 2015, CQGra, 33, 025004
Griffiths, J. B., & Podolský, J. 2009, Exact Space-times in Einstein's General Relativity (Cambridge: Cambridge Univ. Press)
Guckenheimer, J., & Holmes, P. 1983, Nonlinear Oscillations, Dynamical Systems, and Bifurcations of Vector Fields (New York: Springer Science & Business Media)
Laguna, P., Miller, W. A., & Zurek, W. H. 1993, ApJ, 404, 678

Misner, C. W., Thorne, K. S., & Wheeler, J. A. 1973, Gravitation (London: Macmillan)
Mukhopadhyay, B. 2002, ApJ, 581, 427
Mukhopadhyay, B., & Misra, R. 2003, ApJ, 582, 347
Nowak, M. A., & Wagoner, R. V. 1991, ApJ, 378, 656
Paczyński, B., & Wiita, P. J. 1980, A&A, 88, 23
Pettini, M. 2007, Geometry and Topology in Hamiltonian Dynamics and Statistical Mechanics, Vol. 33 (New York: Springer Science & Business Media)
Psaltis, D. 2008, LRR, 11, 1
Sarkar, T., Ghosh, S., & Bhadra, A. 2014, PhRvD, 90, 063008
Sasaki, M., & Tagoshi, H. 2003, LRR, 6, 1
Semerák, O., & Karas, V. 1999, A&A, 343, 325
Tejeda, E., Gafton, E., & Rosswog, S. 2017, MNRAS, submitted (arXiv:1701.00303)
Tejeda, E., & Rosswog, S. 2013, MNRAS, 433, 1930
Tejeda, E., & Rosswog, S. 2014, arXiv:1402.1171
Wegg, C. 2012, ApJ, 749, 183
Weinberg, S. 1972, Gravitation and Cosmology: Principles and Applications of the General Theory of Relativity, Vol. 1 (New York: Wiley)
Witzany, V., Semerák, O., & Suková, P. 2015, MNRAS, 451, 1770

PHYSICAL REVIEW D **96,** 064019 (2017)

Conservation laws and evolution schemes in geodesic, hydrodynamic, and magnetohydrodynamic flows

Charalampos Markakis,[1,2,*] Kōji Uryū,[3,†] Eric Gourgoulhon,[4,‡] Jean-Philippe Nicolas,[5,§] Nils Andersson,[2,‖] Athina Pouri,[6,¶] and Vojtěch Witzany[7,**]

[1]*NCSA, University of Illinois at Urbana-Champaign, Illinois 61801, USA*
[2]*Mathematical Sciences, University of Southampton, Southampton SO17 1BJ, United Kingdom*
[3]*Department of Physics, University of the Ryukyus, Senbaru, Nishihara, Okinawa 903-0213, Japan*
[4]*LUTh, UMR 8102 du CNRS, Observatoire de Paris, Université Paris Diderot, F-92190 Meudon, France*
[5]*Département de Mathématiques, Université de Bretagne Occidentale 6 avenue Victor Le Gorgeu, 29238 Brest Cedex 3, France*
[6]*RCAAM, Academy of Athens, Soranou Efesiou 4, 11527 Athens, Greece*
[7]*ZARM, Universität Bremen, Am Fallturm, 28359 Bremen, Germany*

(Received 4 July 2017; published 13 September 2017)

Carter and Lichnerowicz have established that barotropic fluid flows are conformally geodesic and obey Hamilton's principle. This variational approach can accommodate neutral, or charged and poorly conducting, fluids. We show that, unlike what has been previously thought, this approach can also accommodate perfectly conducting magnetofluids, via the Bekenstein-Oron description of ideal magnetohydrodynamics. When Noether symmetries associated with Killing vectors or tensors are present in geodesic flows, they lead to constants of motion polynomial in the momenta. We generalize these concepts to hydrodynamic flows. Moreover, the Hamiltonian descriptions of ideal magnetohydrodynamics allow one to cast the evolution equations into a hyperbolic form useful for evolving rotating or binary compact objects with magnetic fields in numerical general relativity. In this framework, Ertel's potential vorticity theorem for baroclinic fluids arises as a special case of a conservation law valid for any Hamiltonian system. Moreover, conserved circulation laws, such as those of Kelvin, Alfvén and Bekenstein-Oron, emerge simply as special cases of the Poincaré-Cartan integral invariant of Hamiltonian systems. We use this approach to obtain an extension of Kelvin's theorem to baroclinic (nonisentropic) fluids, based on a temperature-dependent time parameter. We further extend this result to perfectly or poorly conducting baroclinic magnetoflows. Finally, in the barotropic case, such magnetoflows are shown to also be geodesic, albeit in a Finsler (rather than Riemann) space.

DOI: 10.1103/PhysRevD.96.064019

I. INTRODUCTION

A wide variety of compact stellar objects where general relativistic effects are important is currently known. Black holes and neutron stars are involved in many astrophysical phenomena, including binary mergers and gamma ray bursts, which have observable imprints in the electromagnetic and gravitational wave spectrum. Many of these phenomena can be explained by means of general relativistic hydrodynamics. In addition, there is a growing number of observed phenomena where electromagnetic effects play a major role. These include observations of accretion disks around black holes [1], jets in active galactic nuclei or microquasars [2,3], gamma ray bursts, hypernovae, pulsars [4] and magnetars [5–9]. Magnetohydrodynamics (MHD) provides a macroscopic continuum approximation to studying such phenomena. General relativistic magnetohydrodynamics (GRMHD) originates in the works of Lichnerowicz [10] and is a rapidly developing field of modern astrophysics [4,11,12]. Departures from MHD are discussed in [13–15] and references therein. Compact objects such as magnetars or the differentially rotating supramassive remnants of binary neutron-star mergers can have magnetic fields of the order of 10^{15}–10^{17} G which can affect the dynamics and stability [16] of these objects. A fully relativistic description of magnetized neutron stars is thus desirable.

In this article, we develop a geometric treatment of ideal GRMHD. To this aim, we use Cartan's exterior calculus, relying on the nature of the electromagnetic field as a 2-form and the well-known formulation of Maxwell's equations by means of the exterior derivative operator. We also employ the formulation of hydrodynamics in terms of the fluid vorticity 2-form, following Synge [17] and Lichnerowicz [18]. This enables us to formulate GRMHD

*markakis@illinois.edu
†uryu@sci.u-ryukyu.ac.jp
‡eric.gourgoulhon@obspm.fr
§jean-philippe.nicolas@univ-brest.fr
‖N.A.Andersson@soton.ac.uk
¶athpouri@phys.uoa.gr
**witzany@zarm.uni-bremen.de

entirely in terms of exterior forms. Such an approach is not only elegant and fully covariant, but also simplifies some calculations which are tedious in the component approach. In addition, we obtain particlelike *Lagrangian and Hamiltonian descriptions of ideal MHD*, in Newtonian and relativistic contexts, with several theoretical and practical advantages. For example, schemes for evolution in numerical relativity are straightforward to obtain, and conserved quantities whose origin seems *ad hoc* in the component approach, emerge immediately as Noether-related quantities in this canonical approach.

In particular, Synge and Lichnerowicz have shown that barotropic-fluid flows may be described via simple variational principles as geodesic flows in a manifold conformally related to the spacetime manifold. Arnol'd described the nonrelativistic Euler equation as the geodesic equation on the group of volume-preserving diffeomorphisms [19]. This allowed him to apply geometric and group-theoretical methods to the study of this equation, and to develop the now called Arnol'd stability method [20–26].

Carter [27] has used this powerful canonical approach to efficiently derive conservation laws for neutral or charged poorly conducting fluids in general relativity. Markakis [28] has obtained an Euler-Lagrange and a Hamiltonian description of a barotropic fluid valid in Newtonian gravity as well as $3+1$ general relativity. In this article, we extend Carter's framework to perfectly conducting fluids with the aid of the Bekenstein-Oron (BO) formulation of ideal MHD [29–31]. In the canonical approach, conserved circulation integrals, such as those of Alfvén, Kelvin and Bekenstein-Oron, emerge simply as special cases of the Poincaré-Cartan integral invariant of Hamiltonian systems. We further show that the BO description can describe an arbitrary ideal MHD flow without loss of generality and allows one to cast the ideal MHD equations into a circulation-preserving hyperbolic form, which may be useful in numerical simulations of oscillating stars or radiating binaries with magnetic fields in numerical relativity. We generalize the Synge-Lichnerowicz result to perfectly conducting magnetofluids by showing that ideal MHD flows can be described as geodesic flows in a Finsler space.

Finally, Kelvin's circulation theorem has been thought to hold only for barotropic flows. It has been thought not to hold for baroclinic (nonisentropic) flows, except in a weak form (i.e. if the circulation is initially computed along rings of constant temperature or specific entropy [32]). However, using a temperature-dependent time parameter, we obtain a Hamiltonian action principle describing inviscid baroclinic flows within Carter's framework. Moreover, a Poincaré-Cartan integral invariant exists if and only if a system is Hamiltonian. We thus infer that, contrary to common belief, a generalization of Kelvin's theorem to baroclinic flows does exist in the strong form (i.e. the circulation can be initially computed along an *arbitrary* fluid ring). Remarkably, this result can be further extended to perfectly or poorly conducting baroclinic magnetoflows.

Symmetries and conservation laws are very useful because they can provide valuable insight of complicated (magneto)hydrodynamic phenomena; the relevant conserved quantities can be extremely useful in constructing initial data in numerical relativity, or significantly simplify solving for the motion. The examples considered below are applicable, among others, to the mathematical study and numerical simulation of fluid motions in rotating or binary relativistic stars [33–42] and their magnetospheres [43,44], neutron-star or black-hole accretion rings [27,45–47] and cosmological dynamics [48–56].

II. CLASSICAL DYNAMICS IN COVARIANT LANGUAGE

A. Notation

We consider a spacetime $(\mathcal{M}, \boldsymbol{g})$, i.e. a four-dimensional real manifold $\mathcal{M}$ endowed with a Lorentzian metric $\boldsymbol{g}$ of signature $(-+++)$. We assume that $\mathcal{M}$ is orientable, so that we have at our disposal the Levi-Civita tensor $\boldsymbol{\epsilon}$ (also called *volume element*) associated with the metric $\boldsymbol{g}$. Let $\boldsymbol{\nabla}$ be the covariant derivative associated with $\boldsymbol{g}$: $\boldsymbol{\nabla g} = 0$ and $\boldsymbol{\nabla \epsilon} = 0$. The star operator $\star$ denotes the Hodge dual of a differential form. For example, the Hodge dual of the 1-form $\boldsymbol{\omega}$ is a 3-form denoted by $\star\boldsymbol{\omega}$:

$$\star\omega_{\alpha\beta\gamma} := \epsilon_{\alpha\beta\gamma\delta}\omega^{\delta}. \tag{2.1}$$

Similarly, the Hodge dual of the 2-form $\boldsymbol{\Omega}$ is a 2-form denoted by $\star\boldsymbol{\Omega}$:

$$\star\Omega_{\alpha\beta} := \frac{1}{2}\epsilon_{\alpha\beta\gamma\delta}\Omega^{\gamma\delta}. \tag{2.2}$$

More details on these definitions may be found e.g. in Appendix B of Ref. [57].

We shall often use an index-free notation, denoting vectors and tensors on $\mathcal{M}$ by boldface symbols. As in [27], given a linear form $\boldsymbol{\omega}$, we denote by $\vec{\boldsymbol{\omega}}$ the vector associated to it by the metric tensor:

$$\boldsymbol{\omega} =: \boldsymbol{g}(\vec{\boldsymbol{\omega}}, \_). \tag{2.3}$$

In a given vector basis $(\boldsymbol{e}_\alpha)$, the components of $\boldsymbol{g}$, $\vec{\boldsymbol{\omega}}$ and $\boldsymbol{\omega}$ are $g_{\alpha\beta}$, $\omega^\alpha = g^{\alpha\beta}\omega_\beta$ and $\omega_\alpha = g_{\alpha\beta}\omega^\beta$ respectively.

Given a vector $\vec{\boldsymbol{v}}$ and a tensor $\boldsymbol{T}$ of type $(0, n)$ $(n \geq 1)$, i.e. a n-linear form (a linear form for $n = 1$, a bilinear form for $n = 2$, etc.), we denote by $\vec{\boldsymbol{v}} \cdot \boldsymbol{T}$ (respectively, $\boldsymbol{T} \cdot \vec{\boldsymbol{v}}$) the $(n-1)$-linear form obtained by setting the first (respectively last) argument of $\boldsymbol{T}$ to $\vec{\boldsymbol{v}}$:

$$\vec{\boldsymbol{v}} \cdot \boldsymbol{T} := \boldsymbol{T}(\vec{\boldsymbol{v}}, \_, \ldots, \_) \tag{2.4a}$$

$$\boldsymbol{T} \cdot \vec{\boldsymbol{v}} := \boldsymbol{T}(\_, \ldots, \_, \vec{\boldsymbol{v}}). \tag{2.4b}$$

Thanks to the above conventions, we may write the scalar product of two vectors $\vec{u}$ and $\vec{v}$ as

$$\boldsymbol{g}(\vec{u},\vec{v}) = \vec{u}\cdot\boldsymbol{v} = \boldsymbol{u}\cdot\vec{v}. \tag{2.5}$$

We denote by $\boldsymbol{\nabla}\cdot$ the covariant divergence, with contraction taken on the adjacent index. For instance, for a tensor field $\vec{\boldsymbol{T}}$ of type (2,0), $\boldsymbol{\nabla}\cdot\vec{\boldsymbol{T}}$ is the vector field defined by

$$\boldsymbol{\nabla}\cdot\vec{\boldsymbol{T}} \coloneqq \nabla_\beta T^{\beta\alpha}\boldsymbol{e}_\alpha, \tag{2.6}$$

where $\{\boldsymbol{e}_\alpha\}$ is the vector basis with respect to which the components $\nabla_\gamma T^{\alpha\beta}$ of $\boldsymbol{\nabla}\vec{\boldsymbol{T}}$ are taken. [Note that the convention for the divergence does not follow the rule for the contraction with a vector: in (2.4a) the contraction is performed on the *first* index.]

We use greek letters $\alpha,\beta,\gamma,\delta,\ldots$ for abstract and $\mu,\nu,\kappa,\lambda,\ldots$ for concrete spacetime indices. We also use roman letters $a,b,c,\ldots$ for abstract and $i,j,k,\ldots$ for concrete spatial indices. We use geometrized Heaviside-Lorentz units throughout the paper. We use ∇_α or ∂_α to denote the (Eulerian) covariant or partial derivative compatible with a curved or flat metric respectively, and $\partial/\partial x^\alpha$ to denote the (Lagrangian) partial derivative of a function $f(x,v)$ with respect to x for fixed v. We make extensive use of Lie and exterior derivatives: for a pedagogical introduction to using these concepts in relativistic hydrodynamics, the reader is referred to [58,59].

B. Hamiltonian flows

It is often thought that continuum systems necessarily require an infinite dimensional manifold for their description, and one often resorts to a classical field-theory approach, based on an action integral over a Lagrangian density in a spacetime 4-volume. This complicates the derivation of conservation laws from symmetries of the action—one of the main reasons for using an action functional in the first place. In many cases, however, the very definition of a perfect fluid allows one to treat each fluid element as an individual particle interacting with other fluid elements through pressure terms (in addition to electromagnetic or gravitational field terms). If the pressure terms are derivable from a potential, then a particlelike action principle can be found. This approach has been utilized by Carter [27] to derive particlelike conservation laws for neutral perfect fluids and for charged poorly conducting fluids. Here, we review Carter's framework and extend it to baroclinic fluids and perfectly conducting magnetofluids.

1. Lagrangian dynamics

The results derived in this section will apply to *any* classical motion obeying a Lagrangian variation principle. That is, for any particular (particle, fluid or magneto-fluid) flow, there exists a Lagrangian function $L(x,v)$ of the spacetime coordinates x^α and canonical 4-velocity v^α, evaluated at $x^\alpha(\lambda)$ and $v^\alpha(\lambda)$ where $\lambda\in\mathbb{R}$ is a canonical time parameter (which need not necessarily coincide with proper time τ) in terms of which the (not necessarily unit) vector

$$v^\alpha = \frac{dx^\alpha}{d\lambda} \tag{2.7}$$

is defined. The equations of the (particle or fluid-element) worldlines $x^\alpha(\lambda)$ can be obtained from the action functional

$$\mathcal{S} = \int_{\lambda_1}^{\lambda_2} L(x,v)\,d\lambda. \tag{2.8}$$

Extremizing the action keeping the endpoints fixed yields the Euler-Lagrange equations of motion

$$\frac{dp_\alpha}{d\lambda} = \frac{\partial L}{\partial x^\alpha} \tag{2.9a}$$

$$p_\alpha = \frac{\partial L}{\partial v^\alpha} \tag{2.9b}$$

where p_α is the *canonical momentum* 1-form conjugate to x^α. In the context of fluid theory, it is preferable to write the above equations in the (Eulerian) covariant form [27]

$$\pounds_{\vec{v}}p_\alpha = \nabla_\alpha L$$

or, in exterior calculus notation,

$$\pounds_{\vec{v}}\boldsymbol{p} = \mathbf{d}L, \tag{2.10}$$

where $\pounds_{\vec{v}}$ is the Lie derivative along the vector $\vec{v}$ and $\mathbf{d}$ is the exterior derivative [58–60]. The canonical momentum one-form $\boldsymbol{p} = p_\mu \mathbf{d}x^\mu$ is also known as the tautological one-form, the Liouville one-form, the Poincaré one-form the symplectic potential or simply the canonical one-form [61]. Using the definition of the Lie derivative and the chain rule, the above equation[1] can be expressed as

$$\begin{aligned}\pounds_{\vec{v}}p_\alpha - \nabla_\alpha L &\coloneqq v^\beta\frac{\partial p_\alpha}{\partial x^\beta} + p_\beta\frac{\partial v^\beta}{\partial x^\alpha} - \left(\frac{\partial L}{\partial x^\alpha} + \frac{\partial L}{\partial v^\beta}\frac{\partial v^\beta}{\partial x^\alpha}\right)\\ &= \frac{dp_\alpha}{d\lambda} - \frac{\partial L}{\partial x^\alpha} + \left(p_\beta - \frac{\partial L}{\partial v^\beta}\right)\frac{\partial v_\beta}{\partial x^\alpha}.\end{aligned} \tag{2.11}$$

[1] In Eq. (2.9b), the Lagrangian L and canonical momentum $\boldsymbol{p}$ are regarded functions of the time parameter λ, through $\vec{\boldsymbol{x}}(\lambda)$ and $\vec{\boldsymbol{v}}(\lambda)$, and characterize a single fluid element. In Eq. (2.10), the Lagrangian and canonical momentum are regarded functions on spacetime through $\vec{\boldsymbol{x}}$ and $\vec{\boldsymbol{v}}(x)$. They amount to the Lagrangian and canonical momentum of the fluid element located at $\vec{\boldsymbol{x}}$, and changing the argument $\vec{\boldsymbol{x}}$ generally changes the fluid element which L and $\boldsymbol{p}$ refer to.

This quantity vanishes if and only if the Euler-Lagrange Eq. (2.9) are satisfied; the latter are thus equivalent to the covariant Eq. (2.10).

2. Hamiltonian dynamics

The Legendre transformation

$$H = v^\alpha p_\alpha - L \tag{2.12}$$

defines the super-Hamiltonian $H(x, p)$. Then, the equations of motion take the form of Hamilton's equations

$$\frac{dp_\alpha}{d\lambda} = -\frac{\partial H}{\partial x^\alpha} \tag{2.13a}$$

$$\frac{dx^\alpha}{d\lambda} = \frac{\partial H}{\partial p_\alpha}. \tag{2.13b}$$

The above equations can be written covariantly as [27]

$$v^\beta(\nabla_\beta p_\alpha - \nabla_\alpha p_\beta) = -\nabla_\alpha H$$

or, in exterior calculus notation,

$$\vec{v} \cdot \mathbf{d}\boldsymbol{p} = -\mathbf{d}H. \tag{2.14}$$

One may obtain Eq. (2.14) using the Cartan identity

$$\pounds_{\vec{v}} p_\alpha = v^\beta(\nabla_\beta p_\alpha - \nabla_\alpha p_\beta) + \nabla_\alpha(v^\beta p_\beta)$$

or

$$\pounds_{\vec{v}}\boldsymbol{p} = \vec{v} \cdot \mathbf{d}\boldsymbol{p} + \mathbf{d}(\vec{v} \cdot \boldsymbol{p}) \tag{2.15}$$

and the Legendre transformation (2.12) to write the covariant Euler-Lagrange Eq. (2.10) as

$$\pounds_{\vec{v}}\boldsymbol{p} - \mathbf{d}L = \vec{v} \cdot \mathbf{d}\boldsymbol{p} + \mathbf{d}H = 0. \tag{2.16}$$

Alternatively, one may prove the equivalence of Eq. (2.14) to the Hamilton Eq. (2.13a) by proceeding analogously to Eq. (2.11), that is, by using the chain rule to rewrite the (Eulerian) covariant derivative $\nabla_\alpha H = \partial H/\partial x^\alpha + \partial p_\beta/\partial x^\alpha \partial H/\partial p_\beta$ in terms of (Lagrangian) partial derivatives.

C. Conservation laws

1. Poincaré-Cartan integral invariant

The 2-form

$$\Omega_{\alpha\beta} \coloneqq \nabla_\beta p_\alpha - \nabla_\alpha p_\beta$$

or, equivalently,

$$\boldsymbol{\Omega} \coloneqq \mathbf{d}\boldsymbol{p} = \mathbf{d}p_\mu \wedge \mathbf{d}x^\mu \tag{2.17}$$

is the *canonical symplectic form*, also known as the *Poincaré two-form* [61]. Its physical content depends on the action (2.8). In Sec. III it will be shown that, if the action describes a perfect fluid, then $\boldsymbol{\Omega}$ is Khalatnikov's canonical vorticity tensor; if the action describes a purely magnetic field, then $\boldsymbol{\Omega}$ is the Faraday tensor. Nevertheless, the results of Sec. II apply to any generic Hamiltonian flow; no assumptions on the physical content of the action (2.8) will be made prior to Sec. III.

Taking the exterior derivative of (2.10), commuting the exterior derivative $\mathbf{d}$ with the Lie derivative $\pounds_{\vec{v}}$ and using the identity $\mathbf{d}^2 = 0$, we immediately deduce that the canonical symplectic form (2.17) is advected by the flow:

$$\pounds_{\vec{v}}\boldsymbol{\Omega} = 0. \tag{2.18}$$

The above equation also follows directly from the Hamilton Eq. (2.14) and the Cartan identity

$$\pounds_{\vec{v}}\boldsymbol{\Omega} = \vec{v} \cdot \mathbf{d}\boldsymbol{\Omega} + \mathbf{d}(\vec{v} \cdot \boldsymbol{\Omega}). \tag{2.19}$$

The conservation Eq. (2.18) is tied to an important integral invariant: Consider[2] the family Ψ_λ of diffeomorphisms generated by canonical velocity $\vec{v}$, with Ψ_λ^{-1} its inverse. Let c be a ring in the flow, bounding a 2-surface S; let $c_\lambda = \Psi_\lambda(c)$ be the family of rings dragged along by the flow, bounding the 2-surfaces $S_\lambda = \Psi_\lambda(S)$. That is, each point of S_λ is obtained by moving each point of S an affine time λ along the flow through that point. The closed line integral of $\boldsymbol{p}$ around $\mathcal{C}_\lambda$ can then be written as

$$\mathcal{I} \coloneqq \oint_{c_\lambda} \boldsymbol{p} = \int_{S_\lambda} \boldsymbol{\Omega} = \int_S \Psi_\lambda^{-1}\boldsymbol{\Omega} \tag{2.20}$$

where we used the Stokes theorem [relating the circulation integral $\oint_{c_\lambda} p_\alpha dx^\alpha$ with the integral $\int_{S_\lambda} \Omega_{\alpha\beta} dx^\alpha_{(1)} dx^\beta_{(2)}$ of $\boldsymbol{\Omega}$ on S_λ, where $dx^\alpha_{(1)}$ and $dx^\beta_{(2)}$ are infinitesimal vectors tangent to S_λ spanning the tangent space at each point] and the diffeomorphism invariance of an integral [i.e. the identity $\int_{\Psi_\lambda(S)} \Psi_\lambda\boldsymbol{\Omega} = \int_S \boldsymbol{\Omega}$, with $\boldsymbol{\Omega}$ replaced by $\Psi_\lambda^{-1}\boldsymbol{\Omega}$, cf. Eq. (A.81) in [60]]. Eq. (2.18) implies that the above integral is conserved:

$$\frac{d\mathcal{I}}{d\lambda} = \int_S \frac{d}{d\lambda}(\Psi_\lambda^{-1}\boldsymbol{\Omega}) = \int_S \pounds_{\vec{v}}\boldsymbol{\Omega} = 0. \tag{2.21}$$

The closed line integral (2.20) is known in analytical dynamics as the *Poincaré-Cartan integral invariant* associated with Hamiltonian systems [62–64]. Its existence

[2]This derivation follows and generalizes Friedman & Stergioulas' [60] proof of conservation of circulation.

emerges from the Hamiltonian structure of Eq. (2.14). In particular, a dynamical system possesses a Poincaré-Cartan integral invariant *if and only if* it is Hamiltonian [65].

Although this result is well known in analytical dynamics, to our knowledge, its applicability to (magneto)hydrodynamics was only recognized by Carter [27] Some classical mechanics texts mention that the integral (2.20) corresponds to a conserved circulation in phase space, analogous to Kelvin's circulation integral in a barotropic fluid. In fact, this is more than a mere analogy, albeit in the converse direction: Kelvin's circulation *equals* the integral (2.20) if the Lagrangian is chosen to be that of a perfect barotropic fluid element, Eq. (3.20) [27,66]. Similarly, Alfvén's magnetic flux theorem, and the generalizations of Kelvin's theorem to poorly [27] or perfectly conducting [29–31] magnetofluids, emerge also as *special cases* of the Poincaré-Cartan integral invariant (2.20). This will be shown in Sec. III by constructing the appropriate Lagrangians.

2. Irrotational flows

In general, a flow will be called *irrotational* if and only if the canonical vorticity 2-form vanishes:

$$\mathbf{\Omega} = \mathbf{d}\boldsymbol{p} = 0. \tag{2.22}$$

Then, if the domain $\mathcal{D}$ is simply connected, the Poincaré lemma implies the local existence of a single-valued scalar field $\mathcal{S}$ such that

$$\boldsymbol{p} = \mathbf{d}\mathcal{S} \tag{2.23}$$

or, equivalently,

$$p_\alpha = \nabla_\alpha \mathcal{S}.$$

The invariance of the Poincaré-Cartan integral (2.20) guarantees that initially irrotational flows remain irrotational.[3] This is very useful when solving the Cauchy problem with irrotational initial data (cf. [66] for a $3+1$ evolution scheme exploiting this property in barotropic fluids). For an irrotational flow, substituting Eq. (2.23) into the equations of motion (2.10), (2.14), we find that the latter have first integrals:

$$\pounds_{\vec{v}}\mathcal{S} - L = 0 \tag{2.24}$$

$$H = 0 \tag{2.25}$$

respectively. In general, a system with constant H is called *uniformly canonical*. This is the case for irrotational flow, and, more generally, for a perfect fluid that is homentropic or barotropic, as will be shown below.

We note that the above first integrals hold throughout the flow. Indeed, taking the exterior derivative of the above equations and commuting the operator $\mathbf{d}$ with $\pounds_v$ leads back to the equations of motion (2.10), (2.14). In the above integrals, we have dropped an additive integration constant by absorbing it into the definition of the potential $\mathcal{S}$. Note that Eq. (2.24) follows directly from Eq. (2.25) with the aid of Eqs. (2.12) and (2.23) and the definition of the Lie derivative.

Equations (2.24) and (2.25) were derived for an irrotational flow. More generally, the same equations can be shown to hold for helicity-free flows which are representable in the Clebsch form $\boldsymbol{p} = \mathbf{d}\mathcal{S} + \alpha\mathbf{d}\beta$. This follows by substituting the latter expression into the equations of motion (2.10), (2.14) and using the fact that the Clebsch potentials α, β are advected by the flow, that is $\pounds_{\vec{v}}\alpha = 0$, $\pounds_{\vec{v}}\beta = 0$.

3. Poincaré two-form

Let $u^\alpha = v^\alpha(-v^\beta v_\beta)^{-1/2}$ be the unit vector along v^α. In light of Eq. (2.14), we can decompose the 2-form (2.17) into "electric" and "magnetic" parts with respect to u^α as

$$\Omega_{\alpha\beta} = (-v^\beta v_\beta)^{-1/2}(u_\alpha \nabla_\beta H - u_\beta \nabla_\alpha H) + u^\delta \epsilon_{\delta\alpha\beta\gamma}\omega^\gamma$$

or

$$\mathbf{\Omega} = (-\vec{\boldsymbol{v}}\cdot\boldsymbol{v})^{-1/2}\boldsymbol{u}\wedge\mathbf{d}H + \star(\boldsymbol{u}\wedge\boldsymbol{\omega}) \tag{2.26a}$$

$$\star\mathbf{\Omega} = (-\vec{\boldsymbol{v}}\cdot\boldsymbol{v})^{-1/2}\star(\boldsymbol{u}\wedge\mathbf{d}H) - \boldsymbol{u}\wedge\boldsymbol{\omega}, \tag{2.26b}$$

where

$$\omega_\alpha \coloneqq \frac{1}{2}u^\delta \epsilon_{\delta\alpha\beta\gamma}\Omega^{\beta\gamma} = u^\delta \star\Omega_{\delta\alpha}$$

or

$$\boldsymbol{\omega} \coloneqq \vec{\boldsymbol{u}}\cdot\star\mathbf{\Omega}. \tag{2.27}$$

From the antisymmetry properties of $\boldsymbol{\epsilon}$ it follows that

$$\vec{\boldsymbol{u}}\cdot\mathbf{d}H = 0, \qquad \vec{\boldsymbol{u}}\cdot\boldsymbol{\omega} = 0 \tag{2.28}$$

and that the scalar invariants of the 2-form $\mathbf{\Omega}$ are

$$\frac{1}{2}\Omega^{\alpha\beta}\Omega_{\alpha\beta} = \omega^\alpha\omega_\alpha - (-v^\beta v_\beta)^{-1}\nabla^\alpha H\nabla_\alpha H \tag{2.29}$$

$$\frac{1}{2}(\star\Omega^{\alpha\beta})\Omega_{\alpha\beta} = (-v^\beta v_\beta)^{-1/2}\omega^\alpha\nabla_\alpha H. \tag{2.30}$$

By the definition (2.17), $\mathbf{\Omega}$ is an exact 2-form. Because $\mathbf{d}^2 = 0$, any exact 2-form is also closed:

[3] In the context of barotropic fluids, this is known as Helmholtz's third theorem, which is a corollary of Kelvin's circulation theorem.

$$\mathbf{d}\boldsymbol{\Omega} = 0 \Leftrightarrow \nabla_\alpha(\star\Omega^{\alpha\beta}) = 0. \tag{2.31}$$

Given a scalar field $\phi(x)$ on $\mathcal{M}$, one can construct an exact 1-form

$$\boldsymbol{l} = \mathbf{d}\phi \tag{2.32}$$

which is also, by virtue of the identity $\mathbf{d}^2 = 0$, closed:

$$\mathbf{d}\boldsymbol{l} = 0 \Leftrightarrow \nabla_\alpha l_\beta - \nabla_\beta l_\alpha = 0. \tag{2.33}$$

Given a closed 2-form $\boldsymbol{\Omega}$ and a closed 1-form $\boldsymbol{l}$, one can construct a current $j^\alpha := l_\beta \star\Omega^{\beta\alpha}$, or

$$\boldsymbol{j} := \vec{\boldsymbol{l}} \cdot \star\boldsymbol{\Omega}, \tag{2.34}$$

which, by virtue of Eqs. (2.31) and (2.33), is conserved:

$$\nabla_\alpha j^\alpha = \nabla_\alpha(\nabla_\beta\phi\star\Omega^{\beta\alpha}) = 0. \tag{2.35}$$

This conservation law implies a corresponding global conservation of the integrated flux of j^α across a hypersurface.

An infinite number of (not necessarily independent) conservation laws stem from Eq. (2.35) since, in general, $\phi(x)$ can be *any* differentiable function of the coordinates. For example, in a chart $\{x^\mu\} = \{t, x^i\}$, if ϕ is chosen to be the spatial coordinate x^1, the above equation reduces to the x^1 component of Eq. (2.31). If ϕ coincides with coordinate time t, Eq. (3.49) yields a spatial constraint equation. Other combinations of the coordinates give different projections Eq. (2.31). Choosing ϕ to be the super-Hamiltonian H gives rise to a conserved current

$$j^\alpha := \nabla_\beta H \star\Omega^{\beta\alpha}. \tag{2.36}$$

This conservation law holds for *any* Hamiltonian system with a Poincaré 2-form $\boldsymbol{\Omega}$. For a baroclinic fluid, described by Eq. (3.41) below, the time component of this current is the potential vorticity, as shown in Sec. III. The corresponding conservation law, known as *Ertel's theorem* [67,68], arises simply as a special case of Eq. (2.36).

As mentioned earlier, a system with spatially constant super-Hamiltonian H is uniformly canonical. If the uniformity condition $\mathbf{d}H = 0$ holds on an initial hypersurface, then Eq. (2.28) guarantees that the condition is preserved in time. For such systems, Eqs. (2.26) and (2.31) yield the conservation law

$$\mathbf{d}\star(\boldsymbol{u} \wedge \boldsymbol{\omega}) = 0 \Leftrightarrow \nabla_\alpha(u^\alpha\omega^\beta - u^\beta\omega^\alpha) = 0. \tag{2.37}$$

In $3+1$ dimensions, this equation is the curl of Eq. (2.18). Helmholtz's vorticity transport equation [68] and Alfven's magnetic field transport equation [69] are special cases of this general conservation law.

4. Generalized helicity

Equations (2.17), (2.31) and (2.30) imply that, for uniformly canonical systems, the generalized helicity current

$$\boldsymbol{h} := \vec{\boldsymbol{p}} \cdot \star\boldsymbol{\Omega} \tag{2.38}$$

is conserved:

$$\nabla_\alpha h^\alpha = \frac{1}{2}\Omega_{\alpha\beta}\star\Omega^{\beta\alpha} = \omega^\alpha\nabla_\alpha H = 0. \tag{2.39}$$

This conservation law also implies a corresponding global conservation of the integrated flux of h^α across a hypersurface. Specific examples are given in Sec. III [70–72].

5. Noether's theorem

Noether's theorem states that each continuous symmetry of the action implies a quantity conserved by the motion. In particular, the *generalized* Noether theorem may be stated as follows [73]. Consider the ε family of infinitesimal coordinate transformations

$$\vec{\boldsymbol{x}} \to \vec{\boldsymbol{x}}_\varepsilon = \vec{\boldsymbol{x}} + \varepsilon\vec{\boldsymbol{k}}(x, v) \tag{2.40}$$

generated by the vector field $\vec{\boldsymbol{k}}(x, v)$, which can depend on position *and* velocity, for a small parameter ε. If these transformations leave the action (2.8) unchanged or, equivalently, change the Lagrangian $L(x, v)$ by a total derivative of some scalar $K(x)$,

$$L \to L_\varepsilon = L - \varepsilon\frac{dK}{d\lambda}, \tag{2.41}$$

then the quantity

$$\mathcal{C}(x, v) = \frac{\partial L}{\partial v^\alpha}k^\alpha + K \tag{2.42}$$

is a constant of motion:

$$\frac{d\mathcal{C}}{d\lambda} = \pounds_{\vec{v}}\mathcal{C} = 0. \tag{2.43}$$

If $\vec{\boldsymbol{k}}$ depends on velocity, then the family (2.40) of transformations is not generally considered a family of diffeomorphisms. It is, however, a generalized symmetry of the action and Noether related to an invariant of the form (2.42).

Conversely, the inverse Noether theorem [73] may be stated as follows: if the quantity $\mathcal{C}(x, v)$ is a constant of motion, then the ε family of infinitesimal transformations generated by the vector field $\vec{\boldsymbol{k}}(x, v)$, obtained by solving the linear system

$$\frac{\partial^2 L}{\partial v^\alpha \partial v^\beta} k^\beta = \frac{\partial \mathcal{C}}{\partial v^\alpha}, \tag{2.44}$$

is a generalized symmetry of the action.

In the Hamiltonian picture, a scalar quantity $\mathcal{C}(x, p)$, which does not explicitly depend on the time parameter λ, is conserved if it commutes with the super-Hamiltonian, in the sense of a vanishing Poisson bracket:

$$\frac{d\mathcal{C}}{d\lambda} = \pounds_{\vec{\mathbf{r}}}\mathcal{C} = \{\mathcal{C}, H\} \equiv \frac{\partial \mathcal{C}}{\partial x^\gamma}\frac{\partial H}{\partial p_\gamma} - \frac{\partial \mathcal{C}}{\partial p_\gamma}\frac{\partial H}{\partial x^\gamma} = 0. \tag{2.45}$$

Conserved quantities polynomial in the momenta are associated with Killing vectors or tensors and are Noether related to symmetries of the action, as discussed below. The super-Hamiltonian H does not explicitly depend on the affine parameter λ and is itself a constant of motion, in agreement with Eq. (2.28) (this symmetry is Noether related to the metric tensor being a Killing tensor, as discussed in Sec. III).

For barotropic fluids, Eqs. (2.42) and (2.43) or (2.45) give rise to Bernoulli's law, as shown in the next section.

III. EXAMPLES OF HAMILTONIAN FLOWS

A. Perfect fluids

We assume that a part $\mathcal{D} \subset \mathcal{M}$ of spacetime is occupied by a perfect fluid, characterized by the energy-momentum tensor

$$\boldsymbol{T}^{\mathrm{fl}} = (\epsilon + p)\boldsymbol{u} \otimes \boldsymbol{u} + p\boldsymbol{g}, \tag{3.1}$$

where ϵ is the proper energy density, p is the fluid pressure and $u^\alpha = dx^\alpha/d\tau$ is the fluid 4-velocity. Moreover, we neglect effects of viscosity or heat conduction and we assume that the fluid is a *simple fluid*, that is, all thermodynamic quantities depend only on the entropy density s and proper baryon number density n. In particular,

$$\epsilon = \epsilon(s, n). \tag{3.2}$$

The above relation is called the *equation of state* (EOS) of the fluid. The *temperature* T and the *baryon chemical potential* μ are then defined by

$$T \coloneqq \frac{\partial \epsilon}{\partial s} \quad \text{and} \quad \mu \coloneqq \frac{\partial \epsilon}{\partial n}. \tag{3.3}$$

Then, the first law of thermodynamics can be written as

$$d\epsilon = \mu dn + T ds. \tag{3.4}$$

As a consequence, p is a function of (s, n) entirely determined by (3.2):

$$p = -\epsilon + Ts + \mu n. \tag{3.5}$$

Let us introduce the *specific enthalpy*,

$$h \coloneqq \frac{\epsilon + p}{\rho} = g + TS, \tag{3.6}$$

where ρ is the rest-mass density

$$\rho \coloneqq mn, \tag{3.7}$$

g is the *specific Gibbs free energy*

$$g \coloneqq \frac{\mu}{m}, \tag{3.8}$$

$m = 1.66 \times 10^{-27}$ kg is the baryon rest mass, and S is the *specific entropy*, or entropy per particle:

$$S \coloneqq \frac{s}{\rho}. \tag{3.9}$$

The second equality in (3.6) is an immediate consequence of (3.5). From Eqs. (3.4)–(3.9), we obtain the thermodynamic relations

$$d\epsilon = hd\rho + \rho T dS, \qquad dp = \rho(dh - TdS). \tag{3.10}$$

A simple perfect fluid is *barotropic* if the energy density depends only on the pressure, $\epsilon = \epsilon(p)$. This is the case for a cold or a homentropic fluid.

With the aid of Eqs. (3.4)–(3.10), the divergence of the fluid energy-momentum tensor (3.1) can be decomposed as

$$\vec{\boldsymbol{\nabla}} \cdot \boldsymbol{T}^{\mathrm{fl}} = h\boldsymbol{u}[\boldsymbol{\nabla} \cdot (\rho\vec{\boldsymbol{u}})] + \rho[\vec{\boldsymbol{u}} \cdot \mathbf{d}(h\boldsymbol{u}) - T\mathbf{d}S]. \tag{3.11}$$

Conservation of rest mass

$$\boldsymbol{\nabla} \cdot (\rho\vec{\boldsymbol{u}}) = 0, \tag{3.12}$$

and the vanishing of (3.11) yield the relativistic Euler equation for *baroclinic fluids*, in the canonical form:

$$\pounds_{\vec{\boldsymbol{u}}}(h\boldsymbol{u}) + \mathbf{d}h = \vec{\boldsymbol{u}} \cdot \mathbf{d}(h\boldsymbol{u}) = T\mathbf{d}S \tag{3.13}$$

where the first equality follows from the Cartan identity (2.15) and the normalization condition

$$g_{\alpha\beta}u^\alpha u^\beta = -1. \tag{3.14}$$

For *barotropic fluids*, the Euler Eq. (3.13) simplifies to

$$\pounds_{\vec{\boldsymbol{u}}}(h\boldsymbol{u}) + \mathbf{d}h = \vec{\boldsymbol{u}} \cdot \mathbf{d}(h\boldsymbol{u}) = 0. \tag{3.15}$$

Equation (3.15) was obtained in special relativity by Synge (1937) [17] and in general relativity by Lichnerowicz (1941) [18]. The extension (3.13) to baroclinic (nonisentropic) fluids was obtained by Taub (1959) [74] (see also

[27,58,75]). Both of these relativistic hydrodynamic equations are canonical and can be described within the framework of Sec. II, which provides a very efficient approach to the derivation of conservation laws.

B. Barotropic flows

1. Hamilton's principle for a barotropic-fluid element

The Euler Eq. (3.15) for a barotropic fluid is readily in the canonical form (2.14). Thus, a particle variational principle in the form described in Sec. II can be found. Indeed the motions of fluid elements in a barotropic fluid are *conformally geodesic*, that is, they are geodesics of a manifold with metric $h^2 g_{\alpha\beta}$ [17,18,76]. This follows from the fact that Eq. (3.15) is the Euler-Lagrange equation of the action functional

$$\mathcal{S} = -\int_{\tau_1}^{\tau_2} h d\tau = -\int_{\tau_1}^{\tau_2} h\sqrt{-g_{\alpha\beta}\frac{dx^\alpha}{d\tau}\frac{dx^\beta}{d\tau}}d\tau. \tag{3.16}$$

The Lagrangian

$$L(x,u) = -h\sqrt{-g_{\alpha\beta}u^\alpha u^\beta} \tag{3.17}$$

is associated with the canonical momentum 1-form

$$\boldsymbol{p} = h\boldsymbol{u}, \tag{3.18}$$

and the canonical vorticity 2-form

$$\boldsymbol{\Omega} = \mathbf{d}(h\boldsymbol{u}). \tag{3.19}$$

On shell, the condition (3.14) is satisfied, and the Lagrangian (3.17) takes the value $L = -h$. Carter [27] introduced a slightly modified Lagrangian

$$L(x,u) = \frac{1}{2}h g_{\alpha\beta}u^\alpha u^\beta - \frac{1}{2}h, \tag{3.20}$$

that is associated with the same equations of motion and has the same on-shell value, but its action is *not* reparametrization invariant. Thus, if one wishes, for instance, to use reparametrization invariance to replace proper time τ by coordinate time t, in order to obtain a *constrained* Hamiltonian via $3+1$ decomposition, as done in [66], then the action (3.16) is the appropriate starting point. If, on the other hand, one is interested in a *super*-Hamiltonian that describes the dynamics in a 4-dimensional spacetime, then Carter's Lagrangian (3.20) is more suitable. Substituting the latter into the Legendre transformation (2.12) yields the super-Hamiltonian

$$H(x,p) = \frac{1}{2h}g^{\alpha\beta}p_\alpha p_\beta + \frac{1}{2}h \tag{3.21}$$

which vanishes on shell [when Eq. (3.14) holds]. Substituting Eqs. (3.18) and (3.21) into the Hamilton Eq. (2.14) yields the barotropic Euler Eq. (3.15).

2. Conservation of circulation in barotropic flows

For this system, Eq. (2.18) yields a relativistic generalization of *Helmholtz's vorticity conservation* equation:

$$\pounds_{\vec{\boldsymbol{u}}}\mathbf{d}(h\boldsymbol{u}) = 0 \tag{3.22}$$

and the Poincaré-Cartan integral invariant (2.20)–(2.21) gives rise a relativistic generalization of *Kelvin circulation theorem*: the circulation along a fluid ring c_τ dragged along by the flow is conserved:

$$\frac{d}{d\tau}\oint_{c_\tau} h\boldsymbol{u} = 0. \tag{3.23}$$

Conservation of circulation for the nonrelativistic Euler equations was discovered by Cauchy (1815) [77,78] and independently rediscovered by Kelvin (1869) [79]. The extension of this theorem to relativistic barotropic fluids was obtained by Lichnerowicz and [80] Taub [74]. The most interesting feature of the above conservation law is that its derivation does not depend on the spacetime metric or spacetime symmetries. Thus, it is *exact* in time-dependent spacetimes, with gravitational waves carrying energy and angular momentum away from a system. Oscillating stars and radiating binaries, if modeled as barotropic fluids with no viscosity or dissipation other than gravitational waves, exactly conserve circulation [60].

3. Fluid helicity

Since the super-Hamiltonian (3.21) is constant, the system is uniformly canonical, and helicity is conserved. If we substitute Eq. (3.18) into Eq. (2.38), then Eqs. (2.27) and (2.39) imply that the fluid helicity current [27,81,82]

$$\boldsymbol{h}_{\rm fl} \coloneqq h\vec{\boldsymbol{u}}\cdot\star\boldsymbol{\Omega} = h\boldsymbol{\omega} \tag{3.24}$$

is conserved:

$$\nabla_\alpha(hu_\beta\star\Omega^{\beta\alpha}) = \nabla_\beta(h\omega^\beta) = 0. \tag{3.25}$$

This implies a corresponding global conservation of the integrated flux of $h^\alpha_{\rm em}$ across a spatial hypersurface. In a chart $\{t, x^i\}$, the volume integral of the time component of $\vec{\boldsymbol{h}}_{\rm fl}$:

$$h^t_{\rm fl} \coloneqq \vec{\boldsymbol{h}}_{\rm fl}\cdot\boldsymbol{\nabla}t = h\omega^t = hu_i\star\Omega^{it} = -h\omega^i u_i/u_t \tag{3.26}$$

is the relativistic generalization of Moffat's fluid helicity [32,71,72]. The last equality follows from Eq. (2.28). If the vorticity ω^i has sufficient decay, then the total volume integral of the above quantity is conserved by the flow.

4. Killing vector fields and Bernoulli's law

If there exists a vector field $k^\alpha(x)$, that generates a family of diffeomorphisms (2.40) leaving the Langrangian (3.17) unchanged, then Noether's theorem implies the existence of a streamline invariant linear in the momenta, given by Eq. (2.42) (with K set to zero):

$$\mathcal{E}(x,p) = k^\alpha p_\alpha = h u_\alpha k^\alpha. \tag{3.27}$$

As stated by Eq. (2.43), this quantity is conserved along a streamline (i.e. the trajectory of a fluid element):

$$\frac{d\mathcal{E}}{d\tau} = \pounds_{\vec{u}}\mathcal{E} = \vec{\boldsymbol{u}}\cdot\boldsymbol{\nabla}\mathcal{E} = 0. \tag{3.28}$$

The above statement is a generalization of Bernoulli's law to relativistic barotropic fluids. In light of the above, each Bernoulli-type conservation law is Noether related to a continuous symmetry of the flow.

Given the super-Hamiltonian (3.21), one may directly verify when a quantity of the form (3.27) is conserved by computing the Poisson bracket (2.45):

$$\begin{aligned}\frac{d\mathcal{E}}{d\tau} &= \{\mathcal{E}, H\} = \frac{1}{h}p_\alpha p_\beta \nabla^\alpha k^\beta - k^\gamma \nabla_\gamma h \\ &= \frac{1}{2h}u^\alpha u^\beta \pounds_{\vec{k}}(h^2 g_{\alpha\beta})\end{aligned} \tag{3.29}$$

which vanishes for all timelike streamlines if and only if

$$\pounds_{\vec{k}}(h^2\boldsymbol{g}) = 0. \tag{3.30}$$

That is, the necessary and sufficient condition for $\mathcal{E}$ to be a streamline invariant is that $\vec{\boldsymbol{k}}$ be a Killing vector of a manifold with metric $h^2\boldsymbol{g}$. This result is intuitive given the fact that, as mentioned earlier, the fluid streamlines are geodesics of this conformal metric, cf. Eq. (3.16). We remark that the vanishing of both $\pounds_{\vec{k}}\boldsymbol{g}$ and $\pounds_{\vec{k}}h$, as indicated by the first line of Eq. (3.29), is a sufficient but not necessary condition for $\mathcal{E}$ to be conserved.

When the pressure vanishes, i.e. when $h = 1$, the condition (3.30) reduces to the Killing equation $\nabla_{(\alpha}k_{\beta)} = 0$, which is Noether related to the existence of conserved quantities linear in the momenta for geodesic motion [83–85].

As an example, let us consider a helically symmetric, rigidly rotating fluid equilibrium, such as a rigidly rotating star (that may be triaxially deformed [86]), or a tidally locked binary on circular orbits. The flow field may then be written as

$$\vec{\boldsymbol{u}} = u^t\vec{\boldsymbol{k}}, \tag{3.31}$$

where

$$\vec{\boldsymbol{k}} = \vec{\boldsymbol{t}} + \Omega\vec{\boldsymbol{\varphi}} \tag{3.32}$$

is a helical Killing vector field which Lie derives the metric: $\pounds_{\vec{k}}\boldsymbol{g} = 0$. Here, Ω is the rotation frequency, $\vec{\boldsymbol{t}} = \boldsymbol{\partial}_t$ is the generator of time translations and $\vec{\boldsymbol{\varphi}} = \boldsymbol{\partial}_\varphi$ is the generator of rotations about the rotation axis.

Let us assume that the fluid configuration is helically symmetric, that is, the Lie derivatives of all fluid variables (such as ρ, h, $\boldsymbol{u}$) along $\vec{\boldsymbol{k}}$ vanish. Since, by virtue of Eq. (3.30), the system is stationary in a rotating frame, Noether's theorem guarantees that the energy in a rotating frame, given by Eq. (3.27):

$$\mathcal{E} = k^\alpha p_\alpha = p_t + \Omega p_\varphi \tag{3.33}$$

is conserved along streamlines.

In general, this quantity can differ from one streamline to the next. However, a stronger result follows from Eq. (3.31) and the Cartan identity (2.15), which allow one to write the Euler Eq. (3.15) as

$$\vec{\boldsymbol{k}}\cdot\mathbf{d}\boldsymbol{p} = \pounds_{\vec{k}}\boldsymbol{p} - \mathbf{d}(\vec{\boldsymbol{k}}\cdot\boldsymbol{p}) = 0. \tag{3.34}$$

Because $\pounds_{\vec{k}}\boldsymbol{p} = 0$, the first integral (3.27) of the Euler equation is constant throughout the fluid:

$$\boldsymbol{\nabla}\mathcal{E} = 0. \tag{3.35}$$

This stronger conservation law is a relativistic generalization of von Zeipel's law [60]. The energy (3.27) is also a first integral to the Euler equation if a helically symmetric system is irrotational [57,87–94]. Such first integrals are valuable for solving for obtaining fluid equilibria via the self-consistent field method [95]. Generalizations of these first integrals have been used to construct equilibria for spinning [96–99] or eccentric [100,101] compact binaries in numerical relativity.

5. Killing tensor fields and the Carter constant

Geodesic motion of test particles in Kerr (or Kerr-de Sitter) spacetimes is known to admit a fourth constant of motion (in addition to energy, angular momentum, and four-velocity magnitude), known as the Carter constant, which is quadratic in the momenta and is Noether related to the existence of a Killing tensor field [83].

To our knowledge, the concept of a Killing tensor for fluid flows has not been defined before, but the framework outlined Sec. II provides the means to do so. Consider a tensor field $K^{\alpha\beta}(x)$ associated with a streamline invariant quadratic in the momenta,

$$\mathcal{E} = K^{\alpha\beta}p_\alpha p_\beta + K, \tag{3.36}$$

where the scalar $K(x)$ is a function of position. This invariant can be considered a special case of the invariant

(2.42) and follows from the generalized Noether theorem, with $k^\alpha(x,p) = K^{\alpha\beta}(x)p_\beta$ being the generator of the symmetry transformations [102]. For the barotropic fluid super-Hamiltonian (3.21), the Poisson bracket (2.45) is

$$\{\mathcal{E}, H\} = (h^2\nabla_\gamma K_{\alpha\beta} + 2hg_{\alpha\beta}K_{\gamma\delta}\nabla^\delta h - g^{\alpha\beta}\nabla^\gamma K)u^\alpha u^\beta u^\gamma. \tag{3.37}$$

The above bracket vanishes for all timelike streamlines if and only if

$$h^2\nabla_{(\gamma}K_{\alpha\beta)} + 2hg_{(\alpha\beta}K_{\gamma)\delta}\nabla^\delta h - g_{(\alpha\beta}\nabla_{\gamma)}K = 0. \tag{3.38}$$

That is, the quantity (3.36) is conserved along streamlines if and only if $\boldsymbol{K}$ is a Killing tensor of the conformal metric $h^2\boldsymbol{g}$.

In the case of a reducible Killing tensor of the form $K^{\alpha\beta} = k^\alpha k^\beta$, where k^α is a Killing vector satisfying Eq. (3.30), the condition (3.38) is automatically satisfied while K again vanishes.

When the pressure vanishes, $h = 1$, the scalar K must vanish and the above condition reduces to the Killing equation $\nabla_{(\alpha}K_{\beta\gamma)} = 0$, which is the necessary and sufficient condition $K^{\alpha\beta}p_\alpha p_\beta$ being conserved along a geodesic of $g_{\alpha\beta}$. This is the condition satisfied by the Killing tensor in the Kerr spacetime, which is Noether related to the Carter constant [83,84]. In light of this, Eqs. (3.36)–(3.38) generalize the concept of a Carter constant to test fluids in Kerr spacetime. Note, however, that the fluid configuration must satisfy a generalized symmetry (in particular, the Hamilton-Jacobi equation describing the flow [66] must be separable in Boyer-Lindquist coordinates) in order for this constant to exist.

A geodesic flow can be described by the super-Hamiltonian $H = \frac{1}{2}g^{\alpha\beta}p_\alpha p_\beta$, with $p_\alpha = u_\alpha$, which is conserved by virtue of the normalization condition (3.14). This conserved quantity arises from $g^{\alpha\beta}$ being covariantly constant and thus a Killing tensor, and is Noether related to the super-Hamiltonian being independent of the affine parameter τ. For barotropic flow, however, $g^{\alpha\beta}$ is not a Killing tensor, as it does not satisfy the condition (3.38) except in the geodesic limit. (If $g^{\alpha\beta}$ were a Killing tensor, then $g^{\alpha\beta}p_\alpha p_\beta = -h^2$ would be a streamline constant, but this is not true unless $h = 1$.) However, $K^{\alpha\beta} = g^{\alpha\beta}/h$ is a Killing tensor, since it satisfies the condition (3.38) provided that $K = h$. The quadratic streamline constant (3.36) associated with this Killing tensor is simply the super-Hamiltonian (3.21).

C. Baroclinic flows

1. Hamilton's principle for a baroclinic-fluid element

The possibility of expressing the equations of baroclinic (nonisentropic) fluid flows in canonical form has been demonstrated by Carter [27]. An intuitively simple action principle (different from but equivalent to Carter's) may be obtained as follows.

A free test particle of rest mass m, moving along a geodesic of spacetime, extremizes the action $\mathcal{S} = -m\int_{\tau_1}^{\tau_2} d\tau$ [103]. For barotropic flows, as indicated by Eq. (3.16), the pressure force on a fluid element can be accounted for by replacing rest mass by the specific enthalpy hm. For baroclinic flows, in light of Eqs. (3.6), (3.8) and (3.10), the natural generalization is to replace rest mass in the above action by the chemical potential $\mu = gm$ or, equivalently, the specific Gibbs free energy g (the rest mass can be dropped without affecting the equations of motion). Upon inspection, it becomes immediately clear that Eq. (3.13) is indeed the Euler-Lagrange equation of the action functional

$$\mathcal{S} = -\int_{\tau_1}^{\tau_2} g d\tau = -\int_{\lambda_1}^{\lambda_2}\left(h\sqrt{-g_{\alpha\beta}\frac{dx^\alpha}{d\lambda}\frac{dx^\beta}{d\lambda}} - S\right)d\lambda \tag{3.39}$$

provided that the (nonaffine) canonical time parameter

$$\lambda(\tau) \coloneqq \int^\tau T(\tau')d\tau' \tag{3.40}$$

is used to parametrize the action. Note that entropy breaks time-parametrization invariance: unlike the barotropic-fluid action (3.16), the baroclinic fluid action (3.39) is *not* parametrization invariant. Consequently, parameter choices other than (3.40), such as proper time τ or coordinate time t, lead to incorrect equations of motion. The Lagrangian

$$L(x,v) = -h\sqrt{-g_{\alpha\beta}v^\alpha v^\beta} + S \tag{3.41}$$

is associated, by virtue of Eqs. (2.7) and (2.9b), with the canonical velocity and canonical momentum

$$v^\alpha = \frac{dx^\alpha}{d\lambda} = \frac{1}{T}\frac{dx^\alpha}{d\tau} = \frac{1}{T}u^\alpha \tag{3.42a}$$

$$p_\alpha = \frac{\partial L}{\partial v^\alpha} = Thv_\alpha = hu_\alpha. \tag{3.42b}$$

On shell, by virtue of Eq. (3.14), one has $v^\alpha v_\alpha = -T^{-2}$ and the Lagrangian takes the value $L = -g/T = -h/T + S$ and, by virtue of Eq. (2.12), the super-Hamiltonian takes the value $H = -S$. Then, the Euler-Lagrange Eq. (2.10) becomes

$$\pounds_{\vec{u}/T}(h\boldsymbol{u}) = \mathbf{d}(S - h/T) \tag{3.43}$$

and the Hamilton Eq. (2.14) becomes

$$\frac{\vec{\boldsymbol{u}}}{T}\cdot\mathbf{d}(h\boldsymbol{u})=\mathbf{d}S. \tag{3.44}$$

Both of these equations are equivalent expressions of the relativistic Euler Eq. (3.13) for baroclinic fluids.

Carter [27] introduced a different Lagrangian analogous to Eq. (3.20)

$$L(x,v)=\frac{1}{2}Thg_{\alpha\beta}v^{\alpha}v^{\beta}-\frac{1}{2}\left(\frac{g}{T}-S\right), \tag{3.45}$$

that is associated with the same canonical velocity and momentum (3.42), has the same on-shell value as our Lagrangian (3.41), and leads to the same equation of motion (3.43). The Legendre transformation (2.12) yields the super-Hamiltonian

$$H(x,p)=\frac{1}{2Th}g^{\alpha\beta}p_{\alpha}p_{\beta}+\frac{h}{2T}-S, \tag{3.46}$$

which has the same on-shell value and leads to the canonical equation of motion (3.44).

2. Conservation of circulation in baroclinic flows

The canonical momentum and canonical vorticity are given by the same expressions (3.18) and (3.19) as for barotropic flows. However, the vorticity is no longer Lie dragged by the fluid four-velocity $\vec{\boldsymbol{u}}$: the exterior derivative of Eq. (3.13) reads

$$\pounds_{\vec{\boldsymbol{u}}}\mathbf{d}(h\boldsymbol{u})=\mathbf{d}T\wedge\mathbf{d}S. \tag{3.47}$$

Thus, the circulation around a fluid ring $c_\tau=\Psi_\tau(c)$ dragged along by the flow (where Ψ_τ is the family of diffeomorphisms generated by fluid four-velocity $\vec{\boldsymbol{u}}$) is not generally conserved:

$$\begin{aligned}\frac{d}{d\tau}\oint_{c_\tau}h\boldsymbol{u}&=\frac{d}{d\tau}\int_{S_\tau}\mathbf{d}(h\boldsymbol{u})\\&=\int_S\pounds_{\vec{\boldsymbol{u}}}\mathbf{d}(h\boldsymbol{u})=\int_S\mathbf{d}T\wedge\mathbf{d}S.\end{aligned} \tag{3.48}$$

Hence, Kelvin's theorem has been commonly thought to not hold for baroclinic flows, except in a weaker form: the circulation computed initially along a fluid ring of constant temperature or specific entropy is conserved [32,104].

In lieu of a conserved circulation law, one may introduce the *potential vorticity*, defined in general relativity by selecting the scalar field in Eq. (2.34), or the negative Hamiltonian in Eq. (2.36), to coincide with specific entropy S (i.e. setting $\boldsymbol{l}=\mathbf{d}S$), to obtain a flux conservation law of the form (3.49):

$$\nabla_\alpha(\nabla_\beta S\star\Omega^{\beta\alpha})=0. \tag{3.49}$$

Using the continuity equation, this law can also be written in terms of a Lie derivative along fluid velocity and, as mentioned earlier, it is the relativistic generalization of *Ertel's theorem* obtained by Friedman [104] (see also Katz [105]).

Here, we take a different route, and show that Carter's framework [106] implies the existence of a strong circulation law. We have just shown above that an inviscid baroclinic fluid is a Hamiltonian system and, as such, must possess a Poincaré-Cartan integral invariant. Indeed, the exterior derivative of Eq. (3.43) implies that the canonical vorticity (3.19) is Lie-dragged by the *canonical fluid velocity* (2.7):

$$\pounds_{\vec{\boldsymbol{u}}/T}\mathbf{d}(h\boldsymbol{u})=0 \tag{3.50}$$

as dictated by Eq. (2.18). Hence, the circulation around a fluid ring $c_\lambda=\Psi_\lambda(c)$, obtained by moving each point of c a canonical time λ [cf. Eq. (3.40)] along the flow through that point, is indeed conserved:

$$\frac{d}{d\lambda}\oint_{c_\lambda}h\boldsymbol{u}=\frac{d}{d\lambda}\int_{S_\lambda}\mathbf{d}(h\boldsymbol{u})=\int_S\pounds_{\vec{\boldsymbol{u}}/T}\mathbf{d}(h\boldsymbol{u})=0 \tag{3.51}$$

as dictated by Eqs. (2.20)–(2.21). Here, the circulation can be initially computed along an *arbitrary* fluid ring c. Thus, unlike the previous weak form, this circulation theorem is a *strong* form of Kelvin's theorem, applicable to baroclinic fluids.

It will be shown below that this circulation theorem can be further extended to barotropic or baroclinic, perfectly or poorly conducting, magnetofluids. These (new and old) circulation theorems are again special cases of the Poincaré-Cartan integral invariant (2.20). The fluid helicity, on the other hand, is not conserved for baroclinic fluids, as these systems are not uniformly canonical.

D. Ideal magnetoflows

1. Maxwell equations

Consider an electromagnetic field in $\mathcal{M}$, described by the electromagnetic 2-form $\boldsymbol{F}$, known as the *Faraday tensor*, satisfying the Maxwell equations which, in natural Heaviside-Lorentz units, read $\nabla_\alpha(\star F^{\alpha\beta})=0$, $\nabla_\alpha F^{\alpha\beta}=J^\beta$ or

$$\mathbf{d}\boldsymbol{F}=0 \tag{3.52a}$$

$$\mathbf{d}\star\boldsymbol{F}=\star\boldsymbol{J}, \tag{3.52b}$$

where $\star\boldsymbol{F}$ is the 2-form Hodge dual of $\boldsymbol{F}$, namely $\star F_{\alpha\beta}:=\frac{1}{2}\epsilon_{\alpha\beta\gamma\delta}F^{\gamma\delta}$, and $\star\boldsymbol{J}$ is the 3-form Hodge dual of the 1-form $\boldsymbol{J}$ associated with the electric 4-current $\vec{\boldsymbol{J}}$, namely $\star J_{\alpha\beta\gamma}:=\epsilon_{\alpha\beta\gamma\delta}J^\delta$.

The electric 4-current may be decomposed as $\vec{\boldsymbol{J}}=e\vec{\boldsymbol{u}}+\vec{\boldsymbol{j}}$ where $e=-\boldsymbol{u}\cdot\vec{\boldsymbol{J}}$ is the proper charge density, $e\vec{\boldsymbol{u}}$ is the

convection current and $\vec{\boldsymbol{j}}$ is the conduction current, satisfying $\boldsymbol{u}\cdot\vec{\boldsymbol{j}}=0$. For an isotropically conducting medium, Ohm's law can be written as

$$\boldsymbol{j}=\sigma\boldsymbol{E} \tag{3.53}$$

where σ is the conductivity of the medium and $\boldsymbol{E}$ is the electric field measured by an observer comoving with the fluid, given by Eq. (3.60) below. In the perfect conductivity limit, $\sigma\to\infty$, the electric field vanishes, $\boldsymbol{E}\to 0$. In the poor conductivity limit, $\sigma\to 0$, the conduction current vanishes, $\boldsymbol{j}\to 0$.

2. Magnetohydrodynamic Euler equation

The relativistic MHD-Euler equation can be obtained from the conservation law of energy-momentum,

$$\boldsymbol{\nabla}\cdot(\boldsymbol{T}^{\mathrm{fl}}+\boldsymbol{T}^{\mathrm{em}})=0, \tag{3.54}$$

where $\boldsymbol{T}^{\mathrm{em}}$ is the energy-momentum tensor of the electromagnetic field:

$$T^{\mathrm{em}}_{\alpha\beta}=F_{\gamma\alpha}F^{\gamma}_{\ \beta}-\frac{1}{4}F_{\gamma\delta}F^{\gamma\delta}g_{\alpha\beta}. \tag{3.55}$$

This tensor is trace-free: $g^{\alpha\beta}T^{\mathrm{em}}_{\alpha\beta}=0$. Taking the divergence of Eq. (3.55) and using the Maxwell Eqs. (3.52), one obtains the well-known relation

$$\boldsymbol{\nabla}\cdot\boldsymbol{T}^{\mathrm{em}}=-\boldsymbol{F}\cdot\vec{\boldsymbol{J}}. \tag{3.56}$$

Substituting Eqs. (3.11) and (3.56) into the conservation law (3.54) yields the *MHD-Euler* equation for *baroclinic magnetofluids*:

$$\vec{\boldsymbol{u}}\cdot\mathbf{d}(h\boldsymbol{u})=T\mathbf{d}S+\frac{1}{\rho}\boldsymbol{F}\cdot\vec{\boldsymbol{J}}. \tag{3.57}$$

As shown in Ref. [57], the specific form (3.57) is well adapted to the cases where the spacetime exhibits some symmetries. Projecting the MHD-Euler equation along $\vec{\boldsymbol{u}}$ yields $T\pounds_{\vec{u}}S=\frac{1}{\rho}\boldsymbol{E}\cdot\vec{\boldsymbol{J}}$. The right-hand side of this equation, which represents Joule heating, vanishes in the limit of perfect conductivity, whence the flow is adiabatic:

$$\pounds_{\vec{u}}S=\vec{\boldsymbol{u}}\cdot\boldsymbol{\nabla}S=0. \tag{3.58}$$

For *barotropic magnetofluids*, the above equation simplifies to

$$\vec{\boldsymbol{u}}\cdot\mathbf{d}(h\boldsymbol{u})=\frac{1}{\rho}\boldsymbol{F}\cdot\vec{\boldsymbol{J}}. \tag{3.59}$$

In the absence of pressure and currents ($h\to 1$ and $\boldsymbol{J}\to 0$), this equation reduces to the geodesic equation, $\vec{\boldsymbol{u}}\cdot\mathbf{d}\boldsymbol{u}=0$, as expected.

3. Perfectly conducting magnetoflows

The electric field 1-form $\boldsymbol{E}$ and the magnetic field vector $\vec{\boldsymbol{B}}$ measured in the fluid rest frame, by an observer of 4-velocity $\vec{\boldsymbol{u}}$, are given in terms of $\boldsymbol{F}$ by

$$\boldsymbol{E}=-\vec{\boldsymbol{u}}\cdot\boldsymbol{F},\qquad \boldsymbol{B}=\vec{\boldsymbol{u}}\cdot\star\boldsymbol{F} \tag{3.60}$$

and satisfy

$$\boldsymbol{E}\cdot\vec{\boldsymbol{u}}=0,\qquad \boldsymbol{B}\cdot\vec{\boldsymbol{u}}=0. \tag{3.61}$$

Equivalently, we can decompose $\boldsymbol{F}$ into electric and magnetic parts with respect to the rest frame defined by the vector $\vec{\boldsymbol{u}}$, as

$$\boldsymbol{F}=\boldsymbol{u}\wedge\boldsymbol{E}+\star(\boldsymbol{u}\wedge\boldsymbol{B}) \tag{3.62a}$$

$$\star\boldsymbol{F}=\star(\boldsymbol{u}\wedge\boldsymbol{E})-\boldsymbol{u}\wedge\boldsymbol{B}. \tag{3.62b}$$

The scalar invariants of the field are given by

$$\frac{1}{2}F^{\alpha\beta}F_{\alpha\beta}=\vec{\boldsymbol{B}}\cdot\boldsymbol{B}-\vec{\boldsymbol{E}}\cdot\boldsymbol{E} \tag{3.63}$$

$$\frac{1}{2}(\star F^{\alpha\beta})F_{\alpha\beta}=\vec{\boldsymbol{B}}\cdot\boldsymbol{E}. \tag{3.64}$$

In ideal MHD, one assumes that the fluid occupying the part $\mathcal{D}\subset\mathcal{M}$ of spacetime is a *perfect conductor*. By this, we mean that the observers comoving with the fluid measure a vanishing electric field. By virtue of Ohm's law (3.53), this expresses the *infinite conductivity* condition. From (3.60), this condition amounts to

$$\boldsymbol{E}=\boldsymbol{F}\cdot\vec{\boldsymbol{u}}=0. \tag{3.65}$$

The electromagnetic field then reduces to

$$\boldsymbol{F}=\star(\boldsymbol{u}\wedge\boldsymbol{B}) \tag{3.66a}$$

$$\star\boldsymbol{F}=-\boldsymbol{u}\wedge\boldsymbol{B} \tag{3.66b}$$

and the Maxwell Eq. (3.52) simplifies to

$$\mathbf{d}\star(\boldsymbol{u}\wedge\boldsymbol{B})=0\Leftrightarrow\nabla_{\alpha}(u^{\alpha}B^{\beta}-u^{\beta}B^{\alpha})=0. \tag{3.67}$$

This equation is a special case of Eq. (2.37), for reasons that will become clear below. In ideal MHD, one only has to evolve the magnetic field Eq. (3.67). The current has no dynamical degrees of freedom and is merely *defined* in terms of the magnetic field via Eq. (3.66a) and the Maxwell

Eq. (3.52b). One then evolves the MHD-Euler Eq. (3.57) after evaluating the Lorentz force term in its right-hand side.

Alternatively, by writing $\boldsymbol{F}$ in terms of the electromagnetic potential 1-form $\boldsymbol{A}$,

$$\boldsymbol{F} = \mathbf{d}\boldsymbol{A}, \tag{3.68}$$

one automatically satisfies the Maxwell Eq. (3.52). The perfect conductivity condition (3.65) is then used to evolve the electromagnetic potential [107,108]:

$$\boldsymbol{u} \cdot \mathbf{d}\boldsymbol{A} = 0 \Leftrightarrow u^\alpha(\nabla_\alpha A_\beta - \nabla_\beta A_\alpha) = 0. \tag{3.69}$$

In $3+1$ dimensions, Eq. (3.67) is the curl of Eq. (3.69), as shown in Sec. III D 11.

4. Action of a magnetic field frozen into the flow

A magnetic field frozen into the fluid, as defined by the perfect conductivity condition (3.65), is characterized by the action functional

$$\mathcal{S} = \int_{\tau_1}^{\tau_2} A_\alpha \frac{dx^\alpha}{d\tau} d\tau \tag{3.70}$$

where the electromagnetic potential $\boldsymbol{A}$ is considered a function of x only. From the Lagrangian [27]

$$L(x,u) = u^\alpha A_\alpha \tag{3.71}$$

we finds that the canonical momentum 1-form (2.9b) is the electromagnetic potential

$$p_\alpha = \frac{\partial L}{\partial u^\alpha} = A_\alpha \tag{3.72}$$

and the canonical vorticity 2-form (2.17) is simply the Faraday tensor

$$\boldsymbol{F} = \mathbf{d}\boldsymbol{A}. \tag{3.73}$$

Because the super-Hamiltonian (2.12) vanishes,

$$H = 0, \tag{3.74}$$

the canonical equation of motion (2.14) takes the form of the perfect conductivity condition (3.69).

5. Alfvén's theorem: Conservation of magnetic flux

If we express the Lie derivative of $\boldsymbol{F}$ along $\vec{\boldsymbol{u}}$ via the Cartan identity,

$$\pounds_{\vec{u}}\boldsymbol{F} = \vec{\boldsymbol{u}} \cdot \mathbf{d}\boldsymbol{F} + \mathbf{d}(\vec{\boldsymbol{u}} \cdot \boldsymbol{F}), \tag{3.75}$$

and take into account the Maxwell Eq. (3.52a) and the perfect conductivity condition (3.65), we get

$$\pounds_{\vec{u}}\boldsymbol{F} = 0. \tag{3.76}$$

This result, which also follows from Eq. (2.18), is the geometrical expression of *Alfvén's magnetic flux theorem*: the magnetic flux through a fluid ring c_τ dragged along by the flow is conserved

$$\frac{d}{d\tau}\oint_{c_\tau} \boldsymbol{A} = \frac{d}{d\tau}\int_{S_\tau} \boldsymbol{F} = \int_S \pounds_{\vec{u}}\boldsymbol{F} = 0. \tag{3.77}$$

This follows directly from Eq. (2.21) for the Lagrangian (3.71) and is therefore simply a special case of the Poincaré-Cartan integral invariant (2.20). Intuitively, Alfvén's theorem is a consequence of perfect conductivity. If one attempts to change the magnetic field and thus the magnetic flux through the ring c_τ of fluid, then, in accordance with Lenz's law, induced currents will generate a compensatory magnetic field in an attempt to cancel the change of flux. In the limit of perfect conductivity, this cancellation is perfect and the flux is exactly conserved.

6. Magnetic helicity

Since the super-Hamiltonian (3.74) is constant, the system is uniformly canonical, and the magnetic helicity,

$$\boldsymbol{h}_{\text{em}} \coloneqq \vec{\boldsymbol{A}} \cdot \star\boldsymbol{F}, \tag{3.78}$$

obtained by substituting Eqs. (3.72) and (3.73) into (2.38), is conserved

$$\nabla_\alpha h^\alpha_{\text{em}} = 0 \tag{3.79}$$

by virtue of Eq. (2.39). This implies a corresponding global conservation of the integrated flux of h^α_{em} across a spatial hypersurface, which amounts to the relativistic generalization of Woltjer's magnetic helicity [32,70,72].

7. Einstein-Maxwell-Euler spacetimes

The classical action describing an Einstein-Maxwell-Euler spacetime $(\mathcal{M},\boldsymbol{g})$, coupled with a perfect fluid carrying an electric current, is given by [60]

$$\mathcal{A} = \int d^4x\sqrt{-g}\left(-\epsilon + \frac{1}{16\pi}R - \frac{1}{4}F_{\alpha\beta}F^{\alpha\beta} + A_\alpha J^\alpha\right), \tag{3.80}$$

where R is the Ricci scalar. By writing $\boldsymbol{F}$ in terms of a 1-form potential $\boldsymbol{A}$, Eq. (3.68), one satisfies the Maxwell Eq. (3.52). Varying the action with respect to the metric $\boldsymbol{g}$ yields the Einstein equations, varying with respect to the electromagnetic 4-potential $\boldsymbol{A}$ yields the Maxwell

Eq. (3.52b), and varying with respect to the fluid variables yields the MHD Euler Eq. (3.57).

Instead of imposing the perfect MHD condition after varying the action, one may incorporate it into the action. This can be done by replacing the action (3.80) with

$$\mathcal{A} = \int d^4x\sqrt{-g}\Big[-\epsilon + \frac{1}{16\pi}R - \frac{1}{2}B_\alpha B^\alpha + a_\alpha \nabla_\beta (B^\alpha u^\beta - B^\beta u^\alpha)\Big] \tag{3.81}$$

where the 1-form $\boldsymbol{a}$ is a Lagrange multiplier used to enforce the flux freezing condition (3.67). In writing the action functional above, we have taken into account Eq. (3.63) in order to evaluate the magnetic energy term. This action functional differs by a surface term from that of Bekenstein-Oron [29] which, in our notation, reads

$$\mathcal{A} = \int d^4x\sqrt{-g}\left(-\epsilon + \frac{1}{16\pi}R - \frac{1}{2}B_\alpha B^\alpha + b^\alpha F_{\alpha\beta}u^\beta\right).$$

Here, the Lagrange multiplier $\boldsymbol{b}$ is used to enforce the perfect conductivity condition (3.65) and is shown to be the curl of $\boldsymbol{a}$ as indicated by Eq. (3.85) below. Our action (3.81) closely resembles the nonrelativistic action of Bekenstein-Oron [29], which is a more natural starting point and simplifies the discussion below. Variation of the action (3.81) with respect to the multiplier $\boldsymbol{a}$ yields the Maxwell Eq. (3.67), while variation with respect to the magnetic field $\boldsymbol{B}$ and integration by parts yields the equation

$$\vec{\boldsymbol{u}} \cdot \mathbf{d}\boldsymbol{a} = -\boldsymbol{B}. \tag{3.82}$$

The multiplier $\boldsymbol{a}$ may thus be thought of as an auxiliary field, with $\boldsymbol{B}$ the *electric* part of the 2-form

$$\boldsymbol{f} = \mathbf{d}\boldsymbol{a} \tag{3.83}$$

[compare Eq. (3.82) with (3.60)]. Note that the above equation automatically satisfies the orthogonality condition (3.61). Comparing Eqs. (3.82) and (3.60), we infer that the Faraday tensor $\boldsymbol{F}$ must be related to the 2-form $\boldsymbol{f}$ via a relation $\star\boldsymbol{F} = -\boldsymbol{f} + \boldsymbol{w}$ where $\boldsymbol{w}$ is some 2-form satisfying $\vec{\boldsymbol{u}} \cdot \boldsymbol{w} = 0$. Since $\boldsymbol{w}$ has no electric part, it can be written in terms of its magnetic part, $\boldsymbol{b} = \vec{\boldsymbol{u}} \cdot \star\boldsymbol{w}$, as $\boldsymbol{w} = \star(\boldsymbol{u} \wedge \boldsymbol{b})$. Taking Eq. (3.66b) into account, we infer that

$$\boldsymbol{f} = \star(-\boldsymbol{F} + \boldsymbol{u} \wedge \boldsymbol{b}) = \boldsymbol{u} \wedge \boldsymbol{B} + \star(\boldsymbol{u} \wedge \boldsymbol{b}). \tag{3.84}$$

That is, the 2-form (3.83) has an electric part given by Eq. (3.82) and a magnetic part given by the 1-form

$$\boldsymbol{b} = \boldsymbol{u} \cdot \star\mathbf{d}\boldsymbol{a}. \tag{3.85}$$

As pointed out by Bekenstein and Oron [29], the theory has a $\mathrm{U}(1) \times \mathrm{U}(1)$ symmetry, since the observable field $\boldsymbol{B}$ remains invariant under gauge transformations $\boldsymbol{A} \to \boldsymbol{A} + \mathbf{d}\Lambda$ and $\boldsymbol{a} \to \boldsymbol{a} + \mathbf{d}\lambda$.

Taking the exterior derivative of Eq. (3.84) yields the Maxwell Eq. (3.52b), with the Faraday tensor given by Eq. (3.66a) and the current "defined" by

$$J^\alpha = \nabla_\beta (u^\alpha b^\beta - u^\beta b^\alpha) \tag{3.86}$$

or

$$\boldsymbol{J} = \star\mathbf{d}\star(\boldsymbol{u} \wedge \boldsymbol{b}). \tag{3.87}$$

This expression has been obtained in [29] via a lengthy route and will be referred to as the *Bekenstein-Oron current*. Note that the above expression automatically satisfies the continuity equation

$$\boldsymbol{\nabla} \cdot \vec{\boldsymbol{J}} = -\star\mathbf{d}\star\boldsymbol{J} = 0 \tag{3.88}$$

regardless of any assumption about $\boldsymbol{u}$ and $\boldsymbol{b}$. Physically, the above equation expresses the conservation of electric charge. The operator $\star\mathbf{d}\star$ is the *codifferential* and has been expressed as the *divergence* taken with the $\boldsymbol{\nabla}$ connection. For convenience, let us introduce an auxiliary vector $\vec{\boldsymbol{q}}$ and an auxiliary 1-form $\boldsymbol{\eta}$ defined by

$$q^\alpha := b^\alpha/\rho, \qquad \eta_\alpha := F_{\alpha\beta}q^\beta$$

or

$$\vec{\boldsymbol{q}} := \vec{\boldsymbol{b}}/\rho, \qquad \boldsymbol{\eta} := \boldsymbol{F} \cdot \vec{\boldsymbol{q}}. \tag{3.89}$$

One may then use the continuity Eq. (3.12) to write the Bekenstein-Oron current (3.87) as

$$\vec{\boldsymbol{J}} = \pounds_{\vec{q}}(\rho\vec{\boldsymbol{u}}) + \rho\vec{\boldsymbol{u}}(\boldsymbol{\nabla} \cdot \vec{\boldsymbol{q}}). \tag{3.90}$$

This expression can be used to write the Lorentz force term in (3.104b) as

$$\frac{1}{\rho}\boldsymbol{F} \cdot \vec{\boldsymbol{J}} = \frac{1}{\rho}\boldsymbol{F} \cdot \pounds_{\vec{q}}(\rho\vec{\boldsymbol{u}}) = -\vec{\boldsymbol{u}} \cdot \mathbf{d}\boldsymbol{\eta}. \tag{3.91}$$

The last equality follows from projecting the Cartan identity, $\pounds_{\vec{q}}\boldsymbol{F} = \vec{\boldsymbol{q}} \cdot \mathbf{d}\boldsymbol{F} + \mathbf{d}(\vec{\boldsymbol{q}} \cdot \boldsymbol{F})$, along the vector $\rho\vec{\boldsymbol{u}}$ and using Eq. (3.65). By virtue of the above equality, the MHD-Euler Eq. (3.57) takes the canonical form

$$\pounds_{\vec{u}}(h\boldsymbol{u} + \boldsymbol{\eta}) + \mathbf{d}h = \vec{\boldsymbol{u}} \cdot \mathbf{d}(h\boldsymbol{u} + \boldsymbol{\eta}) = T\mathbf{d}S \tag{3.92}$$

which is valid for *baroclinic magnetofluids*. For *barotropic magnetofluids*, the above equation simplifies to

$$\pounds_{\vec{u}}(h\boldsymbol{u}+\boldsymbol{\eta})+\mathbf{d}h=\vec{\boldsymbol{u}}\cdot\mathbf{d}(h\boldsymbol{u}+\boldsymbol{\eta})=0. \quad (3.93)$$

The last equality was obtained by Bekenstein *et al.* [29,31].

The tensor or vector calculus-based derivations in Ref. [29,31] did not clarify the generality of this approach. In particular, one may question whether the Bekenstein-Oron ansatz (3.87) for the current is generic enough to accommodate any given ideal MHD flow. This question boils down to whether Eq. (3.82) can be solved for any given magnetofluid configuration with magnetic field $\boldsymbol{B}$ and 4-velocity $\vec{\boldsymbol{u}}$. The answer may be obtained by using the Cartan identity to write Eq. (3.82) as $\pounds_{\vec{u}}\boldsymbol{a}-\mathbf{d}(\vec{\boldsymbol{u}}\cdot\boldsymbol{a})=-\boldsymbol{B}$ and using the gauge freedom in $\boldsymbol{a}$ to set $\vec{\boldsymbol{u}}\cdot\boldsymbol{a}=0$ (this gauge condition can be shown to be preserved by the flow if satisfied initially). The resulting differential equation, $\pounds_{\vec{u}}\boldsymbol{a}=-\boldsymbol{B}$, is always solvable along the integral curves of $\vec{\boldsymbol{u}}$. We have thus shown that no loss of generality is entailed in the Bekenstein-Oron description of ideal MHD flows. For perfectly conducting magnetofluids, the Einstein-Maxwell-Euler action (3.80) may always be replaced by the action (3.81), and the MHD-Euler Eq. (3.57) may always be replaced by Eq. (3.92).

8. Hamilton's principle for a barotropic magnetofluid element

Carter [27] has allowed the possibility that the perfect fluid be charged. His approach is valid for poorly conducting fluids, but has been considered inapplicable to conducting magnetofluids [30]. Nevertheless, it is shown below that Carter's framework can in fact accommodate perfectly conducting fluids in the context of Bekenstein-Oron magnetohydrodynamics. For a barotropic, perfectly conducting magnetofluid, we generalize the action (3.16) as follows:

$$\mathcal{S}=\int_{\tau_1}^{\tau_2}\left(-h\sqrt{-g_{\alpha\beta}\frac{dx^\alpha}{d\tau}\frac{dx^\beta}{d\tau}}+\eta_\alpha\frac{dx^\alpha}{d\tau}\right)d\tau \quad (3.94)$$

with Lagrangian

$$L(x,u)=-h\sqrt{-g_{\alpha\beta}u^\alpha u^\beta}+\eta_\alpha u^\alpha \quad (3.95)$$

and with $\boldsymbol{\eta}$ given by Eq. (3.89). The canonical velocity and momentum of a magnetofluid element are given by

$$u^\alpha=\frac{dx^\alpha}{d\tau} \quad (3.96a)$$

$$p_\alpha=\frac{\partial L}{\partial u^\alpha}=hu_\alpha+\eta_\alpha. \quad (3.96b)$$

Alternatively, one may introduce a Lagrangian which generalizes that of Carter, Eq. (3.20):

$$L(x,u)=\frac{1}{2}hg_{\alpha\beta}u^\alpha u^\beta-\frac{1}{2}h+\eta_\alpha u^\alpha. \quad (3.97)$$

The associated Hamiltonian,

$$H(x,\pi)=\frac{1}{2h}g^{\alpha\beta}(p_\alpha-\eta_\alpha)(p_\beta-\eta_\beta)+\frac{1}{2}h, \quad (3.98)$$

vanishes on shell, so the Hamilton Eq. (2.14) yields the MHD-Euler equation in the Bekenstein-Oron form, Eq. (3.93).

9. Conservation of circulation in barotropic magnetoflows

The canonical momentum 1-form of a barotropic ideal magnetofluid element is given by Eq. (3.96b). Then, the Poincaré 2-form (2.17) amounts to the *canonical vorticity 2-form*:

$$\boldsymbol{\Omega}=\mathbf{d}(h\boldsymbol{u}+\boldsymbol{\eta}). \quad (3.99)$$

Then, the Cartan identity, combined with Eq. (3.92) and the identity $\mathbf{d}^2=0$, yields

$$\pounds_{\vec{u}}\boldsymbol{\Omega}=0. \quad (3.100)$$

This equation implies that the canonical vorticity of a barotropic, perfectly conducting magnetofluid is preserved by the flow. This leads to a generalization of Kelvin's theorem to magnetized fluids.

Indeed, for the system (3.94), the Poincaré-Cartan theorem (2.21) implies that the circulation through a ring c_τ dragged along by the flow is conserved:

$$\frac{d}{d\tau}\oint_{c_\tau}(h\boldsymbol{u}+\boldsymbol{\eta})=0. \quad (3.101)$$

This law follows directly from Eq. (3.100) and was first obtained by Bekenstein and Oron [29,30]. It is a generalization of the relativistic Kelvin circulation theorem (3.48) (which is recovered in the nonmagnetic limit $\boldsymbol{\eta}=0$) to ideal MHD. The most interesting feature of this conservation law is that it is *exact* in time-dependent spacetimes, with gravitational and electromagnetic waves carrying energy and angular momentum away from a system. In particular, oscillating stars and radiating binaries, if modeled as barotropic magnetofluids with no viscosity, resistivity or other dissipation, exactly conserve circulation.

10. Ideal magnetofluid helicity

Since the super-Hamiltonian (3.98) is constant (zero), the system is uniformly canonical, and helicity is conserved: Substituting Eq. (3.96b) into Eq. (2.38) yields the magnetolfuid helicity

$$\boldsymbol{h}_{\rm mfl} \coloneqq (h\vec{\boldsymbol{u}} + \boldsymbol{\eta}) \cdot \star\boldsymbol{\Omega} \tag{3.102}$$

which, by virtue of Eq. (2.39), is conserved:

$$\nabla_\alpha[(hu_\beta + \eta_\alpha)\star\Omega^{\beta\alpha}] = 0. \tag{3.103}$$

This implies a corresponding global conservation of the integrated flux of $h^\alpha_{\rm mfl}$ across a spatial hypersurface. One may proceed analogously to Eq. (3.26) to obtain a conserved volume integral, which amounts to the generalization of Moffat's fluid helicity [32,71,72] to ideal GRMHD.

11. A canonical evolution scheme for ideal MHD

In binary neutron-star inspiral, the temperature is much lower than the Fermi temperature, and heat conduction, viscosity and resistivity can be neglected [60]. The fluid may then be approximated as *barotropic*, *adiabatic, inviscid* and *perfectly conducting*. In general relativity, such fluids are described by the ideal MHD Eqs. (3.69) and (3.59):

$$u^\alpha(\nabla_\alpha A_\beta - \nabla_\beta A_\alpha) = 0 \tag{3.104a}$$

$$u^\alpha[\nabla_\alpha(hu_\beta) - \nabla_\beta(hu_\alpha)] = \frac{1}{\rho}F_{\beta\alpha}J^\alpha, \tag{3.104b}$$

coupled to the continuity Eq. (3.12). One can evolve Eq. (3.69) for the electromagnetic potential and compute the Faraday tensor via Eq. (3.68). In ideal MHD, as mentioned earlier, the current lacks dynamical degrees of freedom and is merely defined in terms of the electromagnetic potential via the Maxwell Eq. (3.52b). One then evolves the MHD-Euler Eq. (3.104b) after evaluating the Lorentz force term in its right-hand side.

In a chart $\{t, x^i\}$, the above system can be written in $3+1$ hyperbolic form[4] as

$$\partial_t A_i - \partial_i A_t + v^j(\partial_j A_i - \partial_i A_j) = 0 \tag{3.105a}$$

$$\partial_t \pi_i - \partial_i \pi_t + v^j(\partial_j \pi_i - \partial_i \pi_j) = f_i \tag{3.105b}$$

where $v^i = u^i/u^t = dx^i/dt$ is the fluid velocity measured in local coordinates, $\pi_\alpha = hu_\alpha$ denotes a (noncanonical) momentum 1-form and $f_\alpha = (\rho u^t)^{-1}F_{\alpha\beta}J^\beta$ denotes the Lorentz force per particle. The curl of the evolution Eq. (3.105a) is an evolution equation for the magnetic field. In particular, the exterior derivatives of the system (3.105) yield an evolution system for the spatial parts of the 2-forms $\boldsymbol{F} = \mathbf{d}\boldsymbol{A}$ and $\boldsymbol{W} = \mathbf{d}\boldsymbol{\pi}$. In flux-conservative form, this system reads:

$$\partial_t F_{jk} + \partial_i(\delta^{il}_{jk} v^m F_{ml}) = 0 \tag{3.106a}$$

$$\partial_t W_{jk} + \partial_i[\delta^{il}_{jk}(v^m W_{ml} - f_l)] = 0 \tag{3.106b}$$

where $\delta^{il}_{jk} = \epsilon_{jkn}\epsilon^{iln} = \delta^i_j\delta^l_k - \delta^i_k\delta^l_j$ is the generalized Kronecker delta. Eq. (3.106a) is an evolution equation, equivalent[5] to Eq. (3.67), for the magnetic field. Numerical evolution of the latter typically requires techniques such as hyperbolic divergence cleaning or constrained transport to avoid error accumulation from a finite magnetic divergence [109]. Such numerical schemes can also be applied to evolving the system (3.106) [as well as the system (3.110) below]. Etienne *et al.* [107,108] have performed GRMHD simulations that directly evolve the electromagnetic potential $\boldsymbol{A}$ by means of Eq. (3.105a) [or Eq. (3.109a)]. The magnetic field is then computed from the curl of the vector potential and has zero divergence by construction. This numerical scheme can also be applied to evolving the system (3.109) below, which is based on the Bekenstein-Oron formulation.

Equations (3.104)–(3.106) constitute the usual formulation of ideal MHD for barotropic magnetofluids. As shown earlier, the Bekenstein-Oron description of ideal MHD allows one to replace the MHD-Euler Eq. (3.59) by the system of Eqs. (3.82) and (3.93), namely

$$u^\alpha(\nabla_\alpha A_\beta - \nabla_\beta A_\alpha) = 0 \tag{3.107a}$$

$$u^\alpha(\nabla_\alpha a_\beta - \nabla_\beta a_\alpha) = -B_\beta \tag{3.107b}$$

$$u^\alpha(\nabla_\alpha p_\beta - \nabla_\beta p_\alpha) = 0 \tag{3.107c}$$

where

$$\boldsymbol{p} = h\boldsymbol{u} + \boldsymbol{\eta} \tag{3.108}$$

is the canonical momentum 1-form of a magnetofluid element, as shown in the next section.

In a chart $\{t, x^i\}$, the above system can be written in $3+1$ canonical hyperbolic form as

$$\partial_t A_i - \partial_i A_t + v^j(\partial_j A_i - \partial_i A_j) = 0 \tag{3.109a}$$

$$\partial_t a_i - \partial_i a_t + v^j(\partial_j a_i - \partial_i a_j) = -B_i \tag{3.109b}$$

$$\partial_t p_i - \partial_i p_t + v^j(\partial_j p_i - \partial_i p_j) = 0. \tag{3.109c}$$

This system may be evolved analogously to the system (3.104). One evolves the first equation for $\boldsymbol{A}$ and computes the magnetic field $\boldsymbol{B} = \vec{\boldsymbol{u}} \cdot \star\mathbf{d}\boldsymbol{A}$. With this source, one evolves the second equation for $\boldsymbol{a}$ and computes the

[4]The four-momenta $\{A_t, A_i\}$ and $\{\pi_t, \pi_i\}$ can be expressed in terms of quantities normal or tangent to a $t =$ constant hypersurface in a manner described in Ref. [66].

[5]Unlike Eq. (3.67) which contains the metric and its connection, Eq. (3.106a) contains no such dependence, yet both equations are equivalent and exact in curved spacetime.

auxiliary field $\boldsymbol{b} = \vec{\boldsymbol{u}} \cdot \star \mathbf{d}\boldsymbol{a}$. Finally, one solves the last equation of the above system, taking Eqs. (3.89) and (3.108) into account, to evolve the hydromagnetic flow.

The spatial exterior derivatives of the system (3.109) yield an evolution system for the spatial parts of the 2-forms (3.73), (3.83) and (3.99). In flux-conservative form, this system reads

$$\partial_t F_{jk} + \partial_i(\delta^{il}_{jk} v^m F_{ml}) = 0 \tag{3.110a}$$

$$\partial_t f_{jk} + \partial_i[\delta^{il}_{jk}(v^m f_{ml} + B_l)] = 0 \tag{3.110b}$$

$$\partial_t \Omega_{jk} + \partial_i(\delta^{il}_{jk} v^m \Omega_{ml}) = 0. \tag{3.110c}$$

As mentioned above, the numerical schemes developed for the systems (3.105) or (3.106) can also be applied to evolving the systems (3.109) or (3.110). Note that these systems were obtained from equations involving only exterior derivatives, and thus do not involve the spacetime metric or its connection. Thus, these systems are *independent of gravity theory* and they can be shown to be valid as written[6] even in the Newtonian limit. This is generally true for equations of motion written in Euler-Lagrange or in Hamiltonian form, cf. [66] for details. For nonmagnetic fluids, Eq. (3.109c) was obtained from a 3 + 1 constrained Hamiltonian formulation of the Euler equation in Ref. [66], where it was shown to be strongly hyperbolic. Other strongly hyperbolic formulations of the relativistic Euler equation include the Valencia formulation [11] and the symmetric hyperbolic Fraudendiner-Walton formulation [110–113]. The hyperbolicity of the evolution system (3.109) is the subject of future work. A notable feature of the canonical evolution system (3.107) is that it manifestly preserves magnetic flux and circulation, owing to its symplecic structure. Equation (3.109a) can also be obtained from a constrained Hamiltonian. Symplectic evolution schemes based on the Hamiltonians of Eqs. (3.109a) and (3.109c) are expected to numerically preserve such properties. Moreover, if the system admits a Noether symmetry, this canonical form quickly gives rise to first integrals as discussed below.

12. Magnetars with helical symmetry

As an example, let us consider a helically symmetric rigidly rotating system, such as a rigidly rotating magnetar triaxially deformed by its off-axis frozen magnetic field. The flow field may then be written in the form of Eq. (3.31). Let us assume that all observable fields (such as h, $\boldsymbol{u}$, $\boldsymbol{B}$, $\boldsymbol{F}$, $\boldsymbol{g}$) are helically symmetric, that is, their Lie derivatives along the helical Killing vector $\vec{\boldsymbol{k}}$, given by Eq. (3.32), vanish.

Using gauge freedom, one can always find a gauge class for which the electromagnetic potential $\boldsymbol{A}$ inherits the Killing symmetries of $\boldsymbol{F} = \mathbf{d}\boldsymbol{A}$ [57,114–116]. Then, using Eq. (3.31) and the Cartan identity, $\pounds_{\vec{k}}\boldsymbol{A} = \vec{\boldsymbol{k}} \cdot \mathbf{d}\boldsymbol{A} + \mathbf{d}(\vec{\boldsymbol{k}} \cdot \boldsymbol{A}) = 0$, we find that Eq. (3.107a) has the first integral

$$\boldsymbol{A} \cdot \vec{\boldsymbol{k}} = A_t + \Omega A_\varphi = \text{constant}. \tag{3.111}$$

Similarly, using $\pounds_{\vec{k}}\boldsymbol{a} = \vec{\boldsymbol{k}} \cdot \mathbf{d}\boldsymbol{a} + \mathbf{d}(\vec{\boldsymbol{k}} \cdot \boldsymbol{a})$ and imposing the gauge condition $\vec{\boldsymbol{k}} \cdot \boldsymbol{a} = 0$ allows one to write Eq. (3.107b) as $\pounds_{\vec{k}}\boldsymbol{a} = -\boldsymbol{B}/u^t$. This equation has the simple solution

$$\boldsymbol{a} = -\boldsymbol{B}t/u^t, \tag{3.112}$$

where the scalar field t satisfies $t^\alpha \nabla_\alpha t = 1$, so that $\pounds_{\vec{k}} t = (\partial_t + \Omega\partial_\varphi)t = 1$. Note that the auxiliary fields $\boldsymbol{a}$ and $\boldsymbol{b} = \vec{\boldsymbol{u}} \cdot \star \mathbf{d}\boldsymbol{a}$ are not observable and need not satisfy helical symmetry (cf. Appendix B). Finally, Eq. (3.31) and the Cartan identity allow one to write Eq. (3.107c) in the form of Eq. (3.34), which has the first integral

$$\boldsymbol{p} \cdot \vec{\boldsymbol{k}} + f = -h/u^t + f = \text{constant}. \tag{3.113}$$

The first integrals (3.111) and (3.113) are consequences of stationarity in an inertial ($\Omega = 0$) or rotating ($\Omega > 0$) frame and, like Eq. (3.35), can be considered generalizations of *von Zeipel's law* to relativistic magnetoflows. The scalar f is such that $\mathbf{d}f = -\pounds_{\vec{k}}\boldsymbol{p}$ or, by virtue of Eq. (3.108),

$$\mathbf{d}f = -\pounds_{\vec{k}}\boldsymbol{\eta}. \tag{3.114}$$

The right-hand side of this equation is proportional to the Lorentz force. One way to see this is to act with $\pounds_{\boldsymbol{k}}$ on Eq. (3.89),[7]

$$\boldsymbol{\eta} = \mathbf{d}\boldsymbol{A} \cdot \vec{\boldsymbol{b}}/\rho = (B^2/\rho)\boldsymbol{u} - \mathbf{d}\boldsymbol{a} \cdot \vec{\boldsymbol{B}}/\rho, \tag{3.115}$$

and use Eq. (3.112), yielding

$$\pounds_{\vec{k}}\boldsymbol{\eta} = \mathbf{d}(\boldsymbol{B}/u^t) \cdot \vec{\boldsymbol{B}}/\rho. \tag{3.116}$$

Equation (3.114) then implies that the Lorentz force must be the gradient of a scalar potential f in order for helically symmetric corotating configurations solutions to exist. This equation is subject to the integrability condition

$$\mathbf{d}\pounds_{\vec{k}}\boldsymbol{\eta} = -\mathbf{d}^2 f = 0, \tag{3.117}$$

[6]With $-p_t$ replaced by the constrained Hamiltonian $H(p_i, x^j)$, and similarly for $-A_t$ and $-a_t$, Eqs. (3.109) are formally valid in both 3 + 1 general relativity and in Newtonian gravity [66].

[7]Note that, on shell, the fields $\boldsymbol{\eta}$, $\boldsymbol{A}$ and $\vec{\boldsymbol{b}}$ are independent of $\vec{\boldsymbol{u}}$, whereas $\vec{\boldsymbol{B}}$ depends on $\vec{\boldsymbol{u}}$ via Eq. (3.60).

which constitutes a restriction on the magnetic field $\boldsymbol{B}$ on which $\boldsymbol{\eta}$ depends. By virtue of Eq. (3.116), the above condition becomes

$$\mathbf{d}(\boldsymbol{B}/u^t) \wedge \mathbf{d}(\boldsymbol{B}/\rho) = 0. \tag{3.118}$$

For corotating helically symmetric magnetoflows, the system of nonlinear partial differential Eq. (3.107) has been reduced to the system of algebraic Eqs. (3.111)–(3.113) and the partial differential Eq. (3.114). The Newtonian analogue of Eq. (3.117) has been considered in Ref. [117]. A full description of a triaxial magnetar requires specifying boundary (or junction) conditions at the stellar surface for the electromagnetic field, as well as an induced surface current (associated with the fact that the condition (3.111) applies inside the star but not in the vacuum outside the surface). This is beyond the scope of this paper and a subject of future work.

13. Hamilton's principle for a baroclinic magnetofluid element

For a baroclinic, perfectly conducting magnetofluid, we consider the action

$$\mathcal{S} = \int_{\lambda_1}^{\lambda_2} \left(-h\sqrt{-g_{\alpha\beta}\frac{dx^\alpha}{d\lambda}\frac{dx^\beta}{d\lambda}} + \eta_\alpha \frac{dx^\alpha}{d\lambda} + S \right) d\lambda \tag{3.119}$$

with $\boldsymbol{\eta}$ given by Eq. (3.89). Like its nonmagnetic limit (3.39), the above functional is parametrized in terms of canonical time λ, cf. Eq. (3.40). The Lagrangian of a magnetofluid element

$$L(x, v) = -h\sqrt{-g_{\alpha\beta}v^\alpha v^\beta} + \eta_\alpha v^\alpha + S \tag{3.120}$$

is associated with a canonical velocity and canonical momentum

$$v^\alpha = \frac{dx^\alpha}{d\lambda} = \frac{1}{T}\frac{dx^\alpha}{d\tau} = \frac{1}{T}u^\alpha \tag{3.121a}$$

$$p_\alpha = \frac{\partial L}{\partial v^\alpha} = Thv_\alpha + \eta_\alpha = hu_\alpha + \eta_\alpha. \tag{3.121b}$$

On-shell, by virtue of Eqs. (3.14), (3.65) and (3.89), the Lagrangian takes the value $L = -g/T = -h/T + S$ and, by virtue of Eq. (2.12), the super-Hamiltonian takes the value $H = -S$. The Euler-Lagrange Eq. (2.10) thus becomes

$$\pounds_{\vec{\boldsymbol{u}}/T}(h\boldsymbol{u} + \boldsymbol{\eta}) = \mathbf{d}(S - h/T) \tag{3.122}$$

and the Hamilton Eq. (2.14) becomes

$$\frac{\vec{\boldsymbol{u}}}{T} \cdot \mathbf{d}(h\boldsymbol{u} + \boldsymbol{\eta}) = \mathbf{d}S. \tag{3.123}$$

These equations are related via the Cartan identity and are equivalent expressions of the MHD-Euler Eq. (3.92).

Alternatively, one may generalize Carter's Lagrangian (3.45) to perfectly conducting baroclinic magnetofluids: the resulting Lagrangian

$$L(x, v) = \frac{1}{2}Thg_{\alpha\beta}v^\alpha v^\beta + \eta_\alpha v^\alpha - \frac{1}{2}\left(\frac{g}{T} - S\right) \tag{3.124}$$

is associated with the same canonical velocity and momentum (3.96) and leads also to the equation of motion (3.122). The Legendre transformation (2.12) yields the super-Hamiltonian

$$H(x, p) = \frac{1}{2Th}g^{\alpha\beta}(p_\alpha - \eta_\alpha)(p_\beta - \eta_\beta) + \frac{h}{2T} - S, \tag{3.125}$$

which leads to the canonical equation of motion (3.123). Note that the 1-form $\boldsymbol{\eta}$, defined by Eq. (3.89) or (3.115), is consider independent of the four-velocity $\vec{\boldsymbol{u}}$.

14. Conservation of circulation in baroclinic magnetoflows

Like their nonmagnetic counterparts, baroclinic magnetoflows do not Lie drag the vorticity (3.99): the exterior derivative of Eq. (3.92) reads

$$\pounds_{\vec{\boldsymbol{u}}}\mathbf{d}(h\boldsymbol{u} + \boldsymbol{\eta}) = \mathbf{d}T \wedge \mathbf{d}S. \tag{3.126}$$

Thus, as in Eq. (3.48), the circulation around a magnetofluid ring dragged along by the flow is not generally conserved, except in a weak sense, i.e. for rings of constant specific entropy or temperature.

Nevertheless, like their nonmagnetic counterparts, ideal baroclinic magnetoflows are Lie dragged by the canonical fluid velocity (3.96a):

$$\pounds_{\vec{\boldsymbol{u}}/T}\mathbf{d}(h\boldsymbol{u} + \boldsymbol{\eta}) = 0 \tag{3.127}$$

as dictated by Eq. (3.122), and this leads to a strong conservation law. In particular, the circulation around a magnetofluid ring $c_\lambda = \Psi_\lambda(c)$, obtained by moving each point of c a thermal time λ [cf. Eq. (3.40)] along the flow through that point, is indeed conserved:

$$\begin{aligned}\frac{d}{d\lambda}\oint_{c_\lambda} h\boldsymbol{u} + \boldsymbol{\eta} &= \frac{d}{d\lambda}\int_{S_\lambda} \mathbf{d}(h\boldsymbol{u} + \boldsymbol{\eta}) \\ &= \int_S \pounds_{\vec{\boldsymbol{u}}/T}\mathbf{d}(h\boldsymbol{u} + \boldsymbol{\eta}) = 0.\end{aligned} \tag{3.128}$$

Here, the circulation can be initially computed along an *arbitrary* fluid ring c. This conservation of circulation law generalizes the Bekenstein-Oron law (3.101) to baroclinic magnetofluids. The conserved circulation is the Poincaré-Cartan integral invariant of the Hamiltonian system

described by the action (3.119). Although it has not appeared in the literature before, it is a special case of Eqs. (2.20) and (2.21), like all circulation integrals presented earlier.

A very similar conservation of circulation law can be obtained for *a poorly conducting fluid*, simply by replacing η_α with eA_α, where e is the net charge per fluid element, in the action (3.119) and all equations that follow from it (cf. [27] for poorly conducting barotropic fluids). Although conservation of circulation holds in the limits of infinite or zero conductivity, we have not been able to obtain such a law for finite conductivity. This may be attributed to the fact that, for finite conductivity, the MHD-Euler Eq. (3.57) does not follow from a Hamiltonian and, equivalently, does not possess a Poincaré-Cartan integral invariant.

E. The geometry of barotropic flows

1. Hydrodynamic flows as geodesics in a Riemann space

In Riemann geometry, the line element is given by the quadratic expression

$$d\mathcal{S}^2 = -\gamma_{\alpha\beta}(x)dx^\alpha dx^\beta. \tag{3.129}$$

where $\gamma_{\alpha\beta}(x)$ is a Lorentzian metric on a Riemannian manifold $\mathcal{M}$. The distance between two points (or events) 1 and 2 is then given by the integral

$$\mathcal{S} = -\int_1^2 \sqrt{-\gamma_{\alpha\beta}(x)dx^\alpha dx^\beta} = -\int_{\tau_1}^{\tau_2} \sqrt{-\gamma_{\alpha\beta}(x)\dot{x}^\alpha \dot{x}^\beta}\, d\tau \tag{3.130}$$

where $\dot{x}^\alpha = dx^\alpha/d\tau$ is the velocity. This functional is independent of the parameter τ.

It was demonstrated above that if a perfect fluid is barotropic, then the motion of a fluid element is conformally geodesic. In particular, Synge [17] and Lichnerowicz [18] have shown that the motions of fluid elements in a barotropic fluid are geodesics of a manifold $\mathcal{M}$ with metric

$$\gamma_{\alpha\beta}(x) = h(x)^2 g_{\alpha\beta}(x) \tag{3.131}$$

conformally related to the spacetime metric $g_{\alpha\beta}(x)$. As shown earlier, such fluid motions can indeed be obtained from the action (3.16), which represents the arc length (3.130) between two events, and is independent of the parameter τ.

2. Magnetohydrodynamic flows as geodesics in a Finsler space

One may think that the above result of Synge and Lichnerowicz ceases to apply in MHD, due to the highly complicated nature of the MHD-Euler Eq. (3.57). Surprisingly, however, the above results can be extended to magnetofluids that are barotropic and perfectly conducting. Such flows are described by the action (3.94), which is independent of the parameter τ, and are geodesic in a Finsler (rather than Riemann) space [118–120]. In particular, in the context of Finsler spaces, Eq. (3.94) has similarities with the Randers metric [121,122].

As pointed out by Chern [118], Finsler geometry is simply Riemann geometry without the quadratic restriction (3.129). In Finsler geometry, the line element is replaced by the general expression

$$d\mathcal{S} = L(x, dx), \tag{3.132}$$

where $L\colon \mathbb{R}^2 \to \mathbb{R}$ is an arbitrary function that can be identified with the Lagrangian. Then, the distance between two points is given by

$$\mathcal{S} = \int_1^2 L(x, dx) = \int_{\tau_1}^{\tau_2} L(x, \dot{x})d\tau \tag{3.133}$$

where the last equality holds if and only if the function $L(x, \dot{x})$ is homogeneous of degree 1 in the velocity $\dot{x}^\alpha = dx^\alpha/d\tau$:

$$L(x, \kappa\dot{x}) = \kappa L(x, \dot{x}) \quad \forall\, \kappa > 0. \tag{3.134}$$

Lagrangians with this homogeneity property give rise to a parametrization-independent action functional, and lay at the foundation of Finsler geometry.

The Lagrangian in the perfect magnetofluid action functional (3.94) satisfies the above homogeneity property and can thus be expressed in the form of arc length in a Finsler space. To show this explicitly, we proceed as follows. Following Chern [118], we consider the projectivized tangent bundle $\mathcal{PTM}$ (i.e. the bundle of line elements) of the manifold $\mathcal{M}$. All geometric quantities constructed from the Lagrangian L are homogeneous of degree zero in $\dot{x}^\alpha$ and thus naturally live on $\mathcal{PTM}$, although L itself does not. Let $\{x^\mu\}$ be local coordinates on $\mathcal{M}$. Express tangent vectors as $\dot{x}^\mu\partial_\mu$ so that $\{x^\mu, \dot{x}^\mu\}$ can be used as local coordinates of $\mathcal{TM}$ and, with $\dot{x}^\mu$ homogeneous, as local coordinates on $\mathcal{PTM}$. Euler's theorem of homogeneous functions (c.f. Appendix A) can be used to show that

$$L(x, \dot{x}) = \underbrace{\frac{\partial L}{\partial \dot{x}^\alpha}}_{p_\alpha}\dot{x}^\alpha = -\Big(\underbrace{\frac{1}{2}\frac{\partial^2 L^2}{\partial \dot{x}^\alpha \partial \dot{x}^\beta}}_{-\gamma_{\alpha\beta}}\dot{x}^\alpha \dot{x}^\beta\Big)^{1/2}. \tag{3.135}$$

The Hessian

$$\gamma_{\alpha\beta}(x, \dot{x}) := -\frac{1}{2}\frac{\partial^2 L^2}{\partial \dot{x}^\alpha \partial \dot{x}^\beta} \tag{3.136}$$

plays the role of a metric on $\mathcal{PTM}$. This is a metric in a *Finsler* (rather than *Riemann*) space, as it depends on

velocity in addition to position. A Finslerian metric is homogeneous of degree zero in the velocity:

$$\gamma_{\alpha\beta}(x,\kappa\dot{x}) = \gamma_{\alpha\beta}(x,\dot{x}) \quad \forall\, \kappa > 0, \tag{3.137}$$

as implied by Eqs. (3.134) and (3.136). That is, the Finslerian metric $\gamma_{\alpha\beta}(x,\dot{x})$ depends on the direction, but not magnitude, of the velocity $\dot{x}^\alpha$. The line element (3.132) can then be written as

$$d\mathcal{S}^2 = -\gamma_{\alpha\beta}(x,\dot{x})dx^\alpha dx^\beta, \tag{3.138}$$

and the functional (3.133) becomes

$$\begin{aligned}\mathcal{S} &= -\int_1^2 \sqrt{-\gamma_{\alpha\beta}(x,\dot{x})dx^\alpha dx^\beta} \\ &= -\int_{\tau_1}^{\tau_2} \sqrt{-\gamma_{\alpha\beta}(x,\dot{x})\dot{x}^\alpha\dot{x}^\beta}\,d\tau.\end{aligned} \tag{3.139}$$

For our particular application, substituting the ideal MHD Lagrangian (3.95) into the definition (3.136) yields

$$\begin{aligned}\gamma_{\alpha\beta}(x,\dot{x}) = {}& h^2 g_{\alpha\beta} - \eta_\alpha\eta_\beta - h(\eta_\alpha u_\beta + \eta_\beta u_\alpha) \\ & - h q_{\alpha\beta}\eta_\gamma u^\gamma,\end{aligned} \tag{3.140}$$

where $u^\alpha = \dot{x}^\alpha(-g_{\beta\gamma}\dot{x}^\beta\dot{x}^\gamma)^{-1/2}$ is the unit vector along $\dot{x}^\alpha$, $q_{\alpha\beta} = g_{\alpha\beta} + u_\alpha u_\beta$ is the projection tensor orthogonal to that vector, and $g_{\alpha\beta}$ is the Riemannian metric in the spacetime $\mathcal{M}$. As required by the homogeneity condition (3.137), the expression (3.140) gives a metric that depends on the direction, but not the magnitude, of the velocity. Equation (3.140) may be compactly written as $\gamma_{\alpha\beta} = -p_\alpha p_\beta - h q_{\alpha\beta} p_\gamma u^\gamma$ where $p_\alpha = h u_\alpha + \eta_\alpha$. On shell, we have $u^\alpha = \dot{x}^\alpha$ and, by virtue of Eqs. (3.65) and (3.89), $\eta_\alpha u^\alpha = 0$, i.e. the last term in Eq. (3.140) vanishes. The Finsler metric $\gamma_{\alpha\beta}$ plays the role of an effective metric felt by a magnetofluid element. Note that the 1-form η_α, defined by Eq. (3.89) or (3.115), is consider independent of $\dot{x}^\alpha$. Therefore, the Lagrangian is linear in the velocity $\dot{x}^\alpha$ and the relevant Finsler space is of the Randers type [121,122].

With the aid of Eqs. (3.135) and (3.140), the action functional (3.94) takes the form of the length (3.139). This functional is independent of τ and represents the arc length between events 1 and 2. That is, the motions of fluid elements in a barotropic, perfectly conducting flow are geodesics in a Finsler space with metric given by Eq. (3.140).

The geodesic equation is obtained by minimizing the functional (3.139) and using Eqs. (A7)–(A10). This yields

$$\frac{d^2x^\lambda}{d\tau^2} + \Gamma^\lambda_{\mu\nu}\frac{dx^\mu}{d\tau}\frac{dx^\nu}{d\tau} = 0, \tag{3.141}$$

where

$$\Gamma^\lambda_{\mu\nu} := \frac{1}{2}\gamma^{\lambda\kappa}\left(\frac{\partial\gamma_{\kappa\mu}}{\partial x^\nu} + \frac{\partial\gamma_{\kappa\nu}}{\partial x^\mu} - \frac{\partial\gamma_{\mu\nu}}{\partial x^\kappa}\right) \tag{3.142}$$

denote the *Finslerian Christoffel symbols* [119]. Although the above equations are identical to those of Riemannian geometry, the transformation law of the symbols $\Gamma^\lambda_{\mu\nu}$ is more complicated since it involves the *Cartan torsion tensor*:

$$C_{\alpha\beta\gamma} := \frac{1}{2}\frac{\partial\gamma_{\alpha\beta}}{\partial\dot{x}^\gamma} = \frac{3h}{(-g_{\epsilon\zeta}\dot{x}^\epsilon\dot{x}^\zeta)^{1/2}}q_{(\alpha\beta}q_{\gamma)\delta}\eta^\delta. \tag{3.143}$$

By extending the notion of a metric in $\mathcal{M}$ to allow for Finsler geometry, the problem of ideal MHD becomes one of pure geometry. We note that the geometry of the spacetime $\mathcal{M}$ remains Riemannian: no deviation from general relativity has been assumed. In the limit $\eta_\alpha \to 0$, the Cartan torsion tensor vanishes, the geometry of $\mathcal{M}$ also becomes Riemannian, and we recover the Synge-Lichnerowicz result on barotropic fluids.

We note that a similar approach may be used for *poorly conducting fluids*, by replacing η_α with eA_α in the equations above, where e is the net charge per fluid element [27]. Furthermore, with the replacements $h \to 1$, $\eta_\alpha \to eA_\alpha$, we recover the motion of a charged particle under the influence of an electromagnetic field in curved spacetime [121,123–126]. We note, however, that for *baroclinic fluids*, the action is not parametrization invariant, and thus cannot be described within Riemann or Finsler geometry.

IV. DISCUSSION

We have illustrated that barotropic flows and magnetoflows without viscosity, resistivity or other dissipation can be described via simple variational principles. These action principles can be written in terms of a Lagrangian density integrated over spacetime, as done traditionally for fluids, or in terms of a particlelike Lagrangian integrated over a proper-time or affine parameter. The latter approach paves the way for deriving simple *Lagrangian and Hamiltonian descriptions of ideal MHD*, in Newtonian and relativistic contexts. These descriptions are as valuable for fluids as they have been for classical mechanics and carry the same advantages over approaches focused on the equation-of-motion level.

For instance, certain conserved quantities‡ whose origin seems *ad hoc* when obtained by tedious algebraic manipulation of the equations of motion—emerge directly from the action in this geometric canonical approach. In particular, when the ideal MHD Lagrangians (3.71) and (3.120) admit continuous symmetries, Noether's theorem immediately yields the associated quantity conserved along streamlines [76]. As shown by Carter and Lichnerowicz, the relativistic hydrodynamics and magnetohydrodynamics are most naturally expressed in the language of differential forms. Cartan's identity can then be used to simplify calculations

tremendously compared to the usual tensor or vector calculus, as demonstrated above. This approach to MHD is not yet very widely known, but this has been changing in recent years, and it is being used to obtain new results [8,127–136]. For stationary and irrotational or corotating magnetoflows, Cartan's identity implies that these quantities, given by Eqs. (3.111) and (3.113), are constant throughout the fluid. These equations represent relativistic, magnetized generalizations of Bernoulli's principle and provide a way to construct equilibrium solutions via iterative methods [95,137]. Such results can be extended to the case of generalized Noether symmetries generated by Killing tensors (cf. [76] for details) and applied to the theory of black-hole accretion rings [27,47].

Several theoretical insights arise from this formulation. The symplectic geometry of phase space gives rise to various circulation theorems that stem from the Poincaré-Cartan integral invariant. The symplectic structure of the perfect MHD equations can be exploited in numerical simulations that use smoothed-particle hydrodynamic methods [138]. For instance, symplectic or time-symmetric methods can be used to conserve phase-space volume, circulation, and energy.

Geometric considerations have led to deeper understanding of magnetic phenomena in fluids in curved spacetime. Exploring the similarities of geodesic motion to hydrodynamic and magnetohydrodynamic motion, Lasota *et al.* [139] generalized the Penrose process [140] from point particles to fluid particles and jets. Moreover, the Finsler geometry described by the metric (3.140) allows one to represent ideal MHD flows as purely geodesic flows with no loss of generality. A notable feature of both pictures is that they are exact in time-dependent spacetimes, with gravitational and electromagnetic waves carrying energy and angular momentum away from the system. Although such geometrical insights have been sometimes used to construct first integrals for nonmagnetized initial data [137], they have not so far been used for magnetized initial data or for evolving hydrodynamic and magnetohydrodynamic flows in numerical general relativity. The integrals (3.111), (3.113) and the evolution system (3.107) provide avenues for exploiting such geometric properties in the future.

ACKNOWLEDGMENTS

We thank Brandon Carter for pointing out the second line of Eq. (3.29) and a similar remark in the analogous equation for a fluid Killing tensor. We thank Theocharis Apostolatos, Jacob Bekenstein, Brandon Carter, Greg Comer, John Friedman, Roland Haas, David Hilditch, Darryl Holm, David Kaplan, Alan Kostelecky and Panagiotis Stavrinos for very fruitful discussions and comments. This work was supported by JSPS Grant-in-Aid for Scientific Research(C) 20540275, MEXT Grant-in-Aid for Scientific Research on Innovative Area 20105004, the Greek State Scholarships Foundation (IKY), NSF Grant No. PHY1001515, DFG grant SFB/Transregio 7 "Gravitational Wave Astronomy," STFC Grant No. PP/E001025/1 and ANR Grant No. 06-2-134423 *Méthodes mathématiques pour la relativité générale*. K. U. and E. G. acknowledge support from a JSPS Invitation Fellowship for Research in Japan (short-term) and the invitation program of foreign researchers at the Paris observatory. C. M. and J. P. N. thank the Paris Observatory for hospitality during the course of this work.

APPENDIX A: FINSLER GEOMETRY AND EULER'S THEOREM

The homogeneity property (3.134) plays a fundamental role in Finsler geometry. This property gives rise to many important relations by means of *Euler's homogeneous function theorem*: Consider a function $Z(x,v)$ that is positively homogeneous of degree r with respect to v^α, that is,

$$Z(x,\kappa v) = \kappa^r Z(x,v) \quad \forall\, \kappa > 0. \tag{A1}$$

Differentiating with respect to κ and setting $\kappa = 1$ yields

$$v^\alpha \frac{\partial Z(x,v)}{\partial v^\alpha} = rZ(x,v). \tag{A2}$$

This is the mathematical statement of Euler's theorem. Applying the above theorem to the case of the Lagrangian (3.134) yields

$$\dot{x}^\alpha \frac{\partial L(x,\dot{x})}{\partial \dot{x}^\alpha} = L(x,\dot{x}). \tag{A3}$$

Differentiating this expression with respect to $\dot{x}^\alpha$ yields

$$\dot{x}^\alpha \frac{\partial^2 L(x,\dot{x})}{\partial \dot{x}^\alpha \partial \dot{x}^\beta} = 0. \tag{A4}$$

Then, differentiating the relation

$$\frac{1}{2}\frac{\partial L^2(x,\dot{x})}{\partial \dot{x}^\alpha} = L(x,\dot{x})\frac{\partial L(x,\dot{x})}{\partial \dot{x}^\alpha} \tag{A5}$$

with respect to $\dot{x}^\beta$, contracting with $\dot{x}^\alpha \dot{x}^\beta$ and using Eqs. (A3) and (A4) yields

$$L^2(x,\dot{x}) = \underbrace{\frac{1}{2}\frac{\partial^2 L^2(x,\dot{x})}{\partial \dot{x}^\alpha \partial \dot{x}^\beta}}_{-\gamma_{\alpha\beta}} \dot{x}^\alpha \dot{x}^\beta. \tag{A6}$$

Equations (A3) and (A6) reproduce (3.135). From Eqs. (3.134) and (A6) we infer that the metric $\gamma_{\alpha\beta}(x,\dot{x})$ is homogeneous of degree zero in the velocity, Eq. (3.137). Then, applying Euler's theorem (A2) for $\gamma_{\alpha\beta}$ with $r = 0$ yields

$$\dot{x}^\gamma C_{\alpha\beta\gamma} = 0, \tag{A7}$$

where

$$C_{\alpha\beta\gamma} \coloneqq \frac{1}{2}\frac{\partial \gamma_{\alpha\beta}}{\partial \dot{x}^\gamma} = \frac{1}{4}\frac{\partial^3 L^2}{\partial \dot{x}^\alpha \partial \dot{x}^\beta \partial \dot{x}^\gamma} \tag{A8}$$

is the *Cartan torsion tensor*. The last equality, which follows from Eq. (3.136), implies that the above tensor is fully symmetric. From the above definition we infer that $C_{\alpha\beta\gamma}$ is homogeneous of degree $r = -1$ in the velocity. Then, Euler's theorem (A2) yields

$$\dot{x}^\delta C_{\alpha\beta\gamma\delta} = -C_{\alpha\beta\gamma}, \tag{A9}$$

where

$$C_{\alpha\beta\gamma\delta}(x, \dot{x}) = \frac{\partial C_{\alpha\beta\gamma}(x, \dot{x})}{\partial \dot{x}^\delta}. \tag{A10}$$

The geodesic equation in Finsler space can be obtained with the same variational methods as in a Riemann space, with additional use of Eqs. (A7)–(A10). Finsler geometry reduces to Riemann geometry if and only if the Cartan torsion tensor and its derivatives vanish, whence the metric $\gamma_{\alpha\beta}$ is independent of velocity [119].

APPENDIX B: BECKENSTEIN-ORON CURRENT WITH ONE SYMMETRY

Assuming that the system obeys a Killing symmetry, i.e. that there exists a vector field $\vec{k}$ such that

$$\pounds_{\vec{k}} \boldsymbol{g} = 0, \qquad \pounds_{\vec{k}} \boldsymbol{u} = 0, \qquad \pounds_{\vec{k}} \boldsymbol{j} = 0, \tag{B1}$$

$$\pounds_{\vec{k}} \boldsymbol{F} = 0, \qquad \pounds_{\vec{k}} h = 0, \qquad \pounds_{\vec{k}} \rho = 0, \tag{B2}$$

a natural question is whether or not one can impose the same symmetry on the auxiliary quantities $\boldsymbol{a}$ and $\boldsymbol{b}$. First, note that

$$\pounds_{\vec{k}} \boldsymbol{b} = \pounds_{\vec{k}} (\vec{\boldsymbol{u}} \cdot \star \mathbf{d}\boldsymbol{a}) \tag{B3}$$

$$= \vec{\boldsymbol{u}} \cdot \pounds_{\vec{k}} (\star \mathbf{d}\boldsymbol{a}) \tag{B4}$$

$$= \vec{\boldsymbol{u}} \cdot \star \pounds_{\vec{k}} (\mathbf{d}\boldsymbol{a}) \quad (\text{since } \vec{\boldsymbol{k}} \text{ is Killing}) \tag{B5}$$

$$= \vec{\boldsymbol{u}} \cdot \star \mathbf{d}(\pounds_{\vec{k}} \boldsymbol{a}) \quad (\text{since } \mathbf{d} \text{ and } \pounds_{\vec{k}} \text{ commute}). \tag{B6}$$

In addition, using Eq. (3.84), as well as the symmetries (B1), (B2),

$$\pounds_{\vec{k}} \mathbf{d}\boldsymbol{a} = \pounds_{\vec{k}} [\boldsymbol{u} \wedge \boldsymbol{B} + \star(\boldsymbol{u} \wedge \boldsymbol{b})] = \star(\boldsymbol{u} \wedge \pounds_{\vec{k}} \boldsymbol{b}). \tag{B7}$$

We have therefore that

$$\pounds_{\vec{k}} \boldsymbol{b} = 0 \Leftrightarrow \pounds_{\vec{k}} \mathbf{d}\boldsymbol{a} = 0 \Leftrightarrow \pounds_{\vec{k}} \boldsymbol{a} \quad \text{closed} \tag{B8}$$

and of course $\pounds_{\vec{k}} \boldsymbol{a} = 0$ implies $\pounds_{\vec{k}} \boldsymbol{b} = 0$. So in effect, assuming that the auxiliary quantities $\boldsymbol{a}$ and $\boldsymbol{b}$ satisfy the same symmetry as the physical quantities is equivalent to assuming merely $\pounds_{\vec{k}} \boldsymbol{a} = 0$. If on the other hand we are ready to sacrifice $\pounds_{\vec{k}} \boldsymbol{a} = 0$ and to assume only that $\pounds_{\vec{k}} \boldsymbol{b} = 0$, we must still impose that $\pounds_{\vec{k}} \boldsymbol{a}$ is closed.

We first notice that $\pounds_{\vec{k}} \boldsymbol{a} = 0$ is not systematically compatible with the gauge condition $\vec{\boldsymbol{u}} \cdot \boldsymbol{a} = 0$. Indeed, let us consider the case where $\vec{\boldsymbol{u}}$ and $\vec{\boldsymbol{k}}$ are parallel, i.e.

$$\vec{\boldsymbol{u}} = f \vec{\boldsymbol{k}}. \tag{B9}$$

The question is whether we can impose consistently the three equations

$$\vec{\boldsymbol{u}} \cdot \boldsymbol{a} = 0, \tag{B10}$$

$$\pounds_{\vec{u}} \boldsymbol{a} = -\boldsymbol{B}, \tag{B11}$$

$$\pounds_{\vec{k}} \boldsymbol{a} = 0. \tag{B12}$$

Using the Cartan identity, we have

$$-\boldsymbol{B} = \pounds_{\vec{u}} \boldsymbol{a} = f \pounds_{\vec{k}} \boldsymbol{a} + (\vec{\boldsymbol{k}} \cdot \boldsymbol{a}) \mathbf{d}f = (\vec{\boldsymbol{k}} \cdot \boldsymbol{a}) \mathbf{d}f = 0 \tag{B13}$$

since $\vec{\boldsymbol{u}} \cdot \boldsymbol{a} = 0$ implies $\vec{\boldsymbol{k}} \cdot \boldsymbol{a} = 0$. This is in general inconsistent.

Giving up the gauge condition $\vec{\boldsymbol{u}} \cdot \boldsymbol{a} = 0$ does not improve things. Let us put $\phi = \vec{\boldsymbol{u}} \cdot \boldsymbol{a}$ and still assume that $\vec{\boldsymbol{u}}$ and $\vec{\boldsymbol{k}}$ are colinear. Now we have $\pounds_{\vec{u}} \boldsymbol{a} = \vec{\boldsymbol{u}} \cdot \mathbf{d}\boldsymbol{a} + \mathbf{d}(\vec{\boldsymbol{u}} \cdot \boldsymbol{a})$ and instead of (B10)–(B12) we must consider

$$\vec{\boldsymbol{u}} \cdot \boldsymbol{a} = \phi, \tag{B14}$$

$$\pounds_{\vec{u}} \boldsymbol{a} = -\boldsymbol{B} + \mathbf{d}\phi, \tag{B15}$$

$$\pounds_{\vec{k}} \boldsymbol{a} = 0. \tag{B16}$$

Then

$$\pounds_{\vec{u}} \boldsymbol{a} = \phi \mathbf{d}(\log f) = -\boldsymbol{B} + \mathbf{d}\phi, \tag{B17}$$

i.e.

$$\boldsymbol{B} = \phi \mathbf{d}\left(\log \left|\frac{\phi}{f}\right|\right). \tag{B18}$$

This forces the magnetic field $\boldsymbol{B}$ to be exact modulo multiplication by a scalar function, which is not a generic property. Indeed consider the 1-form on $\mathbb{R}^4$

$$\alpha = -y\mathbf{d}x + x\mathbf{d}y \tag{B19}$$

whose divergence vanishes. Can we find a globally defined smooth function ψ such that $\psi\alpha$ be closed? This amounts to

$$2\psi + x\partial_x\psi + y\partial_y\psi = 0, \tag{B20}$$

which imposes that ψ be homogeneous of degree -2 and contradicts the fact that ψ be globally defined and smooth.

We conclude that we cannot in all generality assume that the auxiliary fields $\boldsymbol{a}$ and $\boldsymbol{b}$ satisfy the same symmetry as the physical quantities.

APPENDIX C: FLUID SUPER-HAMILTONIANS

The canonical form of the Euler Eq. (3.13) involves only the thermodynamic variables T, S, h. We thus assert that the super-Hamiltonian for this equation has the general form

$$H = H(h, S, T, N), \tag{C1}$$

where $N \coloneqq g^{\alpha\beta}p_\alpha p_\beta$ is the norm of the (generally non-normalized) canonical momenta p_α, whose nature is to be determined. Furthermore, we assume that the Hamiltonian generates a reparametrization with respect to the proper time of the fluid which we denote by a parameter $\mathrm{d}\lambda = \mathrm{d}\tau/\mathcal{A}$, where $\mathcal{A}$ is some function of the variables involved.

Computing Hamilton's equations and comparing them with the Euler equation we deduce that we are on shell only if $p_\alpha = hu_\alpha$ and thus $N = -h^2$. Additionally, the following equalities must be satisfied by the Hamiltonian on shell in order to reproduce the Euler equation:

$$\frac{\partial H}{\partial T} = 0 \tag{C2}$$

$$\frac{\partial H}{\partial h} = 2h\frac{\partial H}{\partial N} \tag{C3}$$

$$\frac{\partial H}{\partial S} = -T\frac{\partial H}{\partial h} - 2Th\frac{\partial H}{\partial N} \tag{C4}$$

$$\mathcal{A} = 2h\frac{\partial H}{\partial N}. \tag{C5}$$

One way to satisfy this set of constraints on the form of the Hamiltonian is via the expression

$$H = \frac{\mathcal{C}'(S)}{2Th}(g^{\alpha\beta}p_\alpha p_\beta + h^2) - \mathcal{C}(S), \tag{C6}$$

where $\mathcal{C}(S)$ is an arbitrary function of the specific entropy with $\mathcal{C}'(S) \neq 0$ for $S \geq 0$. The on-shell value of the conserved super-Hamiltonian is then $-\mathcal{C}(S)$ and the canonical time parameter λ satisfies $\mathrm{d}\lambda = T\mathrm{d}\tau/\mathcal{C}'$. Carter's baroclinic Hamiltonian (3.125) is obtained simply by setting $\mathcal{C}(S) = S$.

For barotropic fluids one can use a similar approach to obtain a set of Hamiltonians of the form

$$H = -\frac{\mathcal{D}(h)}{2h}(g^{\alpha\beta}p_\alpha p_\beta + h^2) \tag{C7}$$

where $\mathcal{D}(h)$ is an arbitrary function of h, and the parametrization corresponding to this Hamiltonian is $\mathrm{d}\lambda = \mathrm{d}\tau/\mathcal{D}$. The transition between the Hamiltonians (C6) and (C7) for baroclinic and barotropic fluids depends on the form of temperature expressed as a function of entropy and enthalpy $T = T(h, S)$.

For baroclinic magnetofluids, we see from Eq. (3.93) that the streamlines of a perfectly conducting fluid behave as if under the influence of a vector potential $\boldsymbol{\eta}$. We thus assume that there is a canonical momentum p_α such that the Hamiltonian depends only on the normalization $N = g^{\alpha\beta}(p_\alpha - \kappa_\alpha)(p_\beta - \kappa_\beta)$ with κ_α some vector. In that case, we obtain the on-shell values $p_\alpha = hu_\alpha + \eta_\alpha, \kappa_\alpha = \eta_\alpha$ $N = -h^2$ and the same set of constraints as in (C2)–(C5). This means that one class of super-Hamiltonians which reproduce the ideal MHD-Euler Eq. (3.93) is

$$H = \frac{\mathcal{C}'(S)}{2Th}[g^{\alpha\beta}(p_\alpha - \eta_\alpha)(p_\beta - \eta_\beta) + h^2] - \mathcal{C}(S), \tag{C8}$$

where the on-shell value of the super-Hamiltonian is again $-\mathcal{C}(S)$ and the canonical time parameter λ satisfies $\mathrm{d}\lambda = T\mathrm{d}\tau/\mathcal{C}'$.

[1] M. Mościbrodzka, C. F. Gammie, J. C. Dolence, H. Shiokawa, and P. K. Leung, Astrophys. J. **706**, 497 (2009).

[2] Z. Meliani, C. Sauty, K. Tsinganos, E. Trussoni, and V. Cayatte, Astron. Astrophys. **521**, A67 (2010).

[3] S. S. Komissarov, Mem SAIt **82**, 95 (2011).

[4] V. Beskin, *MHD Flows in Compact Astrophysical Objects: Accretion, Winds and Jets* (Springer, New York, 2009).

[5] H. Sotani, A. Colaiuda, and K. D. Kokkotas, Mon. Not. R. Astron. Soc. **385**, 2161 (2008).

[6] H. Sotani, K. D. Kokkotas, and N. Stergioulas, Mon. Not. R. Astron. Soc. Lett. **385**, L5 (2008).

[7] B. Zink, P. D. Lasky, and K. D. Kokkotas, Phys. Rev. D **85**, 024030 (2012).
[8] M. Freytsis and S. E. Gralla, J. Cosmol. Astropart. Phys. 05 (2016) 042.
[9] A. L. Watts, N. Andersson, D. Chakrabarty, M. Feroci, K. Hebeler, G. Israel, F. K. Lamb, M. C. Miller, S. Morsink, F. Özel, A. Patruno, J. Poutanen, D. Psaltis, A. Schwenk, A. W. Steiner, L. Stella, L. Tolos, and M. van der Klis, Rev. Mod. Phys. **88**, 021001 (2016).
[10] A. Lichnerowicz, *Relativistic Hydrodynamics and Magnetohydrodynamics* (W. A. Benjamin, New York, 1967).
[11] J. A. Font, Living Rev. Relativ. **11**, 7 (2008).
[12] L. Antón, J. Miralles, J. Martí, J. Ibanez, M. Aloy, and P. Mimica, Astrophys. J. Suppl. Ser. **188**, 1 (2010).
[13] K. Glampedakis, N. Andersson, and S. K. Lander, Mon. Not. R. Astron. Soc. **420**, 1263 (2012).
[14] N. Andersson, I. Hawke, K. Dionysopoulou, and G. L. Comer, Classical Quantum Gravity **34**, 125003 (2017).
[15] N. Andersson, K. Dionysopoulou, I. Hawke, and G. L. Comer, Classical Quantum Gravity **34**, 125002 (2017).
[16] A. Reisenegger, Astron. Astrophys. **499**, 557 (2009).
[17] J. L. Synge, Proceedings of the London Mathematical Society, sec 2 **43**, 376 (1937).
[18] A. Lichnerowicz, Ann. Sci. École Norm. Sup **58**, 285 (1941).
[19] V. Arnold, Ann. l'institut Fourier **16**, 319 (1966).
[20] D. D. Holm, J. E. Marsden, T. Ratiu, and A. Weinstein, Phys. Rep. **123**, 1 (1985).
[21] D. D. Holm, Physica D: Nonlinear Phenomena **17**, 1 (1985).
[22] D. D. Holm, Physica D: Nonlinear Phenomena **25**, 261 (1987).
[23] D. D. Holm, J. E. Marsden, and T. S. Ratiu, Adv. Math. **137**, 1 (1998).
[24] D. D. Holm, *Geometric Mechanics (Part I: Dynamics and Symmetry)*, 2nd ed. (Imperial College Press, Oxford, 2011).
[25] D. D. Holm, *Geometric Mechanics (Part II: Rotating, Translating and Rolling)*, 2nd ed. (Imperial College Press, Oxford, 2011).
[26] T. Tao, *Compactness and Contradiction* (AMS, Providence, RI, 2013) pp. 205–206.
[27] B. Carter, in *Active Galactic Nuclei*, edited by C. Hazard and S. Mitton (Cambridge University Press, Cambridge, 1979) p. 273.
[28] C. Markakis and L. Barack, arXiv:1406.4865.
[29] J. D. Bekenstein and A. Oron, Phys. Rev. E **62**, 5594 (2000).
[30] J. Bekenstein and A. Oron, Found. Phys. **31**, 895 (2001).
[31] J. Bekenstein and G. Betschart, Phys. Rev. D **74**, 083009 (2006).
[32] J. D. Bekenstein, Astrophys. J. **319**, 207 (1987).
[33] C. Markakis, J. S. Read, M. Shibata, K. Uryu, J. D. E. Creighton, J. L. Friedman, and B. D. Lackey, J. Phys. Conf. Ser. **189**, 012024 (2009).
[34] J. S. Read, C. Markakis, M. Shibata, K. Uryu, J. D. E. Creighton, and J. L. Friedman, Phys. Rev. D **79**, 12 (2009).
[35] C. Markakis, J. S. Read, M. Shibata, K. Uryu, J. D. E. Creighton, and J. L. Friedman, in *12th Marcel Grossman Meet.*, edited by T. Damour, R. Jantzen, and R. Ruffini (World Scientific, Singapore, 2011) pp. 5–7, ISBN-10: 9814374512, ISBN-13: 978-9814374514.
[36] W. E. East, F. Pretorius, and B. C. Stephens, Phys. Rev. D **85**, 124010 (2012).
[37] B. D. Farris, R. Gold, V. Paschalidis, Z. B. Etienne, and S. L. Shapiro, Phys. Rev. Lett. **109**, 221102 (2012).
[38] B. Giacomazzo, L. Rezzolla, and L. Baiotti, Phys. Rev. D **83**, 044014 (2011).
[39] J. S. Read, L. Baiotti, J. D. E. Creighton, J. L. Friedman, B. Giacomazzo, K. Kyutoku, C. Markakis, L. Rezzolla, M. Shibata, and K. Taniguchi, Phys. Rev. D **88**, 044042 (2013).
[40] P. Mosta, B. C. Mundim, J. A. Faber, R. Haas, S. C. Noble, T. Bode, F. Löffler, C. D. Ott, C. Reisswig, and E. Schnetter, Classical Quantum Gravity **31**, 015005 (2014).
[41] K. Dionysopoulou, D. Alic, and L. Rezzolla, Phys. Rev. D **92**, 084064 (2015).
[42] T. Kawamura, B. Giacomazzo, W. Kastaun, R. Ciolfi, A. Endrizzi, L. Baiotti, and R. Perna, Phys. Rev. D **94**, 064012 (2016).
[43] I. Contopoulos, J. Plasma Phys. **82**, 635820303 (2016).
[44] A. Nathanail, A. Strantzalis, and I. Contopoulos, Mon. Not. R. Astron. Soc. **455**, 4479 (2016).
[45] O. Zanotti, L. Rezzolla, L. Del Zanna, and C. Palenzuela, Astron. Astrophys. **523**, A8 (2010).
[46] O. Korobkin, E. Abdikamalov, N. Stergioulas, E. Schnetter, B. Zink, S. Rosswog, and C. D. Ott, Mon. Not. R. Astron. Soc. **431**, 349 (2013).
[47] I. Contopoulos, A. Nathanail, and M. Katsanikas, Astrophys. J. **805**, 105 (2015).
[48] A. P. Kouretsis and C. G. Tsagas, Phys. Rev. D **82**, 124053 (2010).
[49] A. P. Kouretsis and C. G. Tsagas, Phys. Rev. D **88**, 044006 (2013).
[50] J. D. Barrow and C. G. Tsagas, Mon. Not. R. Astron. Soc. **414**, 512 (2011).
[51] C. G. Tsagas, Phys. Rev. D **84**, 043524 (2011).
[52] F. Dosopoulou, F. Del Sordo, C. G. Tsagas, and A. Brandenburg, Phys. Rev. D **85**, 063514 (2012).
[53] J. D. Barrow, C. G. Tsagas, and K. Yamamoto, Phys. Rev. D **86**, 023533 (2012).
[54] J. D. Barrow, C. G. Tsagas, and K. Yamamoto, Phys. Rev. D **86**, 107302 (2012).
[55] F. Dosopoulou and C. G. Tsagas, Phys. Rev. D **89**, 103519 (2014).
[56] U.-L. Pen and N. Turok, Phys. Rev. Lett. **117**, 131301 (2016).
[57] E. Gourgoulhon, C. Markakis, K. Uryu, and Y. Eriguchi, Phys. Rev. D **83**, 104007 (2011).
[58] E. Gourgoulhon, EAS Publ. Ser. **21**, 43 (2006).
[59] E. Gourgoulhon, *Special Relativity in General Frames: From Particles to Astrophysics* (Springer, Paris, 2013).
[60] J. L. Friedman and N. Stergioulas, *Rotating Relativistic Stars* (Cambridge University Press, New York, 2013).
[61] R. Abraham and J. E. Marsden, *Foundations of Mechanics* (AMS Chelsea Publishing, Providence, RI, 2008) p. 826.
[62] H. Poincaré, Acta Math. **13**, 1 (1890).
[63] H. Poincaré, *Les Méthodes Nouvelles de la Mécanique Célèste*, Vol. 3, Chap. 28 (Gauthier-Villars, Paris, 1899).

[64] É. Cartan, *Leçons sur les Invariants Intégraux* (Herman, Paris, 1922).
[65] D. Boccaletti and G. Pucacco, *Theory of Orbits: Volume 1* (Springer, New York, 2003).
[66] C. M. Markakis, arXiv:1410.7777.
[67] H. Ertel and C.-G. Rossby, Pure Appl. Geophys. **14**, 189 (1949).
[68] A. F. Cheviakov and M. Oberlack, J. Fluid Mech. **760**, 368 (2014).
[69] H. Alfvén, Nature (London) **150**, 405 (1942).
[70] L. Woltjer, Proc. NUI. Acad. Sci. **44**, 833 (1958).
[71] H. K. Moffatt, J. Fluid Mech. **35**, 117 (1969).
[72] B. Carter and I. Khalatnikov, Ann. Phys. (N.Y.), **219**, 243 (1992).
[73] P. J. Ioannou and T. A. Apostolatos, *Elements of Theoretical Mechanics*, 1st ed. (Leader Books, Athens, 2004) (in Greek).
[74] A. H. Taub, Ration. Mech. Anal **3** (1959).
[75] D. Christodoulou, Bull. Am. Math. Soc. **44**, 581 (2007).
[76] C. Markakis, Ph.D. Dissertation, University of Wisconsin-Milwaukee, 2011.
[77] A.-L. Cauchy, *Théorie de la propagation des ondes à la surface d'un fluide pesant d'une profondeur indéfinie*, I. Tome (Académie royale des sciences, Paris, 1815), pp. 5–318.
[78] U. Frisch and B. Villone, Eur. Phys. J. H **39**, 325 (2014).
[79] W. Thomson, Trans. R. Soc. Edinburgh **25**, 217 (1868).
[80] A. Lichnerowicz, *Théories Relativistes de la Gravitation et de L'Electromagnetisme* (Masson & Cie, Paris, 1955).
[81] R. Prix, Phys. Rev. D **69**, 043001 (2004).
[82] R. Prix, Phys. Rev. D **71**, 083006 (2005).
[83] C. W. Misner, K. S. Thorne, and J. A. Wheeler, *Gravitation* (Freeman, New York, 1973).
[84] R. M. Wald, *General Relativity* (University of Chicago Press, Chicago, 1984).
[85] C. Markakis, Mon. Not. R. Astron. Soc. **441**, 2974 (2014).
[86] X. Huang, C. Markakis, N. Sugiyama, and K. Uryu, Phys. Rev. D **78**, 124023 (2008).
[87] S. Bonazzola, E. Gourgoulhon, and J.-A. Marck, Phys. Rev. D **56**, 7740 (1997).
[88] S. A. Teukolsky, Astrophys. J. **504**, 442 (1998).
[89] P. Marronetti, G. J. Mathews, and J. R. Wilson, Phys. Rev. D **60**, 087301 (1999).
[90] E. Gourgoulhon, arXiv:9804054.
[91] M. Shibata, Phys. Rev. D **58**, 024012 (1998).
[92] S. Bonazzola, E. Gourgoulhon, and J.-A. Marck, Phys. Rev. Lett. **82**, 892 (1999).
[93] K. Uryu and Y. Eriguchi, Phys. Rev. D **61**, 124023 (2000).
[94] K. Taniguchi and M. Shibata, Astrophys. J. Suppl. Ser. **188**, 187 (2010).
[95] R. H. Price, C. Markakis, and J. L. Friedman, J. Math. Phys. (N.Y.) **50**, 073505 (2009).
[96] P. Marronetti and S. L. Shapiro, Phys. Rev. D **68**, 104024 (2003).
[97] W. Tichy, Phys. Rev. D **84**, 024041 (2011).
[98] W. Tichy, Phys. Rev. D **86**, 064024 (2012).
[99] W. Tichy, Rep. Prog. Phys. **80**, 026901 (2016).
[100] N. Moldenhauer, C. M. Markakis, N. K. Johnson-McDaniel, W. Tichy, and B. Brügmann, Phys. Rev. D **90**, 084043 (2014).
[101] T. Dietrich, N. Moldenhauer, N. K. Johnson-McDaniel, S. Bernuzzi, C. M. Markakis, B. Brügmann, and W. Tichy, Phys. Rev. D **92**, 124007 (2015).
[102] T. Padmanabhan, *Gravitation: Foundations and Frontiers* (Cambridge University Press, Cambridge, 2010) p. 728.
[103] L. D. Landau, *The Classical Theory of Fields*, 4th ed. (Pergamon Press, Oxford, UK, 1975).
[104] J. L. Friedman, Commun. Math. Phys. **62**, 247 (1978).
[105] J. Katz, Proc. R. Soc. London A Math. Phys. Eng. Sci. **391** (1984).
[106] B. Carter, in *Relativistic Fluid Dynamics*, edited by A. M. Anile and Y. Choquet-Bruhat (Springer, Berlin, Heidelberg, 1989) pp. 1–64.
[107] Z. B. Etienne, Y. T. Liu, and S. L. Shapiro, Phys. Rev. D **82**, 084031 (2010).
[108] Z. B. Etienne, V. Paschalidis, Y. T. Liu, and S. L. Shapiro, Phys. Rev. D **85**, 024013 (2012).
[109] C. F. Gammie, J. C. McKinney, and G. Tóth, Astrophys. J. **589**, 444 (2003).
[110] J. Frauendiener, Classical Quantum Gravity **20**, L193 (2003).
[111] R. A. Walton, arXiv:astro-ph/0502233.
[112] T. A. Oliynyk, E. L. C, and D. W. -M. Choquet-Bruhat Y, Classical Quantum Gravity **29**, 155013 (2012).
[113] T. A. Oliynyk, Bull. des Sci. Mathématiques **141**, 105 (2017).
[114] K. Uryu, E. Gourgoulhon, and C. Markakis, Phys. Rev. D **82**, 104054 (2010).
[115] C. Markakis, K. Uryu, and E. Gourgoulhon, in J. Phys. Conf. Ser. **283**, 012021 (2011).
[116] K. Uryu, E. Gourgoulhon, C. M. Markakis, K. Fujisawa, A. Tsokaros, and Y. Eriguchi, Phys. Rev. D **90**, 101501 (2014).
[117] B. Haskell, L. Samuelsson, K. Glampedakis, and N. Andersson, Mon. Not. R. Astron. Soc. **385**, 531 (2008).
[118] S.-S. Chern, Not. Am. Math. Soc. **43**, 959 (1996).
[119] G. S. Asanov, *Finsler Geometry, Relativity and Gauge Theories* (Springer, New York, 1985).
[120] D. Lovelock and H. Rund, *Tensors, Differential Forms, and Variational Principles* (Dover Publications, New York, 1989).
[121] G. Randers, Phys. Rev. **59**, 195 (1941).
[122] S. Basilakos, A. P. Kouretsis, E. N. Saridakis, and P. C. Stavrinos, Phys. Rev. D **88**, 123510 (2013).
[123] G. S. Asanov, Math. Phys. Appl. Math. **11**, 221 (1977).
[124] G. Gibbons and C. Warnick, Contemp. Phys. **52**, 197 (2011).
[125] G. W. Gibbons, C. A. R. Herdeiro, C. M. Warnick, and M. C. Werner, Phys. Rev. D **79**, 044022 (2009).
[126] G. W. Gibbons and C. M. Warnick, Ann. Phys. (Amsterdam) **325**, 909 (2010).
[127] T. D. Brennan, S. E. Gralla, and T. Jacobson, Classical Quantum Gravity **30**, 195012 (2013).
[128] S. E. Gralla and T. Jacobson, Mon. Not. R. Astron. Soc. **445**, 2500 (2014).
[129] T. D. Brennan and S. E. Gralla, Phys. Rev. D **89**, 103013 (2014).
[130] S. E. Gralla and T. Jacobson, Phys. Rev. D **92**, 043002 (2015).

[131] S. E. Gralla, A. Lupsasca, and M. J. Rodriguez, Phys. Rev. D **92**, 044053 (2015).
[132] S. E. Gralla and P. Zimmerman, Phys. Rev. D **93**, 123016 (2016).
[133] S. E. Gralla, A. Lupsasca, and M. J. Rodriguez, Phys. Rev. D **93**, 044038 (2016).
[134] S. E. Gralla, A. Lupsasca, and A. Strominger, Phys. Rev. D **93**, 104041 (2016).
[135] S. E. Gralla, A. Lupsasca, and A. Philippov, Astrophys. J. **833**, 258 (2016).
[136] G. Compère, S. E. Gralla, and A. Lupsasca, Phys. Rev. D **94**, 124012 (2016).
[137] E. Gourgoulhon, arXiv:1003.5015.
[138] S. Rosswog, Living Rev. Comput. Astrophys. **1**, 1 (2015).
[139] J.-P. Lasota, E. Gourgoulhon, M. Abramowicz, A. Tchekhovskoy, and R. Narayan, Phys. Rev. D **89**, 024041 (2014).
[140] R. Penrose and R. M. Floyd, Nature (London) Phys. Sci. **229**, 177 (1971).

Monthly Notices
of the
ROYAL ASTRONOMICAL SOCIETY

MNRAS **473,** 2434–2440 (2018) doi:10.1093/mnras/stx2520
Advance Access publication 2017 September 27

Exploiting the hidden symmetry of spinning black holes: conservation laws and numerical tests

Vojtěch Witzany★
ZARM, University of Bremen, Am Fallturm 2, D-28359 Bremen, Germany

Accepted 2017 September 25. Received 2017 August 29; in original form 2017 July 24

ABSTRACT

The Kerr black hole is stationary and axisymmetric, which leads to conservation of energy and azimuthal angular momentum along the orbits of free test particles in its vicinity, but also to conservation laws for the evolution of continuum matter fields. However, the Kerr space–time possesses an additional 'hidden symmetry', which exhibits itself in an unexpected conserved quantity along geodesics known as the Carter constant. We investigate the possibility of using this hidden symmetry to obtain conservation laws and other identities that could be used to test astrophysical simulations of the evolution of matter fields near spinning black holes. After deriving such identities, we set up a simple numerical toy model on which we demonstrate how they can detect the violations of evolution equations in a numerical simulation. Even though one of the expressions we derive is in the form of a conservation law, we end up recommending an equivalent but simpler expression that is not in the form of a conservation law for practical implementation.

Key words: accretion, accretion discs – black hole physics – methods: analytical – methods: numerical.

1 INTRODUCTION

The observational properties of black holes in systems of various scales from X-ray binaries to active galactic nuclei are computed from the behaviour of various test matter fields evolving in the Kerr space–time, the general-relativistic field of an isolated spinning black hole. For instance, in the case of accretion on to black holes, the consensus has gradually emerged that one needs to include radiation, single-species hydrodynamics and magnetic fields, but also possibly multispecies hydrodynamics or even non-Maxwellian rarefied plasma dynamics to reproduce all the features of a real accretion process in a computer simulation (Abramowicz & Fragile 2013; Blaes 2014).

With the increased complexity and additional layers of physics involved in such computer simulations, the question is how to test either for implementation mistakes or for inherent errors of the numerical evolution schemes. One particular way to do this is to see whether the codes reproduce the behaviour of analytical solutions to the dynamical equations (De Villiers & Hawley 2003; Gammie et al. 2003). However, there is only a very small set of solutions against which one can carry out such tests and they will typically probe only a subset of the implemented physics. Another approach, pursued for instance in Markakis et al. (2016) or Vojtěch (2017), is to find new conservation laws coming from the structure of the equations involved. We focus here on the latter approach, and specifically on formulating a conservation law or a similar expression that should be applicable to the evolution of any test matter field on the Kerr background, thus encompassing any possible model of the accretion process.

To do so, we investigate the possibility of a conservation law coming from the so-called 'hidden symmetry' of the Kerr field. The Kerr space–time is stationary and axisymmetric, which implies the conservation of orbital energy and azimuthal angular momentum along free test particle trajectories. The symmetries also lead to energy and angular moment currents that are conserved for any continuum test matter field evolving on the Kerr background.

This, however, is not a full list of conservation laws in Kerr space–time; a nowadays classical analysis of Carter (1968) showed that there is an additional integral of motion for the free test particle motion, currently known as the Carter constant. The Carter constant is a square of an angular-momentum-like vector dragged along the trajectory and it cannot be linked to any explicit symmetry of the Kerr space–time, only to particular geometric properties of the Kerr metric such as the existence of a so-called Killing-Yano (KY) tensor (Walker & Penrose 1970; Floyd 1973). The existence of the KY tensor and other geometric structures in the Kerr space–time is exactly what is informally referred to as the 'hidden symmetry'.

One would expect a conservation law of a scalar quantity along single-particle trajectories to always have a direct counterpart in conservation laws for the evolution of continuum matter fields. However, in the case of the Carter constant and the hidden symmetry, no conservation law for the evolution of general matter fields was known until now. An intuitive reason for this was given by Grant

★ E-mail: witzany@zarm.uni-bremen.de

& Flanagan (2015), who demonstrated that the sum of the Carter constants of a set of particles is not conserved once we allow for elastic collisions.

We find a loophole to this argument in Section 3 by studying instead the conservation of the sum of the angular-momentum-like vectors associated with the Carter constant, and obtain a conserved current indirectly associated with this conserved sum. None the less, the resulting KY conservation law turns out to have a smaller potential for the detection of computation error than conservation laws coming from explicit symmetries. As a side product of our investigation, we realize that there exists an infinite family of conservation laws with properties similar to the KY conservation law, each of which provides a different 'basis' in probing a possible violation of the equations of motion. Hence, this investigation could be in fact understood as a probe into this family of conservation laws by studying one representative member.

To assess more precisely the applicability of the KY conservation law, we devise a simple numerical demonstration in Section 4. We construct an analytical model of matter infalling into a black hole with a small unphysical acceleration in the direction of the meridional plane and numerically gauge several options of detecting such an acceleration from data given on a finite grid. Even though the KY conservation law can detect violations of the equations of motion undetectable by conventional means, we end up recommending an alternative method of detection based on the KY tensor that is not in the strict form of a conservation law but is much less demanding in terms of implementation and computational power.

2 USUAL CONSERVATION LAWS

We use the $G=c=1$ geometrized units and the $-+++$ signature of the metric. We also assume that we have a 3+1 split of coordinates, where x^i are the coordinates on the spatial hypersurface and t a temporal coordinate.

2.1 Conservation of stress-energy

We assume a general violation of the equations of motion that shows itself as a non-conservation of the stress-energy tensor $T^{\mu}_{\nu;\mu}=r_\nu$, where r_ν is some small non-physical residue induced either by an implementation mistake or numerical error. This equation can then be written as

$$\frac{1}{\sqrt{-g}}\left(T^{\mu}_{\ \nu}\sqrt{-g}\right)_{,\mu}+\frac{1}{2}g_{\alpha\beta,\nu}T^{\alpha\beta}=r_\nu\,. \tag{1}$$

Upon integration over a spatial volume V with a surface S from time t_0 to t_1 and the application of the divergence theorem, we obtain

$$\left[\int_V T^{t}_{\ \nu}\sqrt{-g}\,\mathrm{d}^3x\right]_{t_0}^{t_1}+\int_{t_0}^{t_1}\int_S T^{i}_{\ \nu}\sqrt{-g}\,\mathrm{d}^2S_i\mathrm{d}t + \int_{t_0}^{t_1}\int_V\frac{1}{2}g_{\alpha\beta,\nu}T^{\alpha\beta}\sqrt{-g}\,\mathrm{d}^3x\,\mathrm{d}t=\int_{t_0}^{t_1}\int_V r_\nu\sqrt{-g}\,\mathrm{d}^3x\,\mathrm{d}t, \tag{2}$$

where d^2S_i is the coordinate surface element. It is now possible to apply the integrated form of equations of motion to test for the presence of a residual on the right-hand side. However, this formula (with $r_\nu=0$) is often used directly in the construction of the so-called conservative numerical schemes (such as e.g. HARM, written by Gammie et al. 2003), and testing the code against the integral identities (2) should indicate only coding mistakes, or computational errors that are already well understood. On the other hand, for *non*-conservative schemes such as that of De Villiers & Hawley (2003), equation (2) can serve as an indirect test of the validity of the evolution.

2.2 Conservation from explicit symmetries

If the metric is independent of a coordinate $x^{\hat{\nu}}$ (such as time t or azimuthal angle φ), we have $g_{\alpha\beta,\hat{\nu}}=0$ and equation (2) simplifies as

$$\left[\int_V T^{t}_{\ \hat{\nu}}\sqrt{-g}\,\mathrm{d}^3x\right]_{t_0}^{t_1}+\int_{t_0}^{t_1}\int_S T^{i}_{\ \hat{\nu}}\sqrt{-g}\,\mathrm{d}^2S_i\mathrm{d}t =\int_{t_0}^{t_1}\int_V r_{\hat{\nu}}\sqrt{-g}\,\mathrm{d}^3x\,\mathrm{d}t. \tag{3}$$

This makes the integral test much more powerful because one then needs to integrate only over a domain of dimension 3 to test for violations in a space–time volume of dimension 4.

One particular demonstration of this power is to set the surface S outside of an isolated system (so that $T^{i}_{\ \hat{\nu}}$ vanishes on S at all times), and we then get a quantity $\int T^{t}_{\ \hat{\nu}}\sqrt{-g}\,\mathrm{d}^3x$ that should be conserved at all times. This means that the noise coming from the numerical integration of the left-hand side of equation (2) becomes entirely independent of the time interval $[t_0,\,t_1]$, and we are able to search for an arbitrarily small average value of $r_{\hat{\nu}}$ by letting its effect accumulate over very large times.

A routinely implemented example is the conservation of total azimuthal angular momentum $\int T^{t}_{\ \varphi}\sqrt{-g}\,\mathrm{d}^3x$ or energy $\int T^{t}_{\ t}\sqrt{-g}\,\mathrm{d}^3x$ carried by an isolated matter field evolving in a stationary and axisymmetric space–time. The inherent noise from the computation of total energy or angular momentum contained in the system is independent of the elapsed simulation time and one thus obtains a robust handle on cumulative error.

3 KY CONSERVATION LAW

Let us now turn our attention to the geometrical formulation of explicit symmetry. The fact that the metric does not change along a certain direction ξ^μ can be expressed by the fact that this vector fulfils the so-called Killing equation

$$\xi_{\mu;\nu}+\xi_{\nu;\mu}\equiv 2\xi_{(\mu;\nu)}=0. \tag{4}$$

In the set of coordinates where $x^{\hat{\nu}}$ is the symmetry coordinate, the corresponding Killing vector has the components $\xi^\mu=\delta^{\mu}_{\hat{\nu}}$.

In this language, the integral of geodesic motion is written as $u^\mu\xi_\mu$

$$\frac{\mathrm{d}(u^\mu\xi_\mu)}{\mathrm{d}\tau}=u^{\mu}_{\ ;\kappa}u^\kappa\xi_\mu+u^\mu u^\kappa\xi_{\mu;\kappa}=0, \tag{5}$$

where the first term vanishes due to the geodesic equation and the second term vanishes due to the Killing equation. The conservation law for continuum fields (3) can then be understood as a consequence of the fact that $T^{\mu\nu}\xi_\nu$ is a conserved (divergenceless) current

$$\frac{1}{\sqrt{-g}}(T^{\mu\nu}\xi_\nu\sqrt{-g})_{,\mu}=(T^{\mu\nu}\xi_\nu)_{;\mu}=T^{\mu\nu}_{\ \ ;\mu}\xi_\nu+T^{\mu\nu}\xi_{\nu;\mu}=0. \tag{6}$$

One particular generalization of the Killing equation that is no longer connected to any explicit symmetry of the metric is the antisymmetric KY tensor of rank two $Y_{\mu\nu}=-Y_{\nu\mu}$, which fulfils a direct generalization of the Killing equation of the form $Y_{\mu(\nu;\,\kappa)}=0$. One consequence of the existence of such a tensor is that geodesics

parallel-transport a vector $L_\nu = u^\mu Y_{\mu\nu}$ along their motion

$$\frac{\mathrm{D}}{\mathrm{d}\tau}(L_\nu) = u^\mu_{;\kappa} u^\kappa Y_{\mu\nu} + u^\mu Y_{\mu\nu;\kappa} u^\kappa = 0, \tag{7}$$

where the first term again vanishes due to the geodesic equation and the second term vanishes due to the property $Y_{\mu(\nu;\kappa)} = 0$. The most important consequence is that $L^\kappa L_\kappa$ is then an integral of motion. In the case of the Kerr space–time, there exists a Killing-Yano tensor such that L_κ represents a generalization of the angular momentum vector; $L^\kappa L_\kappa$ can then be understood as a generalized specific angular momentum squared and is known as the Carter constant (Floyd 1973; Penrose 1973).

Our aim is to find a conserved current j^μ, $j^\mu_{;\mu} = 0$ associated with the hidden symmetry of the Kerr space–time so that we can obtain formulas similar to (3).

3.1 Physical motivation and statement of conservation law

We now show the link between the integrals of free test particle motion and conservation laws for continuum fields. Furthermore, we clarify why certain integrals of motion have simple conservation-law counterparts while others do not.

One could naively think that it is sufficient to find a conservation law fulfilled for a cloud of free-streaming particles due to the conservation laws along individual trajectories, and a conservation law for general continuum fields will then always follow. However, we demonstrate that such conservation laws can be spoiled already in the simple case of a cloud of free-streaming particles that are allowed to undergo an occasional elastic collision.

Let $p^\mu_{(i)}$ be the momenta of the particles where i is an index that runs over all the particles, we can then write that in an elastic collision

$$\sum_i p'^\mu_{(i)} - \sum_i p^\mu_{(i)} = 0, \tag{8}$$

where the primed and unprimed quantities always signify quantities right after and before the collision, respectively.

As a consequence, we can contract the momentum conservation (8) with the KY tensor to see that the sums of vectors associated with KY tensors are always trivially conserved

$$\sum_i (Y_{\mu\kappa} p'^\mu_{(i)}) - \sum_i (Y_{\mu\kappa} p^\mu_{(i)}) = 0. \tag{9}$$

Similarly, if we contract (8) with a Killing vector ξ_μ, we see that the sum of $\xi_\mu p^\mu_{(i)}$ is conserved in collisions. However, as was noticed also by Grant & Flanagan (2015), if we try to see what happens to the sum of the quadratic Carter constants $C_{(i)} \equiv K_{\mu\nu} p^\mu_{(i)} p^\nu_{(i)}$, $K_{\mu\nu} \equiv Y_{\mu\kappa} Y^\kappa_{\ \nu}$, in momentum exchanges, we obtain

$$\sum_i C'_{(i)} - \sum_i C_{(i)} = \sum_i \sum_{j\neq i} K_{\mu\nu} p^\mu_{(i)} p^\nu_{(j)} - \sum_i \sum_{j\neq i} K_{\mu\nu} p'^\mu_{(i)} p'^\nu_{(j)}. \tag{10}$$

By Einstein equivalence principle, *every* scattering process will be locally ignorant of the privileged directions of the background space–time and thus also the existence of $K_{\mu\nu}$. Therefore, any scattering process will produce a non-zero right-hand side of (10) and will change the value of the sum of Carter constants.

We will now quickly sketch why these results lead to the fact that collisions will not spoil the divergence-free properties of tensors such as $\rho u^\mu u^\nu \xi_\nu$ or $\rho u^\mu u^\nu Y_{\nu\kappa}$, whereas $\rho u^\mu u^\nu u^\lambda K_{\nu\lambda}$ becomes non-conserved once collisions are included.

Let us assume for simplicity that the collisions are such that particles are not annihilated or created, and that the particle rest mass stays the same at all times. We can then write a distributional or 'skeletonized' total tensor $\rho u^\nu L^\kappa$ using the worldlines of individual particles $x^\mu_{(i)}(\tau)$ as (see e.g. Trautman 2002)

$$\rho u^\nu L^\kappa = \frac{1}{\sqrt{-g}} \sum_i m_i \int_{-\infty}^{\infty} u^\nu_{(i)} L^\kappa_{(i)} \delta^{(4)}\big(x^\mu - x^\mu_{(i)}(\tau)\big)\,\mathrm{d}\tau\,, \tag{11}$$

$$u^\nu_{(i)} = u^\nu_{(i)}(\tau) = \frac{\mathrm{d}x^\nu_{(i)}}{\mathrm{d}\tau}\,,\ L^\kappa_{(i)} = L^\kappa_{(i)}(\tau) = \frac{\mathrm{d}x^\lambda_{(i)}}{\mathrm{d}\tau} Y_\lambda^{\ \kappa}\big(x^\mu_{(i)}(\tau)\big)\,, \tag{12}$$

where $\rho u^\nu L^\kappa$ obviously integrates out only into a function of x^μ. Using the identity

$$\frac{\mathrm{d}x^\nu}{\mathrm{d}\tau}\left[\delta^{(4)}\big(x^\mu - x^\mu_{(i)}(\tau)\big)\right]_{,\nu} = -\frac{\mathrm{d}}{\mathrm{d}\tau}\delta^{(4)}\big(x^\mu - x^\mu_{(i)}(\tau)\big)\,, \tag{13}$$

we then obtain

$$(\rho u^\nu L^\kappa)_{;\nu} = \frac{1}{\sqrt{-g}} \sum_i m_i \int_{-\infty}^{\infty} \frac{\mathrm{D}L^\kappa_{(i)}}{\mathrm{d}\tau} \delta^{(4)}\big(x^\mu - x^\mu_{(i)}(\tau)\big)\,\mathrm{d}\tau. \tag{14}$$

Now let us recall that during the free-streaming of the particle, we have $\mathrm{D}L^\kappa_{(i)}/\mathrm{d}\tau = 0$, and during a collision, the vector $L^\kappa_{(i)}$ jumps to another vector $L^{\kappa\prime}_{(i)} = L^\kappa_{(i)} + \Delta^\kappa_{\mathrm{col}(i)}$. We thus have

$$\frac{\mathrm{D}L^\kappa_{(i)}}{\mathrm{d}\tau} = \sum_{\mathrm{col}} \Delta^\kappa_{\mathrm{col}(i)} \delta(\tau - \tau_{\mathrm{col}(i)})\,, \tag{15}$$

where $\tau_{\mathrm{col}(i)}$ is the value of the proper time at which the collision happens. The expression for $(\rho u^\nu L^\kappa)_{;\,\nu}$ then reduces to

$$(\rho u^\nu L^\kappa)_{;\nu} = \frac{1}{\sqrt{-g}} \sum_{\mathrm{col}} \delta^{(4)}(x^\mu - x^\mu_{\mathrm{col}}) \left(\sum_i m_i \Delta^\kappa_{\mathrm{col}(i)}\right)\,, \tag{16}$$

where $x^\mu_{\mathrm{col}} = x^\mu_{(i)}(\tau_{\mathrm{col}(i)})$ for every particle (i) taking part in the given collision. We can now see that the sum in the round brackets in (16) corresponds to equation (9) computed at every given collision, and we thus obtain

$$(\rho u^\nu L^\kappa)_{;\nu} = 0. \tag{17}$$

If we applied this procedure to $\rho u^\mu K_{\kappa\lambda} u^\kappa u^\lambda$, we would obtain $(\rho u^\mu K_{\kappa\lambda} u^\kappa u^\lambda)_{;\,\mu}$ equal to an expression analogous to the right-hand side of (16), which would, however, not vanish due to the non-conservation of the sum of Carter constants in collisions. We can thus see that the current $\rho u^\mu K_{\kappa\lambda} u^\kappa u^\lambda$ conserved for non-collisional dust cannot be generalized in the case of fully general matter fields.

On the other hand, considering that for dust we have $T^{\mu\nu} = \rho u^\mu u^\nu$, we can write $\rho u^\mu L^\kappa = T^{\mu\nu} Y_\nu^{\ \kappa}$ and the fully general counterpart of (17) can then be alternatively derived using $T^{\mu\nu}_{\ \ ;\mu} = 0$ and the properties of the KY tensor

$$(T^{\mu\nu} Y_\nu^{\ \kappa})_{;\mu} = T^{\mu\nu}_{\ \ ;\mu} Y_{\nu\kappa} + T^{\mu\nu} Y_{\nu\ ;\mu}^{\ \kappa} = 0. \tag{18}$$

Hence, equation (18) could in some sense be understood as the 'hidden conservation law', which follows from the parallel transport of L_κ along free test particle motion. Nevertheless, it has the flaw that it is not in the form of a divergence of a vector or a totally antisymmetric tensor, and will thus have no simple integral counterparts. For that reason, we create a current form by a divergence with respect to the dangling index κ, $j^\mu \equiv (T^{\mu\nu} Y_\nu^{\ \kappa})_{;\kappa} = T^{\mu\nu;\kappa} Y_{\nu\kappa}$, to obtain

$$\begin{aligned}(T^{\mu\nu;\kappa} Y_{\nu\kappa})_{;\mu} &= (T^{\mu\nu} Y_\nu^{\ \kappa})_{;\kappa\mu} = (T^{\mu\nu} Y_\nu^{\ \kappa})_{;\mu\kappa} \\ &= (T^{\mu\nu}_{\ \ ;\mu} Y_{\nu\kappa} + T^{\mu\nu} Y_{\nu\ ;\mu}^{\ \kappa})_{;\kappa} = 0,\end{aligned} \tag{19}$$

where we have used the fact that one can swap the order of divergences in all indices of a tensor.

That is, we come to the final conclusion that a conserved current linked to the non-trivial conservation laws along geodesics or the 'hidden symmetry' is $j^\mu = T^{\mu\nu;\,\kappa} Y_{\nu\kappa}$.

3.2 Generating tensor for ky current

One can easily show that the current j^μ can be (under the assumption of $T^{\mu\nu}_{\ \ ;\mu} = 0$) also rewritten as a divergence of an antisymmetric tensor $j^\mu = F^{\mu\nu}_{\ \ ;\nu}$, where

$$F^{\mu\nu} = 2T^{\kappa[\mu} Y^{\nu]}_{\ \ \kappa}. \tag{20}$$

Both $j^\mu_{\ ;\mu} = 0$ and $j^\mu = F^{\mu\nu}_{\ \ ;\nu}$ are fulfilled due to the properties of the KY tensor and the equations of motion for $T^{\mu\nu}$. Hence, a violation of either is an indication of improper evolution as is shown in more detail in the next Subsection.

On the other hand, this also points towards a general method of generating a large amount of alternative conserved currents with properties similar to j^μ either from general tensors or from KY tensors of higher rank; we discuss this possibility in Appendix A. It is not clear what is the usefulness or proper meaning of the whole class of conserved currents and tensors presented in Appendix A, but we restrict ourselves here only to the study of the current $j^\mu = T^{\mu\nu;\,\kappa} Y_{\nu\kappa}$ as a representative member and leave a deeper investigation of the general class as a possibility for future works.

3.3 Integral forms of ky conservation law

Under the assumption $T^\mu_{\nu;\mu} = r_\nu$, the KY conservation law modifies as $F^{\mu\nu}_{\ \ ;\nu} = j^\mu - r_\alpha Y^{\mu\alpha}$, $j^\mu_{\ ;\mu} = (r_\nu Y^{\nu\mu})_{;\mu}$. If we then integrate over the same ranges as in (3), we obtain

$$\left[\int_V j^t \sqrt{-g}\,\mathrm{d}^3x\right]_{t_0}^{t_1} + \int_{t_0}^{t_1}\int_S j^i \sqrt{-g}\,\mathrm{d}^2S_i\mathrm{d}t = \left[\int_V r_\nu Y^{t\nu}\sqrt{-g}\,\mathrm{d}^3x\right]_{t_0}^{t_1} + \int_{t_0}^{t_1}\int_S r_\nu Y^{i\nu}\sqrt{-g}\,\mathrm{d}^2S_i\mathrm{d}t. \tag{21}$$

In other words, the KY conservation law is weaker in nature than those coming from explicit symmetries because the dimension of the integration region on the left-hand side of (21) is the same as the region in which the residue is detected (the right-hand side). The reason why it is still worthwhile to consider this conservation law is that it will probe components of r_ν, which are not in the direction of the symmetries of the space–time. Indeed, in the Kerr space–time with non-zero spin, the KY tensor is a non-degenerate matrix and by a convenient choice of integration intervals we can, in principle, detect any component of the residue r_ν.

It is also useful to consider the integral form of $F^{\mu\nu}_{\ \ ;\nu} = j^\mu - r_\alpha Y^{\mu\alpha}$ integrated either over a spatial volume V at a fixed time $t = t_0$ or over a spatial surface S from t_0 to t_1 to yield

$$\int_S F^{ti}\sqrt{-g}\,\mathrm{d}^2S_i\Big|_{t=t_0} - \int_V j^t\sqrt{-g}\,\mathrm{d}^3x\Big|_{t=t_0} = -\int_V r_\nu Y^{t\nu}\sqrt{-g}\,\mathrm{d}^3x\Big|_{t=t_0}, \tag{22}$$

$$\left[\int_S F^{ti}\sqrt{-g}\,\mathrm{d}^2S_i\right]_{t_0}^{t_1} - \int_{t_0}^{t_1}\int_S j^i\sqrt{-g}\,\mathrm{d}^2S_i\mathrm{d}t = -\int_{t_0}^{t_1}\int_S r_\nu Y^{i\nu}\sqrt{-g}\,\mathrm{d}^2S_i\mathrm{d}t. \tag{23}$$

The identities (22) and (23) can be combined with (21) as convenient.

In the following, we will also use the integral form of the 'KY-projected equations of motion' $(T^{\mu\nu}Y_\nu^{\ \kappa})_{;\mu} = r^\nu Y_\nu^{\ \kappa}$, which reads

$$\left[\int_V T^{t\nu}Y_\nu^{\ \kappa}\sqrt{-g}\,\mathrm{d}^3x\right]_{t_0}^{t_1} + \int_{t_0}^{t_1}\int_S T^{i\nu}Y_\nu^{\ \kappa}\sqrt{-g}\,\mathrm{d}^2S_i\mathrm{d}t + \int_{t_0}^{t_1}\int_V \Gamma^\kappa_{\mu\lambda}T^{\mu\nu}Y_\nu^{\ \lambda}\sqrt{-g}\,\mathrm{d}^3x\,\mathrm{d}t = \int_{t_0}^{t_1}\int_V r^\nu Y_{\nu\kappa}\sqrt{-g}\,\mathrm{d}^3x\,\mathrm{d}t. \tag{24}$$

4 DEMONSTRATION IN KERR SPACE–TIME

The Kerr metric in Boyer-Lindquist coordinates t, φ, r, ϑ reads

$$\begin{aligned}\mathrm{d}s^2 = &-\left(1-\frac{2Mr}{\Sigma}\right)\mathrm{d}t^2 + \frac{\Sigma}{\Delta}\mathrm{d}r^2 + \Sigma\mathrm{d}\vartheta^2 \\ &+ \sin^2\vartheta\left(r^2 + a^2 + \frac{2Mra^2\sin^2\vartheta}{\Sigma}\right)\mathrm{d}\varphi^2 \\ &- \frac{4Mra\sin^2\vartheta}{\Sigma}\mathrm{d}t\mathrm{d}\varphi,\end{aligned} \tag{25}$$

where M, a are the mass and the spin of the black hole, respectively, $\Sigma = r^2 + a^2\cos^2\vartheta$ and $\Delta = r^2 - 2Mr + a^2$. The components of the Killing-Yano tensor then read (Floyd 1973)

$$\begin{aligned}Y_{rt} &= -Y_{tr} = a\cos\vartheta\,,\\ Y_{r\varphi} &= -Y_{\varphi r} = -a^2\cos\vartheta\sin^2\vartheta,\\ Y_{\vartheta\varphi} &= -Y_{\varphi\vartheta} = (r^2+a^2)r\sin\vartheta,\\ Y_{\vartheta t} &= -Y_{t\vartheta} = -ar\sin\vartheta,\\ Y_{t\varphi} &= -Y_{\varphi t} = Y_{r\vartheta} = -Y_{\vartheta r} = 0.\end{aligned} \tag{26}$$

The Killing-Yano tensor is independent of M and it is invertible for $a \neq 0$. An important property is that all the components $Y_{\mu\nu}$ are antisymmetric with respect to a reflection about the equatorial plane $\vartheta \to \pi - \vartheta$.

4.1 Dust flow

Let us now construct an analytical accretion toy model with a parametrized non-physical deviation; this model will be used to study the applicability of the KY conservation law in the next Subsection. We set up a field of dust $T^{\mu\nu} = \rho u^\mu u^\nu$ that is infalling into a Kerr black hole with a mass density ρ and the four-velocity

$$u_\varphi = u_\vartheta = 0, \tag{27}$$

$$u_t = -1, \tag{28}$$

$$u_r = -\frac{\sqrt{2Mr(r^2+a^2)}}{\Delta} + \varepsilon, \tag{29}$$

where when the dimensionless constant $\varepsilon = 0$ then the velocity field fulfils the geodesic equation $a^\mu = 0$ but violates it for $\varepsilon \neq 0$ by introducing two non-zero components of acceleration

$$a_\vartheta = -\varepsilon\frac{2a^2\sin\vartheta\cos\vartheta\sqrt{2Mr(r^2+a^2)}}{\Sigma^2} + \mathcal{O}(\varepsilon^2)\,, \tag{30}$$

$$a_r = -\varepsilon\left(\frac{\sqrt{2Mr(r^2+a^2)}}{\Sigma}\right)_r + \mathcal{O}(\varepsilon^2). \tag{31}$$

Since the velocity field is purely radial, the continuity equation $(\rho u^\mu)_{;\,\mu} = 0$ has the simple solution

$$\rho = -\frac{\dot{M}(\vartheta)}{2\pi\Delta u_r}, \tag{32}$$

where $\dot{M}(\vartheta)$ is an arbitrary positive function of ϑ, which represents the dust accretion rate through a $\vartheta = \text{const.}$ layer.

This flow is parametrized by the arbitrary function $\dot{M}(\vartheta)$ and the deviation parameter ε. Since the continuity equation is fulfilled, we obtain that the residue vector is $T^\mu_{\nu;\mu} = r_\nu = \rho a_\nu$.

4.2 Integral test

The three 'usual' conservation laws we would check in this situation are conservation of mass $(\rho u^\mu)_{;\,\mu} = 0$, conservation of angular momentum $(T^\mu_\varphi)_{;\mu} = 0$ and conservation of energy $(T^\mu_t)_{;\mu} = 0$. However, it is easy to verify that the example has been constructed so as to automatically fulfil these conservation laws while violating the evolution equations in the 'blind spots' of these tests.

We will now compare the detection of a non-zero ε by the equalities (2), which was obtained from a direct integration of the equations of motion, (24), which was obtained from the KY-projected equations of motion, and (22), which was obtained from the KY conservation law.

As for the implementation of (2), we choose the $\nu = r$ component for our purposes, take the volume V as the volume between r_0 and r_1, and obtain under the assumption of automatic stationarity and axisymmetry

$$\left[\int_{0^\pi} \rho (u_r)^2 \Delta \sin\vartheta \,\mathrm{d}\vartheta\right]_{r_0}^{r_1} - \frac{1}{2}\int_{r_0}^{r_1}\int_{0^\pi} g_{\alpha\beta,r}\,\rho u^\alpha u^\beta \Sigma \sin\vartheta \,\mathrm{d}\vartheta\,\mathrm{d}r$$
$$= \int_{r_0}^{r_1}\int_{0^\pi} \rho a_r \,\Delta \sin\vartheta \,\mathrm{d}\vartheta\,\mathrm{d}r. \tag{33}$$

To implement (24), we must choose a component that detects the non-zero acceleration in the meridional plane. A quick glance at the non-zero components of the KY tensor (26) shows that we can detect the meridional acceleration only through the $\kappa = t, \varphi$ components of (24). Here, we choose the $\kappa = t$ component and obtain similarly to (33)

$$\left[\int_{0^\pi} \rho u_r L^t \Delta \sin\vartheta \,\mathrm{d}\vartheta\right]_{r_0}^{r_1} + \frac{1}{2}\int_{r_0}^{r_1}\int_{0^\pi} \Gamma^t_{\mu\lambda}\,\rho u^\mu L^\lambda \Sigma \sin\vartheta \,\mathrm{d}\vartheta\,\mathrm{d}r$$
$$= \int_{r_0}^{r_1}\int_{0^\pi} \rho (a^r Y^t_r + a^\vartheta Y^t_\vartheta)\,\Sigma \sin\vartheta \,\mathrm{d}\vartheta\,\mathrm{d}r. \tag{34}$$

Finally, we implement (22) with the volume between $r = r_0$ and $r = r_1$ in place of V to obtain

$$\left[\int_{0^\pi} F^{tr} \Sigma \sin\vartheta \,\mathrm{d}\vartheta\right]_{r_0}^{r_1} - \int_{r_0}^{r_1}\int_{0^\pi} j^t \Sigma \sin\vartheta \,\mathrm{d}\vartheta\,\mathrm{d}r$$
$$= \int_{r_0}^{r_1}\int_{0^\pi} \rho (a^r Y^t_r + a^\vartheta Y^t_\vartheta)\,\Sigma \sin\vartheta \,\mathrm{d}\vartheta\,\mathrm{d}r. \tag{35}$$

In all the cases, we have to exclude the black hole from the integration region because its central singularity acts as a sink where conservation laws are violated.

The integrals on the left-hand sides of (33), (34) and (35) should in every case detect deviations (non-zero right-hand sides) that are of order $\mathcal{O}(\varepsilon)$ and correspond to quantities integrated over the same coordinate ranges. Furthermore, the integration regions and components in (34) and (35) were chosen such that they have the identical projections of r_ν on the right-hand sides.

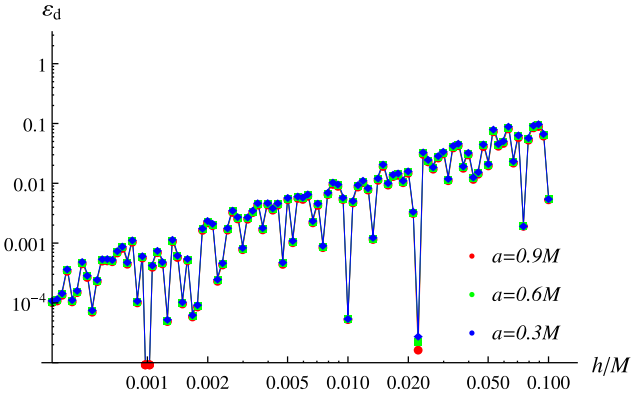

Figure 1. The detection value of the non-physical perturbation ε_d as detected by the integrated equations of motion (33) as a function of grid spacing h. The integration bounds $[r_0, r_1]$ are taken as $[3M, 6M]$ and various values of spin were used.

There is one very important difference between (34) and (35) as compared to (33), and that is the response of these integrals to terms symmetric or antisymmetric with respect to reflection about the equatorial plane. Due to the reflection antisymmetry of $Y_{\mu\nu}$ and the reflectionally symmetric integration region, the KY-based expressions (34) and (35) measure the reflectionally antisymmetric part of ρa^μ, and (33) the symmetric part. Since we have constructed a^μ as reflectionally symmetric, we need to introduce reflection asymmetry in ρ for the KY tests (34) and (35) to yield non-trivial results. We do so by choosing the angular mass influx from (32) as $\dot{M}(\vartheta) = 1 + \cos\vartheta$.

The numerical demonstration of these tests now consists of a detection of a non-zero ε when the dust stress-energy tensor is given to us in terms of double-precision numbers on a finite grid. The grid is constructed in Boyer-Lindquist coordinates r, ϑ with spacing $\delta r = h, \delta\vartheta = h/r$, where h is some given length constant. The left-hand sides of (33), (34) and (35) are then evaluated using numerical integration. To evaluate the integral of j^t we must, however, compute the gradients of the stress-energy tensor by numerical differentiation and only after that perform numerical integration on the finite grid.

We numerically approximate the gradient by the symmetric difference $f'(x) = [f(x+h) - f(x-h)]/2h + \mathcal{O}(h^3)$ and the integrals via the trapezoidal rule $\int f(x)\mathrm{d}x = h(f_0/2 + f_1 + \ldots + f_{n-1} + f_n/2) + \mathcal{O}(h^2)$ in given coordinates. We perform all the computations at double precision and define the 'base-noise' σ_0 as the numerically computed value of the left-hand sides at $\varepsilon = 0$. We then define the detection value ε_d of ε as the value for which the left-hand evaluates as $10\sigma_0$.

4.3 Results

In Figs 1, 2 and 3, we plot the dependence of ε_d on h for various values of the spin parameter a for (33), (34) and (35), respectively.

The results are largely independent of a since the relative sizes of the terms in (33), (34) and (35) stay constant, to linear order in a, independently of the value of spin. When $\varepsilon = 1$, then the deviation of our model velocity from the physical one is of orders of the speed of light, so it is reasonable to require that the numerical test definitely detects $\varepsilon \lesssim 1$. We see in Fig. 3 that the test based on the KY conservation law is noisier due to numerical differentiation and

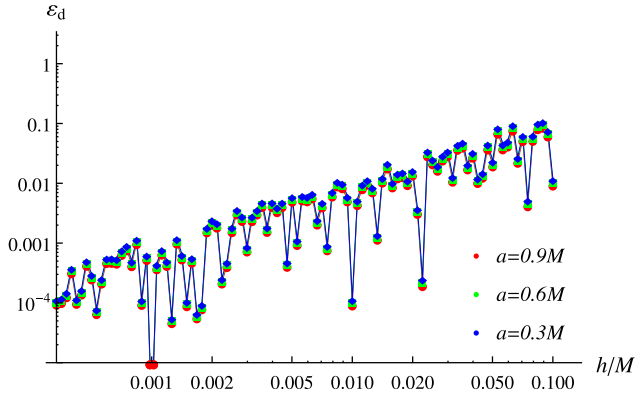

Figure 2. The detection value of the non-physical perturbation ε_d as detected by the KY-projected equations of motion (34) as a function of grid spacing h. Same integration bounds and values of spin as in Fig. 1 are used and the scaling and ranges of axes are also identical to Fig. 1.

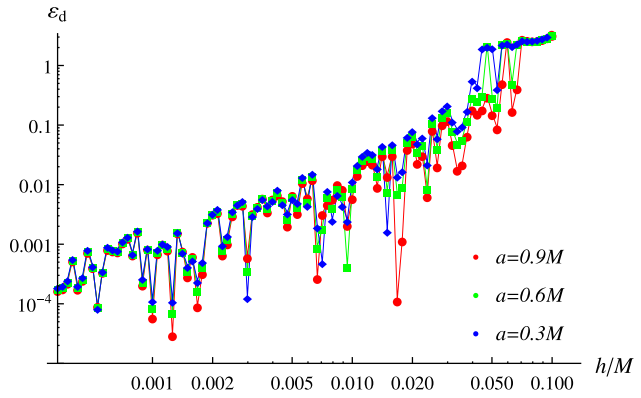

Figure 3. The detection value of the non-physical perturbation ε_d as detected by the KY conservation law (35) as a function of grid spacing h. Same integration bounds and values of spin as in Fig. 1 are used and the scaling and ranges of axes are also identical to Fig. 1.

requires $h \lesssim 0.05M$ to detect perturbations within $\varepsilon \lesssim 1$. On the other hand, the tests (33) and (34) are free of the noise coming from numerical differentiation and detect $\varepsilon \lesssim 1$ already for much larger grid spacings. None the less, once the step is $h \lesssim 0.05M$, the KY conservation law yields comparable results to the (33) and (34).

5 DISCUSSION AND CONCLUDING REMARKS

Even though checking for the conservation of the KY current $j^\mu = T^{\mu\nu;\kappa}Y_{\nu\kappa}$ can detect violations of the equations of motion that are not detectable by checking for the conservation of particle number, energy or azimuthal angular momentum, it does so at a requirement of rather fine grid spacing ($h \lesssim 0.05M$) and at a testing power 'only' comparable to checking the integrated version of the equations of motion $T^{\mu\nu}{}_{;\mu} = 0$ or the 'KY-projected equations of motion' $(T^{\mu\nu}Y_\nu{}^\kappa)_{;\mu} = 0$.

In our example, the KY conservation law as well as the KY projected equations of motion provided information about the reflectionally antisymmetric part of the non-physical perturbation, while the integrated equation of motion provided information about the symmetric part. Since it will be a general pattern that the KY tests provide information independent of the one obtained by the plain coordinate form of the equations of motion, it is advisable to use at least one of the two in a 'testing toolkit' when investigating the validity of numerical evolutions. Clearly, the integrated version of KY-projected equations of motion is preferable amongst the two because it does not require the evaluation of either spatial or temporal gradients of matter variables and thus avoids any difficulties with implementation or excessive requirements on grid spacing.

Nevertheless, we must admit that the exploitation of the hidden symmetry bears less powerful results than we hoped for. A KY conservation law is possible to formulate and link to the properties of geodesic motion, but it turns out to be only a weak one and, albeit a possibly privileged specimen, a member of a larger class of similarly weak conservation laws which have no longer anything to do with the hidden symmetry. In principle, even the KY-projected equation of motion $(T^{\mu\nu}Y_\nu{}^\kappa)_{;\mu} = 0$ can be considered only as a simpler and more elegant member of a general class of identities $(T^{\mu\nu}X_\nu{}^\kappa)_{;\mu} - T^{\mu\nu}X_\nu{}^\kappa{}_{;\mu} = 0$ for arbitrary $X_{\mu\nu}$. On the other hand, the fact that our results are connected to more general mathematical structures does not lessen any of the statements given in the paragraphs above.

In upcoming works, we plan to use the hidden symmetry of the Kerr space–time in a different manner. Specifically, we plan to investigate analytical solutions of fluid flows, already hinted upon in Markakis et al. (2016), that share or generalize the hidden symmetry of the Kerr background.

ACKNOWLEDGEMENTS

I would like to thank Charalampos Markakis, Volker Perlick and Pavel Jefremov for useful discussions on this topic. I am also grateful for the support from a PhD grant of the German Research Foundation within its Research Training Group 1620 *Models of Gravity*.

REFERENCES

Abramowicz M. A., Fragile P. C., 2013, Living Rev. Relativ., 16, 1
Vojtěch W. et al., 2017, MNRAS, preprint (arXiv:1709.03330)
Blaes O., 2014, Space Sci. Rev., 183, 21
Carter B., 1968, Phys. Rev., 174, 1559
De Villiers J.-P., Hawley J. F., 2003, ApJ, 589, 458
Floyd R., 1973, PhD thesis, London Univ., London, England
Gammie C. F., McKinney J. C., Tóth G., 2003, ApJ, 589, 444
Grant A., Flanagan É. É., 2015, Class. Quantum Gravity, 32, 157001
Howarth L., Collinson C., 2000, Gen. Relativ. Gravit., 32, 1845
Krtouš P., Kubiznák D., Page D. N., Frolov V. P., 2007, J. High Energy Phys., 2007, 004
Markakis C., Uryū K., Gourgoulhon E., Nicolas J.-P., Andersson N., Pouri A., Witzany V., 2016, Phys. Rev., 96, 064019
Penrose R., 1973, Ann. New York Acad. Sci., 224, 125
Trautman A., 2002, Gen. Relativ. Gravit., 34, 721
Walker M., Penrose R., 1970, Commun. Math. Phys., 18, 265

APPENDIX A: CONSERVATION LAWS FROM GENERAL TENSORS

Consider an arbitrary tensor $X^{\mu\nu}$ and a tensor analogous to $F^{\mu\nu}$,

$$\tilde{F}^{\mu\nu} = 2T^{\kappa[\mu}X^{\nu]}{}_\kappa . \tag{A1}$$

We then see that independent of the properties of $X^{\mu\nu}$, the following current will be conserved

$$\tilde{j}^\mu = \tilde{F}^{\mu\nu}{}_{;\nu} = T^{\mu\nu;\kappa}X_{\kappa\nu} + T^{\kappa\mu}X^\nu{}_{\kappa;\nu} - T^{\kappa\nu}X^\mu{}_{\kappa;\nu} . \tag{A2}$$

As for the testing power of $\tilde{j}^{\mu}_{\ ;\mu} = 0$, we obtain analogously to (21) the detection of $T^{\mu\nu}_{\ \ ;\mu} = r^{\nu}$ as

$$\left[\int_V \tilde{j}^t \sqrt{-g}\,\mathrm{d}^3x\right]_{t_0}^{t_1} + \int_{t_0}^{t_1}\int_S \tilde{j}^i \sqrt{-g}\,\mathrm{d}^2S_i\mathrm{d}t = \left[\int_V r_\nu X^{t\nu}\sqrt{-g}\,\mathrm{d}^3x\right]_{t_0}^{t_1} + \int_{t_0}^{t_1}\int_S r_\nu X^{i\nu}\sqrt{-g}\,\mathrm{d}^2S_i\mathrm{d}t. \quad \text{(A3)}$$

If we investigate under which conditions the last two terms in (A2) vanish so that a form $\tilde{j}^{\mu} = T^{\mu\nu;\kappa}X_{\kappa\nu}$ similar to the KY conservation law is obtained, we get

$$X_{\mu(\nu;\kappa)} = g_{\mu(\nu}X^{\lambda}_{\ \kappa);\lambda}. \quad \text{(A4)}$$

If $X^{\mu\nu}$ were additionally antisymmetric, then the fulfilment of condition (A4) would make it a so-called conformal KY tensor (of which the usual KY tensors are a subclass with $X^{\lambda}_{\ \kappa;\lambda} = 0$). This suggest that the currents $\tilde{j}^{\mu}$ derived from KY or conformal KY tensors may play a privileged role as compared to those derived from general tensors. A full investigation of whether this is true is out of the scope of this paper.

Similarly, it is possible to generate conserved antisymmetric tensors $\tilde{j}^{\mu_1\cdots\mu_{n-1}}$, $\tilde{j}^{\mu_1\cdots\mu_{n-1}}_{\ \ \ \ ;\mu_{n-1}} = 0$ from any tensor $X^{\mu_1\cdots\mu_n}$. We show the resulting formulas only for $\tilde{j}^{\mu_1\cdots\mu_{n-1}}$ generated from KY tensors.

A KY tensor of arbitrary rank is defined as a totally antisymmetric tensor $Y_{\mu\nu\ldots\kappa} = Y_{[\mu\nu\ldots\kappa]}$ whose gradient is also antisymmetric $Y_{\mu\nu\ldots\kappa;\,\gamma} = -Y_{\mu\nu\ldots\gamma;\,\kappa}$. The tensor analogous to $F^{\mu\nu}$ is then, for a KY tensor of rank n, defined as

$$F^{\mu_1\ldots\mu_n} = \frac{n}{n-1}Y_{\alpha}^{\ [\mu_1\ldots\mu_{n-1}}T^{\mu_n]\alpha}. \quad \text{(A5)}$$

Using the properties of the Killing-Yano tensor and $T^{\mu\nu}_{\ \ ;\nu} = 0$, we then obtain

$$j^{\mu_1\ldots\mu_{n-1}} = F^{\mu_1\ldots\mu_n}_{\ \ \ \ ;\mu_n} = Y_{\alpha\beta}^{\ \ \ [\mu_1\ldots\mu_{n-2}}T^{\mu_{n-1}]\alpha;\beta}. \quad \text{(A6)}$$

It is easy to see that by construction $j^{\mu_1\ldots\mu_{n-1}}_{\ \ \ \ ;\mu_{n-1}} = 0$. Since the tensors $F^{\mu_1\ldots\mu_n}$ and $j^{\mu_1\ldots\mu_{n-1}}$ are totally antisymmetric, integral formulas analogous to the ones in Subsection 3.3 will apply to them.

Some astrophysically relevant space–times admit KY tensors of higher rank (Howarth & Collinson 2000), but these generate redundant conserved quantities for free test particle motion and are thus expected to generate linearly dependent variants of the conservation laws presented in the main text. Of broader theoretical interest is the fact that non-redundant KY tensors of higher rank arise for higher dimensional spinning black holes (Krtouš et al. 2007) and there the formulas above will probably give independent conservation laws.

This paper has been typeset from a TEX/LATEX file prepared by the author.

A&A 614, A75 (2018)
https://doi.org/10.1051/0004-6361/201732361

Astronomy & Astrophysics

New closed analytical solutions for geometrically thick fluid tori around black holes

Numerical evolution and the onset of the magneto-rotational instability

V. Witzany and P. Jefremov

Center of Applied Space Technology and Microgravity (ZARM), Universität Bremen, Am Falturm 2, 28359 Bremen, Germany
e-mail: vojtech.witzany@zarm.uni-bremen.de; paul.jefremow@zarm.unibremen.de

Received 25 November 2017 / Accepted 24 February 2018

ABSTRACT

Context. When a black hole is accreting well below the Eddington rate, a geometrically thick, radiatively inefficient state of the accretion disk is established. There is a limited number of closed-form physical solutions for geometrically thick (nonselfgravitating) toroidal equilibria of perfect fluids orbiting a spinning black hole, and these are predominantly used as initial conditions for simulations of accretion in the aforementioned mode. However, different initial configurations might lead to different results and thus observational predictions drawn from such simulations.
Aims. We aim to expand the known equilibria by a number of closed multiparametric solutions with various possibilities of rotation curves and geometric shapes. Then, we ask whether choosing these as initial conditions influences the onset of accretion and the asymptotic state of the disk.
Methods. We have investigated a set of examples from the derived solutions in detail; we analytically estimate the growth of the magneto-rotational instability (MRI) from their rotation curves and evolve the analytically obtained tori using the 2D magneto-hydrodynamical code HARM. Properties of the evolutions are then studied through the mass, energy, and angular-momentum accretion rates.
Results. The rotation curve has a decisive role in the numerical onset of accretion in accordance with our analytical MRI estimates: in the first few orbital periods, the average accretion rate is linearly proportional to the initial MRI rate in the toroids. The final state obtained from any initial condition within the studied class after an evolution of ten or more orbital periods is mostly qualitatively identical and the quantitative properties vary within a single order of magnitude. The average values of the energy of the accreted fluid have an irregular dependency on initial data, and in some cases fluid with energies many times its rest mass is systematically accreted.

Key words. accretion, accretion disks – black hole physics – magnetohydrodynamics (MHD) – methods: analytical – methods: numerical

1. Introduction

Accretion of matter onto black holes can lead to the release of large amounts of radiation and is responsible for some of the most energetic phenomena in the Universe such as X-ray binaries or active galactic nuclei. When the accretion rate on a black hole is sufficiently high while radial convection of internal energy sufficiently low, the accretion disk surrounding the black hole reaches a state which is well described by the so-called thin disk model (Shakura & Sunyaev 1973; Novikov & Thorne 1973; Abramowicz & Fragile 2013). However, when the accretion rate drops well below the so-called Eddington accretion rate $\dot{M}_{\rm Edd} = 1.39 \times 10^{18} (M/M_\odot) {\rm g\,s^{-1}}$, as is believed to be, for example, the case for the black hole in our Galactic center, the accretion disk enters a rather different mode that is characterized as geometrically thick, optically thin, "hot" in the sense that thermal energies are nonnegligible as compared to gravitational binding energies, and radiatively inefficient. This also implies that the energy losses from the disk are dominated by either direct advection through the horizon or outflows (see Yuan & Narayan 2014, and references therein).

Amongst other things, this means that the radiatively inefficient disk can be, to a first approximation, modeled as a magneto-hydrodynamic (MHD) fluid without radiation back-reaction (see e.g., Dexter et al. 2009). A more accurate model, however, requires the inclusion of radiative cooling and heating, and the partially two-temperature nature of the fluid in this accretion mode, see for example Ryan et al. (2017) and references therein. Consequently, a number of global general-relativistic MHD studies were conducted showing that the MRI-driven turbulence (Balbus & Hawley 1991, 1998) provides the angular momentum transport in the disk, and many features predicted by analytical or semi-analytical models emerge with only a small amount of additional ad-hoc input (see e.g., De Villiers et al. 2003; McKinney & Gammie 2004; Narayan et al. 2012).

For simulations of this type of accretion disks one usually uses initial conditions which are in a smooth equilibrium state. If such equilibria are to be given completely in closed form, then they are predominantly either the fluid tori with constant specific angular momentum $\ell \equiv -u_\varphi/u_t$ of Kozłowski et al. (1978); Abramowicz et al. (1978), or with constant $\ell^* \equiv u_\varphi u^t$ of Fishbone & Moncrief (1976).

However, the angular momentum or angular velocity distributions play a decisive role in the onset of various instabilities. The MRI growth rate is proportional to the angular velocity gradient, and another notable instability, the centrifugal or

Rayleigh–Taylor[1] instability, has a growth rate proportional to the gradient of angular momentum.

Another case where the angular momentum distribution was formerly believed to make a crucial difference is the gravitational runaway instability as studied for example by Font & Daigne (2002); Daigne & Font (2004). In the particular model chosen by the authors of the aforementioned study, the mass parameter of the black hole space-time was allowed to dynamically grow by the amount of accreted matter, possibly leading to an accretion runaway. Then, they found that if specific angular momentum grew with radius, the runaway instability was suppressed, whereas for the ℓ = const. tori it caused the accretion disk to be fully accreted on orbital time-scales. This instability was later shown to disappear when full self-gravity of the torus is accounted for (Montero et al. 2010; Rezzolla et al. 2010; Mewes et al. 2016). However, the study of Font & Daigne (2002); Daigne & Font (2004) demonstrates that the precise shape of the angular momentum distribution can often have a critical influence on the evolution obtained within a given model.

Is it possible that we are missing new dynamical effects or different states of the accretion disks in our simulations because we are restricting ourselves only to a limited number of initial conditions? To answer this question, a variety of closed form solutions corresponding to different gradients of either ℓ or Ω in the initial fluid configurations would be useful.

We present such solutions in this paper in Sect. 2, and demonstrate how these lead, at least in principle, to differences in numerical simulation results in Sect. 3 by implementing and evolving our solutions in the HARM 2D code (Gammie et al. 2003; Noble et al. 2006). A reader looking for an explicit recipe for the construction of the tori will find all the needed formulas in Appendix B. Of interest is also the essentially unknown fact that the fully general solutions for the toroidal equilibria in static space-times (e.g., in the Schwarzschild space-time) are expressible in closed form, which we briefly describe in Sect. 2.2.

2. Analytical solutions for fluid tori near black holes

We use the $G = c = 1$ geometrized units and the $-+++$ signature of the space-time metric. A comma before an index defines a partial derivative with respect to the appropriate coordinate, whereas a preceding semi-colon a covariant derivative with respect to the coordinate.

2.1. Basic equations

The plasma orbiting the black hole is modeled by ideal MHD where molecular dissipation, electric resistivity, self-gravitation, and radiative or nonequilibrium effects are neglected in the dynamics. As a result, the system is governed by the set of equations (cf. Anile 1989)

$$\left(T^{\mu}{}_{\nu}\right)_{;\mu} = \left(T^{\mu}{}_{\nu(\mathrm{m})} + T^{\mu}{}_{\nu(\mathrm{f})}\right)_{;\mu} = 0\,, \tag{1}$$

$$(\mu u^{\mu})_{;\mu} = 0\,, \tag{2}$$

$$(u^{\mu}b^{\nu} - u^{\nu}b^{\mu})_{;\nu} = 0\,, \tag{3}$$

$$T^{\mu\nu}_{(\mathrm{m})} \equiv b^2 u^{\mu}u^{\nu} + \frac{b^2}{2}g^{\mu\nu} - b^{\mu}b^{\nu}\,, \tag{4}$$

$$T^{\mu\nu}_{(\mathrm{f})} \equiv w u^{\mu}u^{\nu} + P g^{\mu\nu}\,, \tag{5}$$

where u^{μ} is the fluid four-velocity, μ its rest-mass density, w its enthalpy density, and P its pressure. The vector b^{μ} is the magnetic field vector in the rest frame of the fluid.

We place the magneto-fluid into an axially symmetric and stationary space-time with the metric

$$\mathrm{d}s^2 = g_{tt}\mathrm{d}t^2 + 2g_{t\varphi}\mathrm{d}t\mathrm{d}\varphi + g_{\varphi\varphi}\mathrm{d}\varphi^2 + g_{rr}\mathrm{d}r^2 + g_{\vartheta\vartheta}\mathrm{d}\vartheta^2. \tag{6}$$

Some useful symbols we use are the rotation frequency of zero-angular-momentum observers (ZAMOs), $\omega \equiv g^{t\varphi}/g^{tt} = -g_{t\varphi}/g_{\varphi\varphi}$; the potential whose gradient generates the acceleration of ZAMOs, $\Phi_{(\mathrm{Z})} \equiv -\ln(-g^{tt})/2$; minus the determinant of the t-φ part of the metric, $\rho^2 \equiv g_{t\varphi}^2 - g_{tt}g_{\varphi\varphi}$; and a radius-like quantity $\mathcal{R} \equiv \sqrt{-g^{tt}g_{\varphi\varphi}}$.

Now let us assume that all the properties of the magneto-fluid are axisymmetric and stationary, the flow is purely circular, $u^r = u^{\vartheta} = 0$, and that the magnetic field is purely toroidal, $b^r = b^{\vartheta} = 0$. Then the Faraday Eq. (3) and the particle-conservation Eq. (2) are trivially fulfilled and we need to solve only the momentum balance equation (relativistic Euler Eq. (1)).

The magnetic part of this equation can under the given assumptions be simplified as

$$\left(T^{\mu}{}_{\nu(\mathrm{m})}\right)_{;\mu} = \frac{(b^2\rho^2)_{,\nu}}{2\rho^2}. \tag{7}$$

This expression was first derived by Komissarov (2006), but we provide, in our view, a more direct and clear rederivation in Appendix A.

There are many different ways how to rewrite the fluid part of the Euler equation, one of them is the form which can be attributed to Fishbone & Moncrief (1976)

$$\left(T^{\mu}{}_{\nu(\mathrm{f})}\right)_{;\mu} = w\left[-\ln(\mathcal{R})_{,\nu}V^2 + \omega_{,\nu}\mathcal{R}V\sqrt{1+V^2} + \Phi_{(\mathrm{Z}),\nu}\right] + P_{,\nu}\,, \tag{8}$$

where $V \equiv u_{\varphi}/\sqrt{g^{\varphi\varphi}}$ is the linear velocity of the fluid as measured in the ZAMO frame.

However, one of the best known forms of the fluid part of the Euler equation for circular equilibria is due to Kozłowski et al. (1978); Abramowicz et al. (1978) and reads

$$\left(T^{\mu}{}_{\nu(\mathrm{f})}\right)_{;\mu} = w\left[-\ln(u^t)_{,\nu} + \frac{\ell}{1-\Omega\ell}\Omega_{,\nu}\right] + P_{,\nu}\,, \tag{9}$$

where $\ell \equiv -u_{\varphi}/u_t$ and $\Omega = u^{\varphi}/u^t$. In all of the Eqs. (7), (8) and (9) the nontrivial components are of course only those with $\nu = r, \vartheta$. We provide brief descriptions of the derivations of the expressions Eq. (8) and (9) in Appendix A.

2.2. Static space-times

In static space-times ($g_{t\varphi} = 0$) the full Euler equation using Eq. (7) and (8) simplifies as

$$-\ln(\mathcal{R})_{,\nu}V^2 = -\frac{P_{,\nu}}{w} - \frac{\tilde{P}_{,\nu}}{\tilde{w}} - \Phi_{(\mathrm{Z}),\nu}\,, \tag{10}$$

where we have introduced the notation $\tilde{P} \equiv b^2\rho^2$, $\tilde{w} \equiv 2w\rho^2$.

[1] In many contexts the "Rayleigh–Taylor instability" is used exclusively for the instability of interfaces of fluids with different densities. Here, we have used the word as also applying to the similar effect in continuous media (see e.g., Gourgouliatos & Komissarov 2018).

Let us now further assume that the configuration of the fluid fulfills the barotropic[2] condition of coincident surfaces of constant pressure and enthalpy $P = P(w)$ and the "magnetotropic" condition of coincident constant $\tilde{P}$ and $\tilde{w}$, $\tilde{P} = \tilde{P}(\tilde{w})$ (see Komissarov 2006). Then the right-hand side of Eq. (10) is a coordinate gradient, and the same must be true also for the left-hand side. Thus we conclude that under the given conditions we necessarily have $V = V(\mathcal{R})$ and the general solution of the Euler equation reads.

$$W(w(r,\vartheta)) + \tilde{W}(\tilde{w}(r,\vartheta)) = -\Phi_{(c)}(\mathcal{R}(r,\vartheta)) - \Phi_{(Z)}(r,\vartheta)\,, \tag{11}$$

where we have defined the effective potentials

$$W(w) \equiv \int \frac{P'(w)}{w}\mathrm{d}w\,, \tag{12}$$

$$\tilde{W}(\tilde{w}) \equiv \int \frac{\tilde{P}'(\tilde{w})}{\tilde{w}}\mathrm{d}\tilde{w}\,, \tag{13}$$

$$\Phi_{(c)}(\mathcal{R}) \equiv -\int \frac{V(\mathcal{R})^2}{\mathcal{R}}\mathrm{d}\mathcal{R}\,, \tag{14}$$

and where the potentials are determined only up to integration constants. The functions W and $\tilde{W}$ can be understood as thermodynamic and magneto-thermodynamic effective potentials respectively, Φ_c has clearly the meaning of a centrifugal potential, and $\Phi_{(Z)}$ is, in the currently discussed case of static space-times, the gravitational potential experienced by static observers.

General solutions for the toroidal equilibria can then be constructed by

1. Prescribing arbitrary distributions $P(w), \tilde{P}(\tilde{w})$ (e.g., as an "enthalpic polytrope" $P = Kw^\gamma$, $\tilde{P} = \tilde{K}\tilde{w}^\kappa$, see Komissarov 2006; Wielgus et al. 2015) and an equally arbitrary rotation profile $V(\mathcal{R})$;
2. Analytically integrating the potentials from Eq. (12)–(14);
3. Solving Eq. (11) for $w(r,\vartheta)$;
4. Using $b^2 = \tilde{P}(2\rho^2 w(r,\vartheta))/\rho^2$ and the relation $b^\mu u_\mu = 0$ to determine b^t, b^φ;
5. Postulating an equation of state such as the ideal-gas $w = \mu + 5\mu k_\mathrm{B}T/(2m)$, where T is the temperature and m the particle mass, to derive the density and entropy field from fundamental thermodynamic relations and the function $P(w)$.

The results presented in this section are probably not original, even though it is hard to find their explicit statement in the literature. They can be, however, seen as easily obtainable consequences of the results of either Abramowicz (1971) or Fishbone & Moncrief (1976) when restricted to static space-times.

Nonetheless, we find it important to state these results explicitly because there is a number of studies that construct tori in static space-times and use somewhat complicated numerical methods tailored for stationary space-times, even though the above-stated general closed solution is available (e.g., Daigne & Font 2004; Narayan et al. 2012; Penna et al. 2013).

[2] The fluid fulfilling the condition $P = P(w)$ is called barotropic by Kozłowski et al. (1978); Abramowicz et al. (1978), while other authors would rather call a fluid where the conditions $P = P(\mu)$ is fulfilled barotropic (see e.g., Tooper 1965). Both conditions coincide in flows with constant entropy per particle and in the Newtonian limit.

2.3. Stationary space-times

We see above that the form of the Euler equation coming from Eq. (8) can be used to construct the entirely general barotropic and magnetotropic solutions in static space-times. Furthermore, Fishbone & Moncrief (1976) used this form even in the case of stationary space-times to obtain equilibria with constant ℓ^*. However, we found it much more fruitful to use Eq. (9) in the general $g_{t\varphi} \neq 0$ stationary space-times.

We obtain the Euler equation under the assumption of barotropicity and magnetotropicity as

$$-\ln(u^t)_{,\nu} + \frac{\ell}{1-\Omega\ell}\Omega_{,\nu} = -W_{,\nu} - \tilde{W}_{,\nu}. \tag{15}$$

Once again, this equation quickly leads to an integrability requirement that either $\Omega_{,\mu} = 0$ or $\ell = \ell(\Omega)$. This result is known as the relativistic von Zeipel theorem (Abramowicz 1971).

However, finding closed analytical solutions is more complicated than in the static case; if we postulate the function $\ell(\Omega)$, we obtain

$$W + \tilde{W} = -L(\Omega) - \frac{1}{2}\ln(-g_{tt} - 2g_{t\varphi}\Omega - g_{\varphi\varphi}\Omega^2)\,, \tag{16}$$

where we have used the fact that $u^t = (-g_{tt} - 2g_{t\varphi}\Omega - g_{\varphi\varphi}\Omega^2)^{-1/2}$ and we define $L(\Omega)$ analogously to the potentials Eq. (12)–(14),

$$L(\Omega) \equiv \int \frac{\ell(\Omega)}{1-\Omega\ell(\Omega)}\mathrm{d}\Omega\,. \tag{17}$$

In other words, the thermodynamic and magneto-thermodynamic potentials are specified by this procedure not only as functions of coordinates but also of an as-of-yet unspecified function $\Omega = \Omega(r,\vartheta)$.

To obtain $\Omega(r,\vartheta)$ from the postulated $\ell(\Omega)$ and thus find the full explicit solution, one has to use the relation

$$\Omega = \frac{u^\varphi}{u^t} = \frac{\ell g^{\varphi\varphi} - g^{t\varphi}}{\ell g^{t\varphi} - g^{tt}}\,, \tag{18}$$

which leads to the equation for Ω

$$(\ell g^{t\varphi} - g^{tt})\Omega - \ell g^{\varphi\varphi} + g^{t\varphi} = 0\,. \tag{19}$$

In general, this equation has to be solved numerically, see examples for nonmagnetized tori in Chakrabarti (1985), Daigne & Font (2004), Qian et al. (2009), Penna et al. (2013), and also more recent examples for magnetized tori in Wielgus et al. (2015), Gimeno-Soler & Font (2017). Nevertheless, if we instead want to obtain $\Omega(r,\vartheta)$ as a closed analytical expression, we must impose some constraints on the form of $\ell(\Omega)$. For instance, if Ω is to be a root of a polynomial equation of order n, it is easy to see that necessarily $\ell = P^{(n-1)}(\Omega)/P^{(n-1)}(\Omega)$, where $P^{(k)}(x)$ are some polynomials of order k.

We have chosen here to focus on the general form of $\ell(\Omega)$ which leads to the expression for Ω as a root of a quadratic equation ($n = 2$)

$$\ell = \frac{\ell_0 + \lambda\Omega}{1 + \kappa\ell_0\Omega}\,, \tag{20}$$

where ℓ_0, κ, λ are some constants.

We chose this particular form of the parametrization of $\ell(\Omega)$ because the case $\kappa = 0, \lambda = 0$ corresponds to the well-known $\ell = \text{const.} = \ell_0$ Polish donuts of Kozłowski et al. (1978);

Table 1. Simulation parameters.

Variable	Value
Black hole spin a	$0.9375\,M$
Resolution	512×512
Inner radius of toroid	$5\,M$
Outer radius of toroid	$12\,M$
Horizon radius $r_{\rm H}$	$M + \sqrt{M^2 - a^2}$
Inner boundary of simulation	$0.98\,r_{\rm H}$
Outer boundary of simulation	$40\,M$

Table 2. Initial condition parameters.

κ	$\ell_0\,[M]$	κ	$\ell_0\,[M]$
–1.11	2.5889	0.15	3.2606
–1.	2.6418	0.26	3.32871
–0.9	2.69052	0.36	3.39239
–0.79	2.74492	0.47	3.46449
–0.69	2.79522	0.57	3.53203
–0.58	2.85157	0.68	3.60865
–0.48	2.90383	0.78	3.68053
–0.37	2.96253	0.89	3.76223
–0.27	3.0171	0.99	3.83902
–0.16	3.07854	1.1	3.92644
–0.06	3.13577	1.2	4.00877
0.05	3.20034	1.31	4.10268

Notes. Parameters for tori with an isobaric contour passing through $r = 5\,M, 12\,M$ while $\lambda = 0$.

Abramowicz et al. (1978), and, on the other hand, $\kappa = 1, \lambda = 0$ corresponds to $\ell^* \equiv u_\varphi u^t = \text{const.} = \ell_0$ of Fishbone & Moncrief (1976). The other choices of κ, λ, however, represent a continuous class connecting and extending these two particular solution families.

The expressions for Ω and the thermodynamic potential as functions of coordinates corresponding to Eq. (20) are given in Appendix B; examples of the obtained rotation curves and density profiles are discussed in the next section. In particular, it is shown that in Kerr space-time the choice $\lambda = 0, \ell_0 > 0$ and a small $\kappa > 0$ generically leads to ℓ growing with radius, whereas $\kappa < 0$ to an angular momentum falling of with radius.

Even more specifically, we will see in the next section that $\kappa < 0$ leads to very thick tori with strongly nonKeplerian rotation profiles. However, since the solutions themselves do not have any direct physical meaning, and since they are used only as initial conditions for an MHD evolution that completely changes their character, we do not exclude any choice of parameters, save perhaps for those leading to outright pathological tori. In return, this allows us to potentially discover new states and behaviors of accretion disks.

3. Numerical simulations

Because the solutions presented in the previous section are in closed form, it is easy to set them up as initial conditions for the evolution in Kerr space-time in existing numerical codes and see whether they bring any variations in the properties of the accretion disks that evolve from them. Hence, we implemented our initial conditions in the 2D HARM code of Gammie et al. (2003); Noble et al. (2006) and conducted the numerical study in a "standard HARM set-up", as described for example in McKinney & Gammie (2004).

We placed the tori with various choices of the solution parameters near a Kerr black hole with spin $a = 0.9375M$, perturbed them with a small poloidal magnetic field with $P/b^2 = 100$ at the pressure maximum of the torus, and evolved the tori for a time period of $3000\,M$ with a 512×512 resolution. As indicated already in Balbus & Hawley (1991, 1998), long-term MHD turbulence requires at least some magnetic field threading the disk vertically and this is the reason why the weak poloidal field is included in the initial conditions. Toroidal fields also trigger the MRI, but on their own they eventually decay (see also Wielgus et al. 2015; Fragile & Sądowski 2017). We have thus decided not to include a toroidal component of the magnetic field in the initial conditions ($\tilde{P} = 0$) and leave the study of its effects to other works.

What follows is a description of some of the properties of the chosen initial conditions and a discussion of the simulation results. We used the default HARM outputs of energy, angular momentum, and rest-mass accretion rates to diagnose the evolutions. The parameters of the simulation are summarized in Table 1.

3.1. Properties of initial conditions

Our main target was to investigate the properties of the tori with the angular-momentum relation Eq. (20) in dependence on the various values of the parameter κ. We set $\lambda = 0$ and determine ℓ_0 by requiring that the toroids have their inner and outer edge at $r = 5\,M$ and $r = 12\,M$ in Boyer–Lindquist coordinates respectively.

The thermodynamic relations were then determined by setting up the gas as initially isentropic, nonmagnetized ($\tilde{P} = 0$), and having a polytropic equation of state $P = K\mu^\gamma$, where μ is mass density and we set $\gamma = 13/9$ to roughly mimic an ideal-gas mixture of relativistic electrons and mostly nonrelativistic ions. Furthermore, we used the HARM convention $K = \mu_{\rm c}^{1-\gamma}$, where μ_c is the density of the toroid at the pressure maximum (see Appendix B).

We constructed 24 such initial conditions with κ in the interval $[-1.11, 1.31]$; a summary of the resulting parameters is given in Table 2, and the properties of the initial conditions can be inspected in Figs. 1–4.

We know from the analysis of von-Zeipel radii by Abramowicz et al. (1978); Kozłowski et al. (1978) that the $\ell = \text{const.}$ toroids in the Kerr space-time will have an angular velocity along the equator falling off with radius, at least as long as we are above the photon orbit. Since $\kappa = 0$, $\lambda = 0$ corresponds to the $\ell = \ell_0 = \text{const.}$ tori, we can then assume that for moderate magnitudes of κ our solutions will also have an angular velocity fall-off, at least if we are far away from the photon sphere. This expectation is fulfilled in the case of our tori, as can be seen on a few examples in Fig. 1.

Furthermore, by examining the angular momentum relation Eq. (20) at $\lambda = 0, \ell_0 > 0, \Omega > 0$ and by assuming that angular velocity is falling off with radius, we conclude that $\kappa > 0$ means angular momentum growing with radius, and a small $\kappa < 0$ (such that the expression Eq. (20) does not become singular) an angular momentum fall-off. This is demonstrated in Fig. 2.

As for the dependence of the vertical structure of the toroid on the parameter κ, that seems to be impossible to characterize by any simple analytical argument. We can only offer the observation that the angular momentum distribution is such that

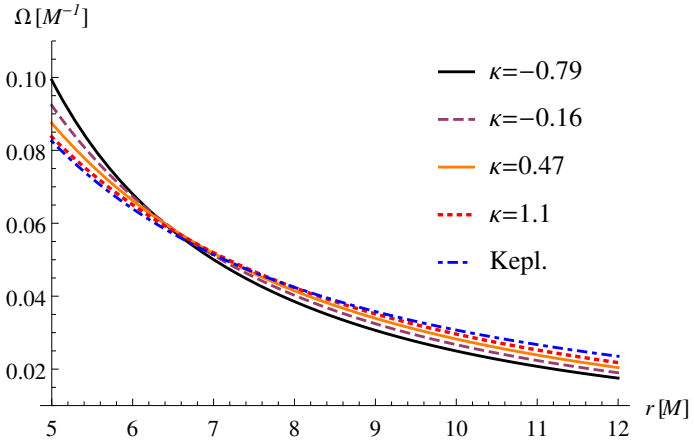

Fig. 1. Profile of the angular velocity Ω inside the tori along the equatorial plane for different values of the parameter κ. In this and all the following graphs we assume $\lambda = 0$ and ℓ_0 is determined by the constraint that the torus has its inner and outer edge at $r = 5\,M$ and $r = 12\,M$ respectively.

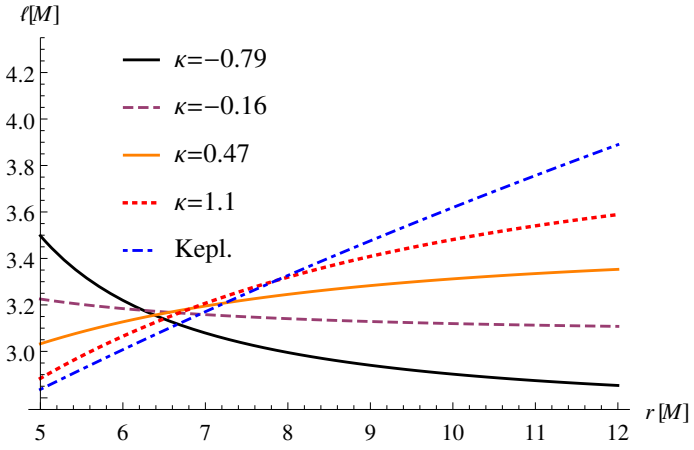

Fig. 2. Profile of specific angular momentum ℓ inside the tori along the equatorial plane for different values of the parameter κ.

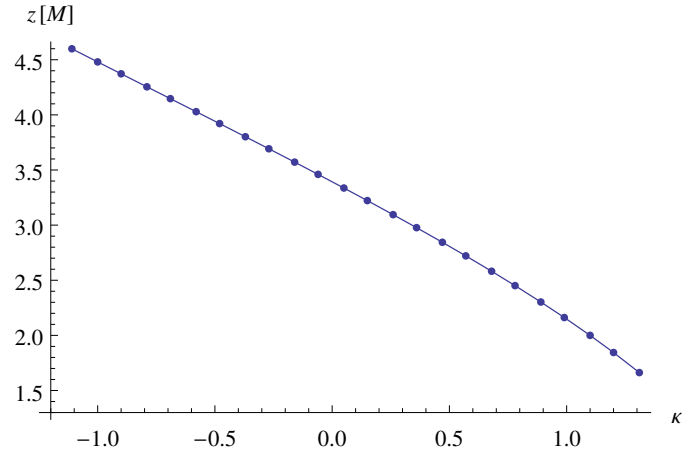

Fig. 3. Vertical extent $z = r\cos\vartheta$ of the tori as a function of the parameter κ.

for $\kappa \gtrsim 1$ the rotation curve in the equatorial plane is closer to Keplerian values and thus the disk should be closer to the canonical "thin disk" also in the vertical structure. This can be seen to hold in Figs. 3 and 4. The $\kappa \gtrsim 1$ ($\lambda = 0$) disks are thus the ones closest to the state assumed to arise from long-term MHD simulations and, as such, could be preferred as initial conditions in astrophysical studies.

Last but not least, the HARM convention $K = \mu_c^{1-\gamma}$ leads to the specific enthalpy $h \equiv w/\mu$ to be equal to $h = (2\gamma - 1)/(\gamma - 1) = 4.25$ at the pressure maximum of every torus. This fact leads to the relativistic Bernoulli parameter $\mathcal{B} \equiv -hu_t$ being much larger than one at the pressure maxima of the tori, a property common to hot accretion flows (Narayan & Yi 1994, 1995). The values of the Bernoulli parameter at the pressure maxima of the tori as a function of κ are plotted in Fig. 5.

3.2. Simulation results

The general scenario of the evolution of any of our tori is up to some intermittent episodes (see Sect. 3.3) qualitatively equivalent to the default HARM simulation with the ℓ^* = const. tori as described for example in McKinney & Gammie (2004). We see the onset of the MRI and a rapid transition to turbulence throughout the disk starting from the inner edge. In parallel, the inner edge extends all the way toward the black hole, forming a plunging region, and the accretion disk reaches a quasi-steady state with a magnetically dominated corona layer above it, and a nearly evacuated magnetized funnel around the poles.

The simulation time $t = 3000\,M$ is about ten orbital periods of the pressure maxima and it is sufficient to see the establishment of these quasi-stationary structures. However, it is not enough to see the ultimate fate of the disk in terms of the accumulation of magnetic flux around the black hole and a possible transition to a magnetically arrested disk, or the spreading of the disk to large radii through angular momentum exchange (for a long simulation see Narayan et al. 2012).

The mathematical analysis of Balbus & Hawley (1991) showed that the MRI grows with a rate which is dependent both on the wave vector of the disturbance and the local angular-velocity gradients in the fluid. To obtain a single numerical estimate of some kind of "typical strength" of the MRI for each torus, we have chosen to use the growth rate of the fastest-growing MRI mode (maximum of the MRI growth rate in the perturbation wave-vector space) $\mathrm{Im}(\omega_{\mathrm{max}})$ evaluated at the location of the pressure maxima of the tori. Gammie (2004) showed that the rate of the fastest growing mode can be computed as half the shear rate in the case of relativistic Keplerian disks, $-\omega_{\mathrm{max}}^2 = \sigma^2/2$ and, even though this result has not been rigorously proven to apply to general relativistic flows, we have used it here as our estimate (for definition and computation of shear rates in Kerr space-times see e.g., Semerák 1998).

The resulting MRI growth-rate estimates are given in Fig. 6, where we see that by variation of κ we get an MRI e-folding time from $10\,M$ to about $20\,M$. As can be seen on a few selected examples of accretion rates in Fig. 7, this leads to the first wave of matter arriving at the black hole at around 100–200 M. This certainly does not mean that the MRI needs approximately ten e-folds to take effect because this time also includes the inspiral time required for the matter released by the instability to arrive to the black hole horizon. In fact, the waves arrive within a few tens of M away from each other, which suggests that matter is released from the tori within approximately five e-folding times of the MRI.

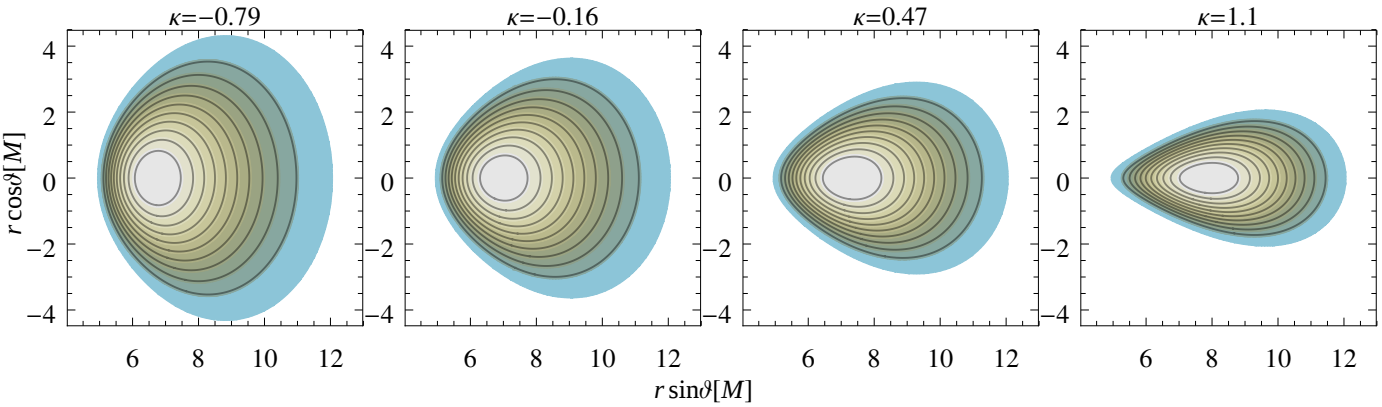

Fig. 4. Meridional sections of the density of the tori for different values of κ. The progression goes from geometrically very thick tori with large pressure gradients at their inner edge up to thinner toroids with a cusp (vanishing pressure gradient) gradually forming at their inner radius.

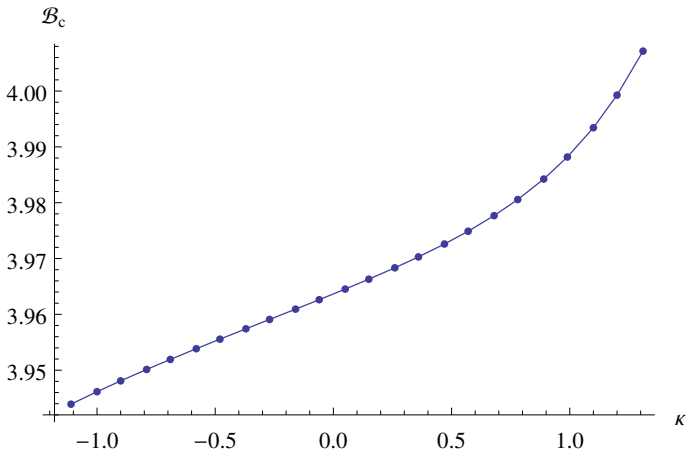

Fig. 5. Relativistic Bernoulli parameter $\mathcal{B} \equiv -hu_t$ at the pressure maxima of the tori ($\mathcal{B} > 1$ corresponds to matter with enough energy to escape to infinity) as a function of the parameter κ. In our case the thermodynamic properties are chosen such that $h = 4.25$ at the pressure maxima of the toroids, so the behavior of $\mathcal{B}_c$ is due to the fact that the maxima are getting farther from the black hole with growing κ.

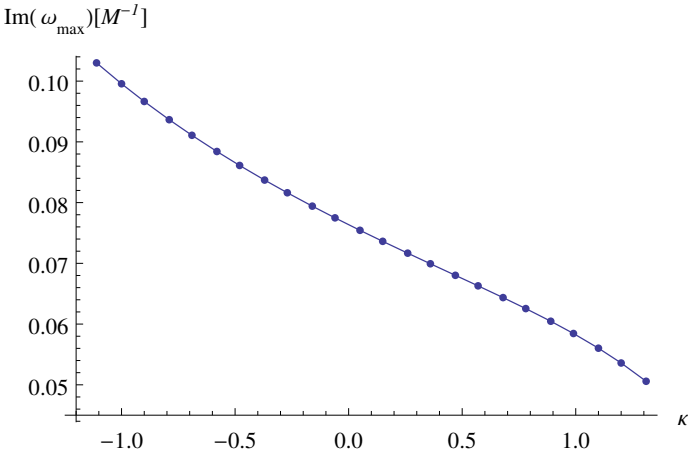

Fig. 6. Growth rates of the fastest-growing MRI mode $\mathrm{Im}(\omega_{\mathrm{max}})$ evaluated at the position of the pressure maxima of the tori plotted as a function of the parameter κ.

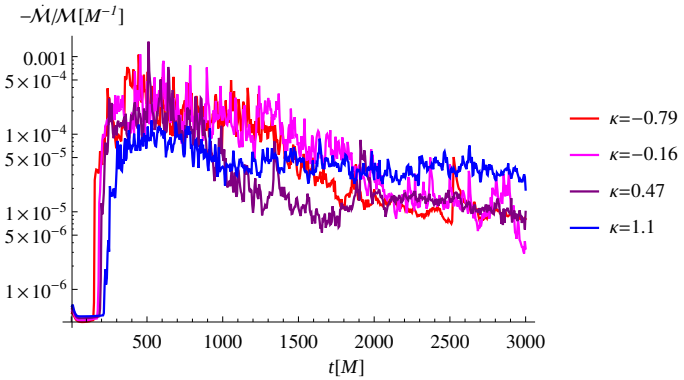

Fig. 7. Some examples of the numerically obtained mass accretion rate $\dot{\mathcal{M}}/\mathcal{M}$ as a function of time. The height of the first peak of the accretion rate is correlated with κ, but the late evolutions are harder to relate to the parameters of the initial conditions.

This observation is further documented in Fig. 8, where we see that the average accretion rates over the first 500 M of evolution are correlated with the initial MRI estimates. This may be explained by noticing from Fig. 7 that the "first accretion waves" arrive earlier from the tori with higher shear (smaller κ), but also that these waves bring larger amounts of matter with them. However, we also see that the correlation starts to be broken for the most shearing tori (with largest MRI growth rates), which is probably because they are already entering the nonlinear mode of evolution in the chosen averaging interval.

Furthermore, if we try to see whether the accretion rates in the last 1000 M of our evolution are correlated to the initial $\mathrm{Im}(\omega_{\mathrm{max}})$, we see in the second part of Fig. 8 that there is no tangible correlation. This is because by that time the tori have evolved to the quasi-stationary "asymptotic[3]" states where their relation to the properties of initial conditions has mostly been washed out, perhaps up to the energy and angular-momentum content. For further details see the next subsection.

3.3. Advected specific energy and nominal efficiency

We also computed the "nominal efficiency" $\tilde{\eta} \equiv 1 - \langle \dot{\mathcal{E}}/\dot{\mathcal{M}} \rangle$ as was done in McKinney & Gammie (2004) but we found negative efficiencies for all of our tori at late times. This is not a mistake

[3] Meaning that they then evolve on timescales much longer than the orbital time.

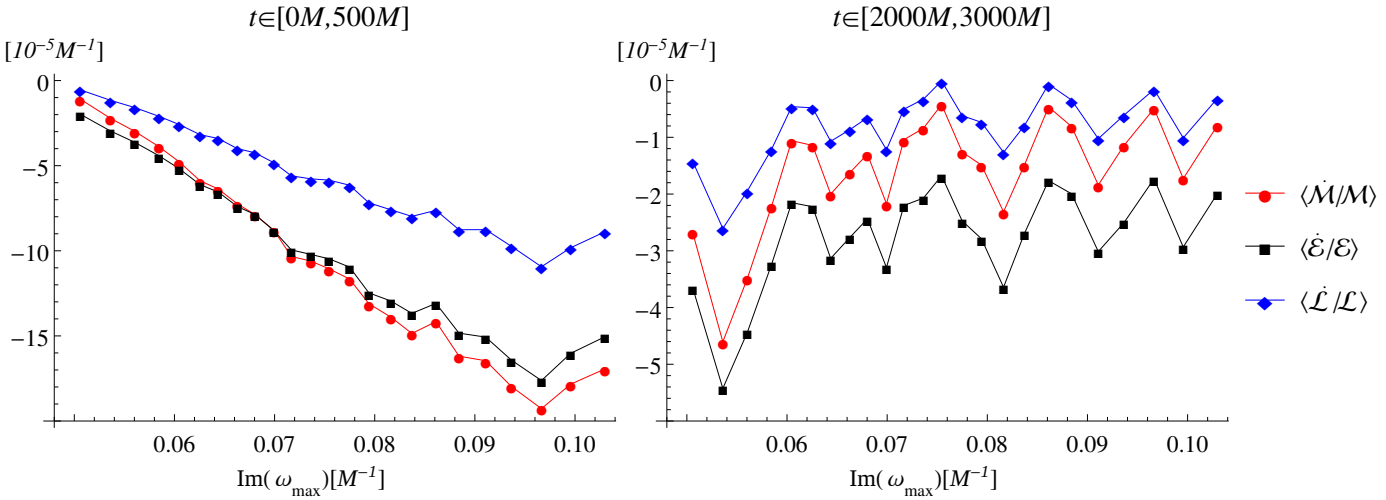

Fig. 8. Numerically obtained accretion rates of rest mass $\langle \dot{\mathcal{M}}/\mathcal{M} \rangle$, energy $\langle \dot{\mathcal{E}}/\mathcal{E} \rangle$ and angular momentum $\langle \dot{\mathcal{L}}/\mathcal{L} \rangle$ averaged over the evolution time intervals $[0, 1000\,M]$ and $[2000\,M, 3000\,M]$ as a function of the initial MRI growth rate estimate $\mathrm{Im}(\omega_{\mathrm{max}})$. We note that a lower negative value of $\dot{\mathcal{M}}, \dot{\mathcal{E}}, \dot{\mathcal{L}}$ corresponds to a higher loss rate of the quantity from the torus and thus a higher accretion rate. The displayed values correspond to the parameter κ in the interval $[-1, 1.31]$.

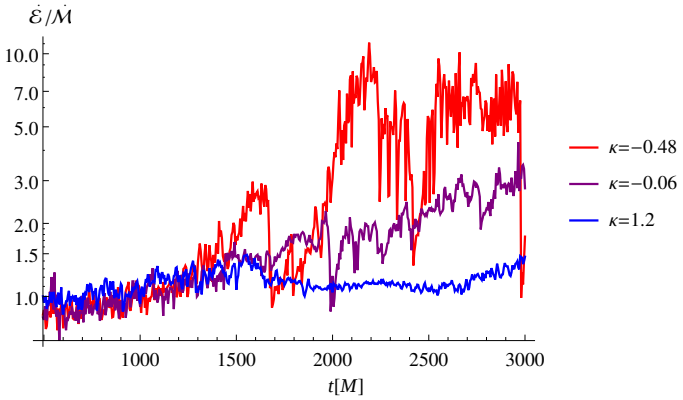

Fig. 9. Accreted specific energy $\dot{\mathcal{E}}/\dot{\mathcal{M}}$ as a function of time for chosen values of the parameter κ.

but, as will be seen from the following, a robust property of this type of simulations with an analytical underpinning. Hence, we must warn against the usage of $\tilde{\eta}$ as any sort of efficiency of the accretion process. Let us now discuss the arguments which explain this phenomenon.

The total energy in the disk is defined as

$$\mathcal{E}(t) = -\int_V T^t_{\ t}\,\sqrt{-g}\,\mathrm{d}^3x = \int \mathcal{B}\mu u^t\,\sqrt{-g} - P\,\sqrt{-g}\,\mathrm{d}^3x + \mathcal{E}_{\mathrm{m}}\,, \tag{21}$$

where V is the spatial volume, and $\mathcal{E}_{\mathrm{m}}$ is the energy in the magnetic fields (initially almost zero). The total rest mass $\mathcal{M}$ is, on the other hand, defined as

$$\mathcal{M}(t) = \int_V \mu u^t\,\sqrt{-g}\,\mathrm{d}^3x\,. \tag{22}$$

The expression $\mu u^t\sqrt{-g}$ is just the coordinate mass density, so for instance $\int \mathcal{B}\mu u^t\sqrt{-g}\mathrm{d}^3x / \int \mu u^t\sqrt{-g}\mathrm{d}^3x$ is simply the mass-averaged Bernoulli parameter.

Thus, we can see that the ratio $\mathcal{E}/\mathcal{M}$ corresponds to the average Bernoulli parameter with contributions to energy from the internal stress in the gas, and the magnetic-field energy. A similar argument leads us to the realization that $\dot{\mathcal{E}}/\dot{\mathcal{M}}$ is the average Bernoulli parameter of the accreted fluid elements plus similar terms. However, since we start with a toroid with most of its elements having $\mathcal{B} > 1$ (see Fig. 5), we should not strictly expect the advection dominated flow to accrete exclusively the portion of the matter with $\mathcal{B} < 1$ and spit the rest out in an outflow. Thus, even when ignoring the pressure and magnetic contribution to energy, we should not be surprised by $\dot{\mathcal{E}}/\dot{\mathcal{M}} > 1$.

The simulation of McKinney & Gammie (2004) did not find the average $\langle \dot{\mathcal{E}}/\dot{\mathcal{M}} \rangle$ to be larger than 1 but we believe that this is only thanks to the fact that their simulation halted at $t = 2000M$. In contrast, we found that for times $t > 2000M$ the irregular advection mechanism is able to push even the high-energy fluid elements into the black hole. This is demonstrated in Fig. 9, where we see that $\dot{\mathcal{E}}/\dot{\mathcal{M}}$ undergoes erratic "build-ups" whose origin seems to be linked with the behavior of the magnetic fields and the coronal layer (see Fig. 10).

Specifically, visual inspection of the plots of the strength of magnetic fields reveals that the build-ups in $\langle \dot{\mathcal{E}}/\dot{\mathcal{M}} \rangle$ are associated with the coronal layer slowly raising all the way to the axis and filling the polar funnel; the abrupt drop in accreted specific energy is then associated with a sudden evacuation of the axis region and the reemergence of the funnel. This of course suggests that what is accreted in the "super-energetic" periods is mostly the magnetically dominated matter from the coronal region around the poles. On the other hand, it also suggests that this phenomenon might be associated with the strictly axisymmetric structure of the simulation and that it would not be reproduced in a 3D simulation. Alternatively, it could be caused by the small topological defect which is introduced in HARM to regularize the coordinate singularity at the axis (see Gammie et al. 2003).

One thing which is clear to us is the fact that this super-energetic accretion cannot be easily related to any parameter of the initial conditions, as we show in Fig. 11. All the properties of the initial conditions vary as smooth, typically monotonous functions of the parameter κ, so if the late $\langle \dot{\mathcal{E}}/\dot{\mathcal{M}} \rangle$ is to depend on any simple property of the initial conditions, it should be obvious from its dependence on κ. Even though the late average $\langle \dot{\mathcal{E}}/\dot{\mathcal{M}} \rangle$

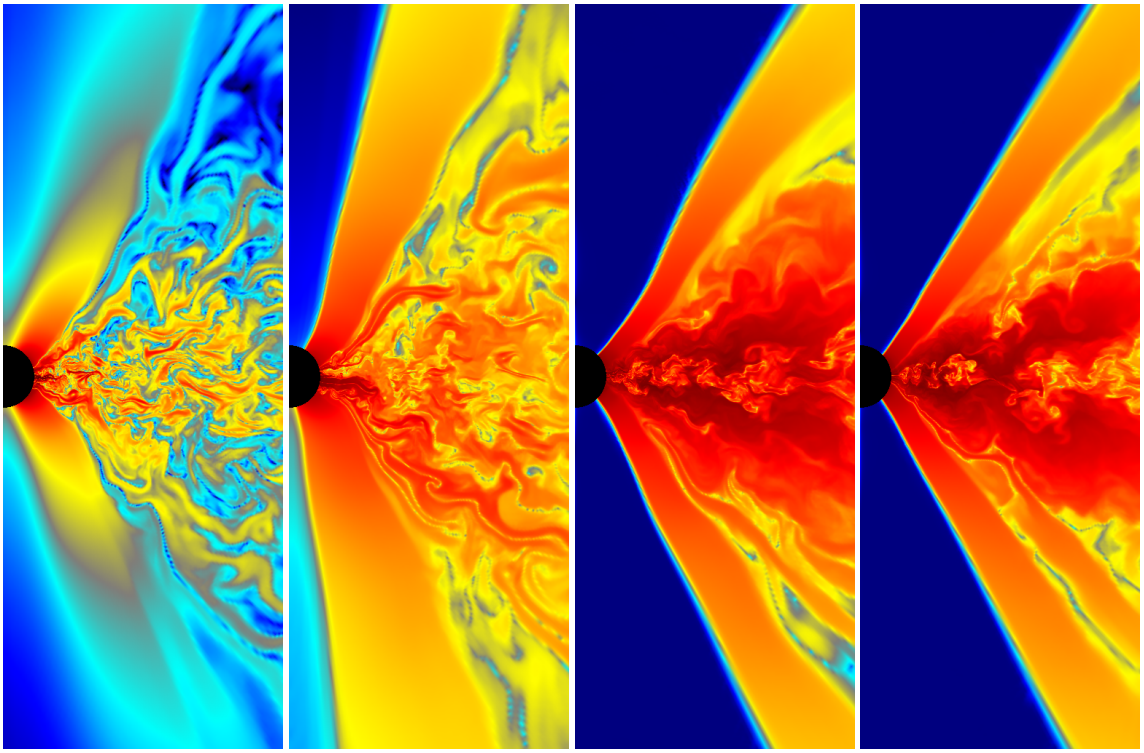

Fig. 10. Snapshots of the structure of the magnetic fields for different tori evolutions plotted in Boyer–Lindquist coordinates. The color indicates $\log(b^2/b^2_{\rm max})$, where $b^2_{\rm max}$ is the maximal strength of the magnetic field in the respective image, the black circle is the interior of the black hole, and the right equatorial edge of the image is at $r = 12M$. The first two images on the left are snapshots for the $\kappa = -0.48$ torus before and after the first $\dot{\mathcal{E}}/\dot{\mathcal{M}}$ peak, at $t = 1200\,M$ and $t = 1700\,M$ respectively (c.f. Fig. 9). The other two images on the right are snapshots for the "$\dot{\mathcal{E}}/\dot{\mathcal{M}}$-quiescent" $\kappa = 1.2$ torus at $t = 1200\,M$ and $t = 1700\,M$ respectively. It appears that the behavior of $\dot{\mathcal{E}}/\dot{\mathcal{M}}$ is linked with the evolution of the coronal layer.

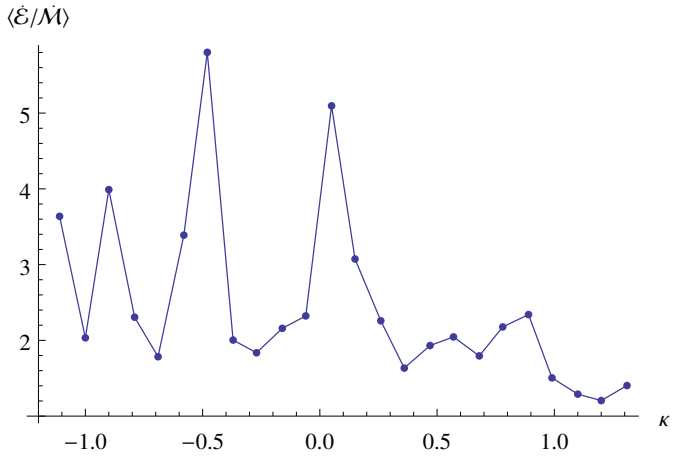

Fig. 11. Accreted specific energy $\dot{\mathcal{E}}/\dot{\mathcal{M}}$ averaged over the interval $t \in [2000\,M, 3000\,M]$ as a function of κ. The vertical axis has its origin at 1, which means that all our flows return a negative nominal efficiency at late simulation times.

can be recognized in Fig. 11 as a continuous function of κ in certain regions, the sampling is not sufficient to understand the structure any further. The only other observation, inferred from Figs. 2 and 11, is that the extremely high values of specific energy seem to be associated with initial rotation curves which are very far away from a Keplerian profile.

We believe that this dependence of $\langle\dot{\mathcal{E}}/\dot{\mathcal{M}}\rangle$ on initial conditions should be studied in more detail in future works. Additionally, a more careful study should separate $\dot{\mathcal{E}}/\dot{\mathcal{M}}$ from the actually accreted Bernoulli parameter because the former involves a significant, or even dominant contribution of the energy of the magnetic field at late evolution times. However, implementing and running diagnostics that would allow us to make such a distinction and shed more light on this numerically observed phenomenon is beyond the scope of the current paper.

4. Conclusions

We presented generalizations of the known closed-form analytical solutions of geometrically thick fluid tori near black holes; our solutions are easy to construct and implement in numerical codes. Unlike the previously known solution families, our family provides a rich spectrum of possibilities for the rotation curve and geometrical shapes even if parameters such as the inner and outer radii are constrained. In particular, our $\kappa \gtrsim 1$ disks have semi-Keplerian rotation profiles and could thus be preferred for initial conditions of astrophysical simulations rather than the ℓ = const. (Abramowicz et al. 1978; Kozłowski et al. 1978) or ℓ^* = const. (Fishbone & Moncrief 1976) tori.

The MRI growth rates for different tori from our new class have different magnitudes and the tori exhibit different numerical evolutions accordingly. Namely, the average normalized accretion rate $\langle\dot{\mathcal{M}}/\mathcal{M}\rangle$ over the first 500 M of the simulation (three or more orbital periods) turns out to be linearly proportional to the growth rate of the fastest-growing MRI mode at the pressure maximum of the torus.

On the other hand, the asymptotic states of the accretion disk which are achieved for an evolution time $\gtrsim$2000 M do not exhibit any correlation of accretion rates with the initial MRI growth rates. Additionally, all of the asymptotic accretion disks

tend to have the same qualitative disk-corona-funnel structure as described by for example McKinney & Gammie (2004) and the normalized accretion rates of their angular momentum, energy and mass vary within a single order of magnitude.

Nevertheless, we see that the disks vary quite wildly in the specific energy of the fluid they accrete; for particular choices of initial conditions and at the most extreme periods, the energy of the accreted elements approaches ten times their rest mass. This seems to be connected with the behavior of the strongly magnetized coronal layer because the extreme accretion episodes are associated with the corona pushing into the funnel, sometimes even up to the point of the short disappearance of the evacuated region. This behavior, however, appeared only for initial conditions far away from a Keplerian rotation profile. Further insights into this question should be obtained by future studies which should also involve more realistic matter models for the disk and better diagnostics ran during the simulation.

Acknowledgements. We would like to thank Claus Lämmerzahl and Volker Perlick for supervision and useful discussions on the topic. We are grateful for the support from a Ph.D. grant of the German Research Foundation (DFG) within Research Training Group 1620 "Models of Gravity". Additionally, PJ kindly acknowledges the support from the Erasmus Mundus Joint Doctorate IRAP program.

References

Abramowicz, M. A. 1971, Acta Astron., 21, 81
Abramowicz, M. A., & Fragile, P. C. 2013, Living Rev. Relativ., 16, 1
Abramowicz, M., Jaroszyński, M., & Sikora, M. 1978, A&A, 63, 221
Anile, A. M. 1989, Relativistic Fluids and Magneto-Fluids: With Applications in Astrophysics and Plasma Physics (Cambridge University Press)
Balbus, S. A., & Hawley, J. F. 1991, ApJ, 376, 214
Balbus, S. A., & Hawley, J. F. 1998, Rev. Mod. Phys., 70, 1
Chakrabarti, S. K. 1985, ApJ, 288, 1
Daigne, F., & Font, J. A. 2004, MNRAS, 349, 841
De Villiers, J.-P., Hawley, J. F., & Krolik, J. H. 2003, ApJ, 599, 1238
Dexter, J., Agol, E., & Fragile, P. C. 2009, ApJ, 703, L142
Fishbone, L. G., & Moncrief, V. 1976, ApJ, 207, 962
Font, J. A., & Daigne, F. 2002, MNRAS, 334, 383
Fragile, P. C., & Sądowski, A. 2017, MNRAS, 467, 1838
Gammie, C. F. 2004, ApJ, 614, 309
Gammie, C. F., McKinney, J. C., & Tóth, G. 2003, ApJ, 589, 444
Gimeno-Soler, S., & Font, J. A. 2017, A&A, 607, A68
Gourgouliatos, K. N., & Komissarov, S. S. 2018, MNRAS, 475, L125
Komissarov, S. S. 2006, MNRAS, 368, 993
Kozłowski, M., Jaroszyński, M., & Abramowicz, M. 1978, A&A, 63, 209
McKinney, J. C., & Gammie, C. F. 2004, ApJ, 611, 977
Mewes, V., Font, J. A., Galeazzi, F., Montero, P. J., & Stergioulas, N. 2016, Phys. Rev. D, 93, 064055
Montero, P. J., Font, J. A., & Shibata, M. 2010, Phys. Rev. Lett., 104, 191101
Narayan, R., & Yi, I. 1994, ApJ, 428, L13
Narayan, R., & Yi, I. 1995, ApJ, 444, 231
Narayan, R., Sądowski, A., Penna, R. F., & Kulkarni, A. K. 2012, MNRAS, 426, 3241
Noble, S. C., Gammie, C. F., McKinney, J. C., & Del Zanna L. 2006, ApJ, 641, 626
Novikov, I., & Thorne, K. S. 1973, Black holes, 6, 343
Penna, R. F., Kulkarni, A., & Narayan, R. 2013, A&A, 559, A116
Qian, L., Abramowicz, M. A., Fragile, P. C., et al. 2009, A&A, 498, 471
Rezzolla, L., & Zanotti, O. 2013, Relativistic Hydrodynamics (Oxford University Press)
Rezzolla, L., Baiotti, L., Giacomazzo, B., Link, D., & Font, J. A. 2010, Class. Quant. Grav., 27, 114105
Ryan, B. R., Ressler, S. M., Dolence, J. C., et al. 2017, ApJ, 844, L24
Semerák, O. 1998, Gen. Rel. Grav., 30, 1203
Shakura, N. I., & Sunyaev, R. A. 1973, A&A, 24, 337
Tooper, R. F. 1965, ApJ, 142, 1541
Wielgus, M., Fragile, P. C., Wang, Z., & Wilson, J. 2015, MNRAS, 447, 3593
Yuan, F., & Narayan, R. 2014, ARA&A, 52, 529

Appendix A: Deriving various forms of Euler equation

A.1. Simplifying $\left(T^{\mu}{}_{\nu(\mathrm{m})}\right)_{;\mu}$

Omitting terms which are zero due to the stationarity and axisymmetry of all quantities, the circularity of velocity field, and toroidality of magnetic field, we obtain

$$\left(T^{\mu}{}_{\nu(\mathrm{m})}\right)_{;\mu} = b^2 a_\nu + \frac{(b^2)_{,\nu}}{2} - b_{\nu;\mu} b^\mu \,. \tag{A.1}$$

Let us now rewrite the a_ν and $b_{\nu;\mu}b^\mu$ terms as

$$u_{\nu;\mu}u^\mu = \frac{1}{2} g^{\alpha\beta}{}_{,\nu} u_\alpha u_\beta \,, \tag{A.2}$$

$$b_{\nu;\mu}b^\mu = \frac{1}{2} g^{\alpha\beta}{}_{,\nu} b_\alpha b_\beta \,. \tag{A.3}$$

We then obtain

$$\left(T^{\mu}{}_{\nu(\mathrm{m})}\right)_{;\mu} = -\frac{b^2}{2} g^{\alpha\beta}{}_{,\nu}\left(-u_\alpha u_\beta + \frac{b_\alpha b_\beta}{b^2}\right) + \frac{(b^2)_{,\nu}}{2} \,. \tag{A.4}$$

We now realize that u_μ and $b_\mu/\sqrt{b^2}$ are two normalized orthogonal vectors exclusively in the $t-\varphi$ direction and we thus have

$$\frac{u_\alpha u_\beta}{u_\mu u^\mu} + \frac{b_\alpha b_\beta}{b^\mu b_\mu} = -u_\alpha u_\beta + \frac{b_\alpha b_\beta}{b^2} = g_{\alpha\beta}|_{(\varphi t)} \,, \tag{A.5}$$

where $g_{\alpha\beta}|_{(\varphi t)}$ is the φ, t-restriction of the metric (that is, $g_{rr}|_{(\varphi t)} = g_{\theta\theta}|_{(\varphi t)} = 0$ but otherwise the same as the metric). We then see that the magnetic part of the structural equations reads

$$\left(T^{\mu}{}_{\nu(\mathrm{m})}\right)_{;\mu} = -\frac{b^2}{2} g^{\alpha\beta}{}_{,\nu} g_{\alpha\beta}|_{(\varphi t)} + \frac{(b^2)_{,\nu}}{2} \,. \tag{A.6}$$

We now compute

$$\begin{aligned} g^{\alpha\beta}{}_{,\nu} g_{\alpha\beta}|_{(\varphi t)} &= (g^{\alpha\beta}|_{(\varphi t)})_{,\nu}\, g_{\alpha\beta}|_{(\varphi t)} = -g^{\alpha\beta}|_{(\varphi t)} (g_{\alpha\beta}|_{(\varphi t)})_{,\nu} \\ &= -\mathrm{Tr}\left[\mathbf{g}|^{-1}_{(\varphi t)} (\mathbf{g}|_{(\varphi t)})_{,\nu}\right] = -\frac{\rho^2_{,\nu}}{\rho^2} \,, \end{aligned} \tag{A.7}$$

where in the last step we have used the formula for the derivative of a determinant of a matrix, and we denote $\rho^2 \equiv -\mathrm{Det}\left(\mathbf{g}|_{(\varphi t)}\right) = g^2_{t\varphi} - g_{tt} g_{\varphi\varphi}$. Using (A.7) we then obtain that the magnetic part of the stress-energy tensor can be written as

$$(T^{\mu(\mathrm{m})}_{\nu})_{;\mu} = \frac{(\rho^2 b^2)_{,\nu}}{2\rho^2} \,. \tag{A.8}$$

A.2. Simplifying $\left(T^{\mu}{}_{\nu(\mathrm{f})}\right)_{;\mu}$

Under the symmetry assumptions and circularity of the flow we obtain

$$\left(T^{\mu}{}_{\nu(\mathrm{f})}\right)_{;\mu} = w a_\nu + P_{,\nu} \,. \tag{A.9}$$

Let us now briefly derive the two possible forms of a_ν useful for the construction of analytical solutions.

A.2.1. Fishbone-Moncrief form of acceleration

The Fishbone-Moncrief form is obtained by expressing the acceleration in terms of the velocity in the ZAMO frame. The linear velocity of the flow in the ZAMO frame is $V = u_\varphi/\sqrt{g_{\varphi\varphi}}$, and the four-velocity components of the circular flow are given as

$$u_\varphi = \sqrt{g_{\varphi\varphi}} V \,, \tag{A.10}$$

$$u_t = -\sqrt{\frac{1+V^2}{-g^{tt}}} - \omega \sqrt{g_{\varphi\varphi}} V \,, \tag{A.11}$$

These expressions are then directly substituted into the four-acceleration $a_\nu = g^{\alpha\beta}{}_{,\nu} u_\alpha u_\beta/2$ to obtain

$$\begin{aligned} a_\nu &= \frac{1}{2}\left(g^{tt}{}_{,\nu} u_t^2 + 2 g^{t\varphi}{}_{,\nu} u_t u_\varphi + g^{\varphi\varphi}{}_{,\nu} u_\varphi^2\right) \\ &= -\ln(\mathcal{R})_{,\nu} V^2 + \omega_{,\nu} \mathcal{R} V \sqrt{1+V^2} + \Phi_{(\mathrm{Z}),\nu} \,. \end{aligned} \tag{A.12}$$

A.2.2. "Polish-donut" form of acceleration

The Polish-donut form of acceleration is derived by realizing that the acceleration can be rewritten as

$$\begin{aligned} u_{\nu;\mu}u^\mu &= \frac{1}{2} g^{\alpha\beta}{}_{,\nu} u_\alpha u_\beta = \frac{1}{2}\left[(g^{\alpha\beta} u_\alpha u_\beta)_{,\nu} + 2 u_\alpha u^\alpha{}_{,\nu}\right] \\ &= u_\alpha u^\alpha{}_{,\nu} = u_t u^t{}_{,\nu} + u_\varphi u^\varphi{}_{,\nu} \,. \end{aligned} \tag{A.13}$$

We now use the four-velocity normalization to express $u_t = -(1+u^\varphi u_\varphi)/u^t$ and obtain

$$a_\nu = -\frac{u^t_{,\nu}}{u^t} + \frac{u^t_{,\nu}}{u^t} u^\varphi u_\varphi + u_\varphi u^\varphi{}_{,\nu} = -\ln(u^t)_{,\nu} + u_\varphi u^t \left(\frac{u^\varphi}{u^t}\right)_{,\nu} \,. \tag{A.14}$$

The last step is to use the four-velocity normalization to obtain the identity $u^t u_t = -1/(1-\Omega\ell)$ and thus $u_\varphi u^t = \ell/(1-\Omega\ell)$ which leads to Eq. (9).

Appendix B: Construction of tori

When we postulate $\ell = (\ell_0 + \lambda\Omega)/(1+\kappa\ell_0\Omega)$, we obtain the angular rotation frequency for $\kappa \neq 1$ as

$$\begin{aligned} \Omega &= \frac{\mathcal{A} - \sqrt{\mathcal{A}^2 + 4(\ell_0 g^{\varphi\varphi} - g^{t\varphi})(\lambda g^{t\varphi} - \kappa\ell_0 g^{tt})}}{2(\lambda g^{t\varphi} - \kappa\ell_0 g^{tt})} \\ \mathcal{A} &= g^{tt} + \lambda g^{\varphi\varphi} - \ell_0 g^{t\varphi}(1+\kappa) \end{aligned} \tag{B.1}$$

When we have $\ell = \ell_0$ (such as when $\kappa = \lambda = 0$), the formerly quadratic equation for Ω in Eq. (19) becomes linear and the quadratic root (B.1) has a formal singularity. In that case we can either take an appropriate limit or directly substitute into Eq. (18) to obtain

$$\Omega = \frac{\ell_0 g^{\varphi\varphi} - g^{t\varphi}}{\ell_0 g^{t\varphi} - g^{tt}} \,. \tag{B.2}$$

The function $L(\Omega)$ from Eq. (17) is easily integrated as (for a general choice of parameters)

$$\begin{aligned} L = &-\frac{1}{2}\ln\left[1 + (\kappa-1)\ell_0\Omega - \lambda\Omega^2\right] \\ &- \frac{\ell_0(1+\kappa)}{2C}\ln\left[\frac{C - \ell_0(1-\kappa) - 2\lambda\Omega}{C + \ell_0(1-\kappa) + 2\lambda\Omega}\right] , \\ C = &\sqrt{\ell_0^2(\kappa-1)^2 + 4\lambda} \,. \end{aligned} \tag{B.3}$$

There are degeneracies in the parametrization when we allow for $\lambda \neq 0$ and we thus recommend to set $\lambda = 0$ for most practical purposes. Then the function L simplifies as

$$L = \frac{1}{\kappa - 1} \ln\left[1 + (\kappa - 1)\ell_0 \Omega\right] . \tag{B.4}$$

The final expression for the thermodynamic potentials (for $\lambda = 0$) then reads

$$\begin{aligned} W + \tilde{W} = &- \ln\left[\left[1 + (\kappa - 1)\ell_0 \Omega\right]^{1/(\kappa-1)}\right] \\ &- \ln\left[\sqrt{-g_{tt} - 2g_{t\varphi}\Omega - g_{\varphi\varphi}\Omega^2}\right] , \end{aligned} \tag{B.5}$$

where we of course need to substitute the $\lambda = 0$ version of (B.1) to obtain a purely coordinate-dependent expression.

The expressions for mass and enthalpy density of an isentropic, nonmagnetized, and polytropic fluid $P = K\mu^\gamma$ read (cf. Rezzolla & Zanotti 2013)

$$\mu = \left[\frac{\gamma - 1}{K\gamma}\Big(\exp[W - W_\mathrm{s}] - 1\Big)\right]^{1/(\gamma-1)} , \tag{B.6}$$

$$w = \mu \exp[W - W_\mathrm{s}] = \mu + \frac{K\gamma}{\gamma - 1}\mu^\gamma . \tag{B.7}$$

where W_s is the value of W at the surface of the torus (conventionally the inner edge).

The dynamical properties of the polytropic gas are invariant with respect to K (see e.g., Rezzolla & Zanotti 2013), so the choice of K is somewhat arbitrary. We choose K in the same way as the original HARM code and that is so that

$$\frac{\mu}{\mu_\mathrm{c}} = \left[\frac{\gamma - 1}{\gamma}\Big(\exp[W - W_\mathrm{s}] - 1\Big)\right]^{1/(\gamma-1)} , \tag{B.8}$$

where μ_c is the maximum density[4] in the torus (i.e., at the pressure maximum). This leads immediately to $K = \mu_\mathrm{c}^{1-\gamma}$.

However, as was mentioned in the main text and can be seen from (B.6) and (B.7), the choice of K does influence the absolute values of specific enthalpy $h = w/\mu$ throughout the fluid. Hence, some of the important physical characteristics of the toroids such as their total specific energy $\mathcal{E}/\mathcal{M}$ or total specific angular momentum $\mathcal{L}/\mathcal{M}$ depend on the value of K even at fixed spatial extent and rotation curves!

If we then fix κ (and $\lambda = 0$), and we want to confine the torus between some r_in and r_out, we must numerically solve the following equation for ℓ_0 using either well-known algorithms or software such as Mathematica or Matlab

$$W(r = r_\mathrm{in}, \theta = \pi/2; \kappa, \ell_0) - W(r = r_\mathrm{out}, \theta = \pi/2; \kappa, \ell_0) = 0 .$$

The parameters which we obtained in the case of $r_\mathrm{in} = 5M$, $r_\mathrm{out} = 12M$ are given in Table 2.

[4] In the HARM code, one actually stores and evolves the dimensionless μ/μ_c instead of μ.